Metabolic engineering of *Saccharomyces cerevisiae* for the biosynthesis of olivetolic acid, a key cannabinoid precursor

Zur Erlangung des akademischen Grades eines

Dr.rer.nat

von der Fakultät Bio- und Chemieingenieurwesen
der Technischen Universität Dortmund
genehmigte Dissertation

vorgelegt von

M. Sc. Kilan Josia Schäfer

aus

Langen (Hessen)

Tag der mündlichen Prüfung: 12.03.2026

1. Gutachter/-in: Prof. Dr. Oliver Kayser

2. Gutachter/-in: Prof. Dr. Vlada Urlacher

Dortmund 2026

TABLE OF CONTENTS

LIST OF FIGURES

LIST OF TABLES

Erklärung zur Reproduktion vorab veröffentlichter Inhalte

Declaration of pre-published contents

Kapitel 3	3.1.1	In Teilen modifiziert aus	**[A]**
	3.1.2	In Teilen modifiziert aus	**[A]**
	3.1.3	In Teilen modifiziert aus	**[A]**
	3.1.4	In Teilen modifiziert aus	**[A]**
	3.1.5	In Teilen modifiziert aus	**[A]**
	3.1.6	In Teilen modifiziert aus	**[A]**
	3.1.7	In Teilen modifiziert aus	**[A]**
	3.2.1	In Teilen modifiziert aus	**[A]**
	3.2.2	In Teilen modifiziert aus	**[A]**
	3.2.3	In Teilen modifiziert aus	**[A]**
	3.2.4	In Teilen modifiziert aus	**[A]**
	3.2.5	In Teilen modifiziert aus	**[A]**
	3.3.2	In Teilen modifiziert aus	**[A]**
	3.3.3	In Teilen modifiziert aus	**[B]**
		Datenerhebung in Teilen aus	**[a]**
	3.3.4	In Teilen modifiziert aus	**[B]**
	3.3.5	In Teilen modifiziert aus	**[B]**
	3.3.6	In Teilen modifiziert aus	**[B]**
	3.3.7	In Teilen modifiziert aus	**[B]**
	3.3.8	In Teilen modifiziert aus	**[B]**
	3.4.1	In Teilen modifiziert aus	**[B]**
	3.4.3	In Teilen modifiziert aus	**[B]**
		Datenerhebung in Teilen aus	**[b]**

Publikationen

Publications

[A] Schäfer, K. J.; Aras, M.; Boles, E.; Kayser, O. Optimizing Hexanoic Acid Biosynthesis in Saccharomyces Cerevisiae for the de Novo Production of Olivetolic Acid. Biotechnol. Biofuels Bioprod. **2024**, 17 (1), 141. https://doi.org/10.1186/s13068-024-02586-2.

[B] Schäfer, K. J.; Chalwatzis, L.; Feka, A. M.; Aras, M.; Boles, E.; Kayser, O. Biochemical and Metabolic Engineering of Saccharomyces Cerevisiae for the Biosynthesis of Olivetolic Acid, a Key Cannabinoid Precursor. Biotechnol. J. **2025**, 20 (6), e70042. https://doi.org/10.1002/biot.70042.

Datenerhebung im Rahmen studentischer Arbeiten

Data collection held within student theses

[a] Chalwatzis, L., 2022, “Genetic engineering of precursor supply for cannabinoid production in yeast,” Masterarbeit, Technische Universität Darmstadt, Darmstadt

[b] Feka, T. M. 2024, “Optimization of olivetolic acid production in *Saccharomyces cerevisiae* by metabolic engineering,” Masterarbeit, Goethe Universität Frankfurt, Frankfurt am Main

1 INTRODUCTION

1.1 *Saccharomyces cerevisiae* in biotechnology and research

The budding yeast *Saccharomyces cerevisiae*, or baker's yeast, has been used in biotechnology for millennia through the fermentation of wine, beer and other alcoholic beverages. In modern biotechnology, *S. cerevisiae* is subject to precise and targeted metabolic and genetic engineering to generate recombinant strains capable of functioning as microbial biocatalysts. This has been made possible by decades of extensive research, resulting in the complete sequencing and a near complete annotation of its genome as well as a deep understanding of its core metabolic pathways. As a single-celled eukaryotic microorganism, *S. cerevisiae* harbors the advantages of both simple microbes and more complex organisms. It can readily take up plasmid DNA from its environment, thereby allowing for quick and efficient heterologous expression in a manner similar to bacterial model organisms, such as *Escherichia coli*. Furthermore, *S. cerevisiae* exhibits fast and robust growth in simple cultivation media containing a carbon source and a nitrogen source. Additionally, it possesses a complex cell wall composed of polysaccharides, proteins and lipids which facilitates interactions with the environment and provides structural stability and robustness.[1] This inherent robustness, combined with its high tolerance towards low pH, ethanol and various stresses such as shear stress, enables it to withstand the harsh conditions typically observed during fermentative processes in bioreactors.[2,3] Moreover, it is metabolically versatile, capable of utilizing a wide range of carbon sources, preferably hexose sugars, and is able to grow in both aerobic and anaerobic conditions. Importantly, it rapidly ferments sugars anaerobically, even in the presence of oxygen in a phenomenon called the "Crabtree effect".[4,5] Metabolically engineering *S. cerevisiae* away from ethanol production and towards value-added bioproducts therefore harbors great potential as sugars can be efficiently converted to products, thus resulting in high productivity.[6] Moreover, *S. cerevisiae* is classified as generally regarded as safe (GRAS) making it suitable for applications for a range of biotechnological industries, including the pharmaceutical and food industries. Thus, *S. cerevisiae* is a well-rounded and promising candidate for applications in diverse industrial settings.

S. cerevisiae additionally shares key features with higher eukaryotes. Most notably, it possesses membrane bound organelles such as a nucleus, endoplasmic reticulum, Golgi apparatus, mitochondria, peroxisomes and vacuoles. Thus, *S. cerevisiae* is able to express large, complex heterologous proteins and incorporate essential post-translational modifications (PTMs), making it possible to reconstitute complex heterologous biosynthetic pathways in *S. cerevisiae* which find their limitations in bacterial species such as *E. coli*. To this end, *S. cerevisiae* is also used as a simple model organism for studying human diseases.[7–10]

1.1.1 Genetic engineering of *S. cerevisiae*

The genome of *S. cerevisiae* is readily accessible and a plethora of tools have been developed which allow rapid and targeted genome modification. It readily undergoes homologous directed repair (HDR) making it able to insert, remove or reshuffle genetic elements containing homologous regions as short as 35 nt.[11–13] This feature has been exploited for genetic engineering through the integration of either dominant or auxotrophic selective markers in order to replace target genes or to facilitate the co-integration of genes of interest (GOIs) by providing selection pressure.[14] In order to recycle genetic markers, the successful use of the prokaryotic Cre-loxP system, a site-specific recombination system, was described for *S. cerevisiae* in 1987.[15] However, this system requires two steps and results in the retention of genetic scars in order to facilitate marker recycling. Consequently, the Cre-LoxP system is constrained by genomic instability, as the accumulation of these scars can render engineered strains susceptible to unwanted recombination events. Nevertheless, more recently, this system has been expanded to allow multiplexed genome editing in *S. cerevisiae*.[16] Despite this, since the advent of a more precise genome modification system, the CRISPR (clustered regularly interspaced short palindromic repeats)/Cas9 (CRISPR-associated protein 9) system, the possibilities and ease of genetic engineering have rapidly expanded across all fields of biotechnology, not least in *S. cerevisiae*. As CRISPR/Cas9 induces double-stranded breaks (DSBs) within the genome, this method can be used to facilitate the integration of DNA molecules containing homology arms for the target locus. Thus, the CRISPR/Cas9 induced DSB can be repaired via HDR using a desired donor DNA molecule as a repair template. In this manner, CRISPR/Cas9 allows the targeted and scarless integration or deletion of genetic elements via a single step, without the requirement of auxotrophic or antibiotic resistance markers.

Briefly, the CRISPR/Cas9 system is a ribonucleoprotein (RNP) complex comprising an endonuclease (Cas9) and two non-coding RNAs, CRISPR RNA (crRNA) and trans-activating crRNA (tracrRNA). Natively, it forms a bacterial adaptive immune system which is used to defend against invading viruses by cleaving foreign DNA. This system was first adopted from *Streptococcus pyogenes* and repurposed for targeted genome editing in 2012[17] and has since been expanded and modified for diverse genome editing strategies.[18–20] The Cas9 protein possesses two catalytic domains which each cleave the phosphodiester bond of the non-complementary (RuvC domain) and the complementary strands (HNH domain), respectively, thereby inducing DSBs within DNA molecules. The tracrRNA is required for activation of the RNP complex whereby it induces the maturation of the crRNA which must be processed from a pre-crRNA via RNase III.[17,21,22] The crRNA forms a base-paired duplex with the tracrRNA and contains a 20 nt sequence, called the protospacer, which is complementary to a specific DNA sequence to which it binds via Watson-Crick base pairing.[23,24] In this way, crRNA is responsible for targeting Cas9 to the site of cleavage. For the purpose of targeted genome editing, the crRNA and tracrRNA elements were fused to form a single guide RNA (sgRNA).[17] This RNA chimera simplifies the system and allows the ability to rapidly design genome editing strategies in which no pre-RNA processing is required and only the protospacer sequence of the crRNA element must be altered to target Cas9 to the desired locus

within the genome. Furthermore, a nuclear localization sequence (NLS), commonly the SV40 NLS sequence,[25] is incorporated to ensure it is targeted to the nucleus of a eukaryotic host.[18] Other than the protospacer itself, DNA cleavage is limited only by the requirement of a protospacer adjacent motif (PAM).[26] For ^{Sp}Cas9, the PAM consists of the simple and highly abundant NGG sequence, where N represents any nucleotide.[27] This potentially allows precise cleavage at almost any desired locus. Cas9 from other organisms require alternative PAM sequences for cleavage, for example the *Staphylococcus aureus* Cas9 requires a PAM comprising the less abundant NNGRRT sequence, where R represents a purine nucleotide,[28–30] while Cas12a (Cpf1) targets T rich PAM sequences.[31,32] Thus, the CRISPR/Cas9 system can be adapted depending on the desired application, for example to allow higher precision or more flexibility. A further innovation of the system is the inactivation of the individual catalytic domains of the endonuclease through the mutation of catalytic residues within the RuvC domain (D10A) or the HNH domain (H840A). This generates Cas9 DNA nickases (Cas9n or Cas9^{H840A}, respectively).[17,20] These mutant enzymes induce single-stranded nicks which is important to allow precise single bp editing. Furthermore, inactivation of both domains allows targeting of a deactivated Cas9 (dCas9) to specific genetic loci without inducing any DNA strand breaks. This application may be desired for transcriptional regulation by fusing repressors (CRISPRi) or activators (CRISPRa) to dCas9[33] or in imaging studies by fusing dCas9 to fluorescent proteins such as green fluorescent protein (GFP).[34,35]

A significant amount of research has been and continues to be conducted in the fields of molecular and synthetic biology for *S. cerevisiae*. This has allowed the development of extensive genetic toolboxes,[36–38] diverse gene editing strategies,[39–44] promoter engineering and plasmid-based expression systems.[45–50] The vast repertoire of data has been compiled in online databases, including the Saccharomyces Genome Database (SGD).[51,52]

1.2 Cannabinoids

1.2.1 Cannabinoid structures, classification and history

Cannabinoids comprise a large class of bioactive secondary metabolites found primarily in the plant species *Cannabis sativa L* (*Cannabaceae*) and some have been identified in other plants species such as those belonging to the genus *Rhododendron* (*Ericaceae*).[53] These compounds are of interest because they exert pharmacological and therapeutic effects in humans. This occurs through their interaction with the endogenous receptors of the endocannabinoid system (ECS), cannabinoid receptor 1 (CB_1) and 2 (CB_2).[54,55] The term “phytocannabinoids” was introduced to distinguish plant derived cannabinoids from the chemically distinct endocannabinoids, which are the natural ligands CB1 and CB_2, and due to the emergence of synthetic, non-natural cannabinoids. However, as this work exclusively focuses on the biosynthesis of the plant-derived compounds, the term “cannabinoids” will hereafter be used to refer to these. Up to 120 different cannabinoids are known to exist to date, the most well-known and well-studied being (–)-Δ^9-*trans*-

tetrahydrocannabinol (Δ^9-THC or THC) and cannabidiol (CBD), of which THC is the main active ingredient responsible for the psychological effects experienced upon cannabis consumption – colloquially known as the "high". In addition, over 560 other chemical compounds have also been identified in cannabis, including over 100 different terpene species.[56–61] Other predominant cannabinoid species are cannabigerol (CBG), cannabichromene (CBC) and cannabinol (CBN).

Structurally, cannabinoids contain a terpenoid moiety and an alkylresorcinol moiety. The most common and typical cannabinoid species, to which THC and CBD belong, have a C_{21} skeleton which contains a monoterpene (C_{10}) and an *n*-pentyl (C_5) moiety bound to a resorcinol core (C_6). However, due to the diverse range of starter units which can be used for the biosynthesis of the isoprenyl and polyketide precursors, from which the terpenoid and *n*-alkyl moieties are derived, the chemical diversity of these compounds is extremely broad.[62] Common examples of non-canonical cannabinoids are those in which the *n*-alkyl substituents vary in length and include natural derivatives of THC and CBD which are found in *C. sativa* in low concentrations. Tetrahydrocannabivarin (THCV) and cannabidivarin (CBDV) contain a shortened *n*-propyl (C_3)

Cannabinoid Type	Structure
CBG	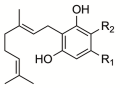
CBD	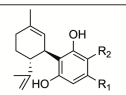
Δ^9-THC	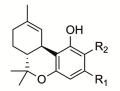
CBC	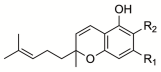
Δ^8-THC	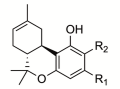
CBN	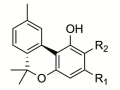
CBE	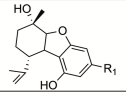
CBL	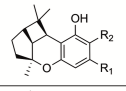
CBND	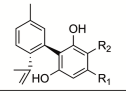
CBT	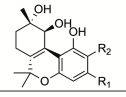

R_1 = Alkyl Side Chain
R_2 = H or COOH

Figure 1 | Cannabinoid structures

Overview of the chemical structures of the cannabinoid types (adapted from Gülck and Møller, 2020). This figure was created using ChemDraw 22.2.0 (PerkinElmer).

sidechain while more recently, tetrahydrocannabiphorol (THCP) and cannabidiphorol (CBDP) were identified which contain longer *n*-heptyl (C_7) sidechains at the *n*-alkyl position.[63,64] Interestingly, the length of the alkyl substituent influences binding affinities as THCP binds to CB_1 and CB_2 with 33-fold greater affinity compared to THC and 63-fold greater affinity compared to that of THCV, thereby making it more potent.[64] To organize this large chemical family, cannabinoids have been classified into 11 different types based on structural differences within the isoprenyl group and the resorcinol core (Figure 1). Of these, the following four classes are synthesized enzymatically: cannabichromenes (CBCs), cannabidiols (CBDs), cannabigerols (CBGs) and (–)-Δ^9-*trans*-tetrahydrocannabinols (Δ^9-THCs). The remaining seven classes, cannabicyclols (CBLs), cannabinols (CBNs), cannabinodiols (CBNDs), cannabitriols (CBTs), cannabielsoins (CBEs), (–)-Δ^8-*trans*-tetrahydrocannabinols (Δ^8-THCs) and miscellaneous species, are formed through the spontaneous rearrangement of the first four classes either as degradation products or due to oxidation.[53,60,62,65] Moreover, cannabinoids are synthesized as C_{22} organic acids, containing a carboxylic acid group on the aromatic ring of the alkylresorcinol moiety, and only exist in their neutral forms following decarboxylation through exposure to light or heat.[66–68] These acidic precursors are sometimes referred to as “pre-cannabinoids”.

Interestingly, cannabis usage has a very long history in human societies which stretches back over multiple millennia. Written records provide strong evidence that indicate the cultivation and medicinal usage of cannabis which dates back to ancient Egyptian and Assyrian civilizations and physical evidence was found suggesting its therapeutic application in the 4th century AD.[69,70] However, the chemical basis of cannabis was not understood until the extraction and isolation of the first cannabinoids which began in the late 19th century with the identification of cannabinol (CBN).[71] This work laid the foundation for subsequent studies into the chemical constituents of cannabis and their pharmacological effects. A number of decades later, the two most prevalent cannabinoids were discovered. CBD was first isolated by Adams and colleagues in 1940 who correctly deduced its chemical formula and proposed an initial chemical structure.[72] However, the correct structure was not solved until the availability of NMR spectroscopy in 1963.[73] This was then shortly followed by the discovery and structural elucidation of Δ^9-THC.[74] CBN was later identified as a degradation product of Δ^9-THC, which is formed through its oxidation.[61,75] Although Δ^9-THC is the primary active ingredient responsible for psychological activity, CBN has been shown to exhibit some psychoactive effects, either via its own potency or by enhancing the effects of Δ^9-THC.[61,75] In contrast, CBD is non-psychoactive.[72] Nevertheless, it exhibits various pharmacological and therapeutic effects which have been extensively investigated in more recent years.[76,77]

1.2.2 The endocannabinoid system

The ECS is a neuromodulatory system present in both the central and peripheral nervous system. It is involved in a range of physiological processes, most notably the regulation of neurologic and behavioral activity.[78–80] It comprises endocannabinoids, their receptors CB_1 and

CB_2, which are seven transmembrane $G_{i/o}$-linked G-protein coupled receptors (GPCRs) and the proteins required for their biosynthesis and degradation.[55,80–82] The cannabinoid receptors were initially identified in the brain and were characterized due to high affinity binding of cannabinoids.[83,84] They were therefore named as such. CB_1 was first cloned in 1990 and is predominantly expressed within the central nervous system (CNS) but it is also distributed at lower levels throughout many tissues within the body, including the exocrine pancreas, the liver, the gastrointestinal tract, adipocytes, skeletal muscle and circulating immune cells.[82,85–88] CB_2 was cloned three years later and found to be primarily expressed in the peripheral immune system but is also distributed within other tissues and peripheral organs.[87,89] However, CB_2 expression is also induced within the CNS upon inflammation or injury, for example in Alzheimer's disease.[90–93] Moreover, CB_1 and CB_2 can form heteromeric complexes within the brain which adds a further layer of complexity to the potential physiological effects exerted through this system.[94]

It was only after their characterization as cannabinoid receptors that their natural ligands were identified. The two most common and well-studied endocannabinoids are *N*-arachidonoylethanolamine (anandamide or AEA) and 2-arachidonoylglycerol (2-AG) (Figure 2).[95–97] Both are eicosanoid-like lipid based signaling molecules, or neurotransmitters, and are both derivatives of the polyunsaturated fatty acid, arachidonic acid. However, their biosynthesis and degradation pathways differ.[98,99] For this reason, they are structurally and chemically distinct to cannabinoids, despite sharing a common target. Both endocannabinoids are resident in the cell membranes as a component of lipids and released on demand into the extracellular matrix via distinct enzymatic pathways. This in contrast to canonical neurotransmitters which are synthesized and stored in intracellular synaptic vesicles.[79,100] There is evidence for multiple distinct biosynthetic routes for 2-AG and AEA from their lipid precursors, phosphatidyl inositol bisphosphate (PIP_2) and *N*-arachidonyl phosphatdiylethanolamine (NAPE), respectively.[99,101–104] 2-AG and AEA are both released in response to elevated Ca^{2+} levels, mediated either by depolarization or through $G_{q/11}$-linked GPCR mediated induction, for example via the group I metabotrophic glutamate receptors (mGluRs).[105–107] 2-AG is much more abundant in the brain receptor and binding to CB_1 and CB_2 is much stronger while AEA binds more weakly, making it act as a partial agonist.[107,108] However, 2-AG has wide ranging applications within the body. It is, for example, hydrolyzed by specific lipases to provide arachidonic acid for prostaglandin synthesis in some organs.[109]

In the context of neurotransmission, AEA and 2-AG interactions with CB_1 and CB_2 are involved in retrograde signaling and were first shown to function by attenuating signal transmission.[110–113] They are released from postsynaptic neurons and activate the presynaptic resident CB_1 and CB_2 receptors. This triggers signal cascades leading to the inhibition of high voltage-gated Ca^{2+} channels, thereby blocking Ca^{2+} entry into the neuron and inhibiting neurotransmitter release. In

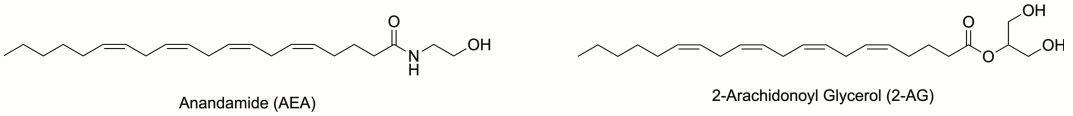

Figure 2 | Endocannabinoid structures

Chemical structures of the two most common endocannabinoids, anandamide (AEA) and 2-Arachidonyl Glycerol (2-AG). This figure was created using ChemDraw 22.2.0 (PerkinElmer).

addition, other GPCRs and ion channels have since been discovered which bind both endocannabinoids and cannabinoids and initiate distinct signaling cascades. GPR55 is activated by THC and AEA and sometimes termed the third cannabinoid receptor (CB_3).[114] GPR18 is activated by THC and *N*-arachidonoyl glycine, a metabolite of AEA, but is antagonized by CBD.[115,116] The transient receptor potential vanilloid 1 (TRPV1) is a non-selective cation channel with signaling roles in thermal and pain perception and is regulated by endocannabinoids and cannabinoids.[117–119] $GABA_A$ is potentiated by 2-AG at low GABA concentrations.[120] Thus, it is evident that endocannabinoids and cannabinoids have wide-ranging influences on neurological and physiological processes through the interaction with the receptors of the ECS and beyond. Details of these effects have been extensively reviewed elsewhere.[79,121–123]

1.2.3 Mechanisms of cannabinoid action

THC exerts its psychotropic effects by binding to CB_1 and CB_2 and activating signaling cascades via the release of G-proteins. It binds in the orthosteric binding sites, thereby highlighting the plasticity of the CB_1 and CB_2 binding pockets given the structural differences between THC and their native ligands. However, it only acts as a partial agonist and can therefore partially antagonize the effects of 2-AG.[124–127] Interestingly, THCA is non-psychoactive, suggesting that the carboxylic acid group prevents or disturbs correct binding. Likewise, CBD is non-psychoactive, despite THC and CBD having identical chemical formulas. This is because they differ in their chemical structures which results in conformational differences and therefore in different binding affinities for CB_1 and CB_2. THC adopts a planar conformation due to an additional ring structure formed by an oxygen bridge between the resorcinol core and the monoterpene moiety.[74,76] In contrast, the two rings are free to rotate around the C-C bond joining the two moieties together in CBD due to the absence of an oxygen bridge. This results in CBD adopting a non-planar conformation and having a lower affinity for the orthosteric binding pocket of CB_1 and CB_2.[128] Moreover, the interactions of CBD with the cannabinoid receptors are more complex and potentially broader. CBD is a strong antagonist of CB_1 and CB_2 and additionally acts as an inverse agonist of CB_2 by actively reducing receptor activity below basal levels.[127,129,130] While it has poor affinity for the primary binding sites, CBD binds to the receptors allosterically, thereby negatively modulating receptor activity and reducing the potency of 2-AG and THC.[131] Furthermore, it blocks fatty acid amide hydrolase (FAAH) and cyclooxygenase (COX) mediated degradation of AEA and 2-AG, which can in turn attenuate psychotic episodes for schizophrenia patients or aid in pain relief.[131–135] AEA seemingly plays a significant role in psychotic episodes in patients suffering from conditions such as schizophrenia by modulating dopamine levels. Levels are significantly elevated, especially in early stages of psychosis, which may act as a protective measure.[136,137] Allosteric regulators are effective therapeutic agents and are highly valued in drug design as they are generally specific and exhibit few side effects.[138] As such, CBD may be an attractive drug candidate. Indeed, antagonization of GPR55 or desensitization of TRPV1 by CBD contribute to a reduction in neuronal hyperexcitability

and pain perception[135,139] and inverse agonism against the 5-HT1A receptor can modulate and treat epileptic seizures.[140] Thus, CBD is considered to have anticonvulsive, neuroprotective and anti-inflammatory properties and is therefore of interest for treating diseases involving the CNS.[141,142]

Research into the less abundant cannabinoids found in cannabis extracts, including THCV, CBDV, CBG, CBN and CBC, also found widespread interactions of these molecules with various receptors, channels and enzymes and their therapeutic potential have also been investigated.[117,143,144] Of these, CBC is among the most abundant of the minor cannabinoids and is often grouped with THC, CBD and CBG as comprising the four major cannabinoids. CBC has gained more traction for research in recent years as a potential therapeutic agent due to its ability to partially antagonize CB_1 and CB_2 and has been shown to reduce gut inflammation in mouse models.[145–147] However, as it is far less abundant than the other major cannabinoid species, representing between 0.02-0.67% of dry weight,[148] gaining high yields through the extraction from plants is extremely difficult . As such, CBC can be synthesized synthetically via chemical processes from olivetol and citral[149,150] and optimization of reaction conditions have improved yields to 75%.[151] Alternatively, efforts to increase the biosynthesis of CBC through engineering of cannabichromenic acid synthase (CBCAS) allowed 22-fold increase in activity in cell lysates.[152] Thus, due to the influence and regulation of the two main cannabinoids, THC and CBD, as well as less abundant species on the ECS and beyond, cannabinoids have become of great interest as therapeutic agents for a range of neurological or behavioral conditions.

1.2.4 Cannabinoids as therapeutic agents

The effects of medicinal cannabis or cannabinoids as therapeutic agents for the treatment of a wide range of diseases and symptoms have long been known. THC has commonly been used to treat glaucoma patients by reducing intraocular pressure through the activation of CB_1 and GPR18.[153] Today, medical cannabis is widely available in a growing number of countries and the therapeutic chemicals CBD (Epidiolex), derived from plant extracts as a purified oil, and the synthetically derived THC (dronabinol) and a THC analogue (nabilone) have been approved for clinical use by the Food and Drug Administration (FDA) in the United States. Older applications include the treatment of human immunodeficiency virus (HIV)/acquired immunodeficiency syndrome (AIDS) to reduce viral load and to counteract weight loss by stimulating appetite,[154–156] and cancer patients to minimize nausea induced by chemotherapy.[157,158] More recently, cannabis has especially proven to be effective in treating neuropathic and chronic noncancer pain such as rheumatoid arthritis and fibromyalgia[159,160] as well as treating symptoms of multiple sclerosis and Huntington disease which include spasticity and pain.[161–163] Moreover, CBD was shown to induce apoptosis in prostate carcinoma cells[164] and is used to treat severe epilepsy in children.[65,165,166] Furthermore, cannabis and cannabinoids have shown effectiveness in treating Alzheimer's disease.[167] Although clinical studies have not always been conclusive and side-effects or modest efficacy have sometimes been reported, the benefits of using cannabis to treat symptoms of certain

severe diseases can lead to a great improvement in patient quality of life, as has been shown for Parkinson disease.[168]

In addition to the bioactivity of cannabinoids in humans and mammals, cannabis possesses antibacterial properties against gram-positive bacterial species including *Staphylococci* and *Streptococci*, however, not against gram-negative bacteria.[169] More recent studies have investigated the antibacterial activity of various cannabinoid species against the highly antibiotic-resistant bacterial strain, methicillin-resistant *S. aereus* (MRSA) commonly found in hospitals.[170,171] CBG displayed the greatest antibiotic activity and low rates of resistance, making it an attractive candidate as an antibiotic.[171] Its mechanism of action was deemed to be at the cytoplasmic membrane of MRSA. Moreover, it was concluded that the lack of potency against gram-negative bacteria was due to the inability to traverse the outer membrane layers and reach the inner membrane. However, by compromising the permeability barrier of the outer membrane using sublethal concentrations of polymyxin B, CBG potency was also high in gram-negative bacteria.[171] Thus, CBG may be useful in combination therapies against gram-negative bacteria. It was also shown that the most potent cannabinoids were the neutral canonical species (CBD, CBG and THC) while the acidic pre-cannabinoids (CBDA, CBGA and THCA) and *n*-propyl derivatives (THCV and CBDV) displayed reduced bioactivity.[171] This is similar to the psychoactive effects of THC which are not exerted in its carboxylated form. Nevertheless, their potencies remained largely tolerant to structural modifications of the prenyl and *n*-alkyl moieties, as long as hydrophobicity was not drastically altered.[170,171] In contrast, modifications to the hydroxyl groups of the resorcinol core greatly affected their potency, suggesting a functional role of the hydroxyl groups in the antibacterial properties of cannabinoids as is common with other phenolic compounds.[170,172] To this end, there is increased research into developing novel synthetic or semi-synthetic antibiotics using cannabinoids as a scaffold to target multi-resistant bacterial strains in the light of growing problem of antibiotic resistance worldwide.[173,174]

1.2.5 The native cannabinoid biosynthesis pathway

The main site of cannabinoid biosynthesis and storage are the stalked glandular trichomes of the female cannabis flower which was initially postulated based on analysis of their chemical profiles.[175–177] More recently, transcriptomic and metabolomic profiling of these glandular trichomes have identified the expression of genes involved in the cannabinoid biosynthetic pathway which cemented these previous findings.[178,179] Δ^9-THC, CBD and CBC are largely related in structure and share the same biosynthetic pathway until the formation of their common precursor, cannabigerolic acid (CBGA). The canonical pathway (Figure 3) begins within the cytosol where hexanoic acid is activated to hexanoyl-CoA by the action of acyl-activating enzyme 1 (AAE1).[180,181] Hexanoic acid is thought to originate from LCFAs, such as palmitic acid, and the proposed mechanism for its

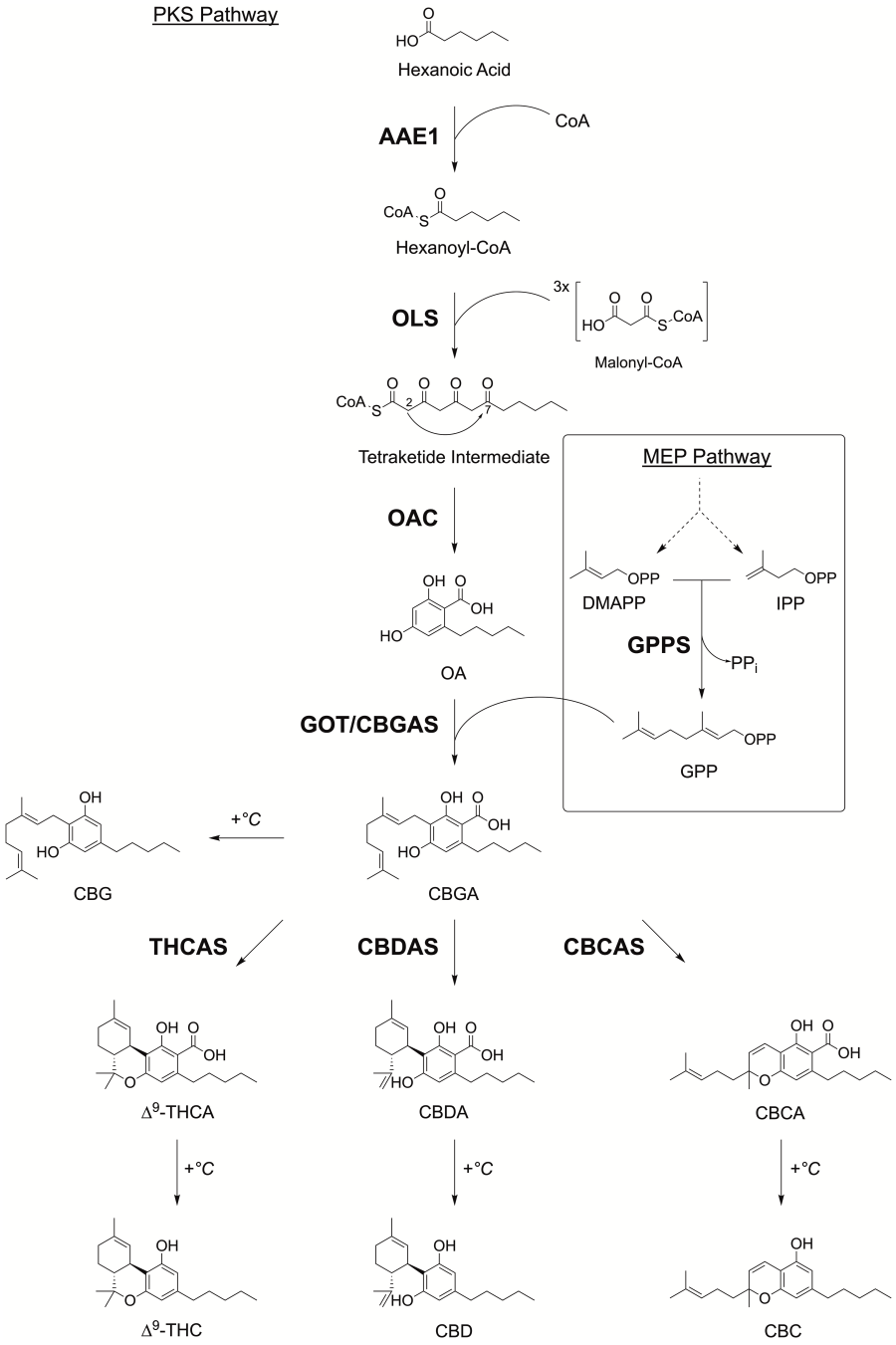

Figure 3 | Overview of the canonical cannabinoid biosynthesis pathway within C. sativa

Enzymes are written in bold. Pathways are underlined. Non-enyzmatic thermal decarboxylation is denoted by +°C. The intramolecular 2→7 aldol condenstation reachion of 3-5-7-trioxododecaneoyl-CoA is represented with an arrow. Dotted lines represent multiple enzymatic steps. This figure was created using ChemDraw 22.2.0 (PerkinElmer).

generation is through the sequential desaturation, lipoxygenation and cleavage of the LCFAs via the lipoxygenase (LOX) pathway. This is based on transcriptomic analyses which revealed high expression of desaturases, LOXs and hydroperoxide lyases (HPLs).[178,181,182] Alternatively, it has been proposed that hexanoyl-CoA may be derived from a premature termination of the fatty acid biosynthesis based on the analysis of a *C. sativa* cDNA library.[182] Hexanoyl-CoA is subsequently condensed with three molecules of malonyl-CoA via decarboxylative Claisen condensation

reactions in an iterative manner. This is catalyzed by a type III polyketide synthase (PKS), named olivetol synthase (OLS) or sometimes referred to as tetraketide synthase (TKS), to form the linear tetraketide intermediate, 3-5-7-trioxododecaneoyl-CoA.[183] OLS exists as a homodimer consisting of two 385 amino acid polypeptide chains with a mass of approximately 42.5 kDa each.[183] Surprisingly, initial *in vitro* and *in vivo* overexpression studies of OLS in the absence of OAC in *E. coli*, found that OLS alone was unable to form olivetolic acid (OA) and that other side-products were formed instead. The primary side product was olivetol (OL) which is formed through the spontaneous and irreversible cyclization of the tetraketide intermediate via a decarboxylative C2→C7 intramolecular aldol condensation reaction. Two further side-products are α-pyrone molecules which are formed through lactonization reactions: the tetraketide hexanoyl triacetic acid lactone (HTAL) and triketide pentyl diacetic acid lactone (PDAL).[183–185] α-Pyrones are commonly formed as spontaneous side products from polyketide precursors synthesized by bacterial type II PKSs in the absence of the cyclase enzymes required for the formation of the correct aromatic polyketide product. One such example is by *whiE* from *Streptomyces coelicolor*.[186] The phenomena of diverse side-product formation by heterologous expression of OLS alone led to the discovery of the cyclase OAC, which is responsible for catalyzing the non-decarboxylative cyclization of the linear tetraketide intermediate to correctly form OA. OAC is a small dimeric α+β barrel (DABB) protein consisting of a 101 amino acid polypeptide chain and the reaction which it catalyzes represents an unusual route for the biosynthesis of aromatic polyketides from type III PKSs in which a separate cyclase is required for product formation.[180,187,188]

OA, which is an *n*-pentylresorcinolic acid, is a key precursor in the cannabinoid biosynthesis pathway but is also of interest itself as a potential antimicrobial, cytotoxic and photoprotective agent. This is due to its structural similarity with lichen derived monoaromatic compounds and various aromatic tetraketide products derived from other plant type III PKSs.[189,190] Interestingly, the lichen species *Cetrelia sanguinea* naturally produces OA, although the biosynthetic route has not been fully investigated.[191] Examples of similar type III PKS derived compounds include the flavonoid precursor naringenin chalcone, catalyzed by chalcone synthase (CHS), and resveratrol, catalyzed by stilbene synthase (STS). As such, the mechanism of OLS was initially compared to that of CHS and STS. However, notable differences were discovered between these pathways. Both compounds are derived from the condensation of the starter unit 4-coumaroyl-CoA with three molecules of malonyl-CoA and in both CHS and STS, the tetraketide intermediate remains bound to the enzymes where the cyclization to the final products is catalyzed.[192–195] However, the mechanism of cyclization differs between the enzymes which allows the formation of distinct products, despite high similarities in their DNA and protein sequences as well as the use of identical substrates. CHS catalyzes a non-decarboxylative intramolecular C6→C1 Claisen condensation reaction,[196] while STS catalyzes a decarboxylative intramolecular C2→C7 aldol condensation reaction.[195,197] In contrast, OLS releases the linear tetraketide intermediate and this is subsequently cyclized by the separate OAC in an intramolecular C2→C7 non-decarboxylative aldol condensation reaction.[180,184] Thus, the cannabinoid biosynthesis pathway represents a distinct biosynthetic route for polyketide aromatization and demonstrates the plasticity within nature for the generation of

secondary metabolites.[180,184] The principals of this pathway may therefore be exploited in biotechnology.

OA is subsequently prenylated at the C3 position with the isoprenyl intermediate geranyl pyrophosphate (GPP) to form CBGA. In plants, GPP is synthesized by both the mevalonate (MVA) pathway in the cytosol and the 2-C-methyl-D-erythritol 4-phosphate (MEP) pathway in plastids.[198] As the MEP pathway is generally involved in secondary metabolism which includes the biosynthesis of terpenoids, it is regarded that the MEP pathway is the source of GPP in cannabinoid biosynthesis. As such, GPP is formed through the condensation of dimethylallyl pyrophosphate (DMAPP) and isopentenyl pyrophosphate (IPP) by the action of GPP synthase (GPPS).[199,200] Prenylation of OA occurs in the plastids and is achieved by the action of the plastid resident transmembrane aromatic prenyltransferase (aPT), which was initially named geranylpyrophosphate:olivetolate geranyltransferase (GOT) but is now commonly referred to as CBGA synthase (CBGAS) or PT4.[201–203] CBGA subsequently undergoes oxidative cyclization and is converted to the acidic precursors of the terminal cannabinoids, Δ^9-tetrahydrocannabinolic acid (THCA), cannabidiolic acid (CBDA) or cannabichromenic acid (CBCA). The oxidative cyclization of CBGA to their respective acidic cannabinoid products is catalyzed by three specific synthases: THCA synthase (THCAS), CBDA synthase (CBDAS) and CBCA synthase (CBCAS). The acidic cannabinoids are the primary species found in the plants and only upon exposure to heat, light or alkaline conditions do they undergo non-enzymatic decarboxylation, forming the neutral terminal cannabinoids THC, CDB and CBC.[204–206] The variation in cannabinoid profiles determines the chemotype of each cannabis strains and is dependent on the varying expression of the corresponding synthases.[207,208] THC is the principal constituent found in the *C. sativa* drug strain, marijuana, while CBD is the most common species in the fiber-type strain, hemp.[209] Plants have typically been bred to increase the contents of THC over the years and plants today can reach potencies of up to 28%.[58,210] Furthermore, strains vary in their ratio of THC and CBD content,[211] which indicates varying expression levels of the synthases. This is because enzymatic conversion between THC and CBD is not apparent in plants, although this can be achieved chemically.[212]

1.2.6 Structure and chemistry of the terminal cannabinoid synthases

The most prominent terminal cannabinoid synthases, THCAS and CBDAS, have been extensively studied and are structurally very similar, sharing 84% amino acid sequence homology.[208] THCAS is a 75 kDa monomeric protein which was first identified and purified in 1995[213] while CBDAS is an approximately 74 kDa monomeric protein which was isolated in the following year.[214] CBCAS was first identified in 1997, purified a year later and was patented in 2015.[215–217] Although it is much less studied than the other two major synthases, it shares great amino acid sequence homology with THCAS (93-96%) and thus likely shares similar mechanisms of action.[53,152,208] CBCAS, has a molecular mass of 71 kDa but, in contrast to THCAS and CBDAS, exists as a 136 kDa homodimer.[216] The final step in the biosynthesis of the terminal cannabinoids

occurs in the extracellular storage cavities of glandular trichomes within the apoplastic space as THCAS, CBDAS and CBGA are localized there.[218,219] Thus, the substrate and the synthases must be transported via the secretory pathway. All three synthases contain a highly similar cleavable N-terminal signal peptide which is required to localize the enzymes to the secretory pathway and is cleaved during maturation of the enzyme. Indeed, it was found that recombinant THCAS and CBDAS entered the secretory pathway of insect (*Spodoptera frugiperda*) and tobacco cells and were secreted into the media.[209,220,221] Similarly, CBCAS was secreted when overexpressed in the yeast *Pichia pastoris*.[208] Despite a lack of direct evidence, all three synthases are thought to be post-translationally modified via *N*-linked glycosylation as the molecular weights determined from purification studies were significantly higher than the theoretical weights based solely on the amino acid sequences.[209,220,222,223] Moreover, as *N*-linked glycosylation of secreted proteins is common in nature,[224] it is highly probable that THCAS, CBDAS and CBCAS carry this post-translational modification (PTM). Interestingly, the glycosylation sites were shown to differentially influence enzyme activity as removal of these sites increased THCAS activity while the same approach in CBCAS resulted in a mild decrease in activity.[152,223,225]

The synthases are enzymatically classified as oxidoreductases as they catalyze the cyclization of a monoterpene moiety and are specifically described as members of the berberine bridge enzyme (BBE)-like family.[226] However, they do not share common characteristics which are typically found in plant terpenoid cyclases. For example, they do not require divalent ions, a common feature of terpenoid cyclases, or external cofactors for activity and they are not inhibited by chelating agents.[214,216,227,228] They are however flavinylated enzymes which contain a single flavin adenine dinucleotide (FAD) molecule, covalently bound at positions H114 and C176, and thus belong to the wider family of oxygen-dependent FAD-linked oxidoreductases.[221,226,229] Moreover, mutations at the positions involved in coordinating FAD binding results in the loss of enzyme activity.[152,209,221,229] FAD binding is further stabilized through various hydrogen-bond interactions with the nitrogen atoms within the backbone of six residues, the nitrogen atoms within the sidechains of two additional residues and with the hydroxyl groups of two tyrosine residues.[229] Binding interactions are expected at similar or identical positions in CBDAS and CBCAS based on their structural similarities.[152] THCAS and CBDAS both also require molecular oxygen and produce hydrogen peroxide (H_2O_2). However, the enzymes differ in their catalytic mechanisms through stereoselectivity during oxidative cyclization of CBGA. The initial steps are identical in which a hydride ion (H^-) is extracted from the C3 position of CBGA and transferred to the bound FAD cofactor, thereby reducing it to $FADH_2$. Next, a basic residue extracts a proton from distinct positions of the substrate which depends on the synthase and results in alternative cyclization mechanisms.[209,221] In THCAS, mutational and structural analyses deduced that Tyr484 deprotonates the hydroxyl group at the O6' position of the alkylresorcinol moiety which ultimately results in the formation of a second ring between the alkylresorcinol moiety and the C8 position of the monoterpene moiety.[229] In contrast, Tyr483 in CBDAS is responsible for deprotonating the terminal methyl group of the monoterpene moiety and thus does not allow the formation of a ring structure between the two moieties.[223] In CBCAS, Tyr484 is proposed to deprotonate the hydroxyl

group at the same position of the alkylresorcinol moiety as in THCAS, however, this leads to a single ring formation between the two moieties, leaving the remainder of the terpene structure open.[152] Interestingly, CBCAS produces a racemic mixture of CBCA suggesting lower stereospecificity of the reaction.[60,230] Finally, molecular oxygen is required to reoxidize $FADH_2$, thereby regenerating FAD, and the reaction is coupled with the release of H_2O_2.[209,221] Initial biochemical studies on CBCAS indicated that molecular oxygen is not required, thus suggesting that FAD is regenerated via oxidation in a distinct manner to THCAS and CBDAS.[216] Nevertheless, it is likely that the mechanism of oxidative cyclization of CBGA catalyzed by CBCAS proceeds in a manner similar to THCAS and CBDAS in which molecular oxygen is reduced to H_2O_2 and this is now generally accepted and is widely described as such.[53,223,226] THCAS and CBDAS also have a similar catalytic capacity (k_{cat} = 0.30 s^{-1} and k_{cat} = 0.19 s^{-1}, respectively) and substrate affinity (134 µM and 137 µM, respectively) for CBGA.[213,214,221] On the other hand, CBCAS exhibits approximately a ten times lower catalytical capacity (0.02 - 0.04 s^{-1}) compared to THCAS and CBDAS. However, this is compensated for by a much greater affinity for CBGA (K_m 9.3 - 23 = µM) which results in a similar overall catalytic rate (k_{cat}/K_m).[216] Finally, CBDAS and THCAS activity is greatest in an acidic environment as a pH of 4.5 was determined to be the optimum for both enzymes.[223] Strikingly, product formation by THCAS shifts towards CBCA production at a higher pH of 7.[223] Taken together, the details of the cannabinoid biosynthesis pathway and the distinctive chemistry of its enzymes offer insights into the occurrence of this unique class of natural products. These insights are essential when considering approaches for producing cannabinoids synthetically using heterologous microbial systems.

1.2.7 Microbial biosynthesis of cannabinoids

The consumption of cannabinoids traditionally occurs via the burning and inhalation or via oral intake of the dried flower buds. Alternatively, the cannabinoids can be extracted from plants, purified and concentrated for use in pharmaceuticals or other products. However, these processes are often labor-intensive, involve the use of solvents and generally result in poor yields. Moreover, due to the high abundance of diverse cannabinoids within the plants, achieving high purity of single species remains difficult, especially in the case of rare cannabinoid species such as CBC or THCV. For these reasons, extracting cannabinoids from plants poses many obstacles for commercialization and up-scaling, particularly in light of an expanding global market due to recent legalization in countries, including the United States, Canada and Germany. Furthermore, considerations of the agricultural land required, as well as the time and costs coupled to growing the plants, render these approaches unsustainable. Although chemical synthesis of the cannabinoids is generally possible for some molecules,[149,151] these methods are limited due to their structural complexity. Nevertheless, the biosynthetic production of cannabinoids using microbial chassis organisms provides a promising alternative and has been the focus of a vast amount of research in recent years. To this end, various parts of the cannabinoid biosynthesis pathway have been implemented in bacterial species, primarily in *E. coli.* Particularly the biosynthesis of OA has

been achieved through the heterologous overexpression of *CsOLS* and *CsOAC*. A study conducted in 2018 demonstrated the first example of engineering an *E. coli* strain for the production of OA, reaching titers of 80 mg L^{-1}.[185] The authors describe various strategies in which the precursor supply was increased through the knocking out of competing pathways and the overexpression of additional enzymes. These "auxiliary" enzymes included the endogenous fatty acyl-CoA synthetase, FadD, capable of activating hexanoic acid to hexanoyl-CoA, acetyl-CoA carboxylase (ACC), to increase the supply of malonyl-CoA, and four heterologous enzymes capable of synthesizing hexanoyl-CoA from acetyl-CoA via a multi-species derived reverse β-oxidation (rBOX) pathway. The rBOX pathway will be discussed in more detail in chapter 1.3.5. Importantly, the final titers reported were derived from bioreactor experiments under controlled and optimized fermentation conditions. However, this system relied on the supplementation of 4 mM hexanoate to provide sufficient amounts of hexanoyl-CoA. Notably, OA titers were extremely limited when relying on the *de novo* biosynthesis of hexanoyl-CoA via the rBOX pathway, reaching only up to 8.4 mg L^{-1}.[185] Nevertheless, this work provided key metabolic engineering insights for the microbial biosynthesis of cannabinoids and their precursors. More recently, the production of 102 mg L^{-1} OA was demonstrated in engineered *E. coli* through a bioconversion system.[231] Here, it was found that two enzymes with short chain acyl-CoA ligase activities from *C. sativa* (AAE3) and *Pseudomonas putida* (IvaE) were more efficient in activating hexanoate to hexanoyl-CoA than fadD, with CsAAE3 proving to be the most efficient. Furthermore, malonyl-CoA supply was enhanced through the overexpression of MatB, a heterologous malonyl-CoA synthetase (MCS) from *Rhodopseudomonas palustris*. Surprisingly, fine-tuning the expression of *CsAAE3* and *RpmatB* for hexanoyl-CoA and malonyl-CoA generation, respectively, indicated that a surplus in *CsAAE3* expression resulted in higher OA production, despite there being a three-fold surplus in the molar equivalents of malonyl-CoA required compared to hexanoyl-CoA for each molecule of OA synthesized. This indicates that the enzymatic activity of CsAAE3 for hexanoate activation is inefficient, leaving room to search for more efficient enzymes to perform this step in microbial OA biosynthesis systems. Additional metabolic engineering strategies were employed to increase the supply of coenzyme A (CoA) and to regenerate ATP as these are consumed at a high rate during activation of hexanoate and malonate to their respective CoA esters. This was achieved through the overexpression of a feedback-resistant heterologous pantothenate kinase (PanK) from *P. putida* (*PpcoaA*) and through the overexpression of a bifunctional polyphosphate kinase from *Cytophaga hutchinsonii* which sequentially phosphorylates AMP to ADP and then ADP to ATP. Finally, the native fatty acid biosynthesis (FAB) pathway was downregulated via promoter engineering to decrease the competition for both malonyl-CoA and hexanoyl-CoA. These strategies led to the final reported titers of 102 mg L^{-1}. However, this system involved the use of two separately engineered strains which required disruption via ultrasonification for bioconversion and relied on supplementation of the cell lysates with 4 mM hexanoate, 12 mM malonate, 2 mM ATP and 2 mM pantothenate.

Despite successful efforts to synthetize OA in *E. coli*, extending the pathway for the biosynthesis of terminal cannabinoids is limited due to difficulties in functionally expressing the transmembrane enzyme, CBGAS, and the inability for *E. coli* to incorporate essential PTMs in

THCAS and CBDAS.[232] The challenge of expressing CBGAS in *E coli* was overcome by expressing a soluble promiscuous aPT derived from the fungal species, *Aspergillus terreus*.[233] This enzyme has also been engineered to improve substrate binding for GPP, OA and OL ($^{At}aPT^{E91Q}$), thereby allowing the biosynthesis of CBGA and CBG.[234] However, this study was designed as a proof-of-concept with titers only being achieved in the µg L^{-1} range.

As a result, alternative microbial cannabinoid production systems have been sought after which allow the functional expression of the terminal cannabinoid synthases. For this, the use of eukaryotic hosts has been investigated. Yeasts possess several advantages over bacteria in the context of cannabinoid biosynthesis. For example, they have an enhanced capacity to express plant genes and are able to incorporate PTMs.[235–237] In 2007, the first example of recombinant THCAS expression in yeast was described using the methanotrophic species *Pichia pastoris* (also named *Komagataella phaffii* or *Komagataella pastoris*).[225] As the terminal cannabinoid synthases enter the secretory pathway,[221] the enzyme was secreted from the recombinant *P. pastoris* cells and exhibited functional activity, as evidenced by the conversion CBGA to THCA at a high rate within the culture medium. Following this, functional intracellular expression of recombinant THCAS was demonstrated in both *P. pastoris* and *S. cerevisiae* by replacing the native 28 amino acid signal peptide with an N-terminal vacuolar localization sequence, comprising 24 amino acids derived from the endogenous proteinase A (Pep4p).[232] Feeding of CBGA to cultures in whole cell bioconversion assays resulted in the biosynthesis of THCA. Subsequent studies demonstrated the ability to co-express a cytosolic THCAS with a soluble bacterial aPT derived from *Streptomyces* sp. strain CL190 (^{Sp}NphB) in both yeast strains.[238] ^{Sp}NphB is able to prenylate diverse aromatic substrates at either the carbon or oxygen positions.[239] It was therefore suggested as a viable alternative to the plant-derived aPT in yeast due to difficulties in expressing CBGAS from *C. sativa* (^{Cs}PT1).[240] However, recombinant protein expression levels in *S. cerevisiae* were deemed too low to accommodate sufficient substrate turnover to CBGA following supplementation of cell lysates with OA and GPP. In contrast, *P. pastoris* was capable of producing detectable amounts of THCA from OA and GPP following co-expression of ^{Sp}NphB and THCAS. Nevertheless, low CBGAS activity limited the supply of substrate for THCAS and the substrate promiscuity of ^{Sp}NphB and preferential regioselectivity for geranylation of the 2-*O* position of OA resulted in higher levels of an *O*-prenylated side-product, 2-*O*-geranyl olivetolic acid (2-*O*-GOA) being obtained. Since then, protein engineering of ^{Sp}NphB which aimed to improve the binding of OA led to the development of mutant constructs which were able to selectively prenylate OA to produce CBGA. These include ^{Sp}NphB$^{G286S/Y288A}$ and ^{Sp}NphB^{Q295F}.[241,242] By implementing the ^{Sp}NphB$^{G286S/Y288A}$ variant in a cell-free system, the production of 744 mg L^{-1} CBGA was achieved via a synthetic biochemistry approach using glucose and OA as inputs.[242]

In 2019, the complete cannabinoid biosynthesis pathway was reconstituted in *S. cerevisiae*, demonstrating the ability to synthesize terminal cannabinoids from the simple sugar galactose.[243] To achieve this, a multi-species rBOX pathway was overexpressed to synthesize hexanoyl-CoA from acetyl-CoA, similar to previous reports in *E. coli* as described above,[185] and ^{Cs}*OLS* and ^{Cs}*OAC* were overexpressed which allowed the biosynthesis of OA. In addition, the native MVA biosynthesis

pathway was engineered to allow the accumulation of GPP. This is because *S. cerevisiae* only transiently produces GPP during isoprenoid biosynthesis due to the lack of a dedicated GPPS. Instead, after its formation, GPP is rapidly elongated to farnesyl pyrophosphate (FPP), a C15 isoprenoid precursor, via condensation with a second IPP (C5) unit. These two steps are catalyzed by the bifunctional FPP synthase Erg20p. As such, the accumulation of GPP was achieved by upregulating the first three enzymatic steps of the MVA pathway by overexpressing the genes *mvaE* and *mvaS*, derived from the gram-positive bacterial species *Enterococcus faecalis*. ^{Ef}*mvaE* encodes a bifunctional enzyme with acetoacetyl-CoA thiolase activity, responsible for condensing two acetyl-CoA units to form acetoacetyl-CoA in the first step of the MVA pathway, and 3-hydroxy-3-methylglutaryl-CoA (HMG-CoA) reductase activity, responsible for reducing HMG-CoA to mevalonate in the third step.[244] ^{Ef}*mvaS* encodes a HMG-CoA synthase, responsible for the formation of HMG-CoA through the condensation of a third acetyl-CoA molecule with acetoacetyl-CoA in the second step of the pathway.[245] Additionally, the endogenous *S. cerevisiae* genes *ERG12, ERG8, ERG19* and *IDI1* were overexpressed. *ERG12* and *ERG8* encode kinases which are responsible for the sequential phosphorylation of mevalonate and mevalonate 5-phosphate, respectively, thereby forming mevalonate 5-diphosphate. Mevalonate 5-diphosphate is subsequently decarboxylated by a mevalonate diphosphate decarboxylase, encoded by *ERG19*, to form IPP. *IDI1* encodes an isomerase which catalyzes the isomerization of IPP to DMAPP. Finally, to accumulate GPP, a mutant *ERG20* was introduced which possess reduced FPP synthase activity through the exchange of phenylalanine at position 69 and asparagine at position 127 with tryptophan (*ERG20*$^{F96W/N127W}$). These mutations function by sterically blocking the active site for FPP synthase activity, thereby significantly reducing its affinity for GPP.[246] Importantly, it is essential for the wildtype *ERG20* to be present in the background in order to maintain viability through sterol biosynthesis. Furthermore, the study by Luo and colleagues identified a specific aPT from *C. sativa*, ^{Cs}*PT4*, which possessed the highest capacity for producing CBGA following removal of the plastid-targeting sequence.[243] ^{Cs}PT4 was subsequently found in the purified microsomal fractions, indicating that it localizes to membrane structures in *S. cerevisiae*. Moreover, ^{Cs}*PT1*, the gene initially postulated to encode CBGAS in yeast, was found to be inactive, consistent with previous observations.[238,240] ^{Sp}NphB was shown to generate CBGA homologues due to alternative prenylation sites[238] which was described above. Furthermore, the promiscuity of ^{Sp}NphB and its engineered variants has been investigated for the conversion of OA analogues, containing alternative *n*-alkyl side-chains, to their corresponding CBGA derivatives, thereby demonstrating the potential for expanding the product profile to unnatural cannabinoids.[247] Finally, the biosynthesis of THCA and CBDA from galactose was achieved when THCAS and CBDAS constructs, which had their secretory signal peptides replaced with a vacuolar localization sequence, were introduced.[232] To further increase production titers, additional copies of ^{Cs}*OLS*, ^{Cs}*OAC* and ^{Cs}*THCAS* were integrated into the strain, thereby allowing the production of 8 mg L^{-1} THCA from galactose. This represented the first report of full microbial cannabinoid biosynthesis from a simple sugar. Moreover, THCVA, CBDVA and CBGVA were detected, likely due to the promiscuity of the cannabinoid biosynthesis enzymes and the availability of butyryl-CoA as a substrate which is

formed as an intermediate during rBOX mediated hexanoyl-CoA biosynthesis. Finally, the pathway was extended to include the production of unnatural cannabinoid analogues by tailoring the input of the starter substrates through feeding of different fatty acid precursors to the engineered microbial strains. This further demonstrated the ability for the cannabinoid biosynthesis enzymes to accept a diverse range of substrates. These included acyl chains of varying lengths, branched acyl chains or acyl chains with an unsaturated terminal group to facilitate post-fermentative modifications through click-chemistry, as demonstrated by azide-alkyne cycloaddition. In this way, the authors demonstrated the ability to tailor the cannabinoids and incorporate further chemical groups, thus expanding the pharmacological potential of these compounds.

The oleaginous yeast, *Yarrowia lipolytica*, which is commonly used for the heterologous production of various natural products, was also recently engineered for the biosynthesis of OA.[248] Here, the authors overexpressed ^{Cs}*OLS* and ^{Cs}*OAC* and applied multiple metabolic engineering strategies to increase the supply of cytosolic hexanoyl-CoA, acetyl-CoA and malonyl-CoA, as well as the supply of ATP and NADPH. After comparing various acyl-CoA ligases for their ability to activate hexanoic acid, ^{Pp}*LvaE* was found to be more efficient than the other candidate enzymes, including ^{Cs}*AAE1*. ^{Pp}*LvaE* was since implemented in the *E. coli* OA producing system, as described above.[231] Furthermore, increasing the malonyl-CoA supply improved OA production 1.8-fold. This was achieved by reducing the transcriptional regulation of ^{Yl}*ACC1*, which encodes the endogenous ACC gene, through the removal of introns.[248] Additionally, the supply of cytosolic acetyl-CoA was increased using multiple strategies. Peroxisomal β-oxidation was enhanced through the overexpression of the peroxisomal matrix protein (^{Yl}*PEX10*), which is involved in the import of peroxisomal matrix proteins, and the peroxisomal ATP/AMP transporter (^{Yl}*ANT1*), which is involved in the import of ATP into the peroxisome. Furthermore, a deregulated *Salmonella enterica* derived acetyl-CoA synthetase (^{Se}*Acs*^{L641P}), in which the leucine residue essential for acetylation-mediated inactivation is mutated,[249] was overexpressed in addition to the *E. coli* pyruvate dehydrogenase complex (^{Ec}*PDH*), which comprises three genes ^{Ec}*aceE* (E1), ^{Ec}*aceF* (E2), and ^{Ec}*lpdA* (E3). The *E. coli* lipoate-protein ligase A (^{Ec}*lplA*), which is required for activation of the E2 subunit via lipoylation, was also overexpressed.[250] Finally, overexpression of malic enzyme from an endogenous source (^{Yl}*MAE1*) and a heterologous source (*MAE2* from *Mucor circinelloides*) was implemented to form pyruvate which can feed into the PDH-mediated acetyl-CoA generating route.[248] Ultimately, despite the final extensive metabolic engineering strategies deployed to increase acetyl-CoA supply, the combination of these approaches only resulted in a modest increase in OA production, reaching 9.18 mg L^{-1} compared to 3.54 mg L^{-1} in the strain overexpressing just single copies of ^{Cs}*OLS*, ^{Cs}*OAC*, *ACC1* and the acyl-CoA synthetase (^{Pp}*lvaE*). Although these were the highest reported titers of OA produced using the canonical biosynthetic route in yeast at the time of publication, this system again relied on exogenous hexanoic acid supplementation and titers remained low. This may be because key bottlenecks within the pathway, such as the activities of ^{Cs}*OLS* and ^{Cs}*OAC*, were not addressed.

To this end, considerable improvements have since been achieved in *S. cerevisiae* cannabinoid biosynthesis systems, principally by incorporating multiple copies of the *C. sativa*

enzymes. Multi-copy integration of *CsOLS* and *CsOAC* was shown to improve the biosynthesis of OA in two recent studies.[251,252] Importantly, a surplus in copy number of *CsOAC* compared to *CsOLS* significantly improved the ratio of OA to OL formation. While Zhang *et al.*[252] implemented a fused OLS-OAC construct, comparable product ratios were achieved using single enzyme constructs.[251] To provide hexanoyl-CoA to the system, both studies relied on the supplementation of cultures with hexanoate and the overexpression of CsAAE1. Screening for other candidate hexanoyl-CoA ligases led to no avail as these enzymes were determined to be less active than CsAAE1.[251] To increase the supply of hexanoyl-CoA, Zhang *et al.*[252] knocked out the *POX1* gene to arrest peroxisomal β-oxidation and prevent the degradation the supplemented hexanoic acid. Moreover, they observed that hexanoyl-CoA can be used a substrate by the endogenous fatty acid synthase (FAS) and is elongated. To reduce the loss of hexanoyl-CoA in this way, the expression of *FAS* was lowered through the replacement of the native *FAS1* promoter with the weaker *RPS25A* promoter. These strategies successfully increased the flux of hexanoyl-CoA towards the cannabinoid biosynthesis pathway.[252] Contrary to these results, however, the presence of *POX1* did not affect the turnover efficiency from hexanoyl-CoA to OA in the study by Schmidt *et al.*[251] However, in this study, it was observed that *HAC1s*, which was overexpressed to aid in the activity of the terminal cannabinoid synthases, had a positive effect on OA biosynthesis.[251] It was suggested that this may be due to the HAC1s-mediated downregulation of genes involved in fatty acid biosynthesis and may therefore either increase the availability of malonyl-CoA or reduce the loss of hexanoyl-CoA to FAS. This would corroborate the findings of Zhang *et al*.[251] To enable the production of CBGA, both studies utilized an overexpressed MVA pathway to supply GPP, as had been previously described,[243] however, the studies diverged in their strategies to facilitate CBGA production. Schimdt *et al.*[251] utilized the soluble aPT SpNphB and increased its copy number.[251] Furthermore, increasing the pH by buffering the cultivation media and fusing SpNphB to ERG20$^{F96W/N127W}$ to facilitate direct transfer of GPP to the aPT improved CBGA formation.[251] In contrast, Zhang *et al.*[252] utilized the membrane bound CsPT4 in which the N-terminal plastid sequence had been removed[243] and, through fluorescence microscopy, were able to determine its localization within the endoplasmic reticulum membrane, facing outwards toward the cytoplasm.[252] Consequently, the authors aimed to increase the size of the endoplasmic reticulum in order to prevent endoplasmic reticulum stress[253] which may occur following overexpression of CsPT4. This was achieved through overexpression of *INO2*, a transcription factor involved in activating the transcription of genes involved in lipid biogenesis.[254] Additionally, the stability of CsPT4 was enhanced by fusing it with an N-terminal superoxide dismutase (Sod1p). As a result, CBGA production was significantly increased, reaching approximately 510 mg L^{-1} from glucose and 3 mM hexanoate.[252] This represents the highest reported CBGA titers to date. Moreover, OA was nearly completely converted to CBGA. However, approximately 109 mg L^{-1} OL also accumulated as a side-product.

Although titers of CBGA were not as high, Schmidt *et al*.[251] were able to produce approximately 6 mg L^{-1} CBGA in shake flask cultures. This was increased to 18 mg L^{-1} in fed-batch bioreactor fermentations from glucose and 0.5 mM hexanoate. However, this is substantially less than in the previous study.[252] Furthermore, high titers of OA accumulated (117 mg L^{-1}), suggesting

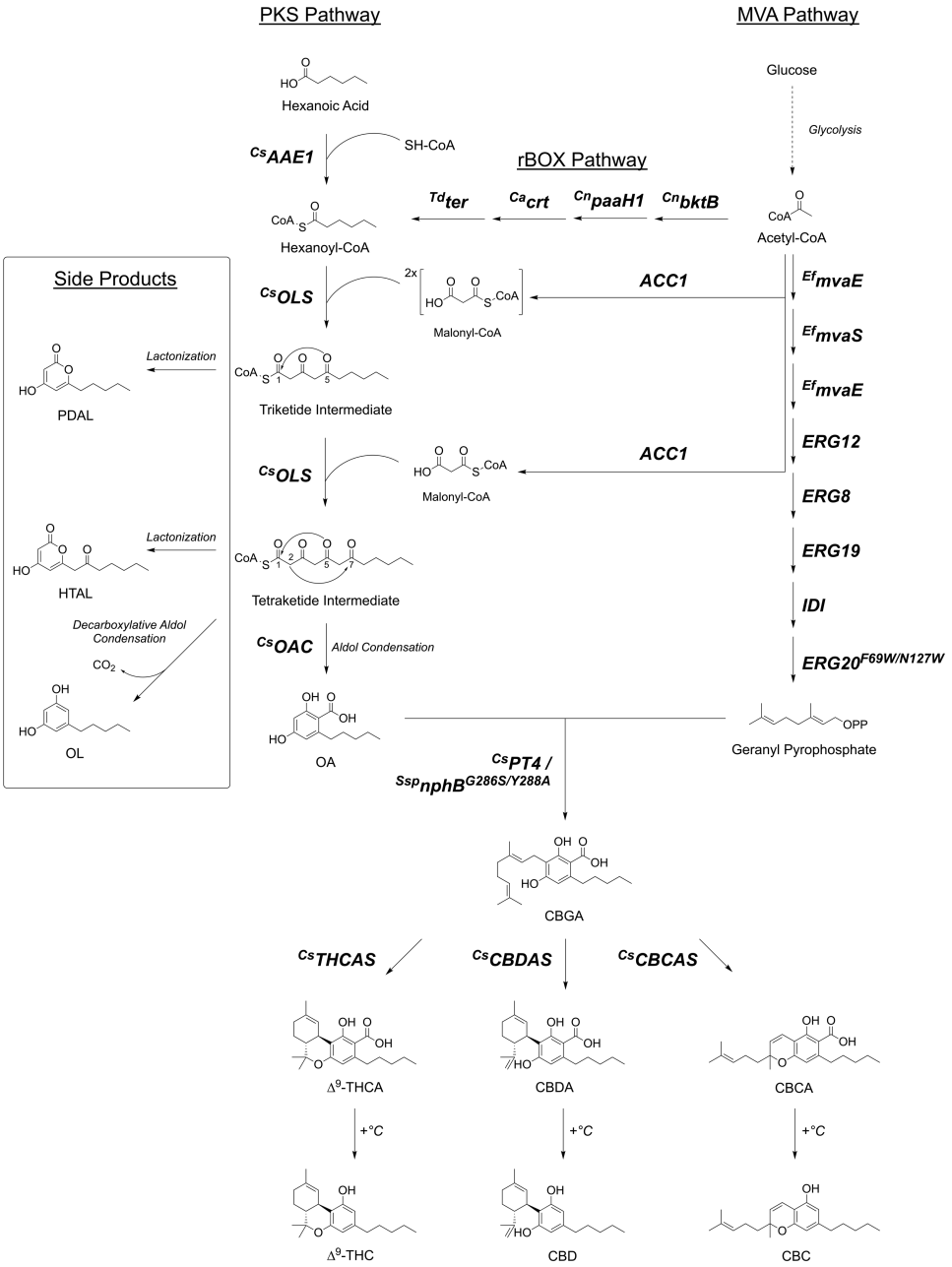

Figure 4 | Overview of a heterologous cannabinoid biosynthesis pathway in *S. cerevisiae*

The heterologous cannabinoid biosynthetsis pathway splits into two arms: (i) a heterologous PKS pathway, to form OA, and (ii) an endogenous MVA pathway, to form GPP. Formation of hexanoyl-CoA is achieved either via activation of exogenous hexanoic acid via overexpression of *CsAAE1* or via a heterologous rBOX pathway using acetyl-CoA derived from a simple carbon source (in this example, glucose). Hexanoyl-CoA is converted to OA via the overexpression of *CsOLS* and *CsOAC*. Malonyl-CoA is derived from acetyl-CoA via *ACC1*. Side products can form through lactonization (C_5 oxygen→C_1) of the triketide or tetraketide intermediates to form PDAL and HTAL, respectively.The main side product, OL, spontaneously forms via a decarboxylative C_2→C_7 intramolecular aldol condensation of the tetraketide intermediate. Overexpression of the MVA pathway can be achieved through the overexpression of bacterial genes (*EfmvaE*/*EfmvaS*) to form MVA. Overexpression of endogenous genes involved in isoprenoid biosynthesis (*ERG12, ERG8, ERG19, IDI*) and of a partially deactivated *ERG20F69W/N127W* allows the accumulation of GPP from acetyl-CoA. Overexpression of an aromatic PT (*CsPT4* or *SspnphBG286S/Y288A*) catalyzes the formation of CBGA from OA and GPP. Overexpression of terminal cannabinoid synthases (*CsTHCAS*/*CsCBDAS*/*CsCBCAS*) catalyzes the conversion of CBGA to the respective acidic pre-cannabinoids which are decarboxylated upon exposure to heat (+°C). Enzymes are written in bold and dotted lines represent multiple enzymatic steps. This figure was created using ChemDraw 22.2.0 (PerkinElmer).

a bottleneck in the supply of GPP or the activity of the aPT in this system.[251] Finally, the pathway

was expanded to demonstrate the production of terminal cannabinoids by introducing the *CsTHCAS*, *CsCBDAS* and *CsCBCAS*, for which the highest production was observed for THCA (1.43 mg L^{-1}). A detailed overview of a general heterologous cannabinoid biosynthesis pathway in *S. cerevisiae* is provided in Figure 4.

An intriguing study in 2021 demonstrated the ability to produce OA and derivatives thereof at significantly higher titers than had previously been reported.[255] OA biosynthesis reached 80 mg L^{-1} while the *n*-heptyl derivative sphaerophorolcarboxylic acid (SA) was produced at 1400 mg L^{-1}. This was achieved using the fungus *Asperigillus nidulans* through a novel biosynthetic route comprising two distinct fungal PKSs which operate in tandem. The first PKS embodies a highly reducing PKS (HRPKS) to provide an ACP-bound primer with a saturated or monosaturated acyl chain of length C_6 or C_8. HRPKSs were tested from different organisms and these were found to vary in the amount and specificity of the acyl-ACP product. The acyl-ACP product is subsequently transferred to a second non-reducing PKS (NRPKS) which performs the iterative condensation of the primer molecule with three malonyl-CoA units and facilitates the intramolecular aldol cyclization reaction, analogous to *CsOLS* and *CsOAC*. Finally, the ACP-bound product was hydrolyzed by a thioesterase (TE) which located on a third protein and fused to a ψACP domain that is not involved in shuttling of the acyl chain but likely aids in the interaction between the TE and the NRPKS. Thus, no plant enzymes were required. This may represent a similar route for OA biosynthesis in the lichen, *Cetrelia sanguinea*, which is a natural producer of OA.[191] SA production was substantially higher than OA, owing to the preferential biosynthesis of octanoyl-ACP (C_8) over hexanoyl-ACP (C_6) in the best performing HRPKS from *Metarhizium anisopliae*.[255]

1.3 Short- and Medium Chain Fatty Acids

1.3.1 Fatty acids and their relevance in biotechnology

Fatty acids (FAs) are key macromolecules which consist of a carboxylic group attached to a long aliphatic chain and have essential roles across almost all forms of life. FAs are extremely diverse and have been classified based on the chemical characteristics of their alkyl chains. These include the degree of saturation (mono- or polyunsaturated FAs), chain length, number of carbons atoms (odd or even), and whether the chain is branched or unbranched (straight chain). Straight chain saturated FAs are typically further categorized into short-chain FAs (SCFAs $\leq C_4$), medium-chain FAs (MCFAs; C_6-C_{14}), long-chain FAs (LCFA; C_{16}-C_{18}) or very long-chain FAs (VLCFA; $\geq C_{20}$) based on their length; although slightly differing uses of the nomenclature exist. In biology, LCFAs and VLCFAs are the most abundant FAs. They are major components of phospholipids which form membrane structures, they can be stored for energy reserves as triacylglycerides (TAGs) through esterification with glycerol and they are used for PTMs of proteins.[256,257] Additionally, they can be involved in signal transduction pathways, following release from lipids as second messengers, or they can be converted to other signaling molecules such as neurotransmitters.[258] In biotechnology,

there is a high demand for FAs as platform compounds as they are direct precursors for many industrially valuable oleochemicals.[259–262] These include, but are not limited to, FA methyl esters (FAMEs) or FA ethyl esters (FAEEs) which are derived through the transesterification of saturated FAs with methanol or ethanol, respectively. They can also serve as biofuels[263] and fatty alcohols (FOHs) which can be used for the production of surfactants and detergents or which can be esterified with FAs to form wax esters.[264,265] MCFAs and their derivatives are also industrially highly valuable. They have direct applications as antimicrobial agents[266–268] while MCFA ethyl esters (MCFAEEs) are desired in the food and wine industry due to their fruity aromas.[269] Furthermore, 1-octanol, a medium-chain FOH, is of great interest as it possesses similar combustion properties to diesel making it a promising candidate for use as a drop-in biofuel or in diesel blends.[270–272] Today, obtaining MCFAs for industrial production of oleochemicals is primarily achieved either through chemical synthesis from fossil fuel-derived feedstocks or from natural sources such as vegetable oils and animal fats. Coconut oil and palm oil naturally have a high content of octanoic to dodecanoic acid while animal fats such as sheep and goat milk additionally contain hexanoic acid.[273–275] However, obtaining high yields of MCFAs from these sources is environmentally harmful and unsustainable. The microbial production of MCFAs offers a sustainable and renewable alternative to these traditional methods. The anaerobic bacterial species *Clostridium kluyveri* and *Megasphaera elsdenii* are natural MCFA producers and have been adopted in biotechnological processes to covert waste biomass to MCFAs.[276–278] They are able to elongate short-chain organic acids, such as acetate or lactate, with ethanol in a process known as chain elongation (CE).[279] Although using these organisms has been harnessed for the production of high MCFAs titers,[276,280,277] the challenges involved in upscaling cultivation systems using anaerobic microorganisms make these organisms poorly suited for industrial-scale production. Moreover, the limited availability of genetic toolboxes and accessibility of their genomes for modification to allow the introduction of more complex biosynthetic pathways are major drawbacks. In contrast, MCFA production can be achieved by using non-natural, synthetic producers which are suitable for industrial upscaling. These include *E. coli* and *S. cerevisiae*. Due to the ability to genetically manipulate these organisms, these systems are not purely limited to MCFA production. Indeed, they can also serve as suitable hosts for reconstituting whole heterologous biosynthetic pathways which enables the direct production of more complex and higher-value MCFA derivatives. A key example is the ability to reconstitute the cannabinoid biosynthesis pathway in *S. cerevisiae* from hexanoyl-CoA, as extensively described above. Two main strategies have been developed and implemented in both *E. coli* and *S. cerevisiae* for the production of MCFAs through their CoA-bound intermediates: (i) the use of a heterologous reverse β-oxidation (rBOX) pathway[281–283] and (ii) through engineering of the endogenous fatty acid biosynthesis (FAB) pathway.[284–287] Other methods have also been explored, for example by modifying the β-oxidation pathway in *S. cerevisiae*.[288] Here, the degradation of the monounsaturated LCFA, oleic acid ($C_{18:1}$), was fine-tuned by knocking out the endogenous acyl-CoA oxidase *POX1*, which is able to accept acyl-CoAs of all chain lengths, and by introducing an acyl-CoA oxidase with specificity for long-chain acyl-CoAs from *Y. lipolytica* (*YlPOX2*). This resulted in the accumulation of MCFAs, however, titers

remained very low (0.5 mg L^{-1}) and most of the FAs were incorporated into the storage pathway rather than the degradation pathway, thereby avoiding the engineered pathway.

1.3.2 The fatty acid biosynthesis (FAB) pathway

The FAB pathway is a highly conserved pathway for the *de novo* biosynthesis of free FAs in all organisms and is achieved by a highly similar set of reactions catalyzed by fatty acid synthases (FASs). There are two types of FAS systems: the eukaryotic type I FAS (FAS I), which is present in the cytosol of mammals and fungi, including *S. cerevisiae*, and the type II FAS (FAS II), which is found in most bacteria, archaea and plants. Exceptions to these rules exist in that a special group of bacteria belonging to the genus' *Mycobacterium*, *Corynebacterium* and *Nocardia* (CMN), possess FAS I systems while FAS II systems are also present in the mitochondria of mammals and yeast.[289–292] FAS I and FAS II systems differ primarily in that FAS I are multidomain enzyme complexes which contain all the functional enzymatic domains required for FA biosynthesis embedded within a single or two polypeptides, whereas FAS II are multienzyme dissociated systems formed by separate proteins which each perform a specific function.[293] Moreover, the mammalian and fungal FASs differ substantially in their structures, although both are FAS I systems.[294] Mammalian FASs comprise a single polypeptide which forms a homodimeric (α_2) complex of approximately 540 kDa[295] while the fungal FAS most commonly comprises two polypeptides, encoded by two single genes, which form much larger and highly structured, heterododecameric ($\alpha_6\beta_6$) megacomplexes of approximately 2.6 MDa (Figure 5).[296,297] Additionally, the bacterial FAS I and that of some fungal species exist as homohexameric complexes comprising a single polypeptide chain encoded by a single gene.[289,298,299]

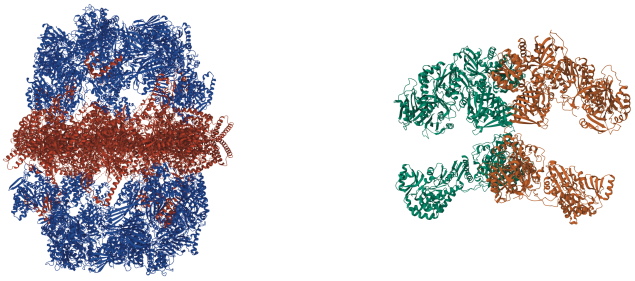

Fungal FAS Mammalian FAS

Figure 5 | Structures of the fungal fatty acid synthase (fFAS) and mammalian (mFAS) complexes

The fFAS consists of six α- (red) and six β- (blue) polypeptide chains arranged in a heterododecameric megacomplex. The six α-chains form a central wheel structure which is capped on either side by two trimeric β-chains which form dome structures. The mFAS consists of two α-polypeptide chains (green and red) which form a homodimeric complex. fFAS - PDB: 2UV8 ; mFAS PDB: 2VZ8

The fundamental steps of FAB are conserved across all organisms, and involve the iterative extension of a growing acyl chain by C_2 units followed by a series of reduction steps using acetyl-CoA as the starter unit and malonyl-CoA as the extension unit (Figure 6). The FAB pathway occurs via four distinct steps: activation, priming, elongation and termination, with slight variations between species. An acyl carrier protein (ACP) is used to covalently bind and transport the growing acyl substrate to the various catalytic domains of FAS, similar to PKS systems.[300–303] ACP is initially modified through the covalent attachment of a 4'-phosphopantetheine (4'-PP) prosthetic group from CoA to the hydroxyl group of a serine residue, changing it from its inactive form (apo-ACP) to its active form (holo-ACP).[304,305] In the fungal FASs, including *S. cerevisiae*, this is catalyzed by the action of an intrinsic 4'-phosphopantetheinyl transferase (PPT) domain, which likely occurs during assembly as the PPT domain sits on the outside of the fully assembled complex.[299,306,307] However, this domain is lacking in the mammalian and CMN FAS I and is instead performed by a separate holo-ACP synthase, similar to the process in FAS II systems.[289,305,308] Next, priming of FAB is achieved through the transacylation of the acetyl group from acetyl-CoA to ACP. This is catalyzed by an acetyltransferase (AT). Once primed, the acetyl group is transferred to a β-ketoacyl synthase (KS) domain via covalent attachment to the thiol group of a cysteine residue (C1305 in *S. cerevisiae*).[284] Next, transacylation of the malonyl group from malonyl-CoA to ACP is catalyzed by a malonyl transferase (MT) domain. In mammalian FAS, a single malonyl:acetyl transferase (MAT) domain is responsible for the transacylation of both the acetyl and malonyl groups. Interestingly, the MAT domain is able to accept a broad range of substrates, thereby opening the potential for engineering towards non-canonical fatty acid derivatives using the mammalian FAS.[309] In contrast, a single AT domain exists in the fungal FAS to facilitate loading of the acetyl group while a bifunctional malonyl:palmitoyl transferase (MPT) domain is responsible for loading the malonyl group and off-loading the fully elongated acyl chain in fungal FAS.[310] The malonyl-bound ACP is then shuttled back to the KS domain which contains the bound acetyl group and both units are condensed in a decarboxylative Claisen condensation reaction,[196] catalyzed by the KS domain. The β-keto group is then subjected to a series of sequential reduction steps. First, β-ketoacyl reductase (KR) reduces the β-keto group to a β-hydroxyl group using NADPH as a cofactor. Next, a β-hydroxyacyl dehydratase (DH) catalyzes the dehydration of the β-hydroxyacyl-ACP to form a 2,3-*trans*-enoyl-ACP. Finally, an enoyl reductase (ER) catalyzes the final reduction step using a second NADPH molecule to form a fully saturated acyl-ACP. The cycle then continues by condensing the acyl-ACP with further malonyl groups until the fully elongated acyl chains, typically palmitoyl-ACP (C_{16}) or stearoyl-ACP (C_{18}), are synthesized. At this point, FAB is terminated. The process of termination differs across species. In most bacteria, the acyl group is transferred directly from ACP to form lipids. In mammals, a TE domain catalyzes the release the acyl group as a free FA[301,311] and in fungi, the acyl-ACP is transferred to the MPT which catalyzes its attachment to CoA, causing its release into the cytoplasm as a fatty acyl-CoA.[312]

To enable the production of MCFAs via the FAB, it is necessary to promote the premature release of the growing acyl chain by engineering FAS. Approaches in modifying the type II FAS in *E. coli* include overexpressing specific enzymes within FAS II, overexpressing heterologous TEs

which have a higher specificity for shorter chain fatty-acyl-ACPs or engineering endogenous TEs to convey higher specificity or interfering with enzymes responsible for chain length control, particularly the KS domain. Tan *et al.*[285] showed that overexpressing 3-hydroxyacyl-ACP

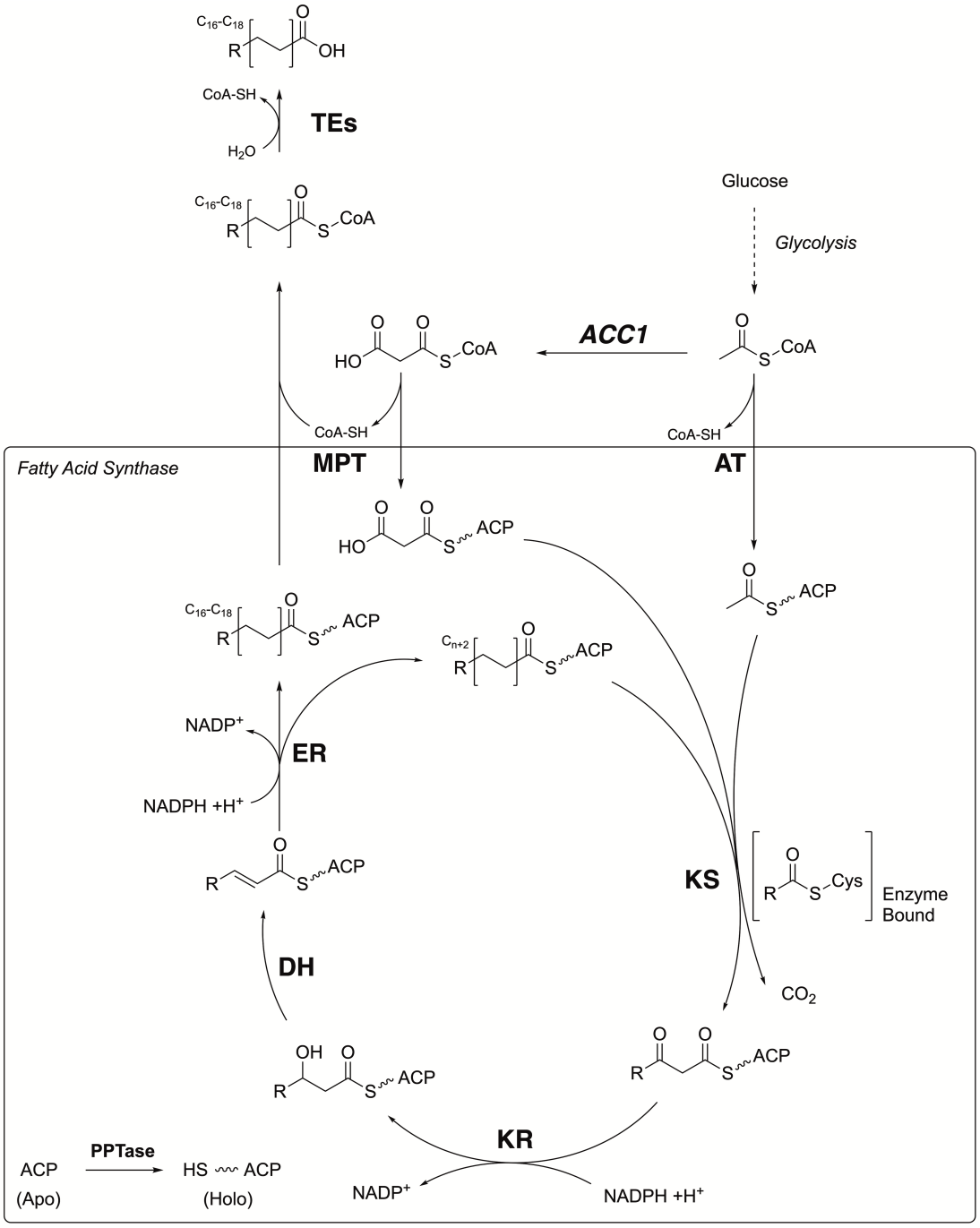

Figure 6 | Overview of the FAB pathway via fungal type I FAS

ACP is phosphopantotheinylated via the FAS resident PPTase domain. Acetyl-CoA is derived a simple carbon source (in this example, glucose) and is transferred to ACP via the AT domain. The acetyl group is then transferred to the KS domain and bound to a cystein residue. Malonyl-CoA is derived from acetyl-CoA via an ACC and the malonyl group is transferred to ACP via the MPT domain. ACP then shuttles the malonyl group to the KS domain where it is condensed with the acetyl group and CO_2 is released. The elongated acyl chain is then shuttled to the KR, DH and ER domains to fully reduce the β-keto group. The reduced acyl chain is then shuttled back to the KS and bound to the cystein residue and the cycle continue. When the acyl chain reached C_{16}-C_{18}, it is transferred to CoA via the MPT domain and released into the cytosol. Enzymes are written in bold and dotted lines represent multiple enzymatic steps. This figure was created using ChemDraw 22.2.0 (PerkinElmer).

dehydratase (*fabZ*) and a heterologous TE from *Anaerococcus tetradius* with specificity for octanoyl-ACP allowed the overproduction of octanoic acid. Torella *et al.*[286] demonstrated that forcibly terminating elongation through the targeted degradation of KS can enable the production of MCFAs. Moreover, the mislocalization and engineering of the endogenous TE ('TesA) from the periplasm to the cytoplasm allowed the premature release of MCFAs in *E. coli*.[313,314]

Harnessing *S. cerevisiae* FAS for the production of MCFAs and their derivatives has also been demonstrated.[270,284] To achieve this, it is essential to understand its biochemical and structural features. Indeed, *S. cerevisiae* FAS has been extremely well studied and a great amount of structural data is available which has enabled protein engineering. The crystal structure of the *S. cerevisiae* FAS was first solved in 2007 by two studies in parallel. Leibundgut *et al*.[302] solved the structure to a resolution of 3.1 Å while Lomakin *et al.*[296] solved the structure to a resolution of 4 Å. Since then, many other structural studies have been performed which have elucidated the intricate mechanisms involved in FAB at higher resolutions using x-ray crystallography or cryo-electron microscopy.[303,315–317] The *S. cerevisiae* FAS forms a symmetrical barrel-shaped structure comprising six α-subunits and six β-subunits ($\alpha_6\beta_6$), encoded by the *FAS2* (5664 bp) and *FAS1* (6156 bp) genes, respectively. *FAS2* is located on chromosome XVI and produces an 1887 amino acid 207 kDa polypeptide (α-chain) while *FAS1* is located on chromosome XI and produces a 2051 amino acid 229 kDa polypeptide (β-chain).[318,319] Single or double *fas* knock-out (KO) mutants are unviable in standard growth medium and require external supplementation of LCFAs, for example oleic acid.[284] The α-subunit (Fas2p) contains the KS, KR, PPT, ACP domains while the β-subunit (Fas1p) contains the AT, ER and DH domains. Interestingly, the MPT domain is split between the C-terminus of the β-subunit and the N-terminus of the α-subunit, likely as a result of an evolutionary gene-splitting event in which the two genes were once joined as single gene.[298] Both polypeptides also contain extensive structural domains that form scaffolds within the final structure, making the architecture very rigid and not easily accessible.[296] The assembly of the complex occurs co-translationally and is intricately regulated.[299,320] Additionally, added layers of transcriptional control exist in which inositol/choline responsive elements (ICREs) located within the promoters of *FAS1* and *FAS2* regulate their induction in response to low inositol and choline levels.[321,322] Furthermore, the presence of Fas1p polypeptide induces *FAS2* expression to regulate stoichiometric ratios of both chains.[323] The six α-subunits (Fas2p) form a central structure resembling a spoked-wheel shape with D3 symmetry and this structure is capped on either side by two identical dome-like structures comprising β-subunit (Fas1p) trimers (Figure 5). As a result, six independent reaction chambers are embedded within the complex and each chamber contains the catalytic domains required for FA biosynthesis within the walls.[296] Each chamber also contains a single ACP domain which is tethered at both the N- and C-terminus to the central structure and the periphery of the interior dome via two flexible α-helical linkers, located at the opposite side to the prosthetic arm.[302] The allows efficient shuttling of the substrate to the various catalytic domains without interference of the substrate-enzyme complex formation. Detailed computational analyses have determined that the shuttling mechanism of ACP by the flexible linkers occurs stochastically but is steered to the catalytic centers by molecular crowding and electrostatic forces.[324] The intricate mechanism and

close proximity of the ACP-bound substrates to the enzymatic domains in *S. cerevisiae* FAS allows FAB to occur extremely efficiently. This is in contrast to FAS II systems, in which free ACP must first find the correct enzyme in the biosynthesis pathway by random diffusion.[293,315,325] Furthermore, the efficiency of *S. cerevisiae* FAS greatly exceeds that of FAS I systems from other organisms as determined through the comparison of kinetic values and their specific activities.[284,306,326,327] Thus, the extreme efficiency of *S. cerevisiae* FAS makes it a suitable target for engineering towards MCFA production. Through a minimally invasive, rational engineering approach, individual residues within the key catalytic domains involved in chain length control were mutated in *S. cerevisiae* FAS which allowed MCFAs production.[284] Moreover, the engineered FAS constructs were overexpressed in a *fas* KO strain to prevent precursor competition and was able complement the FA auxotrophy. The domains subject to engineering were the KS, AT and MPT. The KS domain is presumably the most important domain due to its direct involvement in chain length control as it catalyzes the extension step. On the other hand, the AT and MPT domains can influence on chain length control as they are responsible for the loading of the starter and extension units as well as for the release of the acyl product in the case of MPT. The rationale behind engineering of the KS domain is to spatially restrict the growing acyl chain, thereby preventing extension above a certain chain length. This was achieved by substituting amino acids described to be involved in “gate-keeping” of the hydrophobic KS binding pocket, as revealed by structural studies of a cerulenin-bound FAS complex.[317] Cerulenin is a FAS inhibitor which stalls FAB by forming a covalent bond C1305 within the KS domain which corresponds to the same position bound by the growing acyl chain during FAB.[328] Binding of cerulenin caused an opening of the hydrophobic KS binding pocket by the rotation of M1251 out of the pocket and mutation of the adjacent residue from glycine to a serine (G1250S) rendered FAS more resistant to cerulenin inhibition.[317] It was concluded that this is due to the restricted movement of M1251, thereby blocking access of the inhibitor to C1305. Similarly, during FAB, covalent attachment of the acyl chain at C1305 induces opening of the binding channel allowing the acyl chain to enter. Indeed, it was also shown that incorporation of G1250S and G1250C mutations resulted in an increase in the hexanoic acid derived product, ethyl caproate.[329] By additionally substituting methionine for tryptophan at position 1251 (M1251W) to enhance the steric blockade of the channel, hexanoic and decanoic acid production was improved.[284] Finally, phenylalanine at position 1279 was identified within the KS domain as a promising target as it sits opposite the G1250 and M1251 and extends into the binding channel. However, mutating this to tyrosine (F1279Y) to restrict the binding channel further in combination with the G1250S mutation rendered this construct unable to sufficiently complement the *fas* KO mutation and thus strains were unable to grow and produce MCFAs.[284]

Alternatively, the two transferase domains (AT and MPT) were engineered to tamper with on- and off-loading of the substrates and products. Fungal FAS is known to be able to accept acyl-CoA substrates with longer chain lengths to prime FAB.[252] The MPT domain transfers the malonyl and terminal acyl moieties via the same residue (S1808) and malonyl-CoA was shown to compete with decanoyl-CoA when used as the starter unit for FAB, strongly suggesting that the MPT domain is able to catalyze transacylation of decanoyl-CoA.[310,330] Furthermore, a FAS I from

Corynebacterium ammoniagenes, a member of the CMN group of bacteria, was mutated by inactivating AT domain and shown to be able to accept octanoyl-CoA as a substrate via the MPT domain.[331] These studies suggest that the MPT domain is likely able to facilitate the premature release of ACP-bound medium chain fatty acyls. Gajewski and coworkers[284] therefore also engineered the MPT domain to reduce the uptake efficiency of malonyl-CoA, thereby enhancing the probability of premature product release. By mutating an arginine at position 1834 to lysine (R1834K) within the β-chain, the affinity for the carboxyl group of malonyl-CoA was reduced, resulting in a substantial increase in MCFA production, primarily octanoic acid (C_8). Finally, the AT domain was engineered through an isoleucine to alanine substitution at position 306 (I306A) within the β-chain. This served to concomitantly promote loading of the acetyl group and increase substrate acceptability by broadening the binding channel. Particularly in combination with the MPT mutation (R1834K), the AT mutation (I306A) should promote MCFA biosynthesis by increasing the acetyl:malonyl ratios. Consequently, this promotes priming of a new round of FAB and decreases elongation of growing acyl-chains. Indeed, it has been shown that the ratio of acetyl-CoA to malonyl-CoA influences the FA product spectrum of FAS.[332] All in all, five individual mutations were identified and investigated to produce MCFAs in *S. cerevisiae*.[284] Interestingly, however, the FA output profiles were not definitively predictable and could only be determined experimentally. For example, the I306A mutation was ineffective in isolation but was either able to augment MCFA production when combined with the G1250S/M1251W double mutation in the KS domain or, surprisingly, reduce octanoic acid production when combined with the R1834K mutation within the MPT domain. Similarly, introducing F1279Y to a I306A single mutant improved MCFA production whereas introducing F1279Y to an I306A/R1834K double mutant decreased production. These data demonstrate the complexity behind the interplay of the various mutations. It is therefore necessary to characterize FAS mutants through experimental analysis during engineering strategies for MCFA production.

1.3.3 Acetyl-CoA Carboxylase (ACC) and malonyl-CoA biosynthesis

The formation of malonyl-CoA is the first committed and rate-limiting step in FAB. It is achieved through the carboxylation of acetyl-CoA, catalyzed by biotin (vitamin B7)-dependent acetyl-CoA carboxylases (ACCs) (Figure 7). Similar to FAS, the majority of eukaryotic ACCs form dimeric or oligomeric complexes from a single polypeptide which contains all the necessary catalytic domains.[333] In contrast, bacterial ACCs are typically made up of multiple separate subunits which each possess a single function.[334] The major functional domains of ACCs are biotin carboxylase (BC), the carboxyl transferase (CT) and the biotin carboxyl carrier protein (BCCP). BCCP contains a covalently bound biotin cofactor and is responsible for shuttling biotin between the BC and CT domains. The general reaction mechanism begins with the ATP-dependent carboxylation of biotin by BC using bicarbonate (HCO_3^-). The carboxylated biotin is subsequently transferred to the CT domain which catalyzes the transfer of the carboxyl group from biotin to acetyl-CoA, thereby forming

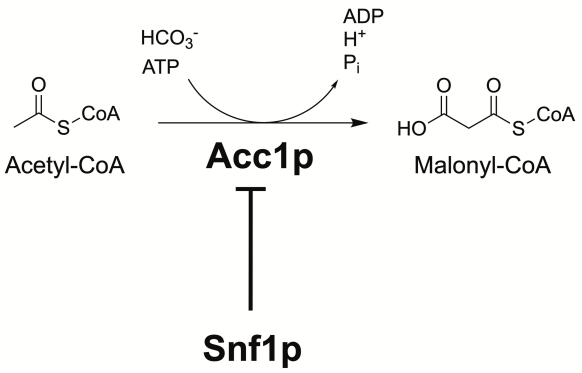

Figure 7 | Malonyl-CoA biosynthesis in *S. cerevisiae*

Malonyl-CoA is formed through the carboxylation of acetyl-CoA, catalyzed by acetyl-CoA carboxylase (Acc1p) using bicarbonate and ATP. Acc1p required biotin as a cofactor and is negatively regulated via Snf1p mediated phosphorylation. This figure was created using ChemDraw 22.2.0 (PerkinElmer).

malonyl-CoA.[335,336] In *S. cerevisiae*, two ACCs exist: Acc1p, which is cytosolic, and Hfa1p, which is localized to the mitochondria. Acc1p also associates with the cytoplasmic face of the endoplasmic reticulum which may allow direct channeling of malonyl-CoA to the endoplasmic reticulum resident elongase enzymes required for VLCFA synthesis.[337,338] Acc1p is encoded by the essential gene, *ACC1*, which is located on chromosome XIV and forms a 2233 aa 250 kDa gene product.[339,340] In its active state, it forms a 500 kDa homodimeric complex and, in addition to the enzymatic domains, Acc1p also contains a large, non-catalytic central domain (CD).[333,341] The mitochondrial homologue of *ACC1*, *HFA1*, is non-essential but is required for FAS II mediated FAB and the production of alpha-lipoic acid (ALA), a derivative of octanoic acid. *HFA1* can complement defective *acc1* mutations when its mitochondrial targeting signal is removed.[342] Dimerization of the BC domains is required for Acc1p to become catalytically active and conformation flexibility of the CD is essential to allow and regulate dimerization.[341] As such, inactivation of Acc1p occurs via disruption of this dimeric complex.[341] This is demonstrated through the mechanism of the antifungal polyketide, soraphen A, which binds at the dimer interface.[343,344] Physiologically, Acc1p is negatively regulated via phosphorylation by the protein kinase Snf1p, a homologue to the mammalian AMP-activated protein kinase (AMPK).[345–347] Snf1p is a regulatory kinase involved in a broad range of cellular processes and is itself positively regulated via phosphorylation.[345,348] It is activated via glucose derepression, thereby triggering the activation of metabolic pathways involved in utilizing alternative or non-fermentable carbon sources while also promoting respiration, peroxisome proliferation and β-oxidation.[348,349] Approximately 31 phosphorylation sites have been predicted within Acc1p based on the Snf1p recognition motifs ΦXR/KXXSXXXΦ (where Φ represents a hydrophobic residue, M, V, L, I or F).[350] While some phosphorylation sites were determined to be involved in inactivating Acc1p *in vitro*, others had no effect on activity.[347]

1.3.4 Increasing malonyl-CoA biosynthesis in *S. cerevisiae* via Acc1p

More recently, specific sites have been identified which are essential for regulation of *S. cerevisiae* Acc1p. S1157 was the first residue identified and is located within regulatory loops between two subdomains of the CD (CD_{C1} and CD_{C2}). Phosphorylation of S1157 results in limited flexibility, thereby preventing BC dimerization and inactivating the enzyme complex.[341,351,352] It is also the main residue involved in inactivating Acc1p and is largely found phosphorylated during the logarithmic growth phase.[352] Accordingly, mutating S1157 to alanine (S1157A) resulted in hyperactivity.[352] In light of biochemical engineering approaches for the biosynthesis of malonyl-CoA derived products in *S. cerevisiae*, increasing the cytosolic pool of malonyl-CoA is essential as its native levels are tightly regulated. Strategies aimed at increasing the malonyl-CoA supply by deregulating Acc1p have been successful in this regard. Overexpressing native *ACC1* has been shown to increase various malonyl-CoA derived products such as 6-methylsalicylic acid (6-MSA), 3-hydroxypropionic acid (3-HP) and FAEEs in *S. cerevisiae*.[288,353,354] However, this approach was unsuccessful in *S. cerevisiae* when engineering FAB,[355] despite being successful for increased FA production in *E. coli* and *Y. lipolytica*.[356,357] This may be due to the negative feedback regulation of Acc1p by long chain fatty acyl-CoAs such as palmitoyl-CoA in *S. cerevisiae*.[358,359] Thus, the benefits of overexpressing native *ACC1* for FA biosynthesis are limited, but this level of feedback regulation would not apply for heterologous malonyl-CoA utilizing pathways which do not accumulate long chain fatty acyl-CoAs. By mutating the phosphorylation site (S1157A), the specific activity of Acc1p was increased by a factor of 9 which resulted in a 3-fold increase in both native FAB and the production of 6-MSA.[360] Moreover, combining *ACC1* overexpression with the deregulation of Acc1p on the protein level is a viable approach. Further phosphorylation sites have also been identified and implemented in metabolic engineering strategies. Combining the S1157A mutation with a mutation of serine at position 659 (S659A) was found to improve the production of malonyl-CoA derived compounds.[353] Finally, mutating serine at position 686 in combination with the S1157A and S659A mutations was shown to further increase malonyl-CoA levels for 3-HP production.[361] In heterologous microbial cannabinoid biosynthetic pathways, increasing the malonyl-CoA pool through modification of *ACC1* expression or phosphorylation dependent regulation has recently emerged as a viable strategy, specifically for the biosynthesis of the malonyl-CoA derived polyketide cannabinoid precursor, OA. For example, the triple mutant $ACC1^{S659A/S686A/S1157A}$ has recently been used to improve CBGA production in *S. cerevisiae*.[362]

1.3.5 The reverse β-oxidation (rBOX) pathway

An alternative method for the biosynthesis of MCFAs using microbial chassis organisms is through a multispecies-derived rBOX pathway. As the name suggests, this pathway is characterized by the reversibility of the individual enzymatic steps involved in the degradative β-oxidation pathway and thus operates in the reverse direction, resulting in the biosynthesis of fatty acids. It comprises four core cytosolic enzymes derived from various bacterial species: an enzyme from the thiolase superfamily, preferably a biosynthetic β-ketoacyl-CoA thiolase (KAT), a β-

hydroxyacyl-CoA dehydrogenase, a β-hydroxyacyl-CoA dehydratase/enoyl-CoA hydratase and an enoyl-CoA reductase.[363] KAT can perform a non-decarboxylative Claisen condensation reaction via an acyl intermediate which is covalently attached to a catalytic cysteine residue.[196,364,365] The enzymes of the rBOX pathway elongate the acyl chain by C_2 units and sequentially reduce the β-keto group in a manner largely analogous to the FAB pathway. However, notable distinctions exist between the two pathways. Firstly, the rBOX pathway uses CoA-bound intermediates and does not involve the transfer of the moieties to ACP, as is the case during FAB. Furthermore, acetyl-CoA is used as the sole building block, acting as both the starter and the elongation unit. As such, the ATP-dependent formation of malonyl-CoA is not required and carbon is not lost in the form of CO_2, thus making the pathway energetically less expensive and resulting in higher theoretical yields compared to FAB.[366] However, the rBOX pathway relies on diffusion of the CoA-bound substrates through the cytosol, similar to bacterial FAS II systems, making it kinetically less efficient than FAB. Interestingly, a reversal of the β-oxidation pathway has been demonstrated by directly incorporating enzymes from the type II FAB pathway,[367] thereby validating the similarities and interchangeability of the two pathways.

The first step in the rBOX pathway involves the formation of the C_4 compound, acetoacetyl-CoA, using two acetyl-CoA molecules catalyzed by KAT. Acetoacetyl-CoA is subsequently reduced at the β-keto position to β-hydroxybutyryl-CoA by a β-hydroxyacyl dehydrogenase and then dehydrated to form crotonyl-CoA by a β-hydroxyacyl dehydratase, also called crotonase. Finally, the acyl chain is fully reduced by an enoyl-CoA reductase to form butyryl-CoA Figure 8. The implementation of this pathway was first described in *E. coli*.[363] This study demonstrated the potential for synthesizing a range of valuable oleochemicals derived from short, medium and long chain fatty acyl-CoA products of the rBOX pathway. These CoA-bound products can be directly used by terminating enzymes to form fatty aldehydes or *n*-alcohols or they can be hydrolyzed to free FAs via TEs. Moreover, the product spectrum can be further expanded by introducing diverse terminating enzymes which act on the different CoA-thioester intermediates with varying degrees of reduction at the β-carbon position. This enables the synthesis of a wide range of oleochemicals which possess differential β-functionalized acidic or alcohol acyl derivatives such as β-ketoacids, 1,3-diols or trans-Δ^2-FAs.[363,366,368]

As all the steps within the rBOX pathway are reversible, this causes in difficulties in driving the reactions in the direction of desired products. To drive the pathway towards completion, methods such as physical sequestration to remove the product are viable options. However, by replacing the flavin dependent enoyl-CoA reductases with an NAD(P)H dependent *trans*-enoyl-CoA reductase (Ter) from *Euglena gracilis* or *Treponema denticola*, the cycle was successfully driven towards to the production of fully saturated acyl chains.[368,369] This is because Ter does not require auxiliary proteins or a flavin cofactor but instead catalyzes the direct transfer of electrons from NAD(P)H to the product which increases the energy barrier required for reoxidation of the product.[369] Furthermore, the pathway can perform multiple cycles in *E. coli* to synthesize LCFAs (C > 10) and *n*-alcohols when incorporating KATs with a broader chain-length specificity.[363] One such KAT is β-ketothiolase B (*bktB*) derived from *Cupriavidus necator* (formerly named *Ralstonia*

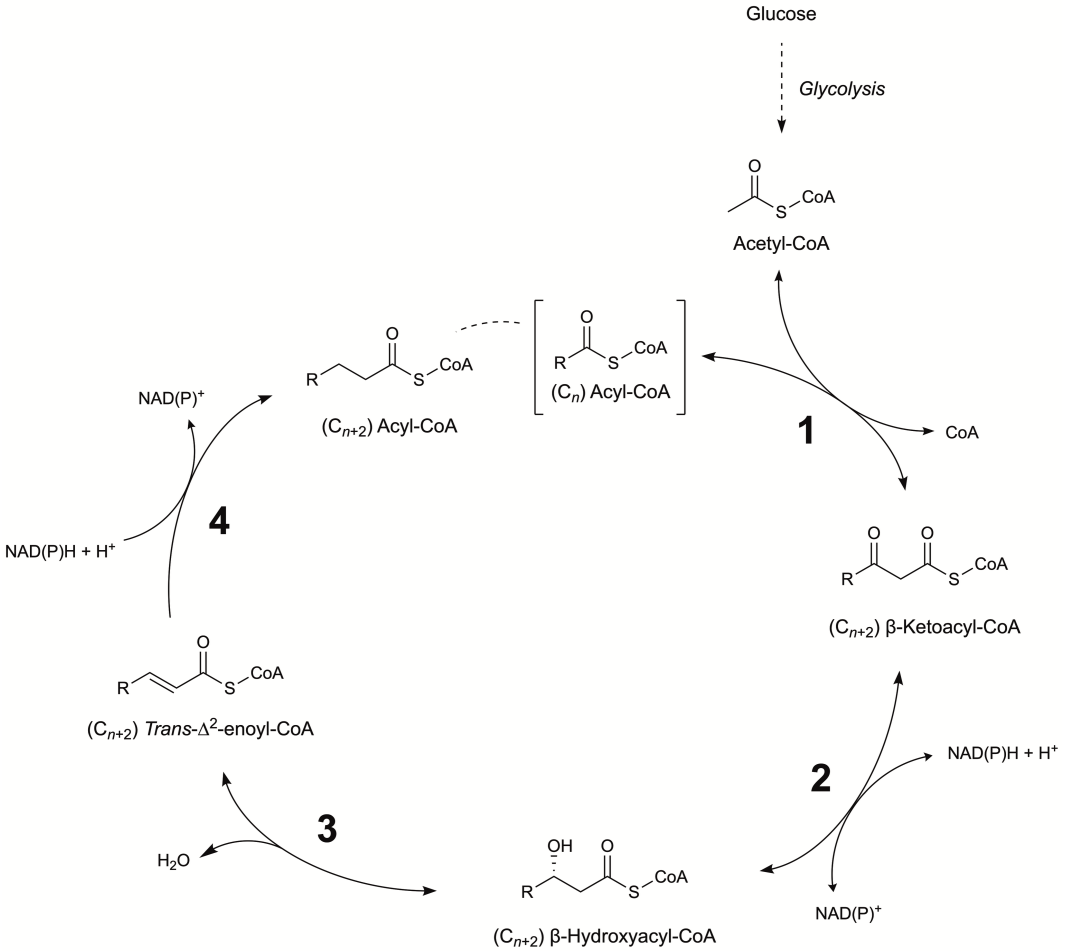

Figure 8 | Overview of the reverse β-oxidation pathway

1 represents a thiolase responsible for catalyzing the Claisen condensation of two acetyl-CoA molecules in the initial step and an acyl-CoA with acetyl-CoA in subsequent rounds of elongation. **2** represents a β-ketoacyl-CoA dehydrogenase causing the reduction of the β-keto group using NAD(P)H as a cofactor. **3** represents a β-hydroxyacyl-CoA dehydratase (or crotonase) which catalyzes the dehydration of the β-hydroxyl group. **4** represents a *trans*-enoyl-CoA reductase which catalyzes the reduction of the enoyl group using NAD(P)H to form the fully reduced, elongated acyl-CoA. This figure was created using ChemDraw 22.2.0 (PerkinElmer).

eutropha).[370,371] The broad substrate specificity of BktB was demonstrated in *E. coli* by its ability to accept a range of precursors.[281,372] These included butyryl-CoA, which enabled the biosynthesis of hexanoyl-CoA via the rBOX pathway, as well as odd-chain (propionyl), branched-chain (isobutyryl) and hydroxylated (glycolyl) acyl-CoA substrates, leading to the biosynthesis of high-value platform compounds such as 3-hydroxy-γ-butyrolactone (3HBL).[281,373] Further research demonstrates the ability to fine-tune and optimize the rBOX pathway to enable high-titer production of MCFAs and their derivatives in *E. coli*.[282,374] Together, these studies exemplify the flexibility and great potential of utilizing the rBOX pathway for the biosynthesis of diverse MCFA-derived products.

1.3.6 The rBOX pathway for MCFA production in *S. cerevisiae*

In *S. cerevisiae* a single cycle of the rBOX pathway was initially implemented to synthesize butyryl-CoA as a platform compound for C_4 bioproducts such as *n*-butanol.[283,375,376] *n*-Butanol is a biofuel produced naturally by many *Clostridium* species, commonly by *Clostridia acetobutylicum*, and is derived from butyryl-CoA via two reduction steps. Butyryl-CoA is synthesized via a pathway using enzymes analogous to the engineered rBOX pathway.[377] As such, reconstitution of the rBOX pathway in yeast utilized enzymes taken from *Clostridium* species, primarily the NADH dependent 3-hydroxybutyryl-CoA dehydrogenase (Hbd), which catalyzes the first reduction step of acetoacetyl-CoA to β-hydroxybutyryl-CoA, and crotonase (Crt), an enoyl-CoA hydratase which catalyzes the subsequent dehydration step to crotonyl-CoA.[283,375,376] However, the native *S. cerevisiae* thiolase Erg10p, which naturally catalyzes the condensation of two acetyl-CoA molecules during the first step of the MVA pathway,[378] was identified as the best candidate to catalyze the initial step in the rBOX pathway.[376] Furthermore, Ters from *E. gracilis* and *T. denticola* were also implemented to catalyze the fourth reaction forming butyryl-CoA and ^{Td}Ter was shown to possess the most activity for crotonyl-CoA.[283,375] Importantly, ^{Td}Ter is also able to convert longer *trans*-Δ^2-enoyl-CoA substrates, with chain lengths of C_6 to C_{12}, making it a suitable candidate for extending the rBOX pathway by multiple cycles.[281,379] To exemplify this, the production of MCFAs with chain lengths of up to C_{10} could also be detected using ^{Td}Ter in *S. cerevisiae*, although titers remained low.[283] Nevertheless, the pathway held promise to be extended in *S. cerevisiae* and allow the production of MCFAs at higher titers. Consequently, the endogenous *ERG10* and the *Clostridium hbd* genes were replaced by two genes from *C. necator* encoding the promiscuous KAT (*bktB*) and a β-hydroxyacyl-CoA dehydrogenase (*paaH1*) which both convey higher affinities for longer chain acyl-CoA intermediates. This enabled an additional iteration of the rBOX pathway for the production of hexanoyl-CoA in *S. cerevisiae*, although titers were low (6 µM corresponding to approximately 5.2 mg L^{-1}).[380]

To metabolically optimize this system and increase the production of rBOX derived molecules, precursor and cofactor supply must be enhanced. Extensive research has focused on engineering *S. cerevisiae* for enhanced cytosolic acetyl-CoA availability and this remains a critical objective in the optimization of acetyl-CoA dependent heterologous biosynthetic pathways.[381–387] Naturally, cytosolic acetyl-CoA is formed via the pyruvate dehydrogenase (PDH) bypass pathway. This pathway involves the decarboxylation of pyruvate, derived from glycolysis, by pyruvate decarboxylases (PDCs) followed by the oxidation of acetaldehyde to acetate by aldehyde dehydrogenases (ALDs) and the subsequent activation of acetate to acetyl-CoA by acetyl-CoA synthetases (ACSs).[388,389] However, due to the Crabtree effect, *S. cerevisiae* preferentially reduces acetaldehyde to ethanol via alcohol dehydrogenases (ADHs) anaerobically. Nevertheless, when glucose has been fully consumed, an extensive rewiring of the metabolic pathways occurs in which ethanol is used as a carbon source for continued growth via aerobic respiration and cytosolic acetyl-CoA is generated via the PDH bypass pathway. This event is termed the diauxic shift.[390]

To increase the supply of acetyl-CoA and NADH for the rBOX pathway in the context of *n*-butanol production, multiple strategies were implemented which redirected the carbon flux towards cytosolic acetyl-CoA.[375,391] The genes encoding six main ADHs (*ADH1-6*) as well as a minor, bifunctional enzyme with alcohol and formaldehyde dehydrogenase activities (*SFA1*) were knocked out to minimize the conversion of acetaldehyde to ethanol. This had the dual effect of increasing the availability of NADH and rerouting the carbon flux towards the formation of cytosolic acetyl-CoA via the PDH bypass pathway for the rBOX pathway. Moreover, multiple ALDs exists which are part of this bypass. Ald2p and Ald3p are cytosolic enzymes which utilize NAD^+ and are induced by ethanol and repressed by glucose. They are therefore active during the diauxic shift. On the other hand, Ald6p is constitutively expressed and uses $NADP^+$ as a cofactor. As such, deletion of the *ADH* genes would likely result in increased Ald6p activity in the presence of glucose, rather than Ald2p and Ald3p, thereby forming NADPH instead of NADH. Furthermore, acetate activation to acetyl-CoA is catalyzed by the ATP-dependent acetyl-CoA synthetase (ACS), of which two isoforms exist in *S. cerevisiae*: the glucose repressed Acs1p and the constitutively expressed Acs2p. One method of metabolically optimizing cytosolic acetyl-CoA formation is by using a prokaryotic acetylating ALD (A-ALD) capable of directly converting acetaldehyde to acetyl-CoA in an ATP-independent manner.[383] Schadeweg and Boles[375] utilized an NAD^+-dependent A-ALD from *E. coli* which had been mutated to preferentially convert acetaldehyde to acetyl-CoA instead of ethanol (*adhE*$^{A267T/E568K}$).[392] To provide additional reducing power, glycerol production was also reduced by knocking out the NADH-dependent glycerol 3-phophate dehydrogenase (*GPD2*) gene. Furthermore, the CoA biosynthesis pathway was upregulated through the overexpression of an *E. coli* pantothenate kinase (*coaA*) which further increased *n*-butanol production upon pantothenate (vitamin B5) supplementation.[375]

Building upon this optimized system, the number of iterations of the rBOX was extended to enable the production of hexanoic acid and octanoic acid by introducing ^{Cn}*bktB* and ^{Cn}*paaH1*.[393] Furthermore, the use of alternative β-hydroxyacyl-CoA dehydratases allowed fine-tuning of the system to produce MCFAs of varying chain length. Here, it was shown that a crotonase from *C. necator* (*crt2*) and an enoyl-CoA hydratase (*ECH*) from *Y. lipolytica* both extended the pathway to produce octanoic acid and low levels of decanoic acid while crotonase from *C. acetobutylicum* (*crt*) resulted in the more specific biosynthesis of hexanoic acid.[393] Thus, the pathway is seemingly halted at the point of β-hydroxyoctanoyl-CoA (C_8) dehydration when implementing ^{Ca}*crt*. In the same study, a comparison of ^{Eg}*ter* and ^{Td}*ter* resulted in higher titers of MCFAs being achieved when using ^{Td}*ter* which is consistent with previous reports.[283] Ultimately, MCFA production titers via the rBOX pathway in *S. cerevisiae* were significantly improved, reaching close to 75 mg L^{-1} hexanoic acid and 60 mg L^{-1} octanoic acid.[393]

1.4 Aims of the thesis

Given the therapeutic benefits of cannabinoids and a rapidly growing global market, engineering recombinant microbial systems for cannabinoid production is an economically lucrative area of research. Furthermore, this topic also holds scientific promise as the ability to specifically synthesize cannabinoid species, particularly rare or unnatural species, can enable further research into the effects of cannabinoids on the human body. While cannabinoid biosynthesis has been demonstrated using different microbial hosts, a common feature in all systems is the dependency of hexanoate supplementation to the cultivation media and the overexpression of a hexanoyl-CoA ligase (*^{Cs}AAE1*) to generate sufficient amounts of hexanoyl-CoA. However, this approach is highly unfavorable in an industrial setting due to cost concerns as well as concerns of toxicity which will likely arise as hexanoate concentrations are increased to meet the requirements for significant cannabinoid production. For these reasons, the objective of this study was to engineer a microbial chassis system for the *de novo* biosynthesis of OA, thereby circumventing the requirement of hexanoate supplementation. *S. cerevisiae* was used as a production host due to the wide availability of genetic toolboxes which enable easy genetic manipulation. This is also facilitated by a well annotated genome. Furthermore, as a eukaryotic host, the entire cannabinoid biosynthesis pathway can be reconstituted in *S. cerevisiae*. Finally, its GRAS status and industrial compatibility allow for transferability from research to industrial settings. As the FAB and rBOX pathways both produce CoA-bound fatty acyl products, we aimed to implement these pathways for production of OA from endogenously produced hexanoyl-CoA.

We first aimed to synthesize hexanoyl-CoA via the FAB pathway by engineering and upregulating the expression of the endogenous FAS complex to shift the product spectrum towards medium chain fatty acyl-CoA production. This approach has not been investigated in microbial cannabinoid biosynthesis systems to date. By testing various combinations of known FAS mutations for MCFA production, we aimed to screen constructs for their ability to produce hexanoyl-CoA via the analysis of exogenous hexanoic acid after cultivation. In parallel, we aimed to implement the rBOX pathway using established enzyme combinations reported to specifically produce hexanoyl-CoA. Subsequently, we aimed to combine both the FAB and rBOX pathways in a single recombinant *S. cerevisiae* strain to increase hexanoyl-CoA biosynthesis, as this approach has also not been investigated hitherto. Furthermore, we envisaged that this combinatorial approach may be applicable for uses beyond the scope of cannabinoid production, as MCFAs and their CoA-esters are industrially valuable platform compounds in their own right.

Following the identification and implementation of the most efficient hexanoyl-CoA biosynthesis pathways, we aimed to address various predicted bottlenecks and further optimize production. We aimed to enhance the supply of cytosolic acetyl-CoA and the availability of cofactors by knocking out competing pathways and redirecting carbon flux away from ethanol production. In addition, we aimed to specifically prevent the degradation of MCFAs, including hexanoic acid, via

peroxisomal β-oxidation. Furthermore, we aimed to increase the supply acetyl-CoA by upregulating the endogenous CoA biosynthesis pathway.

Once the *de novo* production of hexanoyl-CoA had been established and increased to concentrations within the range of hexanoate concentrations supplemented to cultures in previous studies (0.5-3 mM), we aimed to overexpress codon-optimized variants of ^{Cs}*OLS* and ^{Cs}*OAC* to allow the biosynthesis of OA. Moreover, we predicted a bottleneck in the turnover of hexanoyl-CoA to OA as had been consistently reported in the literature and therefore planned to use multicopy expression vectors or to integrate multiple copies of each construct within the genome. Finally, we expected to identify further unpredicted bottlenecks or competing pathways which would be addressed by genetic and metabolic engineering. All in all, our goal was to establish a metabolically optimized *S. cerevisiae* strain capable of synthesizing OA from glucose. Consequently, this strain can be used in further engineering to implement the entire cannabinoid biosynthesis pathway for industrial cannabinoid production.

2 MATERIALS AND METHODS

2.1 Materials

2.1.1 Chemicals

Table 1 | List of chemicals used in this study

Chemicals	Manufacturer
2-Propanol	Roth
Acetic Acid 100% (Glacial) (Cat. Nr.: 3738.1)	Roth
Acetonitrile HPLC Grade (Cat. Nr.: HN44.2)	Roth
Adenine	Roth
Agar-Agar Kobe I	Roth
Agarose (Cat. Nr.: 840004)	Biozym
Ammonium Sulfate	Roth
Carbenicillin	Sigma Aldrich
Calcium-pantothenate (Cat. Nr.: 3812.2)	Roth
Chloramphenicol	Sigma Aldrich
Chloroform (Trichloromethane, $CHCl_3$) GC Grade (Cat. Nr.: 32211)	Sigma-Aldrich
D(+)-Glucose Monohydrate (Cat. Nr.: 6780.2)	Roth
Decanoic acid (Cat. Nr.: C1875)	Sigma-Aldrich
Dimethyl sulfoxide (DMSO)	Roth
Dipotassium hydrogen phosphate (K_2HPO_4)	Roth
Deoxyribonucleotide triphosphates (dNTPs) (Cat. Nr.: N0447S)	New England Biolabs
Ethanol (96%)	Roth
Ethanol (≥99.8%) (Cat. Nr.:9065.1)	Roth
Ethidium bromide	Roth
Ethyl Acetate GC Ultra Grade (Cat. Nr.: KK42.1)	Roth
Ethylenediaminetetraacetic acid (EDTA)	Roth
Formic acid (Cat. Nr.: 4724.1)	Roth
GeneRuler 1 kb Plus DNA Ladder (Cat. Nr.: SM1331)	Thermo Fisher Scientific
Geneticin sulphate (G-418 disulfate salt) (Cat. Nr.: A1720)	Sigma-Aldrich

Chemicals	Manufacturer
Glycerol (Cat. Nr.: 3783.2)	Roth
Heptanoic acid (Cat. Nr.: 75190)	Sigma-Aldrich
Hexane GC Ultra Grade (Cat. Nr.: KK48.1)	Roth
Hexanoic acid (Cat. Nr.: 153745)	Sigma-Aldrich
Hydrochloric acid (HCl) fuming 37%	Roth
Hygromycin B (Cat. Nr.: CP13.3)	Roth
Kanamycin (Cat. Nr.: T832.1)	Roth
L-arginine	Roth
L-histidine	Roth
L-isoleucine	Roth
L-leucine	Roth
L-lysine	Roth
L-methionine	Roth
L-phenylalanine	Roth
L-threonine	Roth
L-tryptophan	Roth
L-tyrosine	Roth
L-valine	Roth
Lithium Acetate (LiOAc)	Roth
Methanol GC Grade (Cat. Nr.: 1.06009)	Sigma-Aldrich
Nourseothricin (ClonNAT) (Cat. Nr.: 5.001.000)	WERNER BioAgents GmbH, Jena, DE
Octanoic acid (Cat. Nr.: 21639)	Fluka
Oleic acid (Cat. Nr.: 20447.293)	VWR
Olivetol	Laboratory Stock (AK Kayser)
Olivetolic acid (Cat. Nr.: A318844)	AmBeed, IL, USA
Polyethylene Glycol (PEG) 4000	Roth
Gibco™ Bacto™ Peptone	BD
Potassium Acetate	Roth
Potassium dihydrogen phosphate (KH_2PO_4)	Roth
Potassium hydroxide (KOH)	Roth
Single stranded carrier DNA (salmon sperm DNA)	Roth

Chemicals	Manufacturer
Sodium chloride (NaCl)	Roth
Sodium hydroxide (NaOH)	Roth
Sulfuric acid (H_2SO_4)	Roth
Tergitol™ solution type NP-40, 70% in H_2O (Cat. Nr.: NP40S)	Sigma-Aldrich
Toluene GC Ultra Grade (Cat. Nr.: KK46.1)	Roth
TRIS (Cat. Nr.: 4855.2)	Roth
Gibco™ Bacto™ Tryptone	BD
Uracil	Sigma-Aldrich
Gibco™ Bacto™ Yeast Extract (Cat. Nr.: 212750)	BD
Gibco™ Bacto™ Yeast Extract (Cat. Nr.: 212720; Lot. Nr. 6272556)	BD
BD Difco™ Yeast nitrogen base without amino acids and ammonium sulphate (Cat. Nr.:233520)	BD
Yeast nitrogen base without amino acids and ammonium sulphate, without calcium-pantothenate (Cat. Nr.: 1512-050)	Sunrise Science Products, TN, USA
Yeast nitrogen base without amino acids and ammonium sulphate, without folic acid and without riboflavin (Cat. Nr.: CYN6501)	FORMEDIUM Ltd., Norfolk, UK

2.1.2 Enzymes

Table 2 | List of enzymes used in this study

Enzymes	Manufacturer
Q5® High-Fidelity DNA Polymerase (Cat. Nr.: M0491)	New England Biolabs
Phusion™ High Fidelity DNA Polymerase (Cat. Nr.: M0530)	New England Biolabs
DreamTaq Green DNA Polymerase (5 U/µL) (Cat. Nr.: EP0711)	Thermo Fisher Scientific
T7 DNA Ligase	New England Biolabs
RNase A (Cat. Nr.: 7156.1)	New England Biolabs
Esp3I-HF	New England Biolabs
BsaI-HFv2	New England Biolabs
NotI-HF	New England Biolabs

2.1.3 Kits

Table 3 | List of kits used in this study

Kits	Manufacturer
GeneJET Plasmid-Miniprep Kit (Cat. Nr.: K0503)	Thermo Fisher Scientific
NucleoSpin Gel and PCR Clean-up Kit	Macherey-Nagel

2.1.4 Analytical devices and columns

Table 4 | List of analytical devices and columns used in this study

Device	Manufacturer
Dionex UltiMate 3000 UHPLC+ system	Thermo Fisher Scientific
Dionex UltiMate 3000 RS Variable Wavelength Detector	Thermo Fisher Scientific
Shodex RI-101 Refractive Index (RI) Detector	Shodex
Clarus® 400 Gas Chromatograph (GC)	PerkinElmer Inc.
Agilent Technologies 7890B GC System detected	Agilent Technologies, Inc.
Agilent Technologies 5977B Mass-Selective Detector (MSD)	Agilent Technologies, Inc.
HP-5MS UI Capillary Column (30 m x 0.25 mm I.D. × 0.25 µm) (Part. Nr.: 19091S-433UI)	Agilent Technologies, Inc.
Zeiss LSM 700 Laser Scanning Confocal Microscope	Carl Zeiss
NUCLEOGEL SUGAR 810 H, 8 – 10 µM, 300 x 7.8 mm column (Cat. Nr.: 719574)	Macherey-Nagel
Agilent Infinity Poroshell 120 EC-C18 column 2.1 x 100 mm, 2.7 µm (Cat. Nr.: 695575-902)	Agilent
Elite-5MS Capillary Column (30 m x 0.25 mm I.D. x 0.25 µm) (Part Nr.: N9316283)	PerkinElmer, Inc.
Vilber Gel Documentation System (E-BOX-VX2/20M)	Vilber Lourmat
Shakers Vibrax® VXR basic	IKA
VXR basic VX 2E reaction vial attachment	IKA
Eppendorf Concentrator 5301	Eppendorf
Bio-Rad Gene Pulser Electroporation System	Bio-Rad

2.2 General Microbiological Methods

2.2.1 Microbial strains

The *Saccharomyces cerevisiae* strain CEN.PK2-1C was used for genetic and biochemical engineering strategies for the biosynthesis of MCFAs and OA as well as for cloning of plasmids via homologous recombination (HR). Pre-existing engineered strains were obtained from the laboratory stock of Prof. Dr. Eckhard Boles at the Goethe University in Frankfurt am Main, Germany and further engineered within the scope of this work. Alternatively, the *S. cerevisiae* strain BY4741 was used for initial experiments testing the mutant FAB pathway. The *E. coli* strain DH10β was used for modular cloning and subcloning of plasmids. All yeast and bacterial strains are listed in Table 5.

Table 5 | List and description of yeast and bacterial strains used in this study

Stock code	Strain Name	Relevant Genotype	Source
		S. cerevisiae	
CEN.PK2-1C	-	*MATa; ura3-52; his3-Δ1; leu2-3,112; trp1-289; MAL2-8C; SUC2*	EUROSCARF[394]
BY4741	-	*MATa; his3Δ1; leu2Δ0; met15Δ0; ura3Δ0*	EUROSCARF[14]
SHY24	*FAS*^{WT}	**BY4741** *Δfaa2*	(395)
SHY34	*fas*^{null}	**BY4741** *Δfas1; Δfas2; Δfaa2*	(395)
GDY15	-	**CEN.PK2-1C** *adh1Δ::loxP; adh2Δ::LEU2; adh3Δ::loxP; adh4Δ::loxP; adh5Δ::loxP; Δgdp2*	(393)
GDY27	-	**GDY15** *ura3Δ::*P_{HHF1}-^{Cn}*bktB-tENO1,* P_{CCW12}-^{Cn}*paaH1-tIDP1,* P_{ENO2}-^{Ca}*crt-tPGK1,* P_{TDH3}-^{Td}*ter-tADH1, kanMX4*	(393)
KSY12	-	**GDY15** *Δfaa2*	This study
KSY13	*yr*BOX1	**GDY27** *Δfaa2*	This study
KSY22	*yr*BOX2	**KSY13** *leu2Δ::*P_{PGK1}-^{Ec}*coaA-tSSA1, natNT2*	This study
KSY23	-	**KSY13** *adh6Δ::*P_{PGK1}-^{Ec}*coaA-tSSA1*	This study
KSY26	*yr*BOX3	**KSY22** P_{FMS1}*Δ::*P_{ADH1}	This study

Stock code	Strain Name	Relevant Genotype	Source
KSY28	-	**KSY13** *adh6Δ::P_{PGK1}-^{Ec}coaA^{R106A}-tSSA1*	This study
KSY29	-	**KSY13** *kanMX4Δ::P_{TEF2}-^{Cs}OLS-tADH1, P_{TEF1}-^{Cs}-OAC-tHXK2*	This study
KSY31	-	***yr*BOX3** *ACC1^{S659A}*	This study
KSY33	-	***yr*BOX3** *ACC1^{S1157A}*	This study
KSY34	-	***yr*BOX3** *ACC1$^{S659A/S1157A}$*	This study
KSY35	*y*OA1	**KSY29** *Ty4::P_{CCW12}-^{Cs}OLS-tENO1, P_{TDH3}-^{Cs}OAC-tTDH1, ^{KI}URA3d, P_{TEF1}-^{Cs}OAC-tSSA1*	This study
KSY39	-	**CEN.PK2-1C** *ura3Δ:: P_{TDH3}-mRuby2-SKL-tENO1, kanMX4*	This study
KSY42	*eGFP-^{Sc}FAA2^{WT}*	**KSY39** *leu2Δ:: P_{HXT7}-$^{1--392}$-eGFP-FAA2^{WT}-tCYC1, natNT2*	This study
KSY44	*eGFP-^{Sc}FAA2-ΔPTS1*	**KSY39** *leu2Δ:: P_{HXT7}-$^{1--392}$-eGFP-FAA2-ΔPTS1-tCYC1, natNT2*	This study
KSY45	-	***y*OA1** *ACC1$^{S659A/S1157A}$*	This study
KSY46	-	***y*OA1** *ACC1^{S659A}*	This study
KSY48	*y*OA2	***y*OA1** *leu2Δ::P_{PGK1}-^{Ec}coaA-tSSA1, natNT2*	This study
KSY49	*eGFP-^{Pc}PCL^{WT}*	**KSY39** *leu2Δ::P_{HXT7}-$^{1--392}$-eGFP-^{Pc}PCL^{T369A}-tCYC1, natNT2*	This study
KSY50	*eGFP-^{Pc}PCL-K^{T}*	**KSY39** *leu2Δ::P_{HXT7}-$^{1--392}$-eGFP-^{Pc}PCL^{T369A}-K-tCYC1, natNT2*	This study
KSY52	*y*OA1_ACC1*	***y*OA1** *ACC1$^{S659A/S686A/S1157A}$*	This study
KSY59	*y*OA3	***y*OA1_*ACC1**** *NSII-3::P_{PGK1}-^{Ec}coaA^{R106A}-tSSA1*	This study
KSY60	*y*OA4	***y*OA1_ACC1*** *416d::P_{TEF1}-^{Pc}PCL^{T369A}-K-tCYC1*	This study
KSY61	*y*OA5	***y*OA4** *NSII-3::P_{PGK1}-^{Ec}coaA^{R106A}-tSSA1*	This study
		E. coli	
DH10β	DH10β	*F– mcrA Δ(mrr-hsdRMS-mcrBC) φ80lacZΔM15 ΔlacX74 recA1 endA1*	New England Biolabs

Stock code	Strain Name	Relevant Genotype	Source
		araD139 Δ (ara-leu)7697 galU galK λ– rpsL(StrR) nupG	

2.2.2 Strain storage and cultivation

All *E. coli* and *S. cerevisiae* strains were stored in 25% (v/v) glycerol at -80 °C. *E. coli* strains were directly inoculated into 5 mL selective liquid LB media from the glycerol stock and incubated at 37 °C under constant shaking at 180 rpm. *S. cerevisiae* strains were initially streaked on appropriate solid media and incubated at 30 °C. Suspension cultures were then inoculated from colonies grown on the solid media. For the biosynthesis of MCFAs or OA as well as for strain propagation as pre-cultures or competent cells, *S. cerevisiae* strains were cultivated as suspension cultures in shake flasks at 30 °C under constant shaking at 180 rpm. Typically, a 100 mL flask was used for culture volumes between 20 and 30 mL while 300 mL flasks were used for culture volumes between 50 and 70 mL. Alternatively, suspension cultures up to a volume of 5 mL were cultivated in glass culture tubes at 30 °C and under constant shaking for applications including screening of individual colonies during strain engineering.

2.2.3 Cultivation Media

Microorganisms were either cultivated in liquid or on solid media. Solid media was formed by adding 19 g L^{-1} agar-agar to the media before autoclaving. *E. coli* was cultivated in lysogeny broth (LB) media and selection was achieved through supplementation with appropriate antibiotics. *S. cerevisiae* was cultivated in either complex media consisting of yeast extract and peptone (YP), synthetic complete (SC) media or synthetic minimal (SM) media and 20 g L^{-1} glucose (D) was added to the media as the primary carbon source. For MCFA and OA biosynthesis, a specific yeast extract was used as this was shown to result in higher MCFA production (BD, lot Nr.: 6272556). Buffered media describes the addition of 0.1 M potassium phosphate buffer (KP_i) at pH 6.5 and was primarily used in fermentations for MCFA and OA production. Selective media describes the addition of appropriate antibiotics to the media or the leaving out of components required for complementation of auxotrophy markers. All media was sterilized by autoclaving before the addition of glucose, KP_i or antibiotics. 10X stock concentrations of glucose (200 g L^{-1}) and KP_i (1 M) were prepared and sterilized separately while 1000x stock concentrations of antibiotics were prepared and sterilized via filtration using 0.22 µm CME syringe filters for aqueous solutions or 0.2 µm nylon syringe filters for organic solutions. Selection in complex media was achieved through the addition of appropriate antibiotics. To complement *fas* KO mutations, YPD media was supplemented with 0.016% (v/v) oleic acid (VWR), which was sterile filtered and added after autoclaving. To facilitate dissolving of oleic acid, the detergent 1%(v/v) Tergitol™ NP-40 (70% in H_2O) was added to the media before autoclaving. SCD and SMD media contained uracil, histidine, tryptophan and leucine to

complement strain auxotrophies and selection was achieved by omitting the appropriate component (for example: uracil$^-$). In some applications, antibiotics were used for selection in synthetic media. Pantothenate-free synthetic media was made by using a modified yeast nitrogen base (YNB) devoid of calcium pantothenate (Sunrise Science Products, Knoxville, TN, USA) and low-fluorescence synthetic media was made by using a modified YNB without amino acids, folic acid and riboflavin (ForMedium™, Norfolk, UK).

Table 6 | List and composition of microbial cultivation media used in this study

Media or Additives	**Component**	**Concentration**
	E. coli	
Lysogeny broth (LB)	Tryptone	10 g L^{-1}
	Yeast extract	5 g L^{-1}
	NaCl	5 g L^{-1}
	NaOH	Adjusted to pH 7.5
Antibiotics	Carbenicillin	100 µg L^{-1}
	Kanamycin	50 µg L^{-1}
	Chloramphenicol	100 µg L^{-1}
	S. cerevisiae	
Yeast extract peptone (YP)	Peptone	20 g L^{-1}
	Yeast extract	10 g L^{-1}
Synthetic complete (SC)	YNB without amino acids and ammonium sulfate	1.7 g L^{-1}
	Ammonium sulfate	5 g L^{-1}
	AA and nucleobase mix	1x
	Uracil	0.171 mM
	Histidine	0.124 mM
	Tryptophan	0.093 mM
	Leucine	0.439 mM
	KOH	Adjusted to pH 6.3
Synthetic minimal (SM)	YNB without amino acids and ammonium sulfate	1.7 g L^{-1}
	Ammonium sulfate	5 g L^{-1}
	KH_2PO_4	20 mM
	Uracil	0.171 mM
	Histidine	0.124 mM

Media or Additives	Component	Concentration
	Tryptophan	0.093 mM
	Leucine	0.439 mM
	KOH	Adjusted to pH 6.3
1M Potassium phosphate buffer (KP_i)	K_2HPO_4	0.3372 M
	KH_2PO_4	0.6628 M
Antibiotics	Nourseothricin	100 µg L^{-1}
	Hygromycin B	200 µg L^{-1}
	Geneticin (G-418)	200 µg L^{-1}

2.3 General Molecular Biotechnological Methods

2.3.1 Microbial Transformation

2.3.1.1 Transformation of S. cerevisiae via heat shock

For transformation of *S. cerevisiae*, a method was used based on the high-efficiency lithium acetate (LiOAc)/single stranded (ss) DNA/polyethylene glycol (PEG) transformation method described by Gietz and Schiestl.[396] Competent cells were grown in 20-50 mL liquid cultures, depending on the number of transformations required, to the mid-exponential growth phase and the OD_{600} was measured. The cells were harvested via centrifugation (3000 x*g*, 2 min) and the supernatant was discarded. The cells were washed twice using sterile ddH_2O and the pellet was transferred to fresh 2 mL microcentrifuge tubes. The cells were then pelleted (3000 x*g*, 30s) and resuspended in 0.015 × OD_{600} × culture volume sterile ddH_2O. Next, 50 µL aliquots of the cell suspension were prepared and the cells were pelleted (3000 x*g*, 30s). The cells were then resuspended in 74 µL DNA mix which contained 500-1000 ng plasmid DNA or 1-10 µg linearized donor DNA for integration in sterile ddH_2O. Next, 286 µL high-efficiency transformation mix (240 µL 50% (w/v) PEG 4000, 36 µL 1 M LiOAc, 10 µL 10 mg mL^{-1} salmon sperm ssDNA) was added to the cell and DNA suspension and mix thoroughly. A 50X master mix of the high-efficiency transformation mix was prepared by adding 1.8 mL sterile 1 M LiOAc to 12 mL sterile 50% (w/v) PEG 4000 and thoroughly mixing before placing the mix on ice. Next, 500 µL 10 mg mL^{-1} salmon sperm carrier DNA was incubated at 98 °C for 5 min to denature it to ssDNA and then added to the cold LiOAc/PEG 4000 mix. This transformation master mix was kept at 4 °C and was stable for multiple months. Prior to transformation, the transformation master mix was vortexed and 286 µL was added to each 74 µL transformation aliquot containing the cells and the DNA and was mixed well by pipetting. The cells were subsequently heat-shocked by incubating the transformation suspension at 42 °C for 45-60 min. The cells were subsequently pelleted (3000 x*g*, 30s) and the

supernatant was removed using a pipette. For selection using auxotrophic markers, cells were plated directly onto solid selective SCD media. For selection using antibiotics, cells were regenerated in 5-20 mL of YPD medium at 30 °C under constant shaking at 180 rpm. Regeneration times were typically 2 h for plasmid-based transformations and at least 4 h for genome editing transformations. Cells were harvested via centrifugation (3000 x*g*, 2 min) and plated on solid selective YPD media containing the appropriate antibiotic.

2.3.1.2 Transformation of E. coli via electroporation

E. coli cells were transformed via electroporation. For this, electrocompetent DH10β (NEB) cells were prepared by inoculating 5 mL pre-cultures in LB media which was grown overnight at 37 °C under constant shaking at 180 rpm. Next, 400 mL of prewarmed LB media was inoculated with the pre-culture and grown at 30 °C until the culture reached an OD_{600} of 0.6-0.7. The culture was then aliquoted in pre-chilled 50 mL tubes and incubated for 30 min on ice. Cells were then harvested via centrifugation (4000 x*g*, 15 min, 4 °C) and the pellets were washed in 25 mL ice-cold ddH_2O. Next, the cells were pelleted again (4000 x*g*, 15 min, 4 °C) and the pellets were pooled together in a single 50 mL tube. The pooled pellet was subsequently resuspended in 4 mL 10% (w/v) glycerol which had been sterile filtered and pre-chilled on ice. The cells were pelleted again (4000 x*g*, 15 min, 4 °C), resuspended in the same 4mL 10% (w/v) glycerol solution and finally aliquoted into 50 µL aliquots which were stored at -80 °C. For transformation, either 20 ng purified plasmid DNA (2.3.2.4) or 1-2 µL Golden Gate assembly reaction mix (2.3.5.2) were added to the frozen electrocompetent aliquots and chilled on ice for 5-10 min. The cell and DNA mixture was transferred to electroporation cuvettes with a gap width of 4 mm and an electrical pulse of 1.8-2.5 kV was applied using a Bio-Rad Gene Pulser set at a resistance of 200 Ω and a capacitance of 25 µF. The cells suspension was transferred to microcentrifuge tubes and resuspended in 1 mL LB media to allow regeneration at 37 °C and constant shaking (500-600 rpm) for up to 1 h. After this, cells were harvested (6000 x*g*, 2 min) and plated on selective solid LB media containing the appropriate antibiotic.

2.3.2 Isolation of microbial DNA

Genomic and plasmid DNA was isolated from *S. cerevisiae* via ethanol precipitation. Genomic DNA was used for PCR-based applications while plasmid DNA was isolated from *S. cerevisiae* during cloning procedures. Two protocols were used for genomic DNA isolation depending on the desired application.

2.3.2.1 Extraction of genomic DNA from S. cerevisiae for quick analysis

This protocol allowed for quick isolation of genomic DNA but was limited in the purity achieved and was therefore generally used during strain engineering to screen large numbers of

colonies via PCR using the DreamTaq™ DNA Polymerase. It was based on an existing protocol which relied on chemical cell lysis.[397] A small amount of cell material was taken from a colony grown on solid media, resuspended in 100 µL lysis buffer (1% SDS, 200 mM LiOAc) and incubated at 70 °C for 15 min. Next, 300 µL 96% ethanol were added and the suspension was centrifuged (3 min, 15,000 x*g*) to pellet the DNA. The pellet was washed twice with ice cold 70% (v/v) ethanol and the ethanol was completely removed after the final washing step. Finally, the DNA was dried at 70 °C and the pellet was resuspended in 50 µL sterile ddH_2O.

2.3.2.2 Extraction of genomic DNA from S. cerevisiae with high purity

This protocol allowed for the isolation of genomic DNA with higher purity and implemented both chemical and mechanical cell lysis while utilizing three separate buffers (Table 7). It was used to purify DNA from verified strains which was subsequently used for PCR-based applications during molecular cloning, sequencing or strain engineering. Alternatively, it was used for screening colonies following certain genetic engineering events due to improved accessibility of genomic regions if PCR amplification was unsuccessful when using the quick protocol. Cell material was either taken from colonies on solid media and resuspended in sterile ddH_2O or approximately 5 OD_{600} units were harvested from overnight cultures. Cells were pelleted via centrifugation (2 min, 3000 x*g*) and resuspended in 400 µL cold Buffer I and chemically lysed through the addition of 400 µL Buffer II. Cells were then subject to mechanical lysis via glass bead beating and vigorous shaking at 2200 rpm using the Shakers Vibrax® VXR basic (IKA). The suspension was then centrifuged (30 min, 18,000 x*g*, 4 °C) and 650 µL of the supernatant were transferred to fresh 1.5 mL microcentrifuge tubes. Next, 325 µL ice cold Buffer III was added to the solution which was then vortexed and incubated on ice for 10 min to allow the DNA to precipitate. The DNA was pelleted via centrifugation (5 min, 18,000 x*g*, 4 °C) and washed twice using ice cold 70% (v/v) ethanol. The ethanol was then completely removed with a pipette, and the DNA was dried at 70 °C. Finally, the pellet was resuspended in 30 µL sterile ddH_2O.

Table 7 | Components of the buffers used for *t*he isolation of genomic DNA from *S. cerevisiae*

Name	**Component**	**Final Concentration**
Buffer I	EDTA /Titriplex III	10 mM
	Tris-HCl (pH 8)	25 mM
	RNase A	0.1 g/L
Buffer II	NaOH	0.2 M
	SDS	1% (w/v)
Buffer III	K-Acetate (pH 5.5 using glacial acetic acid)	3 M

2.3.2.3 Isolation of plasmid DNA from S. cerevisiae

Plasmid DNA was isolated from *S. cerevisiae* during cloning procedures based on HR. Here, DNA was isolated following the same protocol as described in chapter 2.3.2.2 until the addition of Buffer III and the subsequent centrifugation step. After this, the plasmid DNA was purified using the GeneJET Plasmid Miniprep kit. For this, 700 µL of the supernatant were loaded onto the spin column and purified according to the manufacturer's instructions. The plasmid DNA was eluted in 50 µL elution buffer.

2.3.2.4 Isolation of plasmid DNA from E. coli

During molecular cloning procedures, plasmid DNA was extracted and purified from *E. coli* to analysis and verification. Alternatively, known plasmids which were stored in *E. coli* were purified for transformation in *S. cerevisiae*. Briefly, cells were pelleted from 5 mL overnight suspension cultures via centrifugation (2 min, 3000 x*g*). Plasmid DNA was then purified using the GeneJET Miniprep kit following the manufacturer's instructions and eluted in 50 µL elution buffer.

2.3.3 Polymerase chain reaction

2.3.3.1 Amplifying genetic elements for cloning or genetic engineering

Polymerase chain reaction (PCR) was used to amplify genetic elements from genomic or plasmid DNA. Depending on the application, various polymerases were used, and the conditions as well as the PCR cycle program were adjusted accordingly. Either Q5® High-Fidelity DNA Polymerase or Phusion® High-Fidelity DNA Polymerase were used. Annealing temperatures were deduced using the online NEB Tm calculator tool (NEB) and the extension time was adjusted according to the DNA synthesis rate of the DNA polymerase, the length of the amplicon and the complexity of the template DNA. The dNTP solution mix (NEB) was used for all PCRs and either nuclease free water which was supplied with the kits or sterile ddH_2O was used. Table 8 provides an overview of the PCR temperature cycle program used.

Table 8 | Temperature program for polymerase chain reactions

Steps	Temperature (°C)	Time	Cycles
Initial Denaturation	98	1-3 min	1
Denaturation	98	20-30 s	
Annealing	45-72	30 s	25-35
Extension	72	15-60 s	
Final Extension	72	5 min	1

Steps	Temperature (°C)	Time	Cycles
Hold	10	∞	1

Q5® High-Fidelity DNA Polymerase was used for cloning procedures and amplification of genetic elements for genomic integration or sequencing analysis due to the proofreading ability and low error rate of the enzyme. The reactions were performed according to the manufacturer's protocol using 50 µL reaction volumes. Either 1-2 µL of purified genomic DNA or approximately 15-30 ng of purified plasmid DNA was used as template DNA. An overview of the reaction mix is displayed in Table 8.

Table 9 | Composition of reaction mix for Q5® High-Fidelity DNA polymerase

Component	Final Concentration	Volume (µL)
Q5® Reaction Buffer (5X)	1X	10
dNTPs (2 mM)	0.2 mM	5
Forward Primer (10 µM)	0.5 µM	2.5
Reverse Primer (10 µM)	0.5 µM	2.5
Q5® High-Fidelity DNA Polymerase (2 U/µL)	0.02 U/µL	0.5
Template DNA	15-30 ng (plasmid)	Variable
Nuclease-free water	-	Up to 50

Phusion® High-Fidelity DNA Polymerase was used for cloning procedures and amplification of genetic elements for genomic integration or sequencing analysis due to the proofreading ability and low error rate of the enzyme. The reactions were performed according to the manufacturer's protocol using 50 µL reaction volumes. Either 1-2 µL of purified genomic DNA or approximately 15-30 ng of purified plasmid DNA was used as template DNA. An overview of the reaction mix is displayed in Table 10.

Table 10 | Composition of reaction mix for Phusion® DNA polymerase

Component	Final Concentration	Volume (µL)
Phusion® HF Buffer (5X)	1X	10
dNTPs (2 mM)	0.2 mM	5
Forward Primer (10 µM)	0.5 µM	2.5
Reverse Primer (10 µM)	0.5 µM	2.5
Phusion® High-Fidelity DNA polymerase (2 U/µL)	0.02 U/µL	0.5
Template DNA	15-30 ng (plasmid)	Variable
Nuclease-free water	-	Up to 50

2.3.3.2 Colony PCR

To screen colonies for genetic mutations during strain engineering in which a difference in DNA fragment size was expected, colony PCRs were performed using the non-proofreading Thermo Scientific™ DreamTaq™ DNA polymerase. For this, genomic DNA was isolated via the quick extraction method (2.3.2.1). In cases where colony PCRs were unsuccessful, possibly due to insufficient opening of the genomic DNA to allow access to the region of interest, the DNA extraction method for high purity (2.3.2.2) was implemented. An overview of the reaction mix is displayed in Table 11.

Table 11 | Composition of reaction mix for Phusion® DNA polymerase

Component	**Final Concentration**	**Volume (µL)**
DreamTaq™ Green Buffer (10X)	1X	2
dNTPs (2 mM)	0.3 mM	3
Forward Primer (10 µM)	0.5 µM	1
Reverse Primer (10 µM)	0.5 µM	1
DreamTaq™ DNA polymerase (5 U/µL)	0.025 U/µL	0.1
Genomic DNA	-	1-2
Nuclease-free water	-	Up to 20

2.3.4 Agarose gel electrophoresis

PCR amplified DNA or restriction digested plasmid DNA was analyzed via gel electrophoresis using 1% (w/v) agarose dissolved in TAE buffer (40 mM Tris base, 20 mM acetic acid and 1 mM EDTA). A voltage of between 80-120 kV was applied to the gel for 45-60 min and the gel was subsequently stained with ethidium bromide in a TAE buffer bath for 20 min. The stained DNA bands were visualized under exposure to UV light using a Vilber Gel Documentation System (Vilber Lourmat).

2.3.5 Cloning of plasmid DNA

A variety of cloning techniques were implemented to clone plasmid DNA. Plasmids generally contained a bacterial and a yeast selection marker and origin of replication to allow propagation in both *E. coli* and *S. cerevisiae*. Integration plasmids did not contain yeast origin of replications and integration plasmids which were used in combination with CRISPR/Cas9 additionally did not contain a yeast selection marker. A list of all plasmids used in this study can be found in Table 12.

Table 12 | List of all plasmids used in this study

Stock Code	Plasmid Name	Relevant Description	Source
		Expression Plasmids	
ALSV7	*fusFAS^{RK}*	*CEN4/ARS6, Amp^{R}, hphNT1, P$_{TDH3}$-FAS1^{RK}-FAS2-tFAS2*	Lab stock Prof. Dr. Boles (Alina Schrodt)
ALSV9	*fusFAS^{RKFY}*	*CEN4/ARS6, Amp^{R}, hphNT1, P$_{TDH3}$-FAS1^{RK}-FAS2^{FY}-tFAS2*	Lab stock Prof. Dr. Boles (Alina Schrodt)
ALSV11	*fusFAS^{IAGSMWFY}*	*CEN4/ARS6, Amp^{R}, hphNT1, P$_{TDH3}$-FAS1^{IA}-FAS2^{GSMWFY}-tFAS2*	Lab stock Prof. Dr. Boles (Alina Schrodt)
ALSV13	*fusFAS^{IARKGSMWFY}*	*CEN4/ARS6, Amp^{R}, hphNT1, P$_{TDH3}$-FAS1^{IARK}-FAS2^{GSMWFY}-tFAS2*	Lab stock Prof. Dr. Boles (Alina Schrodt)
KSV8	*fusFAS^{IAGS}*	*CEN4/ARS6, Amp^{R}, hphNT1, P$_{TDH3}$-FAS1^{IA}-FAS2^{GS}-tFAS2*	This study
KSV9	*fusFAS^{IARKGS}*	*CEN4/ARS6, Amp^{R}, hphNT1, P$_{TDH3}$-FAS1^{IARK}-FAS2^{GS}-tFAS2*	This study
KSV10	*fusFAS^{IAGSMW}*	*CEN4/ARS6, Amp^{R}, hphNT1, P$_{TDH3}$-FAS1^{IA}-FAS2^{GSMW}-tFAS2*	This study
KSV30	*fusFAS^{IAGSMWFY}*	*CEN4/ARS6, Amp^{R}, kanMX4, P$_{TDH3}$-FAS1^{IA}-FAS2^{GSMWFY}-tFAS2*	This study
KSV47	*^{Cs}OLS*	*2µ, Kan^{R}, hphNT1, P$_{TEF2}$-^{Cs}OLS-tADH1*	This study
KSV51	*^{Ec}coaA*	*2µ, Kan^{R}, HIS3, P$_{PGK1}$-^{Ec}coaA-tSSA1*	This Study
KSV52	*^{Ec}coaA*	*2µ, Kan^{R}, hphNT1, P$_{PGK1}$-^{Ec}coaA-tSSA1*	This study

Stock Code	Plasmid Name	Relevant Description	Source
KSV66	*P_{ADH1}-FMS1*	*2µ, Kan^R, URA3, P_{ADH1}-FMS1-tTDH1*	This study
KSV67	*P_{HSP26}-FMS1*	*2µ, Kan^R, URA3, P_{HSP26}-FMS1-tTDH1*	This study
KSV68	*P_{TEF1}-FMS1*	*2µ, Kan^R, URA3, P_{TEF1}-FMS1-tTDH1*	This study
KSV69	*^{Cs}OLS*	*2µ, Kan^R, URA3, P_{TEF2}-^{Cs}OLS-tADH1*	This study
KSV74	*^{Cs}OLS-^{Cs}OAC*	*2µ, Kan^R, URA3, P_{TEF2}-^{Cs}OLS-tADH1, P_{TEF1}-^{Cs}OAC-tHXK2*	This study
KSV99	*$^{Sc}FAA2^{WT}$*	*2µ, Kan^R, hphNT1, P_{TEF1}-$^{Sc}FAA2^{WT}$-tCYC1*	This study
KSV100	*^{Sc}FAA2-ΔPTS1*	*2µ, Kan^R, hphNT1, P_{TEF1}-^{Sc}FAA2-ΔPTS1-tCYC1*	This study
KSV101	*$^{Pc}PCL^{WT}$*	*2µ, Kan^R, hphNT1, P_{TEF1}-$^{Pc}PCL^{WT}$-tCYC1*	This study
KSV102	*^{Pc}PCL-K*	*2µ, Kan^R, hphNT1, P_{TEF1}-^{Pc}PCL-K-tCYC1*	This study
KSV103	*^{Cs}AAE1*	*2µ, Kan^R, hphNT1, P_{TEF1}-^{Cs}AAE1-tCYC1*	This study
KSV105	*^{Cs}AAE3-K*	*2µ, Kan^R, hphNT1, P_{TEF1}-^{Cs}AAE3-K-tCYC1*	This study
KSV107	*^{At}AAE11-K*	*2µ, Kan^R, hphNT1, P_{TEF1}-^{At}AAE11-K-tCYC1*	This study
KSV108	*^{At}AAE11-ΔPTS1*	*2µ, Kan^R, hphNT1, P_{TEF1}-^{At}AAE11-ΔPTS1-tCYC1*	This study
LCV6	*^{Cs}OLS + ^{Cs}AAE1*	*2µ, Kan^R, URA3, P_{TEF2}-^{Cs}OLS-tADH1, P_{TEF1}-^{Cs}AAE1-tCYC1*	This study (Lukas Chalwatzis Master Thesis)

Stock Code	Plasmid Name	Relevant Description	Source
LCV7	*^{Cs}OLS + ^{Cs}AAE3*	*2µ, Kan^{R}, URA3, P_{TEF2}-^{Cs}OLS-tADH1, P_{TEF1}-^{Cs}AAE3-tCYC1*	This study (Lukas Chalwatzis Master Thesis)
LCV8	*^{Cs}OLS + ^{Sc}FAA2*	*2µ, Kan^{R}, URA3, P_{TEF2}-^{Cs}OLS-tADH1, P_{TEF1}-^{Sc}FAA2-tCYC1*	This study (Lukas Chalwatzis Master Thesis)
LCV11	*^{Cs}OLS + ^{Pc}PCL*	*2µ, Kan^{R}, URA3, P_{TEF2}-^{Cs}OLS-tADH1, P_{TEF1}-^{Pc}PCL-tCYC1*	This study (Lukas Chalwatzis Master Thesis)
LCV12	*^{Cs}OLS + ^{At}AAE11*	*2µ, Kan^{R}, URA3, P_{TEF2}-^{Cs}OLS-tADH1, P_{TEF1}-^{At}AAE11-tCYC1*	This study (Lukas Chalwatzis Master Thesis)
LCV13	*^{Cs}OLS + ^{Tm}AAE15*	*2µ, Kan^{R}, URA3, P_{TEF2}-^{Cs}OLS-tADH1, P_{TEF1}-^{Tm}AAE15-tCYC1*	This study (Lukas Chalwatzis Master Thesis)
LCV28	*^{Cs}OLS + ^{Cs}AAE3-K*	*2µ, Kan^{R}, URA3, P_{TEF2}-^{Cs}OLS-tADH1, P_{TEF1}-^{Cs}AAE3-K-tCYC1*	This study (Lukas Chalwatzis Master Thesis)
LCV29	*^{Cs}OLS + ^{Sc}FAA2-ΔPTS1*	*2µ, Kan^{R}, URA3, P_{TEF2}-^{Cs}OLS-tADH1, P_{TEF1}-^{Sc}FAA2-ΔPTS1-tCYC1*	This study (Lukas Chalwatzis Master Thesis)
LCV30	*^{Cs}OLS + ^{Sc}FAA2-K*	*2µ, Kan^{R}, URA3, P_{TEF2}-^{Cs}OLS-tADH1, P_{TEF1}-^{Sc}FAA2-K-tCYC1*	This study (Lukas Chalwatzis Master Thesis)
LCV31	*^{Cs}OLS + ^{Pc}PCL-K*	*2µ, Kan^{R}, URA3, P_{TEF2}-^{Cs}OLS-tADH1, P_{TEF1}-^{Pc}PCL-K-tCYC1*	This study (Lukas Chalwatzis Master Thesis)
LCV32	*^{Cs}OLS + ^{At}AAE11-ΔPTS1*	*2µ, Kan^{R}, URA3, P_{TEF2}-^{Cs}OLS-tADH1, P_{TEF1}-^{At}AAE11-ΔPTS1-tCYC1*	This study (Lukas Chalwatzis Master Thesis)
LCV33	*^{Cs}OLS + ^{At}AAE11-K*	*2µ, Kan^{R}, URA3, P_{TEF2}-^{Cs}OLS-tADH1, P_{TEF1}-^{At}AAE11-K-tCYC1*	This study (Lukas Chalwatzis Master Thesis)

Stock Code	Plasmid Name	Relevant Description	Source
TFV3	$^{Ec}coaA^{R106A}$	*2µ, Kan^{R}, hphNT1, P_{PGK1}-$^{Ec}coaA^{R106A}$-tSSA1*	This study (Athanasia M. Feka Master Thesis)
		CRISPR/Cas9 Plasmids	
LBGV071	pRCC-N	*2µ, Amp^{R}, natNT2, P_{ROX3}-^{Sp}Cas9-tCYC1, pSNR52-sfGFP-sgRNA-tSUB4*	Lab stock Prof. Dr. Boles (Leonardo Beltran Guzman)
LBGV072	pRCC-H	*2µ, Amp^{R}, hphNT1, P_{ROX3}-^{Sp}Cas9-tCYC1, pSNR52-sfGFP-sgRNA-tSUB4*	Lab stock Prof. Dr. Boles (Leonardo Beltran Guzman)
SiHV138	pRCC-K	*2µ, Amp^{R}, kanMX4, P_{ROX3}-^{Sp}Cas9-tCYC1, pSNR52-sfGFP-sgRNA-tSUB4*	Lab stock Prof. Dr. Boles (Simon Harth)
KSV55	pRCC-N-*ADH6*	*2µ, Amp^{R}, natNT2, P_{ROX3}-^{Sp}Cas9-tCYC1, pSNR52-[ADH6]-sgRNA-tSUB4*	This study
KSV75	pRCC-H-P_{FMS1}	*2µ, Amp^{R}, hphNT1, P_{ROX3}-^{Sp}Cas9-tCYC1, pSNR52-[P_{FMS1}]-sgRNA-tSUB4*	This study
KSV78	pRCC-H-*ACC1-S659*	*2µ, Amp^{R}, hphNT1, P_{ROX3}-^{Sp}Cas9-tCYC1, pSNR52-[ACC1-S659]-sgRNA-tSUB4*	This study
KSV79	pRCC-H-*ACC1-S686*	*2µ, Amp^{R}, hphNT1, P_{ROX3}-^{Sp}Cas9-tCYC1, pSNR52-[ACC1-S686]-sgRNA-tSUB4*	This study
KSV80	pRCC-H-*ACC1-S1157*	*2µ, Amp^{R}, hphNT1, P_{ROX3}-^{Sp}Cas9-tCYC1, pSNR52-[ACC1-S1157]-sgRNA-tSUB4*	This study
KSV96	pRCC-N-*ACC1-S659*	*2µ, Amp^{R}, natNT2, P_{ROX3}-^{Sp}Cas9-tCYC1, pSNR52-[ACC1-S659]-sgRNA-tSUB4*	This study

Stock Code	Plasmid Name	Relevant Description	Source
KSV115	pRCC-K-*416d*	*2µ, Amp^R, kanMX4, P_{ROX3}-^{Sp}Cas9-tCYC1, pSNR52-[416d]-sgRNA-tSUB4*	This study
SARV84	pRCC-H-*NSII-3*	*2µ, Amp^R, hphNT1, P_{ROX3}-^{Sp}Cas9-tCYC1, pSNR52-[NSII-3]-sgRNA-tSUB4*	Lab stock Prof. Dr. Boles (Sandra Lehner)
SHV29	pRCC-N-*kanMX4*	*2µ, Amp^R, natNT2, P_{ROX3}-^{Sp}Cas9-tCYC1, pSNR52-[kanMX]-sgRNA-tSUB4*	(395)
SHV42	pRCC-N-*FAA2*	*2µ, Amp^R, natNT2, P_{ROX3}-^{Sp}Cas9-tCYC1, pSNR52-[FAA2]-sgRNA-tSUB4*	(270)
		Integration Plasmids	
KSV53	^{Ec}*coaA* integration	*Kan^R, LEU2 5' HR, P_{PGK1}-^{Ec}coaA-tSSA1, natNT2, LEU2 3' HR*	This study
KSV81	^{Ec}*coaA^{R106A}* integration	*2µ, Kan^R, LEU2 5' HR, P_{PGK1}-^{Ec}coaA^{R106A}-tSSA1, natNT2, LEU2 3' HR*	This study
KSV84	*mRuby2-SKL* integration	*Kan^R, URA3 5' HR, P_{TDH3}-mRuby2-SKL-tENO1, kanMX4, URA3 3' HR*	This study
KSV88	*eGFP-^{Sc}FAA2^{WT}* integration	*Kan^R, LEU2 5' HR, P_{HXT7}-$^{1-392}$-eGFP-^{Sc}FAA2^{WT}-tCYC1, natNT2, LEU2 3' HR*	This study
KSV90	*eGFP-^{Sc}FAA2-ΔPTS1* integration	*Kan^R, LEU2 5' HR, P_{HXT7}-$^{1-392}$-eGFP-^{Sc}FAA2-ΔPTS1-tCYC1, natNT2, LEU2 3' HR*	This study
KSV97	*eGFP-^{Pc}PCL^{WT}* integration	*Kan^R, LEU2 5' HR, P_{HXT7}-$^{1-392}$-eGFP-^{Pc}PCL^{WT}-tCYC1, natNT2, LEU2 3' HR*	This study
KSV98	*eGFP-^{Pc}PCL-K* integration	*Kan^R, LEU2 5' HR, P_{HXT7}-$^{1-392}$-eGFP-^{Pc}PCL-K-tCYC1, natNT2, LEU2 3' HR*	This study

Stock Code	Plasmid Name	Relevant Description	Source
pCS_Can10	pCfb2791-*OLS-OAC-OAC-URA3d*	*Amp^R, Ty4 5' HR, P_{CCW12}-^{Cs}OLS-tENO1, P_{TDH3}-^{Cs}OAC-tTDH1, ^{KlURA}3d, P_{TEF1}-^{Cs}OAC-tSSA1, Ty4 3' HR*	(251)
KSV114	*^{Ec}coaA^{R106A} integration*	*Kan^R, NSII-3 5' HR, P_{TEF1}-eGFP-^{Pc}PCL^{WT}-tCYC1, NSII-3 3' HR*	This study
		Templates	
FWV132	pRS313H-*fusFAS^{WT}*	*CEN4/ARS6, Amp^R, hphNT1, P_{TDH3}-FAS1-FAS2-tFAS2*	(395)
pVS5_4	*^{Ec}coaA* template	*2µ, natNT2, Amp^R, ^{Ec}coaA*	(375)
pRS41K	*kanMX4* template	*CEN4/ARS6, Amp^R, kanMX4*	(50)
pDionysos_^{Cs}AAE1	*^{Cs}AAE1* template	*2µ, URA3, dLEU2, Amp^R, P_{TEF1}-^{Cs}AAE1*	Lab Stock Prof. Dr. Kayser (Christina Schmidt)
pDionysos_^{Cs}AAE3	*^{Cs}AAE3* template	*2µ, URA3, dLEU2, Amp^R, P_{TEF1}-^{Cs}AAE3*	Lab Stock Prof. Dr. Kayser (Christina Schmidt)
pDionysos_^{Ec}fadD	*^{Ec}fadD* template	*2µ, URA3, dLEU2, Amp^R, P_{TEF1}-^{Ec}fadD*	Lab Stock Prof. Dr. Kayser (Christina Schmidt)
pDionysos_^{Pc}PCL^{T369A}	*^{Pc}PCL^{T369A} template*	*2µ, URA3, dLEU2, Amp^R, P_{TEF1}-^{Pc}PCL^{T369A}*	Lab Stock Prof. Dr. Kayser (Christina Schmidt)
		Empty Vectors/Backbones	
KSV48	EV (pRS313K)	*CEN4/ARS6, Amp^R, kanMX4*	This study
pRS313	pRS313	*CEN4/ARS6, Amp^R, HIS3*	AddGene

Stock Code	Plasmid Name	Relevant Description	Source
pRS41H	EV	*CEN4/ARS6, Amp^R, hphNT1*	(50)
SiHV005	EV / Backbone	*2µ, Kan^R, URA3, sfGFP*	Lab stock Prof. Dr. Boles (Simon Harth)
SiHV007	EV / Backbone	*2µ, Kan^R, HIS3, sfGFP*	Lab stock Prof. Dr. Boles (Simon Harth)
SiHV010	EV / Backbone	*2µ, Kan^R, hphNT1, sfGFP*	Lab stock Prof. Dr. Boles (Simon Harth)
		MoClo-pYTK and extended parts	
pGG3.70	OLS	Part 3, *Cml^R, ColE1*	Lab stock Prof. Dr. Boles
pGG3.71	OAC	Part 3, *Cml^R, ColE1*	Lab stock Prof. Dr. Boles
pGG3.198	FMS1	Part 3, *Cml^R, ColE1*	This study
pGG3.196	^{Ec}coaA	Part 3, *Cml^R, ColE1*	This study
pGG3.202	^{Ec}coaA^{R106A}	Part 3, *Cml^R, ColE1*	This study
pGG2.1	$P_{HXT7}$$^{-1--392}$	Part 2, *Cml^R, ColE1,* $P_{HXT7}$$^{-1--392}$	Lab stock Prof. Dr. Boles
pGG2.25	P_{ADH1}	Part 2, *Cml^R, ColE1,* P_{ADH1}	(36)
pGG2.8	P_{HSP26}	Part 2, *Cml^R, ColE1,* P_{HSP26}	(36)
pGG3a.eGFP	eGFP	Part 3a, *Cml^R, ColE1, eGFP*	This study
pGG3b.10	FAA2^{WT}	Part 3b, *Cml^R, ColE1,* ^{Sc}*FAA2^{WT}*	This study

Stock Code	Plasmid Name	Relevant Description	Source
pGG3b.12	FAA2-ΔPTS1	Part 3b, *Cml^R, ColE1, ^{Sc}FAA2-ΔPTS1*	This study
pGG3b.13	^{Pc}PCL^{WT}	Part 3b, *Cml^R, ColE1, ^{Pc}PCL^{T369A}*	This study
pGG3b.14	^{Pc}PCL-K	Part 3b, *Cml^R, ColE1, ^{Pc}PCL^{T369A}-K*	This study
pGG4.12	tCYC1	Part 4, *Cml^R, ColE1, tCYC1*	(36)
pGG4.10	tHXK2	Part 4, *Cml^R, ColE1, tHXK2*	(36)
pGG4a.1	PTS1	Part 4a, *Cml^R, ColE1, SKL*	This study
LCV14	^{Cs}AAE1	Part 3, *Cml^R, ColE1, ^{Cs}AAE1*	This study (Lukas Chalwatzis Master Thesis)
LCV15	^{Cs}AAE3	Part 3, *Cml^R, ColE1, ^{Cs}AAE3*	This study (Lukas Chalwatzis Master Thesis)
LCV16	^{Sc}FAA2	Part 3, *Cml^R, ColE1, ^{Sc}FAA2*	This study (Lukas Chalwatzis Master Thesis)
LCV17	^{Ec}fadD	Part 3, *Cml^R, ColE1, ^{Ec}fadD*	This study (Lukas Chalwatzis Master Thesis)
LCV18	^{Ec}fadK	Part 3, *Cml^R, ColE1, ^{Ec}fadK*	This study (Lukas Chalwatzis Master Thesis)
LCV19	^{Pc}PCL	Part 3, *Cml^R, ColE1, ^{Pc}PCL^{T369A}*	This study (Lukas Chalwatzis Master Thesis)
LCV20	^{At}AAE11	Part 3, *Cml^R, ColE1, ^{At}AAE11*	This study (Lukas Chalwatzis Master Thesis)
LCV21	^{Tm}AAE15	Part 3, *Cml^R, ColE1, ^{Tm}AAE15*	This study (Lukas Chalwatzis Master Thesis)

Stock Code	Plasmid Name	Relevant Description	Source
LSV22	^{Cs}AAE3-K	Part 3, *Cml^R, ColE1, ^{Cs}AAE3-K*	This study (Lukas Chalwatzis Master Thesis)
LCV23	^{Sc}FAA2-ΔPTS1	Part 3, *Cml^R, ColE1, ^{Sc}FAA2-ΔPTS1*	This study (Lukas Chalwatzis Master Thesis)
LCV24	^{Sc}FAA2-K	Part 3, *Cml^R, ColE1, ^{Sc}FAA2-K*	This study (Lukas Chalwatzis Master Thesis)
LCV25	^{Pc}PCL-K	Part 3, *Cml^R, ColE1, ^{Pc}PCL^{T369A}-K*	This study (Lukas Chalwatzis Master Thesis)
LCV26	^{At}AAE11-ΔPTS1	Part 3, *Cml^R, ColE1, ^{At}AAE11-ΔPTS1*	This study (Lukas Chalwatzis Master Thesis)
LCV27	^{At}AAE11-K	Part 3, *Cml^R, ColE1, ^{At}AAE11-K*	This study (Lukas Chalwatzis Master Thesis)
pYTK001	Entry Vector	*Cml^R, ColE1, sfGFP*	(36)
pYTK002	ConLS (connector)	Part 1, *Cml^R, ColE1*	(36)
pYTK003	ConL1 (connector)	Part 1, *Cml^R, ColE1*	(36)
pYTK009	P_{TDH3}	Part 2, *Cml^R, ColE1,* P_{TDH3}	(36)
pYTK011	P_{PGK1}	Part 2, *Cml^R, ColE1,* P_{PGK1}	(36)
pYTK013	P_{TEF1}	Part 2, *Cml^R, ColE1,* P_{TEF1}	(36)
pYTK014	P_{TEF2}	Part 2, *Cml^R, ColE1,* P_{TEF2}	(36)
pYTK034	mRuby2	Part 3, *Cml^R, ColE1, mRuby2*	(36)
pYTK052	tSSA1	Part 4, *Cml^R, ColE1, tSSA1*	(36)

Stock Code	Plasmid Name	Relevant Description	Source
pYTK053	tADH1	Part 4, *Cml^R, ColE1, tADH1*	(36)
pYTK056	tTDH1	Part 4, *Cml^R, ColE1, tTDH1*	(36)
pYTK061	tENO1	Part 4b, *Cml^R, ColE1, tENO1*	(36)
pYTK067	ConR1	Part 5, *Cml^R, ColE1*	(36)
pYTK072	ConRE (connector)	Part 5, *Cml^R, ColE1*	(36)
pYTK095	Backbone for subcloning	*Cml^R, ColE1, sfGFP*	(36)
SARV79	Integration backbone for *NSII-3* locus	Kan^R, *NSII-3* 5' HR, *sfGFP*, *NSII-3* 3' HR	Lab stock Prof. Dr. Boles (Sandra Lehner)
SiHV033	Integration backbone for *URA3* locus	*Kan^R, URA3 5' HR, sfGFP, kanMX4, URA3 3' HR*	Lab stock Prof. Dr. Boles (Simon Harth)
SiHV110	Integration backbone for *LEU2* locus	*Kan^R, LEU2 5' HR, sfGFP, natNT2, LEU2 3' HR*	Lab stock Prof. Dr. Boles (Simon Harth)

2.3.5.1 Cloning FAS plasmids via homologous recombination

Cloning of the mutant fused fatty acid synthase (fusFAS) plasmids (KSV8, KSV9, KSV10, KSV30) and the corresponding EV, pRS313K (KSV48) was achieved via HR in *S. cerevisiae*. All fusFAS plasmids were derived from the pRS313 plasmid. Genetic elements were amplified via PCR using mutagenic primers to incorporate the desired mutations within the *FAS* genes and the pRS313H-*fusFAS^{WT}* plasmid (FWV132) as a template in which the *HIS3* yeast auxotrophic selection marker had been replaced with the antibiotic *hphNT1* selection marker.[395] PCR products were purified using the NucleoSpin Gel and PCR Clean-up (Macherey-Nagel) according to the manufacturer's instructions. To clone KSV8, KSV9 and KSV10, five or six DNA fragments, which contained homologous sequences of approximately 20-40 bp, were co-transformed into the CEN.PK2-1C strain and each fragment was added in equimolar amounts relative to 500 ng of the largest fragment. KSV30 and the EV (pRS313K) were cloned by replacing the yeast selection markers in ALSV11 (*hphNT1*) and pRS313 (*HIS3*) with the *kanMX4* cassette, respectively. The

kanMX4 cassette was amplified from pRS41K using primers with overhangs of approximately 20 bp homologous the regions flanking the selection markers in ALSV11 and pRS313. The plasmids were linearized using restriction enzymes which cut within the respective selection marker and co-transformed with the purified *kanMX4* PCR product into the CEN.PK2-1C strain. Transformation was performed via heat shock (2.3.1.1), cells were regenerated in YPD media at 30 °C for 2 h and then plated on selective solid media corresponding to the selection marker on the assembled plasmid. After 1-2 days, colonies were scraped from the plate and pooled together to extract the plasmid DNA (2.3.2.3). Next, the DNA was transformed into *E. coli* (2.3.1.2) and plated on solid LB media containing the appropriate antibiotic corresponding to the selection marker on the plasmid. Assembled plasmids were screened by preparing plasmid DNA from individual *E. coli* colonies and analyzing these through restriction digestion and sequencing.

2.3.5.2 Modular cloning via Golden Gate assembly

All other plasmids were cloned via golden gate assembly using a modular cloning yeast toolkit (MoClo-YTK) as described by Lee *et al.*[36] and purchased from AddGene (Kit #1000000061). The kit comprises 96 plasmids, or parts (pYTK), which each contain a characterized genetic element, including promoters, terminators, selection markers, origins of replication and protein tags, and specific 4 bp overhangs which allows assembly of these parts in a defined sequence while allowing quick interchangeability. As such, cloning using this kit is time-efficient and various elements, such as promoters or selection markers, can be rapidly exchanged. This is facilitated by the addition of recognition sites for the Type IIS restriction enzymes BsaI and BsmBI (or Esp3I) flanking the genetic element. Cloning therefore occurs by restriction and ligation, during which the endonuclease recognition site is removed. The Golden Gate assembly was achieved in a single, one-pot reaction containing each of the desired parts, the appropriate Type IIS restriction enzyme (either BsaI-HF®v2 or Esp3I, NEB), a T7 DNA ligase (NEB) and a T4 DNA ligase buffer (NEB) (Table 13). The Golden Gate assembly mix was incubated at various temperatures according to the program in Table 14. The optimal temperature for the Type IIS restriction enzymes is 37 °C and for the T7 DNA ligase is 16 °C. Following the reaction cycle, 0.5 µL of the assembly mix was transformed into *E. coli* cells via electroporation (2.3.1.2) and cells were plated on selective solid media containing appropriate antibiotics. Individual colonies were screened by isolating plasmid DNA (2.3.2.4) and analyzing via restriction digestion and sequencing.

Table 13 | Composition of Golden Gate assembly mix

Component	Stock Concentration	Volume (µL)	Final Concentration
Plasmid DNA (parts)	variable	variable	5 ng/µL
Type IIS Restriction Enzyme (BsaI-HF®v2/Esp3I)	10,000-20,000 U mL^{-1}	0.5	5-10 U

Component	Stock Concentration	Volume (µL)	Final Concentration
T7 DNA ligase	3,000,000 U mL^{-1}	0.5	1,500 U
T4 DNA ligase buffer	10X	1	1X
ddH_2O	-	Up to 5 or 10	-

Table 14 | Temperature program for Golden Gate assembly

Step	Temperature (°C)	Time (min)	Cycles
Initial digestion	37	10	1
Digestion	37	1.5	15-25
Annealing and ligation	16	3	
Final Digestion	37	5	1
Inactivation	80	10	1

The MoClo-YTK kit was expanded through the incorporation of desired genetic elements (e.g. ORFs or the C-terminal PTS1) with appropriate flanking sequences containing Esp3I and BsaI recognition sites, as well as the corresponding 4 bp overhang to facilitate correct assembly Table 15. Genetic elements incorporated into this system in this study were either amplified from genomic DNA or existing plasmid DNA templates or were ordered as synthetic genes. Next, the genetic element was initially cloned into the MoClo-YTK entry vector pYTK001. The pYTK001 plasmid contains an *E. coli* origin of replication, a chloramphenicol resistance cassette (Cml^R) and a superfolder GFP (*sfGFP*) expression cassette flanked by BsmBI cut sites. During cloning, the Esp3I recognition sites are removed and the *sfGFP* cassette is replaced by the genetic element of choice. As such, selection of positive colonies can be simplified by analyzing non-fluorescent (white) colonies. Furthermore, plasmid backbones were pre-assembled and existed as lab stocks which comprised various combinations of yeast origins of replication and selection markers, the bacterial kanamycin resistance cassette (Kan^R) and the *sfGFP* cassette flanked by BsaI and Esp3I recognition sites (Table 12). This allowed cloning of single expression cassettes, comprising a promoter (part 2), an ORF (part 3) and a terminator (part 4), into a backbone of choice which replaces the *sfGFP* cassette during cloning. Moreover, the Kan^R allowed counterselection against any non-digested part plasmids in the Golden Gate assembly mix.

Table 15 | Overhang sequences for Golden Gate assembly into the entry vector (pYTK001)

Golden Gate assembly overhang for pYTK001	5' → 3' sequence
5' overhang sequence	CGTCTCGTC**GGTCTC**AXXXX
3' overhang sequence	CGTCTCAGGTC**GGTCTC**AXXXX

Underlined sequences represent Esp3I recognition site. Bold sequences represent BsaI recognition sites. Xs represent variable 4 bp overhang.

To clone multiple yeast expression cassettes into a single vector, an extra subcloning step was required using the MoClo-YTK vector pYTK095. This plasmid contained an ampicillin resistance cassette (*Amp*^{R}) and the *sfGFP* expression cassette flanked by BsaI and Esp3I recognition sites. Each yeast expression cassette was first individually cloned into pYTK095 via BsaI-HFv2 digestion by incorporating the desired promoter (part 2), ORF (part 3) and terminator (part 4) as well as appropriate upstream (part 1) and downstream (part 5) connectors. These connectors facilitated the correct assembly of the final multiple expression cassette plasmids in the subsequent step. The final step was achieved via Esp3I digestion of one of the pre-assembled backbone plasmids and each yeast expression cassette cloned into pYTK095 in the previous step.

CRISPR/Cas9 plasmids were generated via BsaI-HF®v2 mediated Golden Gate assembly using backbone plasmids which contained an expression cassette for the *Streptococcus pyogenes* Cas9 protein with a C-terminal NLS under the control of the weak *ROX3* promoter (P_{ROX3}), a single guide RNA (sgRNA) under the control of the polymerase III *SNR52* promoter (P_{SNR52}) and an antibiotic resistance marker. The *sfGFP* cassette was located between the P_{SNR52} and the downstream structural element of the sgRNA. Protospacer sequences were designed to contain flanking sequences which facilitated Golden Gate assembly into the CRISPR/Cas9 plasmid backbone to replace the *sfGFP* cassette and were purchased as two individual reverse-complementary single-stranded synthetic oligonucleotides (Table 16). These oligonucleotides were annealed prior to cloning. Three backbone plasmids existed which differed in the yeast selection markers contained. The marker cassettes used were: *hphNT1* for hygromycin B resistance (pRCC-H), *natNT2* for nourseothricin resistance (pRCC-N) or the *kanMX4* for geneticin resistance (pRCC-K).

Integrational plasmids were cloned via BsaI-HF®v2 mediated Golden Gate assembly using preexisting integration backbones which contained the bacterial *Kan*^{R} selection marker, homologous regions of approximately 500 bp upstream (5' HR) and downstream (3' HR) to the genomic target locus, a yeast selection marker and the *sfGFP* cassette which was replaced during cloning. For integration plasmids which were used in conjunction with CRISPR/Cas9, no yeast selection marker was present.

2.3.6 Synthetic DNA

Synthetic genes were ordered as Twist Gene Fragments from Twist Bioscience, CA, USA and codon-optimized for expression in *S. cerevisiae* according to the yeast glycolytic codon usage as described by Wiedemann and Boles.[398] Any genes which were used for Golden Gate assembly were designed with appropriate flanking regions as described in chapter 2.3.5.2 and, importantly, any internal BsaI or Esp3I recognition sites were removed. A list of the heterologous synthetic genes and their nucleotide sequences used in this study are listed in Supplementary Table 1.

Synthetic oligonucleotides, which were either used as primers for PCR amplification, as genetic elements for cloning or as donor DNA in genetic engineering to repair CRISPR/Cas9

induced DSBs, were ordered from Microsynth AG, Switzerland. Oligonucleotides used for cloning or genome editing are listed in Table 16.

Table 16 | List of oligonucleotides used for cloning and genome editing in this study

Oligonucleotides	**5' → 3' Sequence**	**Application**
ALSP7	GTTGTGTTCTACAAAGGTATGAC	Forward primer for insertion of R1834K mutation in *FAS1*
ALSP8	GTCATACCTTTGTAGAACACAAC	Reverse primer for insertion of R1834K mutation in *FAS1*
ALSP13	GGCAATTACTGTATTATTCTTCGCCGGTGTTCGTTGTTACG	Forward primer for insertion of I306A mutation in *FAS1*
ALSP14	CGTAACAACGAACACCGGCGAAGAATAATACAGTAATTGCC	Reverse primer for insertion of I306A mutation in *FAS1*
ALSP15	GTTCTGGTTCTAGTTGGGGTGGTGTTTC	Forward primer for insertion of G1250S and M1251W mutations in *FAS2*
ALSP16	GAAACACCACCCCAACTAGAACCAGAAC	Reverse primer for insertion of G1250S and M1251W mutations in *FAS2*
KSP20	GTTCTGGTTCTTCTATGGGTGGT	Forward primer for insertion of G1250S in *FAS2*
KSP21	ACCACCCATAGAAGAACCAGAAC	Reverse primer for insertion of G1250S in *FAS2*
KSP37	TTAACTATGCGGCATCAGAGCAGATTGTACTGAGAGTGCACCATCAGCGACATGGAGGCC	Forward primer for amplification of *kanMX4* cassette with overhangs for pRS313 to replace marker (*hphNT1* or *HIS3*)
KSP38	TCTCCTTACGCATCTGTGCGGTATTTCACACCGCATATGATCCGGACACTGGATGGCGGC	Reverse primer for amplification of *kanMX4* cassette with overhangs for pRS313 to replace marker (*hphNT1* or *HIS3*)
KSP70	CTTAGAGGTCTCAGATCCTAGGGCCCAAGTCAAACAGGTTTTGAGACCGACGTCCTG	Forward oligonucleotide containing protospacer sequence to target *ADH6* and overhangs for CRISPR/Cas9 plasmid assembly

Oligonucleotides	**5' → 3' Sequence**	**Application**
KSP71	CAGGACGTCGGTCTCAAAACCT GTTTGACTTGGGCCCTAGGATC TGAGACCTCTAAG	Reverse oligonucleotide containing protospacer sequence to target *ADH6* and overhangs for CRISPR/Cas9 plasmid assembly
KSP72	GAGGAAGAAATTCAACACAACA ACAAGAAAAGCCAAAATCGTGA GTAAGGAAAGAGTGAG	Forward primer for amplifying ^{Ec}*coaA* cassette from KSV52 with overhangs for *ADH6* integration locus
KSP73	AAAGAAAGGAGCTACATTTATCA AGAGCTTGACAACATAAAATTAA AGTAGCAGTACTTC	Reverse primer for amplifying ^{Ec}*coaA* cassette from KSV52 with overhangs for *ADH6* integration locus
KSP86	CTTAGAGGTCTCAGATCGACCA ACATGTGGTAAGGTGGTTTTGA GACCGACGTCCTG	Forward oligonucleotide containing protospacer sequence to target P_{FMS1} and overhangs for CRISPR/Cas9 plasmid assembly
KSP87	CAGGACGTCGGTCTCAAAACCA CCTTACCACATGTTGGTCGATCT GAGACCTCTAAG	Reverse oligonucleotide containing protospacer sequence to target P_{FMS1} and overhangs for CRISPR/Cas9 plasmid assembly
KSP88	ACGGTTCAATCGCAATTTCTCCG GAAAGTGCAGTAGCAACTGTAG CCCTAGACTTGATAG	Forward primer for amplifying P_{ADH1} from *S. cerevisiae* genome with overhangs for P_{FMS1} locus
KSP112	CCACCGCTGCTGTTTTGCAAG	Forward primer for inserting R106A mutation in ^{Ec}*coaA*
KSP113	CTTGCAAAACAGCAGCGGTGG	Reverse primer for inserting R106A mutation in ^{Ec}*coaA*
KSP118	CTTAGAGGTCTCAGATCCTGCG TCAACTATCTGATGGGTTTTGAG ACCGACGTCCTG	Forward oligonucleotide containing protospacer sequence to target *ACC1* S659 and overhangs for CRISPR/Cas9 plasmid assembly
KSP119	CAGGACGTCGGTCTCAAAACCC ATCAGATAGTTGACGCAGGATC TGAGACCTCTAAG	Reverse oligonucleotide containing protospacer sequence to *ACC1* S659 and overhangs for CRISPR/Cas9 plasmid assembly
KSP120	TCAATGGTTCTAAATGTGATATC ATA**T**T**AA**G**G**CAA**T**T**G**GCAGA**C**G	Donor DNA for inserting S659A mutation in *ACC1*

Oligonucleotides	5' → 3' Sequence	Application
	GTGGTCTTTTGATTGCCATAGGC GGTAAATCGCAT	
KSP121	CTTAGAGGTCTCAGATCCAAAGT AGTCATAGAGTCAAGTTTTGAGA CCGACGTCCTG	Forward oligonucleotide containing protospacer sequence to target *ACC1* S686 and overhangs for CRISPR/Cas9 plasmid assembly
KSP122	CAGGACGTCGGTCTCAAAACTT GACTCTATGACTACTTTGGATCT GAGACCTCTAAG	Reverse oligonucleotide containing protospacer sequence to *ACC1* S686 and overhangs for CRISPR/Cas9 plasmid assembly
KSP123	CCATCTATTGGAAAGAAGAAGTT GCTGCTACAAGATTAGCTGTAG ATTCTATGACTACTTTGTTGGAA GTTGAAAACGAT	Donor DNA for inserting S686A mutation in *ACC1*
KSP124	CTTAGAGGTCTCAGATCATCTAA AATGGGTATGAACAGTTTTGAGA CCGACGTCCTG	Forward oligonucleotide containing protospacer sequence to target *ACC1* S1157 and overhangs for CRISPR/Cas9 plasmid assembly
KSP125	CAGGACGTCGGTCTCAAAACTG TTCATACCCATTTTAGATGATCT GAGACCTCTAAG	Reverse oligonucleotide containing protospacer sequence to *ACC1* S1157 and overhangs for CRISPR/Cas9 plasmid assembly
KSP126	CGTTCTCCACCTTTCCAACTGTT AAATCTAAAATGGG**A**ATGAA**T**AG **A**GCTGTTGCTGTTTCAGATTTGT CATATGTTGCA	Donor DNA for inserting S1157A mutation in *ACC1*
KSP127	GCTGAGCAGTTACAGAGATGTT ACGAACCACTAGTGCACTGCAG TACAGTTTGCAGACGAACGTTG ATAGGTC	Forward primer for amplifying ^{Cs}*OLS* and ^{Cs}*OAC* cassettes from KSV74 with overhangs upstream of *kanMX4* cassette in *ura3*Δ::rBOX, *kanMX4* locus
KSP128	CGTCATTATAGAAATCATTACGA CCGAGATTCCCGGGGCAGTGGA TTCAAGTGCTCTCATCTCTGTAA CTGCTCAGCTG	Reverse primer for amplifying ^{Cs}*OLS* and ^{Cs}*OAC* cassettes from KSV74 with overhangs downstream of *kanMX4* cassette in *ura3*Δ::rBOX, *kanMX4* locus

Oligonucleotides	**5' → 3' Sequence**	**Application**
KSP175	CATAGAGTCAACGGCTAATCTTG TAGCAGC	Reverse primer for inserting S686A mutation in *ACC1*
KSP176	GCTGCTACAAGATTAGCCGTTG ACTCTATG	Forward primer for inserting S686A mutation in *ACC1*
KSP196	CTTAGAGGTCTCAGATCTAGTG CACTTACCCCACGTTGTTTTGAG ACCGACGTCCTG	Forward oligonucleotide containing protospacer sequence to target *416d* locus on Chr IV locus and overhangs for CRISPR/Cas9 plasmid assembly
KSP221	CAGGACGTCGGTCTCAAAACAA CGTGGGGTAAGTGCACTAGATC TGAGACCTCTAAG	Reverse oligonucleotide containing protospacer sequence to *416d* locus on Chr IV and overhangs for CRISPR/Cas9 plasmid assembly
KSP226	CTATTATCTTCTACGCTGACAGT AATATCAAACAGTGACCTTGCCA ACAGGGAGTTCTTC	Forward primer for amplifying ^{Pc}*PCL-K* cassette from KSV102 with overhangs for *416d* integration locus
KSP227	ATTGCATAAAAGACCGTGTGATG GCTTGGCGGCGAATTGGGTACC GGCCGCAAATTAAAG	Reverse primer for amplifying ^{Pc}*PCL-K* cassette from KSV102 with overhangs for *416d* integration locus
LCP23	CGTCTCAGGTCGGTCTCAGGAT TCACTTCATGTTGGACCTGACCT TTTG	Reverse primer for inserting C-terminal lysine (K) residue in ^{Cs}*AAE3*
LCP26	CGTCTCAGGTCGGTCTCAGGAT CTATGTCTTGACTAGTGAACCTT CGGC	Reverse primer for removing Δ*PTS1* in ^{Sc}*FAA2*
LCP27	CGTCTCAGGTCGGTCTCAGGAT CTACTTAAGCTTTTCTGTCTTGA CTAGTGAACCTTC	Reverse primer for inserting C-terminal lysine (K) residue in ^{Sc}*FAA2*
LCP24	CGTCTCAGGTCGGTCTCAGGAT TTACTTGATCTTGGAACCTGCTT TTCTTC	Reverse primer for inserting C-terminal lysine (K) residue in ^{Pc}*PCL*
LCP29	CGTCTCAGGTCGGTCTCAGGAT TTACTTCAATCTAGAAGAAACGT GTTCGATA	Reverse primer for inserting C-terminal lysine (K) residue in ^{At}*AAE11*

Oligonucleotides	5' → 3' Sequence	Application
LCP28	CGTCTCAGGTCGGTCTCAGGATTTAAGAAACGTGTTCGATAGATCTTTGG	Reverse primer for removing Δ*PTS1* in ^{At}*AAE11*
SHP110	TGACTGCGATGATAGGAGG	Forward primer for amplifying Δ*faa2* locus in SHY24
SHP222	GTGCACCAAGTCAAGTTACG	Reverse primer for amplifying Δ*faa2* locus in SHY24
VSP375	TTTGGCTGGTGAAACTGTATTCATTGTATATGAGATAGTTGATTGTATGC	Reverse primer for amplifying P_{ADH1} from *S. cerevisiae* genome with overhangs for P_{FMS1} locus

Underlined sequences represent insertions or missense mutations. Bold letters indicate silent mutations.

2.3.7 Strain engineering of *S. cerevisiae*

Genetic modifications in yeast strains were engineered based either on the simplified, plasmid-based CRISPR/Cas9 genome editing method for *S. cerevisiae*[40] or via antibiotic resistance marker mediated HR.[11,13] The 20 bp protospacer sequences used in this study to target the genomic loci during CRISPR/Cas9 mediated genetic engineering are listed in Table 17.

Table 17 | List of protospacer sequences used in CRISPR/Cas9 mediated genetic editing.

Genomic Target	Protospacer Sequence	Plasmid Stock Code
FAA2	GAAGATTTTGAAACCTTACG	SHV42
ADH6	CTAGGGCCCAAGTCAAACAG	KSV55
P_{FMS1}	GACCAACATGTGGTAAGGTG	KSV75
kanMX4	TTACTCACCACTGCGATCCC	SHV29
ACC1 S659	CTGCGTCAACTATCTGATGG	KSV78 and KSV96
ACC1 S686	CAAAGTAGTCATAGAGTCAA	KSV79
ACC1 S1157	ATCTAAAATGGGTATGAACA	KSV80
NSII-3 on ChrII	CATTCTCATCGTCCTCTCAA	SARV84
416d on ChrIV	TAGTGCACTTACCCCACGTT	KSV115

For genomic integration, linearized genetic elements were obtained either through restriction digestion (NotI) of 1-10 µg integrational plasmids or via PCR amplification using primers containing specific overhangs for the desired integration locus. Alternatively, genetic elements were

purchased as 60-80 bp synthetic oligonucleotides. These were either transformed alone, if the integration constructs contained a resistance marker, or co-transformed with the corresponding CRISPR/Cas9 plasmid. Cells were subsequently regenerated in 5-20 mL complex media (YPD) or in synthetic uracil drop-out media (SCD-U) for the *y*OA1 and all strains derived from *y*OA1 which contained the *URA3d* selection cassette. Regeneration times were dependent on the fitness of the strains, and ranged from 4 h to 24 h to allow sufficient cell doubling times during which DNA repair and editing can take place. The cultures were pelleted and plated on appropriate selection plates corresponding to the selection marker contained in the CRISPR/Cas9 plasmid or within the linearized DNA integration fragment during HR mediated

Multiple copies of ^{Cs}*OLS* and ^{Cs}*OAC* were integrated into the genome to generate the strain *y*OA using the multicopy integration plasmid pCfb2791-*OLS*-*OAC*-*OAC*-*URA3d* which targets the *Ty4* elements.[251] The S659A, S686A and S1157A mutations were sequentially incorporated into the WT *ACC1* allele via site-directed mutagenesis using CRISPR/Cas9. Synthetic, single-stranded oligonucleotides which contained silent mutations to modify the protospacer recognition sequence were used to incorporate the S659A and S1157A mutations. The S686A mutation was incorporated via PCR using mutagenic primers and the genomic DNA of a *ACC1*$^{S659A/S1157A}$ mutant strain as a template to generate a single double stranded DNA product containing all three mutations. This fragment was purified and transformed into *y*OA1 together with both CRISPR/Cas9 plasmids to induce two DSBs in parallel at positions S659 (KSV96) and S1157 (KSV80) of the WT *ACC1* gene, thereby generating *y*OA1_*ACC1**.

2.3.8 DNA sequencing

To verify correct cloning or genomic editing, plasmid DNA or PCR amplified genomic DNA was sequenced via the Sanger sequencing analysis service provided by Microsynth AG, Switzerland according to the service provider's instructions. PCR amplified DNA was first purified using the NucleoSpin Gel and PCR Clean-up (Macherey-Nagel) according to the manufacturer's instructions.

2.4 Analytical Methods

2.4.1 Sample preparation

2.4.1.1 Fatty acid extraction

Fatty acids (FAs) were extracted from the media as previously described.[270,284,399] For this, a 10 mL sample of the culture supernatant was prepared by separating the cell suspension via centrifugation (3000 x*g*, 15 min). 0.02 g L^{-1} heptanoic acid was added as an internal standard.

These deemed to enable correction of the FA concentration measured after analysis to account for any loss of compounds during the extraction and derivatization processes. FAs were then extracted through the addition of 1 mL 1 M hydrochloric acid (HCl) and 2.5 mL of a 1:1 solution of $CHCl_3$ and MeOH. The phases were thoroughly mixed through vigorous shaking and then separated via centrifugation (3000 x*g*, 10 min). The chloroform phase containing the fatty acids was transferred to fresh 1.5 mL microcentrifuge tubes and evaporated using a vacuum concentrator (Eppendorf Concentrator 5301) at 60 °C. Extracted FAs were stored at -20 °C.

2.4.1.2 Derivatization of fatty acids to fatty acid methyl esters

To analyze free FAs via gas chromatography (GC), it is essential to derivatize them to fatty acid methyl esters (FAMEs) through esterification with a methyl group using methanol. Methylation of free FAs increases their volatility, allowing them to enter the gas phase, and increases their thermal stability, thereby making them suitable for GC analysis. FFAs in contrast are less volatile and thermally less stable. The method used in this study was based on the method described by Ichihara and Fukubayashi. [400] Extracted FAs (2.4.1.1) were resuspended in 200 µL toluene and transferred to DURAN® glass cultures tubes with a screw cap (GL14, 9 mL) that contained a solution comprising 1.5 mL methanol and 300 µL of an 8% (v/v) HCl diluted in methanol, which was prepared using 37% fuming HCl (Roth). The solution was then incubated at 100 °C for 3 h to allow transesterification using methanol. After this, the tubes were allowed to cool and the FAMEs were extracted by adding 1 mL hexane and 1 mL distilled water and mixing the phases through vigorous shaking. The hexane phase was then transferred to ND9 autosampler vials for GC analysis.

2.4.1.3 Olivetol and olivetolic acid extraction

Small organic molecules can be easily measured and separated using high-performance liquid chromatography (HPLC). Therefore, OA and OL were extracted from cultures and prepared for HPLC analysis in this study. To analyze extracellular and intracellular OA and OL concentrations, samples were taken as cell suspensions directly from cultures. Thus, OA and OL were extracted by mixing 300 µL cell culture with an ice-cold mixture of 870 µL acetonitrile and 30 µL formic acid. Cells were mechanically lysed using glass beads and vigorous shaking using the Shakers Vibrax® VXR basic (IKA) at 4 °C. The samples were then centrifuged (15,000 x*g*, 30 min, 4 °C) and the supernatant was filtered into ND9 autosampler vials using 0.2 µm nylon filters.

2.4.1.4 Preparation of sugars and alcohols for analysis

Sugars and small organic molecules can be easily measured and separated using high-performance liquid chromatography (HPLC). Therefore, in this study, glucose consumption and

ethanol formation were analyzed via HPLC. To prepare samples, cell cultures were harvested via centrifugation (15,000 x*g*, 5 min) and 450 µL supernatant were transferred to fresh microcentrifuge tubes. To precipitate proteins and ensure none are transferred to the HPLC system and analytical columns, 50 µL of 50% (w/v) 5-sulfosalicylic acid was added. The solution was then vortexed, centrifuged (15,000 xg, 5 min) and 400 µL supernatant was transferred to ND9 autosampler vials for analysis.

2.4.2 High-performance liquid chromatography (HPLC)

The consumption of glucose consumption as well as the production of ethanol, OA and OL were analyzed via high-performance liquid chromatography (HPLC). Analytes were separated based on their chemical and physical properties using appropriate analytical columns and various conditions were tested to establish the most appropriate and efficient separation method.

2.4.2.1 Separation of sugars and alcohols

Glucose and ethanol were analyzed together using the UHPLC+ system by Thermo Scientific (Dionex UltiMate 3000) equipped with NUCLEOGEL SUGAR 810 H, 8-10 µM, 300 x 7.8 mm column (Macherey-Nagel) which separates analytes based on an ion-exchange and ion-exclusion mechanisms as well as hydrophobicity and size-exclusion. A refractive index (RI) detector (Thermo Shodex RI-101) was used to detect analytes and the system was operated at 30 °C. The mobile phase used was 0.5 mM sulfuric acid at a constant flow rate of 0.600 mL min^{-1}.

2.4.2.2 Separation of olivetolic acid and olivetol

OA and OL samples were analyzed via reverse-phase chromatography in which compounds are separated based on hydrophobicity. This was done by using the UHPLC + system by Thermo Scientific (Dionex UltiMate 3000) equipped with an Agilent Infinity Poroshell 120 EC-C18 column 2.1 x 100 mm, 2.7 µm and a UV detector (Dionex UltiMate 3000 RS Variable Wavelength Detector) which was operated at 40 °C. The mobile phase consisted of 0.1% (v/v) formic acid in water (solvent A) and acetonitrile (solvent B) A sample volume of 5 µL was injected into the column and analytes were separated using a gradient at a constant flow rate of 0.600 mL min^{-1}. Separation began with 70% solvent A and 30% solvent B which was held for 1.5 min. Next, solvent B was linearly increased to 100% until 9.5 min and immediately linearly decreased to 30% until 10 min. This was held for a final 1 min. OA and OL were detected using a wavelength of 225 nm and identification and quantification were achieved using real standards. The OA standard was purchased from Sigma-Aldrich, Germany (AmBeed, IL, USA) and the OL

standard was chemically synthesized within Prof. Dr. Dr. h.c. Kayser's laboratory and its structure was confirmed via mass spectrometry and nuclear magnetic resonance.

2.4.3 Gas chromatography

2.4.3.1 Separation of fatty acid methyl esters

FAMEs were analyzed via gas chromatography (GC) using the Clarus® 400 GC (PerkinElmer) and detected using a flame ionization detector (FID). 1 µL sample was injected into the column using helium as the carrier gas (90 kPa). The injection temperature was set to 250 °C and the sample was split with ratio of 1:20. The detection temperature was set to 300 °C. FAMEs were separated over the course of 42.67 min using an Elite 5ms capillary column 30 m x 0.25 mm I.D. x 0.25 µm (Perkin Elmer) and the following temperature program (Table 18).

Table 18 | Temperature program for FAME separation using the PerkinElmer Clarus® 400 GC

Temperature (°C)	**Increment (°C min^{-1})**	**Hold (min)**
50	-	5
120	10	5
220	15	10
300	20	5

Alternatively, FAMEs were analyzed using the Agilent Technologies 7890B GC System and detected using the Agilent Technologies 5977B Mass-Selective Detector (MSD). 1 µL sample was injected into the column with a split ration of 1:10 using helium as the carrier gas (13 psi) and a flow of 19.5 mL min^{-1}. The injection temperature was set to 250 °C and the sample was split with ratio of 1:10. The detection temperature was set to 300 °C. Separation of the FAMEs was achieved using a HP-5MS Capillary column (30 m x 0.25 mm I.D. x 0.35 µm, Agilent Technologies, Inc.) over the course of 40.67 min using the following temperature program (Table 19).

Table 19 | Temperature program for FAME separation using the Agilent Technologies 7890B GC System

Temperature (°C)	**Increment (°C min^{-1})**	**Hold (min)**
50	-	5
120	10	5
220	15	10
300	40	5

Analytical standards of hexanoic acid, heptanoic acid, octanoic acid and decanoic acid were derivatized to FAMEs using the same protocol (2.4.1.2) to allow identification and quantification of the peaks (Sigma-Aldrich, Germany).

2.4.4 Fluorescence Microscopy

Recombinant *S. cerevisiae* strains were used to visualize the subcellular localization of AAEs via fluorescence microscopy. An overexpression cassette containing the genes encoding the fluorophore, mRuby2, tagged with a PTS1 comprising a C-terminal tripeptide sequence serine-lysine-leucine (SKL) was integrated into the genome of CEN.PK2-1C to visualize the peroxisomes (KSY39). Subsequently, one of either the WT or mutant ^{Sc}*FAA2* or ^{Pc}*PCL* constructs tagged with an N-terminal eGFP were integrated into KSY39 to generate four distinct strains. These were grown to the mid-exponential phase in YPD prior to being washed and diluted to an OD_{600} of 3 in low-fluorescence SCD media. 5 µL of the culture was applied on agarose pads (1% agarose in 89 mM Tris-borate, 2 mM EDTA, pH 8) and mounted on glass slides. The pads were covered with a glass cover slip and kept from light exposure. Confocal fluorescent images were captured using a laser scanning microscope (Zeiss LSM 700) equipped with the Plan-Apochromat 63 × 1.40 Oil DIC objective using the Zeiss LSM Software. The LED laser was set to wavelengths of 488 nm and 555 nm at an intensity of 2% to excite eGFP and mRuby2, respectively. To capture the signal, a PMT detector with an SP555 filter was used and the gain was set to a range of 600-800 V. Images were processed using the open-source image analysis software, Fiji. [401]

2.4.5 Statistical analysis

The data shown represent the mean ± standard deviation (s.d.) of biological replicates. Biological replicates were defined as individual main cultures which each derived from a separate pre-culture. Pre-cultures originated from either a single colony or multiple colonies which were picked from a transformation plate. There was no overlap in colonies between pre-cultures to ensure biological independence. The number of biological replicates for each experiment is stated as *n* within the figure legends. Statistical significance was determined using the two-tailed unpaired *t*-test and was performed using GraphPad Prism (v10.2.0).

3 RESULTS AND DISCUSSION

3.1 Biosynthesis of hexanoyl-CoA in *S. cerevisiae*

3.1.1 Screening mutant FAS constructs for hexanoic acid production

We began our efforts of generating and endogenous hexanoyl-CoA supply from glucose by engineering the FAB pathway. For this, we used a previously described fused FAS (fusFAS) construct in which the α- and β-subunits were joined together via a short linker sequence (DEWGS), designed based on alignments with a single gene fungal FAS from the species *Ustilago maydis*.[299,395] This sequence replaced the four amino acids (YEQS) at the C-terminus of FAS1 and the two amino acids (MK) at the N-terminus of FAS2 (Figure 9).

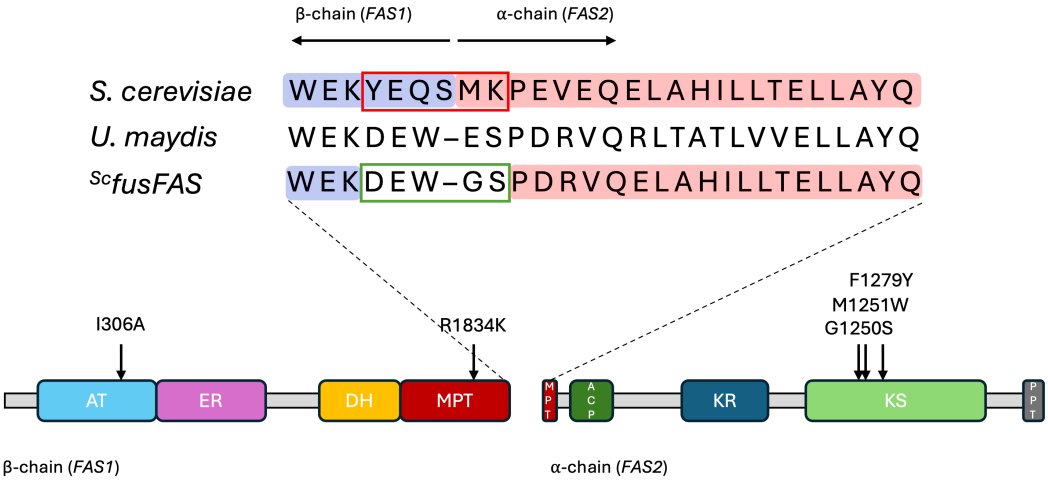

Figure 9 | Schematic of the *S. cerevisiae* fused fatty acid synthase (fusFAS) peptide sequence and domains

(Upper) Sequence alignment of the α-chain C-terminus (blue) and the β-chain N-terminus (red) from *S. cerevisiae* with the single-chain sequence of *Ustilago maydis* FAS and the *S. cerevisiae* fusFAS construct containing the peptide linker sequence DEWGS (green box) which replaced six residues from wildtype *S. cerevisiae* FAS (red box). (Lower) Illustration of the position of the linker within the MPT domain to fuse the two chains together and the individual protein domains with the approximate locations of the mutations introduced to engineer catalytic domains involved in chain length control. AT – acetyltransferase; ER – enoyl reductase; DH – dehydratase; MPT – malonyl/palmitoyl transacylase; ACP – acyl carrier protein; KR – ketoacyl reductase; KS – ketoacyl synthase; PPT – phosphopantetheinyl transferase.

The fused *FAS1* and *FAS2* genes had previously been cloned under the control of the strong glycolytic TDH3 promoter (P_{TDH3}) into a centromeric (CEN6/ARS4) plasmid which contained the dominant marker *hphNT1* (FWV132). From this construct, we constructed six mutant fusFAS constructs by incorporating various combinations of the following amino acid substitutions within the catalytic domains involved in chain length control: I306A (AT), R1834K (MPT), G1250W, M1251W and F1279Y (KS domain) (Table 20).

Table 20 | Name and description of mutant fused fatty acid synthase (fusFAS) plasmids.

Gene	Vector	Marker	Origin of Replication
fusFAS	FWV132	*hphNT1*	*CEN6/ARS4*
fusFAS^{RK}	ALSV7	*hphNT1*	*CEN6/ARS4*
fusFAS^{RKFY}	ALSV9	*hphNT1*	*CEN6/ARS4*
fusFAS^{IAGSMWFY}	ALSV11	*hphNT1*	*CEN6/ARS4*
fusFAS^{IARKGSMWFY}	ALSV13	*hphNT1*	*CEN6/ARS4*
fusFAS^{IAGS}	KSV8	*hphNT1*	*CEN6/ARS4*
fusFAS^{IARKGS}	KSV9	*hphNT1*	*CEN6/ARS4*
fusFAS^{IAGSMW}	KSV10	*hphNT1*	*CEN6/ARS4*
fusFAS^{IAGSMWFY}	KSV30	*kanMX4*	*CEN6/ARS4*

To determine their capability of synthesizing hexanoyl-CoA, we overexpressed each construct in the fatty acid auxotrophic *S. cerevisiae* strain, SHY34, and indirectly determined hexanoyl-CoA production by measuring the amount of free hexanoic acid which accumulates in the medium due to endogenous TE activity. SHY34 derives from the BY4741 stain and is contains a double *fas1 fas2* KO mutation as well as a KO mutation in the gene which encodes the medium chain fatty acyl-CoA synthase *FAA2* (Δ*fas1* Δ*fas2* Δ*faa2*). The strain is hereafter referred to as *fas^{null}*. By using a *fas* KO strain, the competition for precursors and cofactors should be greatly reduced. Moreover, this provided certainty that the source any hexanoic acid production was indeed the mutant fusFAS construct and not a result of the unregulated premature release of hexanoyl-CoA from WT FAS. Furthermore, the Δ*faa2* mutation prevented the degradation of MCFAs, which allowed hexanoic acid to accumulate extracellularly and was therefore able to provide a clearer picture of the production profiles of the fusFAS constructs. Furthermore, as the *fas^{null}* strain is unable to synthesize LCFAs, it is unviable. This can be compensated for by supplementation of the cultures with LCFAs for example in the form of oleic acid. However, the auxotrophy can be partially complemented by the well-studied *FAS^{RK}* construct, which primarily synthesizes octanoic acid, due to the leaky production of LCFAs. Nevertheless, in this case growth of *fas^{null}* is reduced compared to a WT *FAS* strain. Therefore, the *fusFAS^{RK}* construct (ALSV7) was used as a control for complementation of *fas^{null}* and MCFA production in our initial experiments. In addition to identifying a construct capable of producing hexanoic acid, we also determined the specificity of production by analyzing the production of the other MCFAs, octanoic acid and decanoic acid. FAs of longer chain length were not detected. Thus, the total MCFA output of the individual mutant *fusFAS* constructs in the *fas^{null}* strain was analyzed after 48 h cultivation in selective buffered YPD media and growth was determined as measured by the final OD_{600} values (Figure 10).

As expected, *fusFAS^{RK}* was able to complement the auxotrophy of the *fas^{null}* strain and predominantly produced octanoic acid (48.9 ± 1.2 mg L^{-1}). Low levels of hexanoic acid (3.2 ± 0.09 mg L^{-1}) and decanoic acid (6.6 ± 1.2 mg L^{-1}) were also detected. Of the six additional mutant *fusFAS* constructs, *fusFAS^{IAGS}* (KSV8), *fusFAS^{IARKGS}* (KSV9) and *fusFAS^{IAGSMW}* (KSV10)

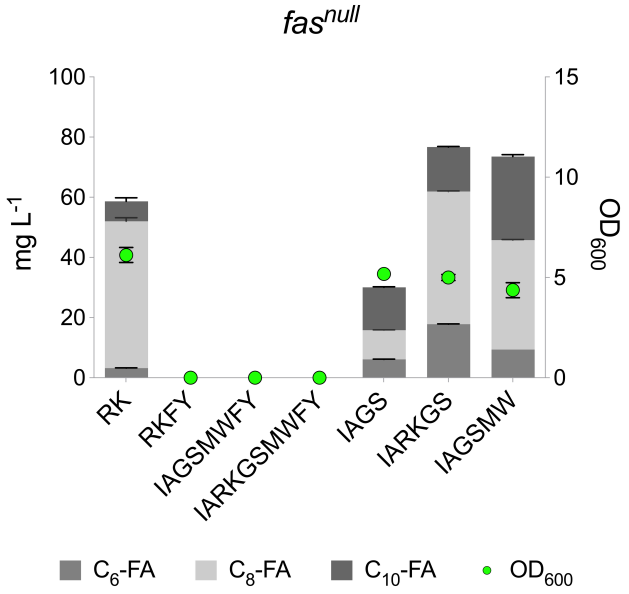

Figure 10 | MCFA production by mutant *fusFAS* constructs in *fas^{null}* strain

Analysis of C_6-FA, C_8-FA and C_{10}-FA biosynthesis as well as growth (OD_{600}) after 48 h in selective buffered YPD media following overexpression of different fusFAS constructs containing various combinations of mutations in a Δ*fas1* Δ*fas2* Δ*faa2* triple knockout strain (*fas^{null}*). MCFA – medium chain fatty acid; C_6-FA – hexanoic acid; C_8-FA – octanoic acid; C_{10}-FA – decanoic acid; OD_{600} – optical density at 600 nm. *n* = 2 biologically independent samples. Data represent mean ± s.d.

were similarly able to complement the *fas* KO mutations and produced higher titers of hexanoic acid compared to *fusFAS^{RK}*. The highest hexanoic acid titer produced was by *fusFAS^{IARKGS}* (17.8 ± 0.15 mg L^{-1}) followed by *fusFAS^{IAGSMW}* (9.4 ± 0.01 mg L^{-1}) and *fusFAS^{IAGS}* (6.2 ± 0.03 mg L^{-1}). Interestingly, although octanoic acid production remained highest with *fusFAS^{RK}*, decanoic acid was approximately 2- or 4-fold higher in the other constructs with the highest production being achieved with *fusFAS^{IAGSMW}* (27.8 ± 0.64 mg L^{-1}). Furthermore, the total MCFA output was higher in *fusFAS^{IARKGS}* (76.8 mg L^{-1}) and *fusFAS^{IAGSMW}* (73.5 mg L^{-1}) compared to *fusFAS^{RK}* (58.7 mg L^{-1}), however, total MCFA output was decreased in *fusFAS^{IAGS}* (30.1 mg L^{-1}). Strikingly, the strains overexpressing the remaining three constructs (*fusFAS^{RKFY}*, *fusFAS^{IAGSMWFY}* and *fusFAS^{IARKGSMWFY}*), were unable to grow. Therefore, no MCFA production was detected. As the common feature of these three constructs was the presence of the F1279Y mutation, we hypothesized that the addition of this mutation results in a more stringent blockade of the growing acyl chain, thereby preventing the leaky production of LCFAs. This observation would suggest that these constructs may actually be more efficient for MCFA production. To investigate this, we repeated the experiment in the WT FAS strain SYH24 (Figure 11). Similar to *fas^{null}*, SHY24 contained the Δ*faa2* mutation to prevent degradation of MCFAs but differed in that it contained the *FAS1* and *FAS2* genes. This strain is therefore referred to as *FAS^{WT}*.

Overexpression of all the mutant *fusFAS* constructs in *FAS^{WT}* resulted in improved growth compared to *fas^{null}* and MCFA production was detected in all constructs, including those which contained the F1279Y mutation. Indeed, in line with the expectation that the constructs containing the F1279Y mutation may be more efficient at synthesizing MCFAs, the highest amount of total

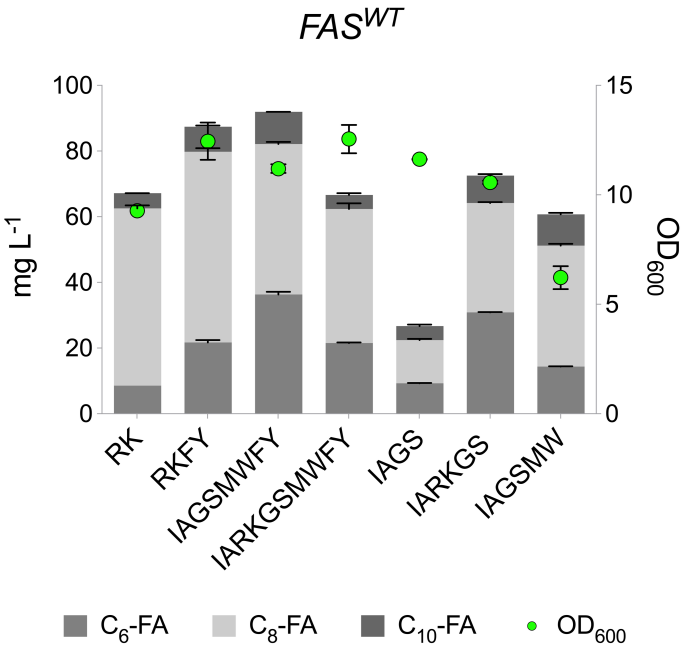

Figure 11 | MCFA production by mutant *fusFAS* constructs in *FAS^{WT}* strain

Analysis of C_6-FA, C_8-FA and C_{10}-FA biosynthesis as well as growth (OD_{600}) after 48 h in selective buffered YPD media following overexpression of different *fusFAS* constructs containing various combinations of mutations in a Δ*faa2* single knockout strain (*FAS^{WT}*). MCFA – medium chain fatty acid; C_6-FA – hexanoic acid; C_8-FA – octanoic acid; C_{10}-FA – decanoic acid; OD_{600} – optical density at 600 nm. *n* = 2 biologically independent samples. Data represent mean ± s.d.

MCFAs were synthesized by *fusFAS^{RKFY}* and *fusFAS^{IAGSMWFY}* constructs, reaching 87.4 mg L^{-1} and 91.9 mg L^{-1}, respectively. Furthermore, the highest titer of hexanoic acid detected was by *fusFAS^{IAGSMWFY}* (36.4 ± 0.79 mg L^{-1}), which corresponds to approximately 40% of the total MCFA output. However, this was followed by the *fusFAS^{IARKGS}* which also produced in the *fas^{null}* strain (30.9 ± 0.11 mg L^{-1}) and corresponded to approximately 43% of its total MCFA output. Interestingly, hexanoic acid biosynthesis increased between 1.5- and 2.7-fold in the four constructs which were also active in the *fas^{null}* strain. This may be attributed to the increase in biomass, however, as the total production of MCFAs was similar in *FAS^{WT}* following overexpression of *fusFAS^{IAGS}* (26.7 mg L^{-1}), *fusFAS^{IARKGS}* (72.5 mg L^{-1}) or *fusFAS^{IAGSMW}* (60.8 mg L^{-1}) compared to in *fas^{null}* (Figure 10), this would suggest that increased biomass is not the sole explanation for increased hexanoic acid biosynthesis.

3.1.2 Comparison of mutant FAS output in *fas* KO and WT *FAS* strain

It is commonly regarded that using a Δ*fas1* Δ*fas2* knockout strain is beneficial for MCFA production when engineering the FAB pathway and this has been shown to be true in the case of octanoic acid production.[270,284,395,402] However, contrary to this trend, our data suggest that the synthesis of hexanoic acid is preferred in the presence of WT FAS rather than in its absence. To investigate this further, we analyzed the data collected from a number of different experiments

which had been conducted using the *fusFAS*^{lARKGS} construct. This construct was selected as it was the best hexanoic acid producer which was active in both the *fas*^{null} and *FAS*^{WT} strains. From these data, we compared the proportion of hexanoic acid, octanoic acid and decanoic acid as a percentage of the total MCFA output. This allowed us to compensate for the natural fluctuations in absolute titers which exist between individual experiments. Indeed, we were able to observe a change in the proportion of each MCFA which was dependent on the presence of WT FAS (Figure 12).

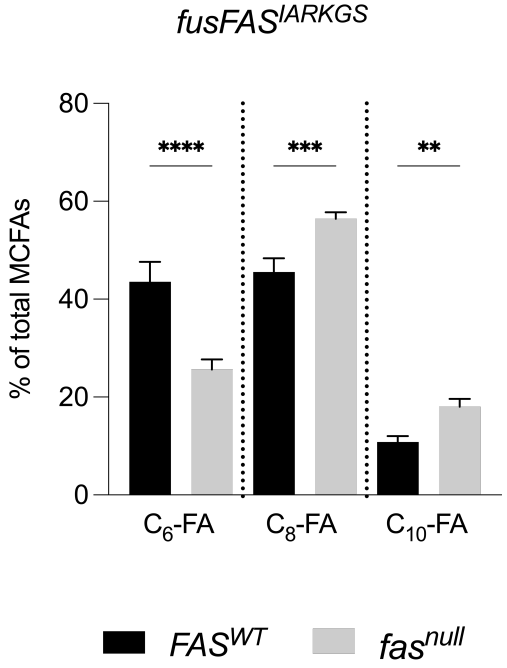

Figure 12 | MCFA production spectrum of mutant *fusFAS* in *FAS*^{WT} and *fas*^{null} strain

Analysis of C_6-FA, C_8-FA and C_{10}-FA biosynthesis after 48 h in buffered selective YPD media as percentages of total MCFA output following overexpression of *fusFAS*^{lARKGS} in either a *FAS* wildtype (*FAS*^{WT}) or *fas* knockout (*fas*^{null}) strain. *n* = 4 independent experiments, each representing the mean of two biologically independent samples. Data represent mean ± s.d. Statistical analysis was performed using the two-tailed unpaired *t*-test. $p > 0.05$ = ns (not significant); $p < 0.05$ = *; $p < 0.01$ = **; $p < 0.001$ = ***; $p < 0.0001$ = ****.

Consistent with literature, we observed an increase in the percentage of octanoic acid in the *fas*^{null} strain comprising 56.4% of the total MCFA output compared to in the *FAS*^{WT} strain, in which it comprised only 45.6%. Similarly, the portion of decanoic acid was also higher in the *fas*^{null} strain, comprising 18.0% compared to 10.8% in the *FAS*^{WT} strain. In contrast, the proportion of hexanoic acid was higher in the *FAS*^{WT} strain, comprising 43.6% compared to 25.6% in the *fas*^{null} strain. This led us to believe that the output of the mutant FAS constructs is dynamic and varies depending on the metabolic or nutritional requirements of the cells.

To explain the varying MCFA production spectra and phenotypes observed when incorporating the different mutations, it is important to understand the roles and positions of the amino acids in the FAS complex. Gajewski *et al.*[284] reported growth deficiencies following introduction of the F1279Y mutation to existing mutations. As phenylalanine at position 1279 protrudes into the acyl binding channel of the wildtype KS domain on the opposite side to glycine

at position 1250 and methionine at position 1251, combining the F1279Y with any of these mutations within the KS domain may completely prevent the elongation of the growing acyl chain, thus rendering the *fusFAS*^{IAGSMWFY} and *fusFAS*^{IARKGSMWFY} constructs unable to complement the *fas* KO mutations through leaky LCFA production. On the other hand, mutating the KS domain by incorporating either the F1279Y mutation alone or the G1250S and M1251W mutations either alone or in combination would allow space for the acyl chain to grow via the opposite side of the channel, albeit with a reduced efficiency. Thus, the premature release of MCFAs is promoted, however, leaky production of LCFAs is still possible. Consequently, combing the FY mutation with a mutation in another domain, such as I306A within the AT domain, complemented the *fas* KO mutations and resulted in some MCFA production, although the titers were modest.[284] Similarly, we observed the least total MCFA production when combining a single KS mutation (G1250S) with the AT domain mutation (I306A). Although the I306A mutation is expected to increase the likelihood of initiating FA biosynthesis by promoting acetyl-CoA loading, without a concomitant reduction in malonyl-CoA uptake through the MPT domain mutation (R1834K) the premature release of incompletely synthesized acyl-CoA molecules is seemingly limited. Moreover, of the three mutations which can be introduced into the KS domain, the G1250S mutation arguably has the least effect, as it acts to reduce flexibility of the M1250 residue but does not contribute greatly to steric hinderance.

An explanation for the growth deficiencies observed when combining only the F1279Y and R1834K mutations may be that sterically hindering chain length elongation (KS mutations) and reducing malonyl-CoA uptake efficiency (MPT domain) act synergistically to prevent elongation. Additionally, we observed an increase in the proportion of the longer MCFAs, octanoic acid and decanoic acid, in the absence of FAS. This may be due to the pressure for cells to synthesize LCFAs to ensure their survival. However, when this pressure is removed through the presence of WT FAS, the product spectra of the same mutant construct is altered in favor of hexanoic acid production. A reason for this may be the higher tolerance of *S. cerevisiae* to hexanoic acid than to octanoic and decanoic acid.[403] Finally, an explanation for the generally much lower titers of decanoic acid may be detoxification mechanisms which involves degradation via β-oxidation through its activation by the long chain fatty acyl-CoA ligase (Faa1p) which displays activity for decanoic acid or via the acyl-CoA:ethanol O-acyltransferase (Eeb1p) mediated esterification of decanoic acid to decanoate ethyl ester.[404]

A further method to increase MCFA and hexanoic acid production may be to overexpress the best producing construct *fusFAS*^{IAGSMWFY} in the *fas*^{null} strain and to supplement the cultures with oleic acid which would allow viability and also maximize acetyl-CoA, malonyl-CoA and NADPH supply for the mutant construct. However, supplementation of oleic acid would not be economically feasible in an industrial setting and was therefore not tested in this study, as this would break the aim of this work which was to engineer a strain capable of synthesizing hexanoyl-CoA without the supplementation of FAs. Alternatively, downregulating WT *FAS* expression may achieve viability while lowering precursor competition. Indeed, this approach was tested by Zhang *et al.* [252] within the context of CBGA biosynthesis, however, with a different rationale. Here, the hypothesis was made that FAS is able to accept hexanoyl-CoA as a substrate and elongate this further. As such,

inhibition of FAS with cerulenin or downregulation through a promoter exchange resulted in an increase in CBGA biosynthesis. It is therefore plausible that the medium chain fatty acyl-CoAs produced by our mutant *fusFAS* constructs may be elongated in the FAS^{WT} strain. Thus, downregulation of WT *FAS* may improve MCFA output.

3.1.3 Temporal analysis of FAS mediated MCFA biosynthesis

Having now identified the most efficient FAS mediated hexanoic acid production system to be overexpression of $fusFAS^{lAGSMWFY}$ in the FAS^{WT} strain, we extended the cultivation time to deduce whether production increases over time. We expected this to be true, as FAB generally occurs after rapidly fermentable sugars such as glucose have been consumed and ethanol can be oxidized during the diauxic shift. [284,395,402] This would lead to an increased availability of cytosolic acetyl-CoA and malonyl-CoA for FAB. Extending the cultivation time to 72 h and 96 h led to a hexanoic acid production of 51.2 ± 1.6 mg L^{-1} and 57.4 ± 2.3 mg L^{-1}, respectively (Figure 13).

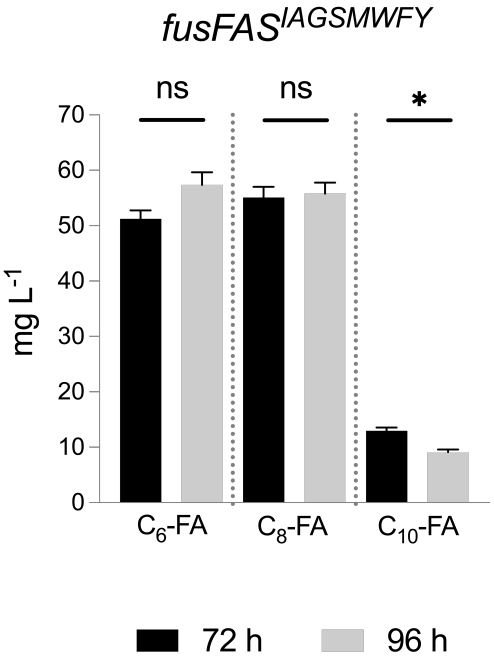

Figure 13 | Extending the cultivation time FAS mediated hexanoic acid biosynthesis

Analysis of C_6-FA, C_8-FA and C_{10}-FA production after 72 h and 96 h in selective buffered YPD media following overexpression of $fusFAS^{lAGSMWFY}$ in a Δ*faa2* KO strain (FAS^{WT}). C_6-FA – hexanoic acid; C_8-FA – octanoic acid; C_{10}-FA – decanoic acid; *n* = 2 biologically independent samples. Data represent mean ± s.d. Statistical analysis was performed using the two-tailed unpaired *t*-test. p > 0.05 = ns (not significant); p < 0.05 = *; p < 0.01 = **; p < 0.001 = ***; p < 0.0001 = ****.

However, this increase was mild and statistically not significant, possible due to the use of duplicates instead of triplicates. Similarly, octanoic acid titers reached 55.1 ± 1.9 mg L^{-1} after 72 h which did not increase after 96 h (55.8 ± 2.0 mg L^{-1}). In contrast, decanoic acid titers were much lower overall, reaching 13.0 ± 0.60 mg L^{-1} after 72 h which was slightly reduced to 9.1 ± 0.50 mg L^{-1} after 96 h. This difference may be due to the ability for decanoic acid to be activated by Faa1p or

due to its conversion to decanoate ethyl ester via Eeb1p as a detoxification mechanisms.[404,405] This may generally explain the much lower titers of decanoic acid measured compared to hexanoic and octanoic acid when using mutant *fusFAS* constructs. Thus, the total MCFA output reached a maximum of 122.3 mg L^{-1} after 96 h which, despite the lack of a direct comparison in a single experiment, is consistently higher than the titers recorded after 48 h when using the same construct in our previous experiments (Figure 11). We therefore deduced that longer cultivation times results in improved MCFA titers and hereafter cultivated strains for a minimum of 72 h when overexpressing a mutant *fusFAS* construct.

3.1.4 Combining mutant FAS constructs in a single strain

Following the conclusion that the *fusFAS*^{IAGSMWFY} was unable to complement a *fas* knockout mutation and required the presence of WT *FAS* to provide LCFAs, we hypothesized hexanoic acid production may increase by combining two mutant *fusFAS* constructs. We therefore co-expressed *fusFAS*^{IAGSMWFY} (KSV030) with *fusFAS*^{IARKGS} (KSV010) in the *fas*^{null} strain. KSV030 was generated by replacing the *hphNT1* marker in ALSV11 with the *kanMX4* marker. By doing so, we aimed to minimize precursor competition and hexanoyl-CoA elongation by WT *FAS* while concomitantly allowing viability through overexpression of *fusFAS*^{IARKGS}. We also compared the total MCFA output

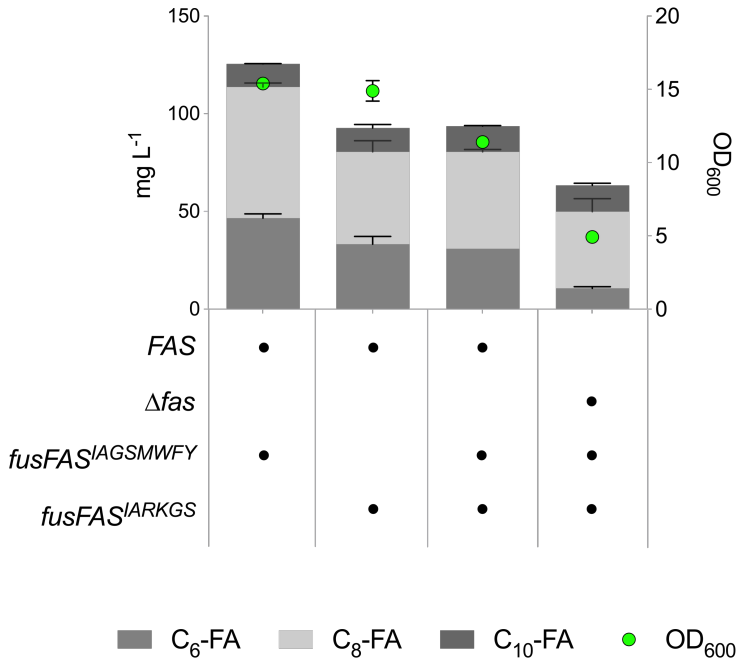

Figure 14 | Combining mutant *fusFAS* constructs in a single *FAS*^{WT} or *fas*^{null} strain

Analysis of MCFA production after 96 h in selective buffered YPD media following overexpression *fusFAS*^{IAGSMWFY} or fusFAS^{IARKGS} individually or together in either the *FAS*^{WT} strain (*FAS*) or the *fas*^{null} strain (Δ*fas*). C_6-FA – hexanoic acid; OD_{600} – optical density at 600 nm. n = 2 biologically independent samples. Data represent mean ± s.d.

in this system to the overexpression of each construct individually. Moreover, this system was compared to the overexpression of both constructs in the *FAS*^{WT} strain (Figure 14).

However, the highest total MCFA (125.5 mg L^{-1}) and hexanoic acid (46.6 mg L^{-1}) production remained when *fusFAS*^{IAGSMWFY} was overexpressed in the *FAS*^{WT} strain, similar to our observations in previous experiments. Meanwhile, the lowest total MCFA (63.4 mg L^{-1}) and hexanoic acid (10.7 mg L^{-1}) production was observed following co-expression in the *fas*^{null} strain. This may be due to diminished growth as the total amount of biomass accumulated was reduced from an OD_{600} of 15.4 and 14.9 following single overexpression of *fusFAS*^{IAGSMWFY} and *fusFAS*^{IARKGS} in the *FAS*^{WT} strain, respectively, to an OD_{600} of 11.4 and 4.9 following co-expression in the *FAS*^{WT} and *fas*^{null} strains, respectively. We therefore conclude that overexpression of multiple large FAS complexes inflicts a metabolic burden on the cells which negatively impacts growth and ultimately MCFA production.

3.1.5 Hexanoic acid biosynthesis via the reverse β-oxidation pathway

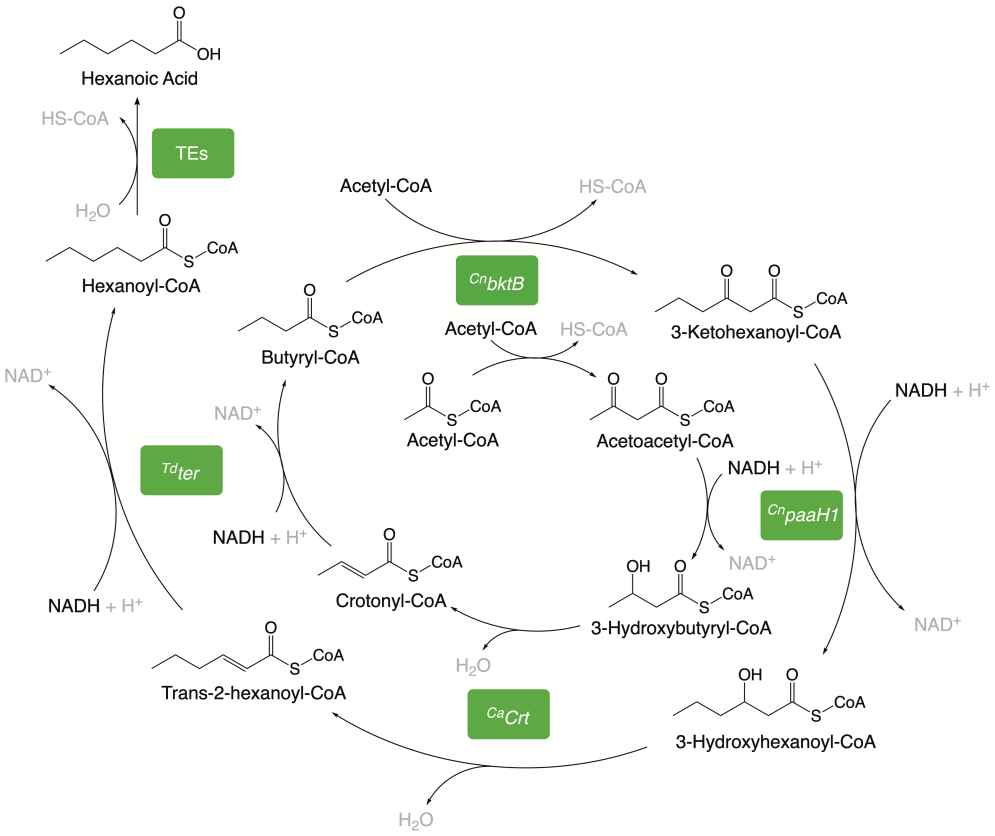

Figure 15 | Overview of the multi-species derived heterologous reverse β-oxidation pathway used to synthesize hexanoyl-CoA in *S. cerevisiae*

Overexpression of a β-ketothiolase (bktB) and a 3-hydroxyacyl-CoA dehydratase (paaH1) from Cupriavidus necator, an enoyl-CoA hydratase (crt) from Clostridium acetobutylicum and a *trans*-enoyl-CoA reductase (ter) from Treponema denticola allows the biosynthesis of hexanoyl-CoA from three molecules of acetyl-CoA while four molecules of NADH are consumed. Hexanoyl-CoA is subsequently hydrolyzed to hexanoic acid via the action of endogenous thioesterases (TEs). This figure was created using ChemDraw 22.2.0 (PerkinElmer).

As an alternative method for synthesizing hexanoyl-CoA in *S. cerevisiae*, we utilized a heterologous rBOX pathway using genes derived from three distinct bacterial species (Figure 15). A β-ketothiolase (*bktB*) and a 3-hydroxyacyl-CoA dehydratase (*paaH1*) were both derived from *Cupriavidus necator* (formally known as *Ralstonia eutropha*), an enoyl-CoA hydratase (*crt*) was derived from *Clostridium acetobutylicum* and a *trans*-enoyl-CoA reductase (*ter*) was derived from *Treponema denticola.* Importantly, these enzymes were able to catalyze the same reactions with substrates of longer chain length, thus allowing the cycle to be repeated using butyryl-CoA and acetyl-CoA as substrates to synthesize hexanoyl-CoA which is hydrolyzed to hexanoic acid, similar to the engineered FAB.

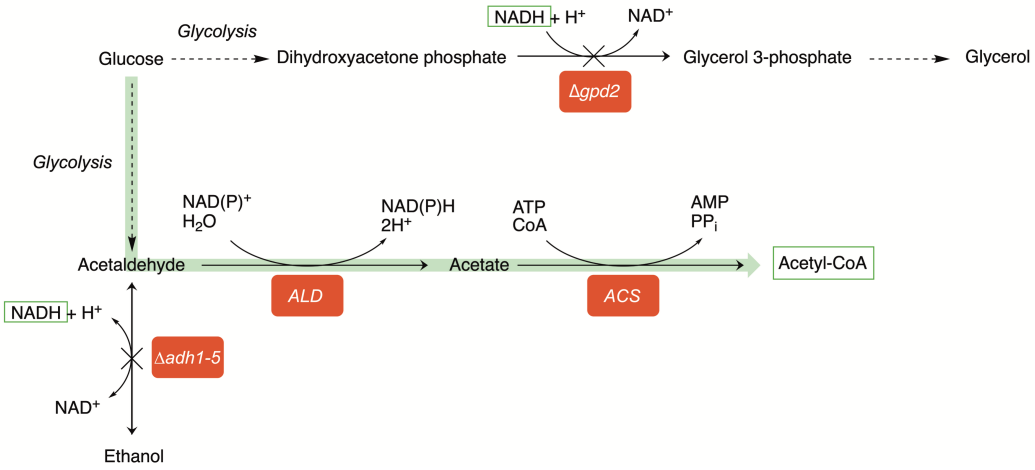

Figure 16 | Overview of KO mutations implemented to optimize hexanoyl-CoA biosynthesis

KO mutations of five *ADH* genes (Δ*adh1-5*) limits ethanol formation and redirects the carbon flux towards acetyl-CoA formation (green arrow). KO mutations of *GPD2* (Δ*gpd2*) reduces glycerol formation. Together, the mutations increase the availability of acetyl-CoA and NADH for rBOX mediated hexanoyl-CoA biosynthesis (green boxes). *ADH* – alcohol dehydrogenase; *GPD* – glycerol 3-phopshate dehydrogenase; *ALD* – aldehyde dehydrogenase; *ACS* – acetyl-CoA synthetase. Figure was created using ChemDraw 22.2.0 (PerkinElmer).

We began by using the strain GDY27 as the rBOX pathway had already been stably integrated into the genome of this strain and it had been metabolically optimized by the knocking out of competing pathways (Figure 16).[393] The modifications included KOs of the five genes encoding ADHs (Δ*adh1-5*) to minimize the reduction of acetaldehyde to ethanol following glycolysis. This has the two-fold effect of increasing cytosolic acetyl-CoA and NADH levels. Acetyl-CoA levels are increased in the absence of ADHs by allowing acetaldehyde to be oxidized by aldehyde dehydrogenases (ALDs), thereby forming acetate. In turn, acetate is activated by acetyl-CoA synthetase (ACS) to form acetyl-CoA. Furthermore, as NADH is oxidized during ethanol production, knocking out *ADHs* concomitantly reduces NADH consumption. Additionally, *GPD2*, which encodes the NADH-dependent glycerol 3-phosphate dehydrogenase and is involved in the formation of glycerol, was knocked out, thus further increasing the availability of NADH for rBOX mediated hexanoyl-CoA biosynthesis.

3.1.6 Preventing hexanoic acid degradation in *S. cerevisiae*

As in the case of engineering of the FAB pathway, we aimed to prevent the degradation of hexanoic acid via peroxisomal β-oxidation which occurs after TE mediated hydrolysis hexanoyl-CoA. This was achieved by introducing an *faa2* KO mutation in GDY27 using CRISPR/Cas9. The accumulation of hexanoic acid in the media of the Δ*faa2* strain (KSY13, hereafter referred to as *yr*BOX1) was compared to the *FAA2* parent strain (GDY27) after 48 h and 72 h of cultivation in buffered YPD media (Figure 17A). We observed a 42% increase in hexanoic acid titer after 48 h in *yr*BOX1 (56.0 ± 1.4 mg L^{-1}) compared to the parent strain (39.4 ± 5.3 mg L^{-1}). However, after 72 h, the *FAA2* strain completely consumed the hexanoic acid which had accumulated in the media (0.22 ± 0.02 mg L^{-1}). In contrast, the titers remained stable in *yr*BOX1 (56.3 ± 2.4 mg L^{-1}). This would suggest that the degradation of hexanoic acid begins before 48 h or occurs concomitantly to biosynthesis. Analysis of glucose consumption over time showed that glucose was fully consumed by 48 h (Figure 17B). As hexanoic acid titers did not increase after 48 h, we deduce that biosynthesis of hexanoyl-CoA via the rBOX pathway is directly coupled to glucose consumption and terminates once glucose is depleted.

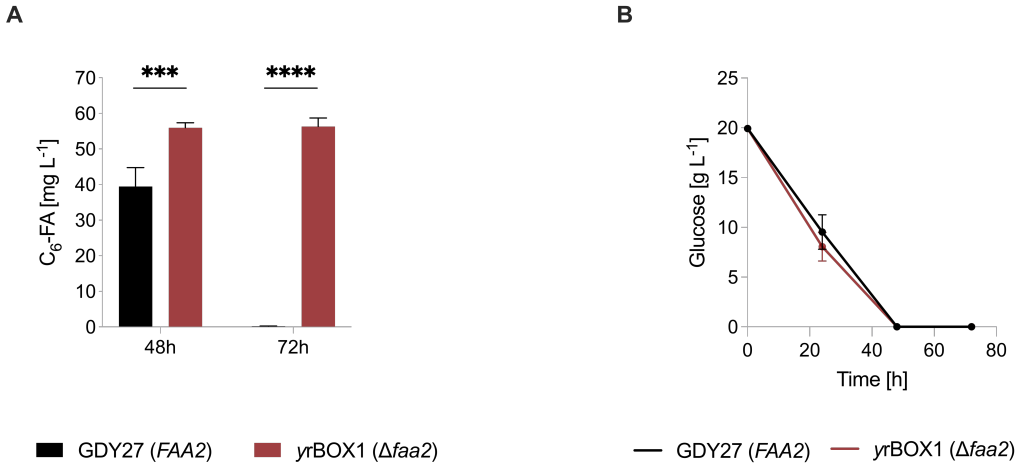

Figure 17 | Preventing hexanoic acid degradation by knocking out *FAA2*

(A) Comparison of *FAA2* (GDY27) and *faa2* KO mutation (yrBOX1) on hexanoic acid titers after 48 h and 72 h in buffered YPD media. **(B)** Analysis of glucose consumption over time. C_6-FA – hexanoic acid. n = 3 biologically independent samples. Data represent mean ± s.d. Statistical analysis was performed using the two-tailed unpaired t-test. $p > 0.05$ = ns (not significant); $p < 0.05$ = *; $p < 0.01$ = **; $p < 0.001$ = ***; $p < 0.0001$ = ****.

3.1.7 Combining the rBOX and FAB pathways in a single strain

Due to the observations that rBOX mediated hexanoyl-CoA biosynthesis occurs during the glucose consumption stage (3.1.6) and engineered FAS mediated MCFA biosynthesis occurs at later growth stages (3.1.3), we envisaged that co-expression of the rBOX and the FAB pathways in a single strain may increase hexanoyl-CoA production due to the temporal distribution of MCFA biosynthesis. To investigate this, we overexpressed *fusFAS*^{IAGSMWFY} (KSV30) in *yr*BOX1 and

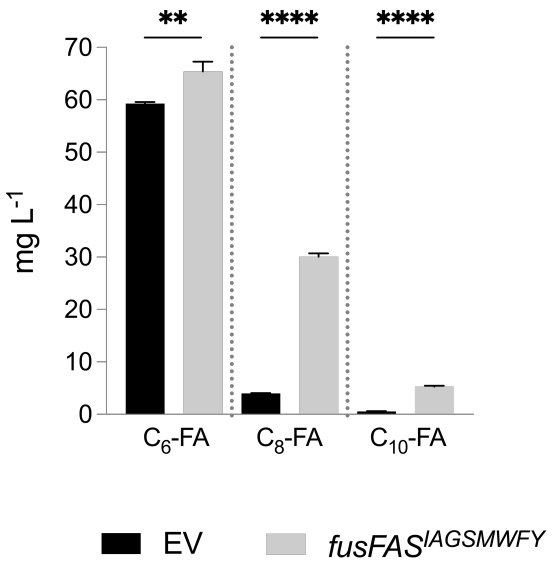

Figure 18 | Combining the rBOX and engineered FAB pathways

The *fusFAS*^{lAGSMWFY} construct (KSV30) was overexpressed in the rBOX strain, *y*rBOX1. MCFA output was analyzed after 96 h of cultivation in selective buffered YPD media. C_6-FA – hexanoic acid; C_8-FA – octanoic acid; C_{10}-FA – decanoic acid. rBOX – reverse β-oxidation; FAB – fatty acid biosynthesis; MCFA – medium chain fatty acid. *n* = 3 biologically independent samples. Data represent mean ± s.d. Statistical analysis was performed using the two-tailed unpaired *t*-test. $p > 0.05$ = ns (not significant); $p < 0.05$ = *; $p < 0.01$ = **; $p < 0.001$ = ***; $p < 0.0001$ = ****.

observed an increase of 10% hexanoic acid reaching 65.4 mg L^{-1} compared the EV control (pRS313K) (59.3 mg L-1) after 96 h of cultivation in selective buffered YPD (Figure 18).

A more notable increase of 7.5-fold and 9.5-fold was observed for octanoic acid (30.1 ± 0.66 mg L^{-1}) and decanoic acid (5.3 ± 0.13 mg L^{-1}) production when *fusFAS*^{lAGSMWFY} was overexpressed compared to the EV control. This is in line with our previous data which show that the spectrum of MCFA production is broader when modifying the FAB pathway compared to the rBOX pathway which is much more specific for hexanoic acid production. Thus, the total MCFA increased by 63%, reaching 100.8 mg L^{-1}.

3.2 Optimizing hexanoyl-CoA biosynthesis in *S. cerevisiae*

3.2.1 Increasing endogenous coenzyme A biosynthesis

The increase in hexanoic acid derived from *fusFAS*^{IAGSMWFY} was substantially lower when overexpressed in the rBOX optimized strain *yr*BOX1 (3.1.7) than when *fusFAS*^{IAGSMWFY} was overexpressed in the *FAS*^{WT} strain which did not contain the rBOX pathway (3.1.3). We therefore suspected a limitation in acetyl-CoA supply when both pathways were combined. To address this, we proceeded by upregulating CoA biosynthesis as CoA supply directly correlates with increased cytosolic acetyl-CoA.[406] We began by cloning a codon-optimized PanK gene derived from *E. coli* (*^{Ec}coaA*) under the control of the strongly expressed glycolytic 3-phosphoglycerate kinase 1 promoter (P_{PGK1}), into a high-copy (*2μ*) plasmid containing either the *HIS3* marker (KSV51) or the *hphNT1* maker (KSV52). These constructs were tested in *yr*BOX1 and hexanoic acid production was measured after 24 h, 48 h and 72 h in selective buffered SCD media (Figure 19A) or selective buffered YPD media (Figure 19B). We observed an increase in hexanoic acid production when overexpressing *^{Ec}coaA* in both synthetic and complex media, and production increased over time. Titers were higher in complex media reaching a maximum of 62.7 ± 4.3 mg L^{-1} after 72 h compared to 39.0 ± 2.5 mg L^{-1} in the EV control. This corresponds to an increase of 61%.

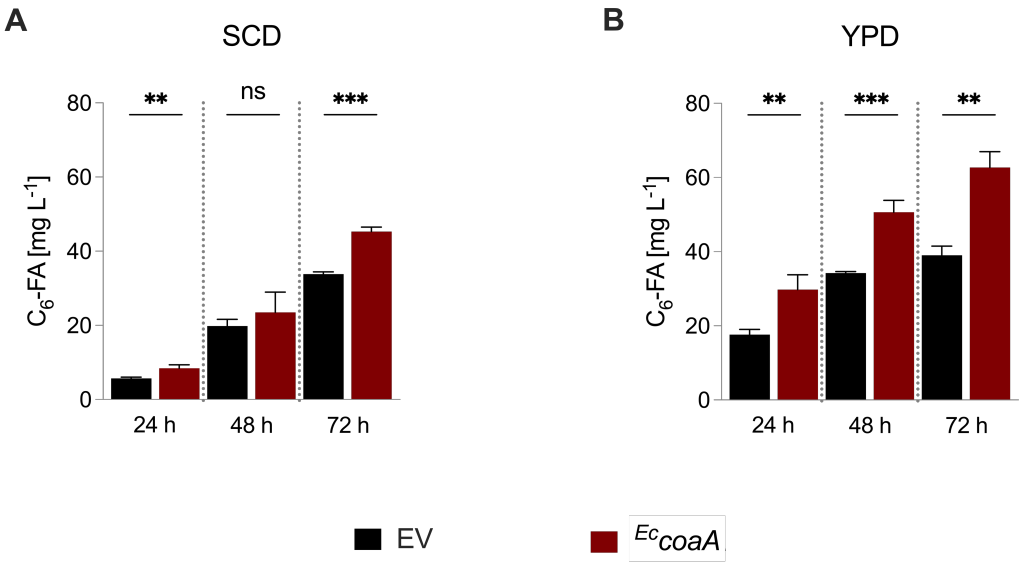

Figure 19 | Plasmid-based overexpression of *E. coli* pantothenate kinase (PanK) in rBOX optimized strain

An *E. coli* derived PanK (*^{Ec}coaA*) was cloned using an auxotrophic marker (KSV51) or a dominant marker (KSV52) and overexpressed in the rBOX pathway optimized strain *yr*BOX1. C_6-FA production was measured after 24 h, 48 h and 72 h of cultivation in either **(A)** selective buffered synthetic media (SCD) or **(B)** selective buffered complex media (YPD) and compared to an empty vector (EV) control. C_6-FA – hexanoic acid; rBOX – reverse β-oxidation. *n* = 3 biologically independent samples. Data represent mean ± s.d. Statistical analysis was performed using the two-tailed unpaired *t*-test. p > 0.05 = ns (not significant); p < 0.05 = *; p < 0.01 = **; p < 0.001 = ***; p < 0.0001 = ****.

As we observed positive effects through plasmid-based overexpression of PanK, we subsequently stably integrated *Ec*coaA into the genome of *yr*BOX1. For this, we used two approaches. First, we integrated *Ec*coaA into the *LEU2* locus via HR. For this, the integration plasmid KSV53 was used which contained a downstream *natNT2* resistance marker, thereby replacing the inactive *leu2-3,112* gene. The resultant strain, KSY22, hereafter referred to as *yr*BOX2, increased hexanoic acid production 2.2-fold, reaching a titer of 89.9 ± 4.5 mg L^{-1} after 72 h compared to 40.1 ± 3.0 mg L^{-1} in *yr*BOX1 (Figure 20A). Moreover, growth of *yr*BOX2 was reduced as the total biomass decreased from an OD_{600} of 11.5 ± 0.53 in the parent strain to 8.5 ± 0.42 (Figure 20B). This may be due to the toxicity of increased concentrations of hexanoic acid or due to the increased consumption of ATP by PanK as well as the downstream enzymes, Cab4p and Cab5p, which are involved in CoA biosynthesis. Notably, ethanol production remained stable reaching approximately 3.5 g L^{-1} in both strains (Figure 20C).

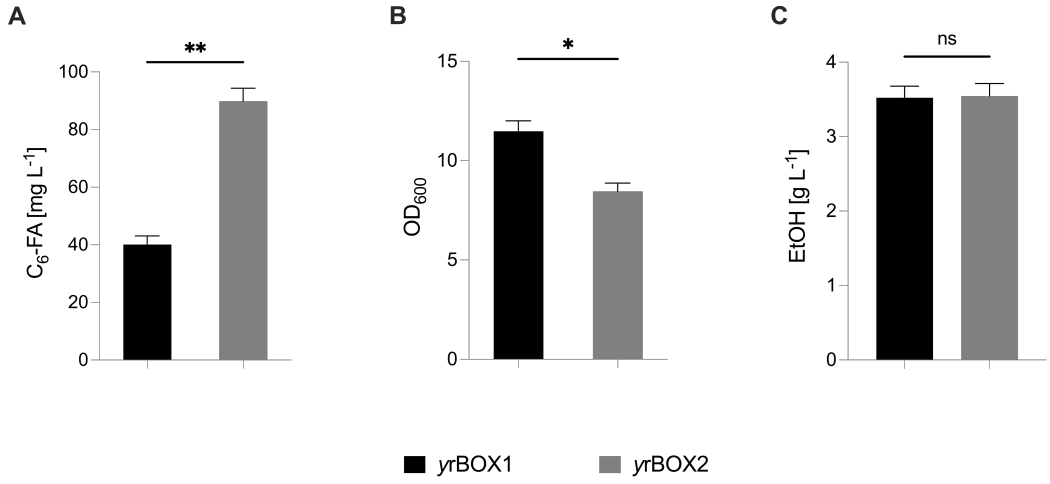

Figure 20 | Genomic integration of *E. coli* pantothenate kinase (PanK) in rBOX optimized strain

Genomic integration of an *E. coli* derived PanK (*Ec*coaA) into the *LEU2* locus of the rBOX pathway optimized strain *yr*BOX1 via HR. **(A)** C_6-FA production, **(B)** growth (OD_{600}) and **(C)** ethanol production were measured after 48 h cultivation in buffered YPD media. rBOX – reverse β-oxidation; C_6-FA – hexanoic acid; OD_{600} – optical density at 600 nm; EtOH – ethanol. *n* = 2 biologically independent samples. Data represent mean ± s.d. Statistical analysis was performed using the two-tailed unpaired *t*-test. p > 0.05 = ns (not significant); p < 0.05 = *; p < 0.01 = **; p < 0.001 = ***; p < 0.0001 = ****.

Alternately, we integrated *Ec*coaA via CRISPR/Cas9 into the *ADH6* locus of *yr*BOX1, thereby knocking out a gene encoding an additional ADH. The *Ec*coaA overexpression cassette was amplified from the expression plasmid KSV52. Through this, we aimed to increase CoA biosynthesis and concomitantly decrease ethanol formation, which in turn should increase carbon flux from acetaldehyde to acetate and therefore result in a greater supply of acetyl-CoA. Moreover, through the scarless integration process of using CRISPR/Cas9, we prevented an unnecessary introduction of the *natNT2* resistance marker into the genome. However, the resultant strain, KSY23, produced less hexanoic acid after 48 h (7.0 ± 0.16 mg L^{-1}) than *yr*BOX1 (45.8 ± 0.71 mg L^{-1}; Figure 21A). This is likely due to poor growth as the OD_{600} was significantly lower after 48 h in KSY23 (0.98 ± 0.03) than in the parent strain (11.5 ± 0.81; Figure 21D). This was also reflected in the slow glucose consumption, as only approximately 9% had been consumed after 48 h in KSY23

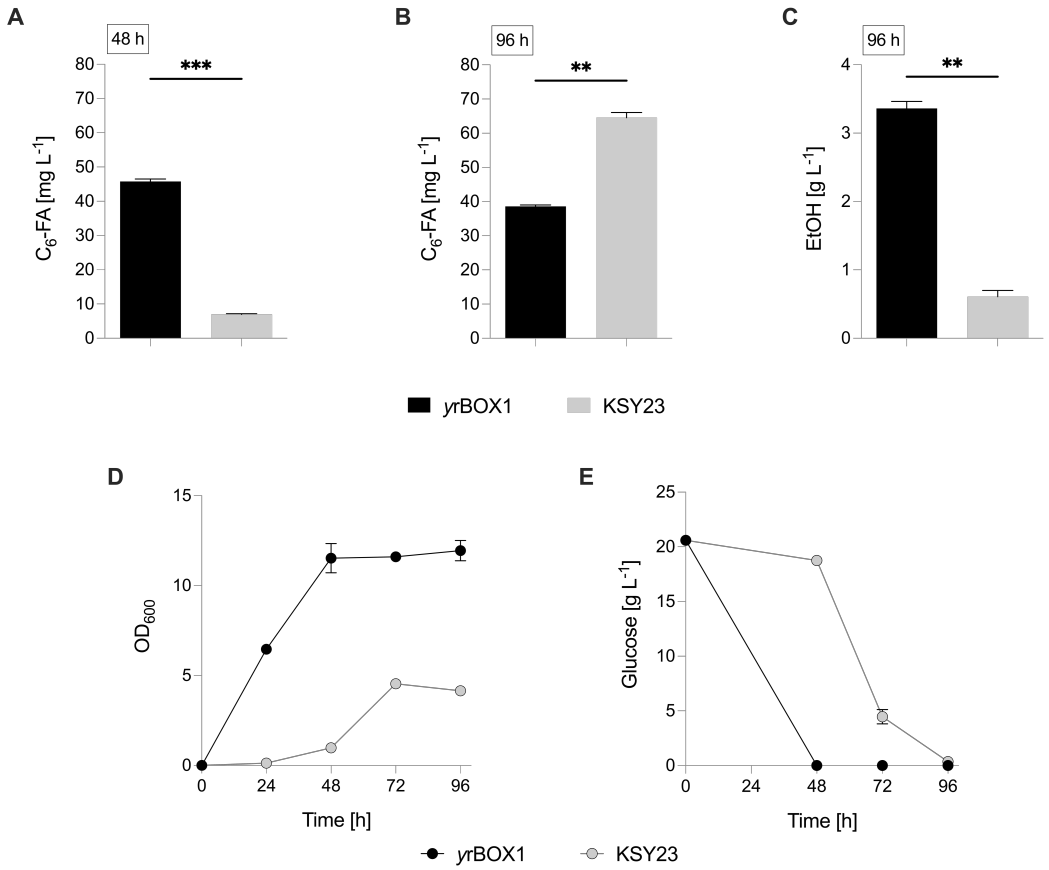

Figure 21 | Integration of *E. coli* PanK into *ADH6* locus

E. coli PanK (*Ec*coaA) was introduced into the genome of the rBOX pathway optimized strain, *yr*BOX1, by replacing the *ADH6* gene (KSY23) and the strains were cultivated in buffered YPD media. **(A-B)** C_6-FA production was measured after 48 h and 96 h and **(C)** ethanol production was measured after 96 h. **(D)** growth (OD_{600}) and **(E)** glucose consumption were measured over time. PanK – pantothenate kinase; rBOX – reverse β-oxidation; C_6-FA – hexanoic acid; EtOH – ethanol; OD_{600} – optical density at 600 nm. *n* = 2 biologically independent samples. Data represent mean ± s.d. Statistical analysis was performed using the two-tailed unpaired *t*-test. p > 0.05 = ns (not significant); p < 0.05 = *; p < 0.01 = **; p < 0.001 = ***; p < 0.0001 = ****.

while glucose was completely consumed in *yr*BOX1 at the same time-point (Figure 21E). We therefore extended the cultivation time until 96 h to allow complete glucose consumption. Indeed, KSY23 continued to grow and consume glucose after 48 h which was translated into a 67% increase in hexanoic acid biosynthesis (64.5 ± 1.5 mg L^{-1}) compared to *yr*BOX1 (38.6 ± 0.42 mg L^{-1}; Figure 21B). *yr*BOX1 did not continue to grow significantly after 48 h, however, the total accumulation of biomass of KSY23 was greatly reduced reaching a final OD_{600} after 96 h of 4.2 ± 0.28 compared to 12.0 ± 0.57 (Figure 21D). Although a reduction in biomass was expected after observing growth effects following PanK integration in *yr*BOX2 (*leu2*Δ::*Ec*coaA, *natNT2*), the effect was much stronger in the *adh6* KO strain. This is likely due to the limited ability for the strain to reduce cytosolic acetaldehyde to ethanol following the KO of a sixth *ADH* gene, and this was reflected in the 82% decrease in ethanol production (0.61 ± 0.09 g L^{-1}) compared to *yr*BOX1 (3.4 ± 0.10 g L^{-1}; Figure 21C). Thus, acetaldehyde is forcibly oxidized to acetate which increases its intracellular concentration during the exponential growth phase. This increase in acetate may be a cause of toxicity resulting in the growth defects observed in KSY23.[407–409] Indeed, many studies

have focused on reducing acetate formation or increasing the tolerance of *S. cerevisiae* towards acetate in biotechnological applications, particularly due to the presence of high acetic acid concentrations released following pretreatment of lignocellulosic acid, an attractive substrate commonly used in industrial processes.[409,410] One example of reducing acetate formation is through its detoxification by upregulating the expression of acetyl-CoA synthetases (*ACS1/2*).[411,412] This may be a beneficial approach in our system as we aim to increase cytosolic acetyl-CoA, although this would further increase ATP consumption which may negatively impact growth and strain fitness. Nevertheless, our data suggest that the metabolic flux was successfully redirected away from ethanol formation and towards acetyl-CoA through the synchronized KO of *ADH6* and the introduction of *^{Ec}coaA*. This ultimately resulted in increased hexanoic acid biosynthesis; however, it also came at the cost of strain fitness.

Finally, as it would be industrially unfavorable to extend bioproduction processes until 96 h, we analyzed the production of hexanoic acid of *yr*BOX1, *yr*BOX2 (*leu2*Δ::*^{Ec}coaA, natNT2*) and KSY23 (*adh6*Δ::*^{Ec}coaA*) after 48 h to achieve a direct comparison of the strains. Similar to our previous results, we observed the highest production of hexanoic acid in *yr*BOX2 (71.0 ± 6.9 mg L^{-1}), corresponding to a 2.1-fold increase over *yr*BOX1 (33.8 ± 0.55 mg L^{-1}) and a 2-fold increase over KSY23 (34.8 ± 1.1 mg L^{-1}; Figure 22A). Interestingly, KSY23 production was similar to *yr*BOX1 after 48 h in contrast to our previous results. Accordingly, glucose consumption was higher at this time-point compared to the previous experiment, as approximately 64% had been consumed by 48 h (Figure 22B). This reflects slight differences in experimental conditions. In contrast, glucose was fully consumed by both *yr*BOX1 and *yr*BOX2 after 48 h. We also observed a decrease in growth in both PanK overexpressing strains, reaching final OD_{600} values of 9.0 ± 0.33 (*yr*BOX1) and 6.9 ± 0.46 (KSY23) compared to 12.0 ± 0.19 (*yr*BOX1; Figure 22C). Finally, ethanol production was again almost identical in *yr*BOX1 (3.4 ± 0.03) and *yr*BOX2 (3.4 ± 0.05) whereas no ethanol was detected in KSY23 (Figure 22D). These data reinforce our previous data and allow us to conclude

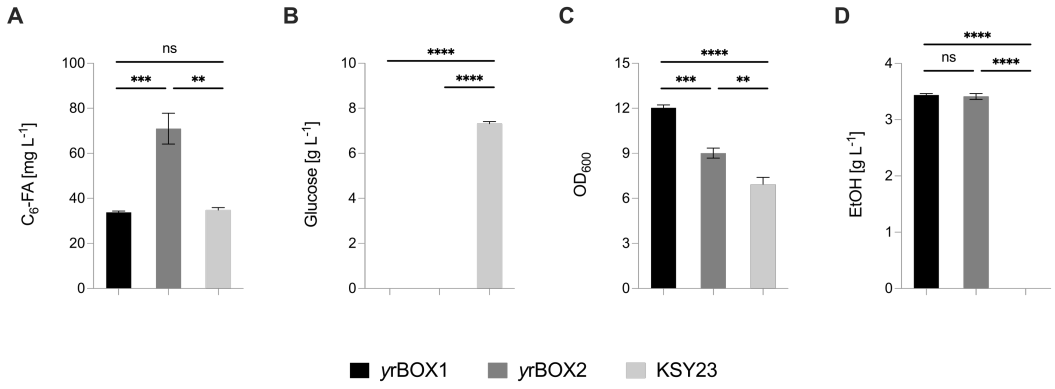

Figure 22 | Comparison of PanK overexpressing strains

The PanK overexpressing strains *yr*BOX1 (*leu2*Δ::*^{Ec}coaA*, *natNT2*) and KSY23 (*adh6*Δ::*^{Ec}coaA*) were compared to their common parent strain, *yr*BOX1. **(A)** C_6-FA production, **(B)** growth (OD_{600}), **(C)** EtOH production and **(D)** glucose consumption were measured after 48 h cultivation in buffered YPD media. PanK – pantothenate kinase; C_6-FA – hexanoic acid; OD_{600} – optical density at 600 nm; EtOH – ethanol. *n* = 3 biologically independent samples. Data represent mean ± s.d. Statistical analysis was performed using the two-tailed unpaired *t*-test. p > 0.05 = ns (not significant); p < 0.05 = *; p < 0.01 = **; p < 0.001 = ***; p < 0.0001 = ****.

that overexpression of PanK increases rBOX mediated hexanoic acid biosynthesis by increasing the supply of acetyl-CoA. However, this also has a negative impact on growth which is exacerbated through the *adh6* KO mutation, thus reducing hexanoic acid production in KSY23. We also conclude that the strains require a basal level of ADH activity to maintain sufficient strain fitness and thereby achieve higher production titers. Taking these aspects into consideration, we continued engineering an OA producing strain using *yr*BOX2.

3.2.2 Preventing feedback regulation of *E. coli* derived PanK

E. coli PanK (*^{Ec}coaA*) is allosterically regulated via feedback inhibition by free CoA. It was found that binding of CoA was prevented through the mutation of arginine to alanine at position 106 (R106A). However, the mutant enzyme only retained only 54% of its catalytic activity.[413] We incorporated this mutation into the codon-optimized *^{Ec}coaA* gene and cloned this into an integration plasmid containing the *natNT2* selection marker (KSV81). The feedback resistant *^{Ec}coaA^{R106A}* gene was subsequently integrated into the genome of *yr*BOX1 at the *LEU2* locus in a manner identical to the engineering of *yr*BOX2 (*leu2*Δ::*^{Ec}coaA*, *natNT2*), thereby generating KSY28 (*leu2*Δ::*^{Ec}coaA^{R106A}*, *natNT2*). However, following the screening of 14 individual colonies which had been positively verified via PCR analysis, no improvement in hexanoic acid biosynthesis was observed when compared to strain *yr*BOX2 which contained the WT *^{Ec}coaA* construct (Figure 23). Nevertheless, both strains improved biosynthesis over their common parent strain, *yr*BOX1.

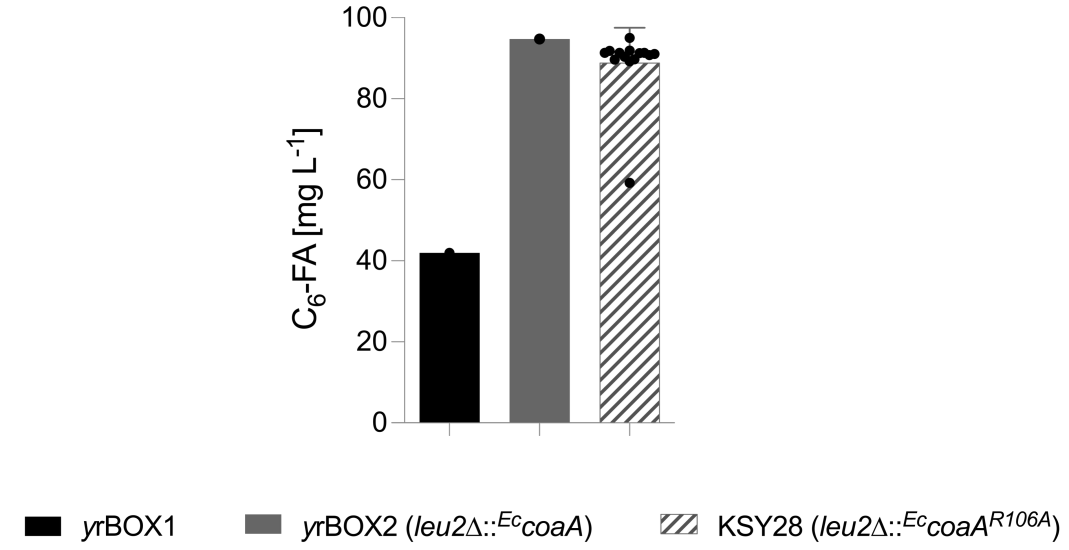

Figure 23 | Inhibiting feedback regulation of *E. coli* PanK

A feedback resistant variant of *E. coli* PanK containing an arginine to alanine substitution (*^{Ec}coaA^{R106A}*) was introduced into the *LEU2* locus of *yr*BOX1 (KSY28). 14 positive clones were verified via PCR and C_6-FA production was analyzed after 48 h cultivation in buffered YPD media. Production was compared to non-feedback resistant *^{Ec}coaA* strain (*yr*BOX2) and their common parent strain (*yr*BOX1). C_6-FA - hexanoic acid; *Ec* – *E. coli*; Data represent *n* = 1 biological sample (*yr*BOX1 and *yr*BOX2) and *n* = 14 biologically independent clones of *leu2*Δ::*^{Ec}coaA^{R106A}*. No statistical analysis was performed.

Various explanations for the lack of improvement in hexanoic acid biosynthesis may exist. As previously mentioned, a decrease in the catalytic activity of ^{Ec}CoaA^{R106A} may counter the positive effects of prolonged activity due to feedback inhibition, thereby resulting in a net zero effect. Alternatively, the explanation could be rooted in the low levels of unacetylated cytosolic CoA present in *S. cerevisiae*, as free CoA is generally directly used for acetate activation. Thus, the second explanation would render the R106A mutation redundant in our strains and therefore would only lead to a decrease in catalytic activity. However, as we did not observe a decrease in hexanoic acid biosynthesis compared to the WT construct, we cannot confidently verify this as the sole explanation. Finally, an explanation may be found when considering the endogenous PanK, encoded by *CAB1*. Unlike the bacterial PanK, Cab1p is regulated via feedback inhibition by acetyl-CoA, similar to PanK found in other eukaryotes.[414,415] If we can assume an increase in cytosolic acetyl-CoA when deregulating ^{Ec}CoaA, then an increase in acetyl-CoA mediated inhibition of Cab1p may explain the net zero effect observed, as both PanKs presumably work in parallel to phosphorylate pantothenate. To address this, Cab1p can be made resistant to inhibition by acetyl-CoA by mutating tryptophan to arginine at position 331 (W331R).[414] *CAB1^{W331R}* was shown to increase catalytic activity 4-fold compared to the WT variant and overexpression of *CAB1^{W331R}* in addition to the remaining genes involved in the endogenous CoA biosynthesis pathway (*CAB2, CAB3, HAL2, CAB4, CAB5*) improved CoA biosynthesis in *S. cerevisiae* 15-fold.[414] Thus, applying these modifications to our pathway may improve MCFA titers, including hexanoic acid, as well as other acetyl-CoA derived natural products including polyketides, terpenoids or, as will be demonstrated in this work, olivetolic acid (OA). Therefore, in this work, later strains were constructed using the feedback resistant *^{Ec}coaA^{R106A}* construct in consideration of potential engineering approaches which may lead to an increase in free cytosolic CoA or in a deregulated endogenous PanK.

3.2.3 Combining rBOX and mutant FAB pathways with PanK overexpression

Having now increased the supply of acetyl-CoA through PanK overexpression, we attempted to increase hexanoic acid biosynthesis by combining the rBOX and mutant FAB pathways. For this, we overexpressed *fusFAS^{IAGSMWFY}* (ALSV11) in the dual PanK and rBOX overexpressing strain *yr*BOX2 and the rBOX overexpressing strain *yr*BOX1. MCFA production and growth were measured after 120 h cultivation in selective buffered YPD (Figure 24). The cultivation time was extended to 120 h to take into consideration the slower growth and production rates which were observed in the PanK overexpressing strains and to ensure sufficient time for FAS mediated biosynthesis.

Consistent with our previous data, we observed 10.7% increase in hexanoic acid production of when *fusFAS^{IAGSMWFY}* was overexpressed in *yr*BOX1 (58.4 ± 3.0 mg L^{-1}) compared to the EV control (52.7 ± 1.1 mg L^{-1}; Figure 24A). Furthermore, hexanoic acid production was increased 2.2-

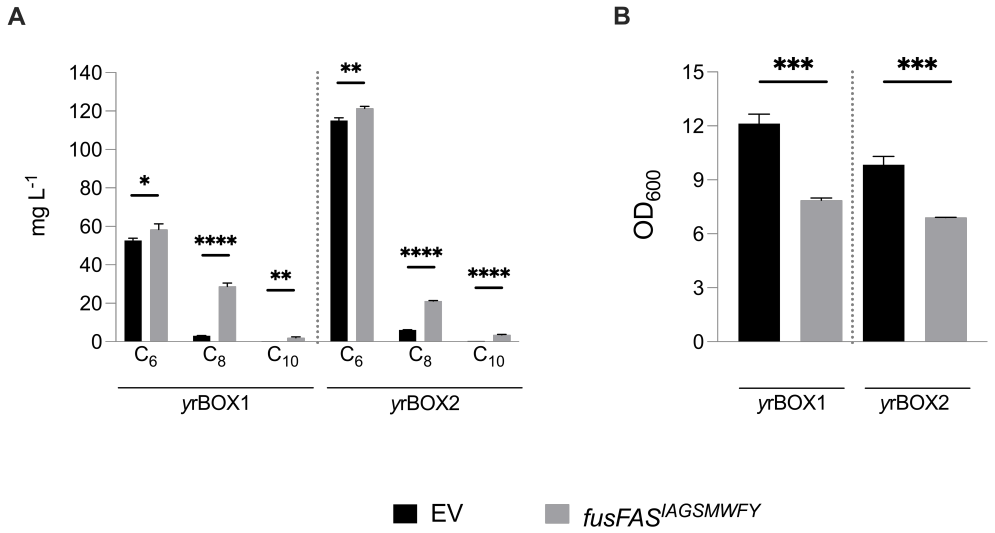

Figure 24 | Combining mutant FAB pathway and rBOX pathway in PanK overexpressing strain.

fusFAS^{IAGSMWFY} (ALVS11) was overexpressed in an rBOX optimized strain with basal PanK expression (*yr*BOX1) or with PanK overexpression (*yr*BOX2) and compared to an EV control. **(A)** MCFA production and **(B)** growth (OD_{600}) were measured after 120 h cultivation in selective buffered YPD media. MCFA – medium chain fatty acid; C_6 – hexanoic acid; C_8 – octanoic acid; C_{10} – decanoic acid; OD_{600} – optical density at 600 n; EV – empty vector. *n* = 3 biologically independent samples. Data represent mean ± s.d. Statistical analysis was performed using the two-tailed unpaired *t*-test. p > 0.05 = ns (not significant); p < 0.05 = *; p < 0.01 = **; p < 0.001 = ***; p < 0.0001 = ****.

fold in the *yr*BOX2 EV control (115.1 ± 1.4 mg L^{-1}) compared to the *yr*BOX1 EV control as expected. Finally, overexpression of *fusFAS*^{IAGSMWFY} in *yr*BOX2 increased hexanoic acid production further to 121.4 ± 1.1 mg L^{-1}. However, this only corresponded to a 5.5% increase over its respective EV control. Moreover, similar to our previous observations (3.1.7), octanoic acid and decanoic acid titers also increased substantially in both strains when overexpressing *fusFAS*^{IAGSMWFY}. Octanoic acid production increased from 2.7 ± 0.05 mg L^{-1} to 27.1 ± 1.0 mg L^{-1} in *yr*BOX1 and from 5.6 ± 0.10 mg L^{-1} to 20.1 ± 0.76 mg L^{-1} in *yr*BOX2. Similarly, decanoic acid production increased from 0.49 ± 0.01 mg L^{-1} to 3.9 ± 0.81 mg L^{-1} in *yr*BOX1 and from 0.65 ± 0.02 mg L^{-1} to 5.4 ± 0.26 mg L^{-1} in *yr*BOX2. Furthermore, growth was reduced by 35% in *yr*BOX1 and by 30% in *yr*BOX2 following the overexpression of *fusFAS*^{IAGSMWFY} (Figure 24B). Although hexanoic acid production increased when combining both pathways, increasing the supply of acetyl-CoA through PanK overexpression did not improve engineered FAS mediated MCFA biosynthesis but surprisingly seemed to have the opposite effect as its overall contribution to MCFA biosynthesis was reduced. The total MCFA output increased by 59% from 56.0 mg L^{-1} to 89.1 mg L^{-1} when overexpressing *fusFAS*^{IAGSMWFY} in *yr*BOX1, whereas the increase from 121.6 mg L^{-1} to 146.1 mg L^{-1} observed in *yr*BOX2 corresponded to only 20%. As the overexpression of *fusFAS*^{IAGSMWFY} also had a significant effect on growth, we considered this to be the cause of the reduction in total MCFA contribution. Indeed, upon closer analysis of MCFA titers in relation to biomass, it was revealed that overexpression of *fusFAS*^{IAGSMWFY} contributed more to total MCFA biosynthesis per cell in *yr*BOX1 (11.3 mg L^{-1} OD_{600}^{-1}), corresponding to a 2.5-fold increase over the EV control (4.6 mg L^{-1} OD_{600}^{-1}), than in *yr*BOX2 (21.2 mg L^{-1} OD_{600}^{-1}), corresponding to a 1.7-fold increase over its EV control (12.3 mg L^{-1} OD_{600}^{-1}). Taking these observations together, we conclude that combining the rBOX and

mutant FAB pathways increases the production of hexanoic acid, however, there is a significant reduction in the contribution of the mutant FAB pathway towards MCFA biosynthesis when PanK is overexpressed. There must therefore be additional factors which limit the production capacity of the mutant FAB pathway. A possible explanation is the supply of malonyl-CoA which will be discussed later (3.3.7). Moreover, introducing the FAB pathway substantially decreases the specificity of hexanoic acid production which is not preferable in the context of OA production. Nevertheless, in applications in which an increase in total MCFA output is desired, we demonstrate that combining the pathways is a viable option.

3.2.4 Investigating pantothenate limitation following upregulated CoA biosynthesis

Next, we aimed to investigate whether pantothenate is limiting the biosynthesis of hexanoic acid following overexpression of the *E. coli* derived PanK (*^{Ec}coaA*). To achieve this, we cultivated the *^{Ec}coaA* overexpressing strain *yr*BOX2 and its parent strain, *yr*BOX1, in pantothenate-free SMD media. The cultures were then supplemented with increasing concentrations of pantothenate (0, 20, 40, 60, 80 or 100 µM) and cultivated for 168 h (Figure 25). Without supplementation of pantothenate, comparable titers of hexanoic acid were produced by *yr*BOX1 (31.5 ± 6.3 mg L^{-1}) and *yr*BOX2 (34.1 ± 2.7 mg L^{-1}). However, a notable difference was observed upon supplementation of

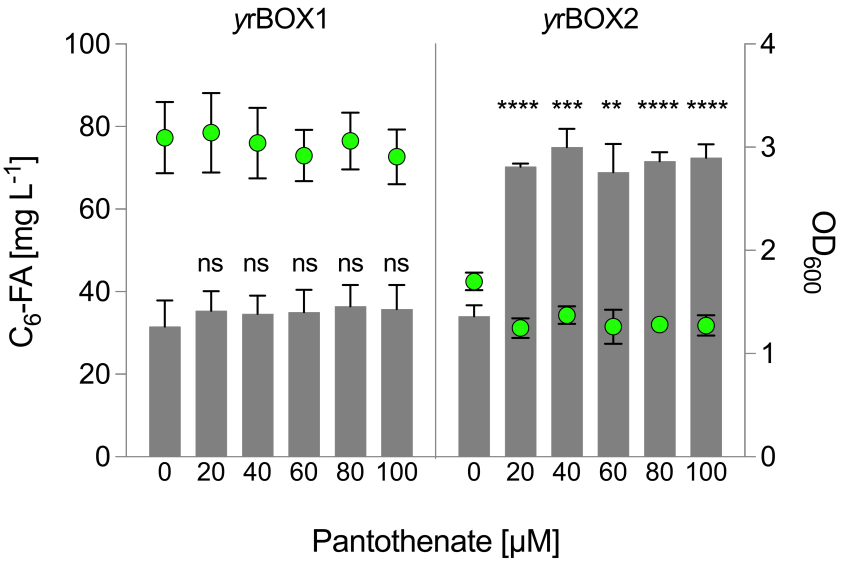

Figure 25 | Investigating the limitation of pantothenate supply following PanK overexpression

The rBOX pathway optimized strains with normal PanK expression (*yr*BOX1) or PanK overexpression (*yr*BOX2) were cultivated in SMD media supplemented with increasing concentrations of Ca-Pantothenate (0, 20, 40, 60, 80 or 100 µM) for 168 h and C_6-FA production and growth (OD_{600}) were measured. PanK – pantothenate kinase; C_6-FA – hexanoic acid; OD_{600} – optical density at 600 nm. *n* = 3 biologically independent samples. Data represent mean ± s.d. Statistical analysis was performed using the two-tailed unpaired *t*-test. p > 0.05 = ns (not significant); p < 0.05 = *; p < 0.01 = **; p < 0.001 = ***; p < 0.0001 = ****.

the cultures with 20 µM pantothenate. A mild, non-significant increase was observed in *yr*BOX1 (35.4 ± 4.7 mg L^{-1}) while production increased 2.1-fold in *yr*BOX2 (70.3 ± 0.8 mg L^{-1}). Despite this, increasing the concentration of pantothenate above 20 µM had no further implication on hexanoic acid biosynthesis in either strain. This would suggest saturation of pantothenate supply for PanK and the occurrence of another limiting factor such as PanK or downstream enzyme activity within the CoA biosynthesis pathway.

3.2.5 Increasing endogenous pantothenate biosynthesis

Having deduced that pantothenate is limiting CoA biosynthesis when PanK is overexpressed, we aimed to upregulate the endogenous supply of pantothenate through the overexpression of the FAD-dependent polyamine oxidase, *FMS1*.[416] We initially used a plasmid-based approach and tested three promoters of varying expression strengths and temporal regulation to control *FMS1* expression using high copy (*2µ*) plasmids containing the *URA3* selection marker. The promoters tested were the ADH1 promoter (P_{ADH1}; KSV66) which had previously been demonstrated for the overexpression of *FMS1* to enhance pantothenate biosynthesis in yeast,[391,417] the heat shock protein 26 promoter (P_{HSP26}; KSV67) and the translation elongation factor 1 alpha promoter (P_{TEF1}; KSV68). These constructs were overexpressed in *yr*BOX2 (Figure 26).

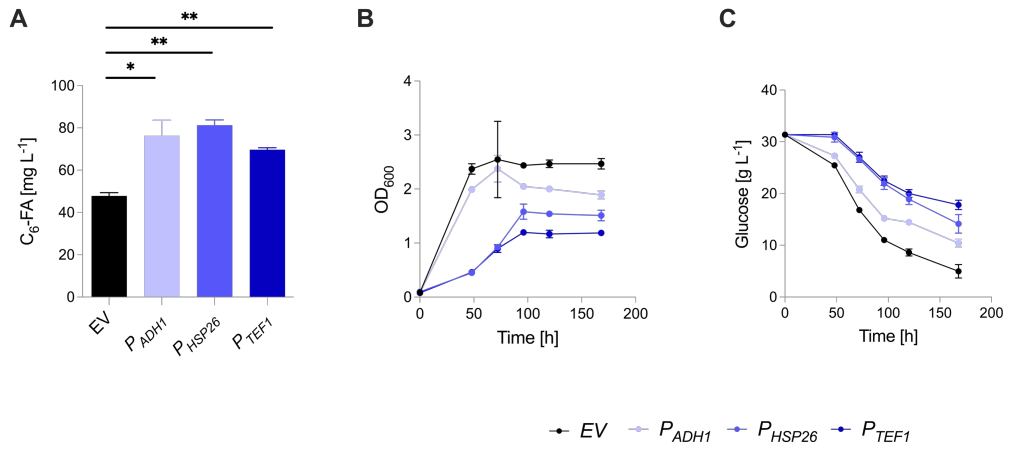

Figure 26 | Plasmid-based overexpression of *FMS1* in PanK overexpressing strain

The FAD-dependent polyamine oxidase gene, *FMS1*, was cloned under the control of either the *ADH1* promoter (P_{ADH1}), the *HSP26* promoter (P_{HSP26}) or the *TEF1* promoter (P_{TEF1}). The constructs were overexpressed in the rBOX optimized strain *yr*BOX2 which contained the *E. coli* derived PanK (^{Ec}*coaA*). **(A)** C_6-FA production was measured after 168 h of cultivation in buffered SCD uracil$^-$ media. **(B)** Growth (OD_{600}) and **(C)** glucose consumption were monitored over time. C_6-FA – hexanoic acid; OD_{600} – optical density at 600 nm. *n* = 3 biologically independent samples. Data represent mean ± s.d. Statistical analysis was performed using the two-tailed unpaired *t*-test. p > 0.05 = ns (not significant); p < 0.05 = *; p < 0.01 = **; p < 0.001 = ***; p < 0.0001 = ****.

We observed an increase in hexanoic acid production with all *FMS1* constructs over the EV control (47.9 ± 1.5 mg L^{-1}) after 168 h of cultivation in SCD uracil$^-$ media. The highest titer was observed with P_{HSP26} (81.3 ± 2.5 mg L^{-1}), followed by P_{ADH1} (76.3 ± 7.3 mg L^{-1}) and P_{TEF1} (69.7 ± 0.9 mg L^{-1}); although the difference between P_{HSP26} and P_{ADH1} was not significant (Figure

26A). A significant difference between the constructs was however observed in both growth (OD_{600}) and glucose consumption (Figure 26B-C). Although growth was reduced in all *FMS1* overexpressing strains compared to the EV control (OD_{600} of 2.47 ± 0.10), P_{ADH1} strains grew better reaching a final OD_{600} of 1.89 ± 0.07 compared to P_{HSP26} (1.51 ± 0.10) and P_{TEF1} (1.19 ± 0.04). Furthermore, within the first 72 h, growth and glucose consumption of P_{ADH1} was more comparable to the control than the other promoters. We therefore decided to continue engineering using P_{ADH1} to control the expression of *FMS1* due to greater strain fitness and production.

We subsequently performed a genomic exchange of P_{FMS1} with P_{ADH1} in the PanK overexpressing strain, *yr*BOX2, thereby generating KSY26. This strain was capable of increasing the endogenous pantothenate supply and is hereafter referred to as *yr*BOX3. Hexanoic acid production and growth were analyzed and compared to the parent strain *yr*BOX2 and to its parent strain, *yr*BOX1, after 48 h of cultivation in buffered YPD media (Figure 27).

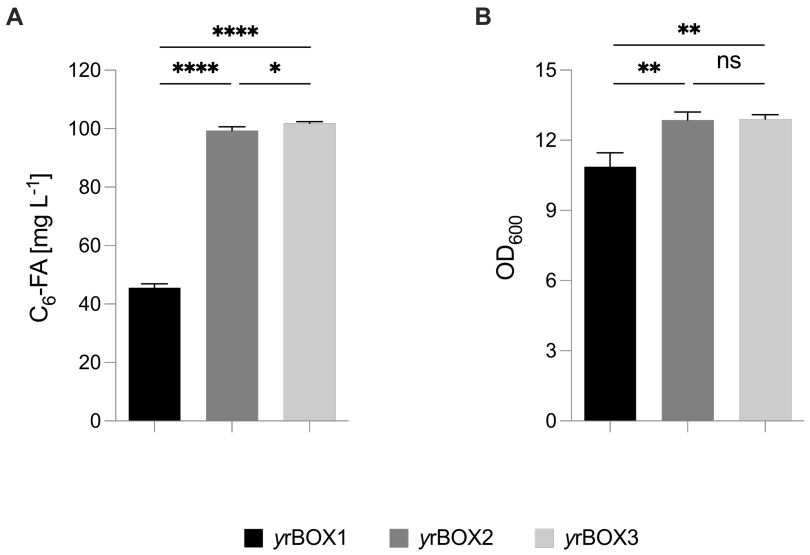

Figure 27 | Increasing endogenous pantothenate supply through genomic upregulation of *FMS1*

(A) C_6-FA production and **(B)** growth (OD_{600}) of the rBOX optimized strain (*yr*BOX1), the PanK overexpressing strain (*yr*BOX2) and the PanK/*FMS1* dual overexpressing strain (*yr*BOX3) were compared after 48 h cultivation in buffered YPD media. C_6-FA – hexanoic acid; OD_{600} – optical density at 600 nm. *n* = 3 biologically independent samples. Data represent mean ± s.d. Statistical analysis was performed using the two-tailed unpaired *t*-test. p > 0.05 = ns (not significant); p < 0.05 = *; p < 0.01 = **; p < 0.001 = ***; p < 0.0001 = ****.

Consistent with our previous results, production was approximately 2.2-fold higher in *yr*BOX2 (99.3 ± 1.4 mg L^{-1}) than *yr*BOX1 (45.6 ± 1.3 mg L^{-1}), while production was only marginally improved in the dual PanK/*FMS1* overexpressing strain *yr*BOX3 (101.8 ± 0.65 mg L^{-1}; Figure 27A). This is presumably due to the sufficient amounts of exogenous pantothenate available in complex media which likely saturate PanK, thus masking the benefit of an increased internal supply of pantothenate in *yr*BOX3. Growth was also comparable in *yr*BOX2 and *yr*BOX3 as the final OD_{600} reached 12.9 in both strains (Figure 27B). Surprisingly, the final OD_{600} of *yr*BOX1 was slightly lower (10.9) which is in contrast to our previous data. Consequently, we tested all three strains in pantothenate-free SCD media to investigate the effect of using only endogenously synthesized

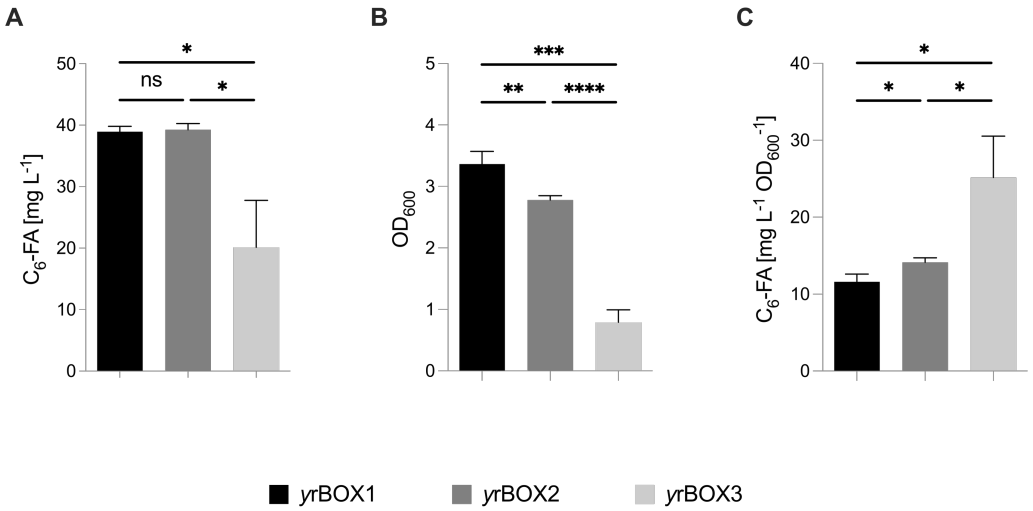

Figure 28 | Investigating the effect of increased pantothenate biosynthesis in pantothenate-free media

(A) C_6-FA production and **(B)** growth (OD_{600}) of the rBOX optimized strain (*yr*BOX1), the PanK overexpressing strain (*yr*BOX2) and the PanK/*FMS1* dual overexpressing strain (*yr*BOX3) were compared after 144 h cultivation in buffered pantothenate-free SCD media. **(C)** Analysis of C_6-FA production normalized to biomass accumulation. C_6-FA – hexanoic acid; OD_{600} – optical density at 600 nm. *n* = 3 biologically independent samples. Data represent mean ± s.d. Statistical analysis was performed using the two-tailed unpaired *t*-test. p > 0.05 = ns (not significant); p < 0.05 = *; p < 0.01 = **; p < 0.001 = ***; p < 0.0001 = ****.

pantothenate for hexanoic acid biosynthesis (Figure 28). We used SCD media to ensure a sufficient supply of methionine and valine which are required for pantothenate biosynthesis. Hexanoic acid production in *yr*BOX1 (38.9 ± 0.88 mg L^{-1}) was similar to *yr*BOX2 (39.2 ± 1.0 mg L^{-1}; Figure 28A). This would be expected as the absence of an external supply of pantothenate results in it become a limiting factor. As both strains rely on the regular internal pantothenate biosynthesis, the benefit of overexpressing PanK is made redundant. This was observed in the pantothenate feeding experiments when cultures were not supplemented with pantothenate (3.2.4). However, growth in *yr*BOX2 (2.78 ± 0.07) was less than in *yr*BOX1 (3.4 ± 0.21), despite similar production (Figure 28B). This may suggest against hexanoic acid mediated toxicity. Nevertheless, when comparing the production of hexanoic acid in relation to the amount of biomass accumulated, we observe that the individual cells synthesize 21% more hexanoic acid in *yr*BOX2 (14.1 ± 0.58 mg L^{-1} OD_{600}^{-1}) than *yr*BOX1 (11.61 ± 0.99 mg L^{-1} OD_{600}^{-1}) which may speak in favor of hexanoic acid mediated toxicity (Figure 28C). Interestingly, cultivation in pantothenate-free media had a significant negative effect on hexanoic acid production in the PanK/*FMS1* dual overexpressing strain (*yr*BOX3) as only 20.2 ± 7.6 mg L^{-1} was produced (Figure 28A). This corresponds to a reduction of almost 50% compared to *yr*BOX2. The poor production is likely a result of poor growth as this was strongly perturbed in *yr*BOX3, reaching an OD_{600} of only 0.79 ± 0.20 after 144 h (Figure 28B). Nevertheless, *yr*BOX3 synthesized approximately 80% more hexanoic acid per cell (25.2 ± 5.4 mg L^{-1} OD_{600}^{-1}) than *yr*BOX2 (Figure 28C). This suggests that the endogenous biosynthesis of pantothenate was indeed upregulated in *yr*BOX3, however, the negative impact on growth results in an overall lower hexanoic acid production in this strain.

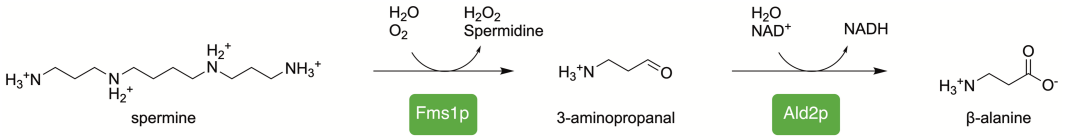

Figure 29 | Overview of the spermine oxidation pathway involving Fms1p

Spermine is oxidized by the FAD-dependent polyamine oxidase Fms1p to form 3-aminopropanal (3-AP). 3-AP is further oxidized by aldehyde dehydrogenase 2 (Ald2p) to β-alanine which is required for pantothenate biosynthesis.

It is unlikely that hexanoic acid mediated toxicity is the sole cause of the drastic growth effect observed in this strain. Additional explanations may be found in the reaction pathway involving Fms1p which oxidizes spermine to 3-aminopropanal (3-AP) (Figure 29). Thus, overexpression of *FMS1* may results in the overproduction of H_2O_2, a reactive oxygen species (ROS). H_2O_2 leads to oxidative stress and can damage proteins by reacting with the thiolate group of amino acids, thereby leading to a global arrest in protein synthesis.[418,419] Moreover, H_2O_2 can react with metal ions such as ferrous iron (Fe^{2+}), in a reaction known as the Fenton Reaction.[420] This has the dual effect of degrading iron-sulfur clusters,[421] thereby inactivating a range of enzymes, as well as decomposing H_2O_2 to form hydroxyl radicals ($^{\bullet}OH$), a highly reactive ROS which can damage different macromolecules.[422,423] In all cases, poor growth is a logical consequence of H_2O_2 overproduction. In *S. cerevisiae* the cytosolic catalase Ctt1p is responsible for protecting cells against H_2O_2 induced stress by efficiently catalyzing its conversion to H_2O and O_2.[424] Consequently, Ctt1p protein levels increase 15-fold upon exposure to H_2O_2.[425] Analyzing Ctt1p protein levels in our *FMS1* overexpressing strain may therefore provide more clarity of whether there are elevated levels of H_2O_2. Alternatively, one could analyze the expression levels of *CTT1* via RT-qPCR or use of a reporter gene controlled by a H_2O_2 inducible promoter, such as *SSA1*.[426] Finally, it has been shown that H_2O_2 strongly induces Ctt1p activity when cells are cultivated in nutrient rich media whereas activity is depressed when cultivated in nutrient-free media. [427] This may help explain the difference in strain fitness and hexanoic acid production following *FMS1* overexpression in synthetic compared to complex cultivation media. As such, the cells become hypersensitive to an overproduction of H_2O_2 when nutrients become limiting in SCD media.

Alternatively, toxicity may arise as a result of 3-AP accumulation. 3-AP is a polyamine-derived aminoaldehyde, and this class of molecules have been shown to cause toxicity to cells. Specifically, 3-AP damages the lysosomal membrane which leads to apoptosis or necrosis.[428] To overcome this, it may prove beneficial to overexpress *ALD2* or *ALD3* which encode cytosolic ALDs that can catalyze the oxidation of 3-AP to β-alanine and are both induced by ethanol.[417] As ethanol production is limited in our strains through the deletion of *ADH1-5*, there may already be a lower level of *ALD2/3* expression which contributes to an accumulation of 3-AP. Overexpression of *FMS1* may therefore exacerbate this effect. Furthermore, as *ALD2* and *ALD3* preferentially use NAD^+ as a cofactor,[429] overexpression may additionally aid in recycling NADH which is required by the rBOX pathway. Moreover, the conversion of acetaldehyde to acetate may be promoted in the case of *ALD2* leading to increased cytosolic acetyl-CoA biosynthesis.

Finally, another explanation for the reduced fitness of *yr*BOX3 in synthetic media may be an increase consumption of methionine or valine which are both required for pantothenate biosynthesis and may therefore negatively impacting global protein biosynthesis.[391,416,417] Particularly methionine may be consumed more as it is a precursor for the *FMS1* harboring pathway. It is possible that YPD contains high enough amounts of methionine and valine to meet the metabolic demands of *yr*BOX3, therefore allowing comparable growth to the parent strain in complex media. It may help to answer whether the growth deficits are due to a limitation in methionine and valine by conducting experiments in which increasing concentrations of methionine and valine are supplemented to synthetic media to surpass those which were used in our standard SCD media composition.

3.3 Biosynthesis of OA from endogenous hexanoyl-CoA

3.3.1 Olivetol biosynthesis and extraction methods

Next, we turned our attention to the conversion of rBOX derived hexanoyl-CoA to OA. We initially started by overexpressing *CsOLS* alone and measuring the production of OL. This deemed to minimize the complexity of the system, thereby allowing us to determine the turnover efficiency of hexanoyl-CoA by *CsOLS*. We therefore cloned a codon optimized *CsOLS* gene under the control of the strong *TEF2* promoter onto a multicopy plasmid (*2μ*) with the antibiotic resistance marker *hphNT1* (KSV47). We subsequently transformed the hexanoic acid producer strain, *yr*BOX1 (3.1.6), with KSV47 and measured the production of OL and hexanoic acid after 72 h in selective buffered YPD media by testing five different OL extraction methods (Figure 30).

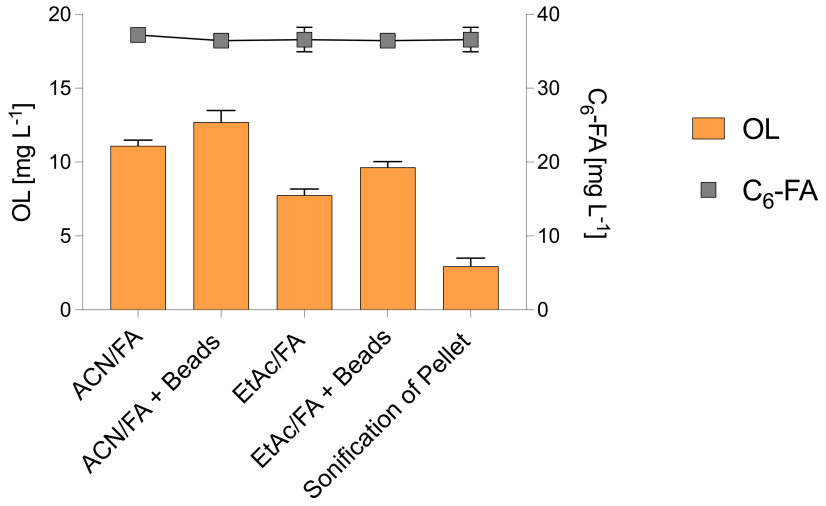

Figure 30 | Comparison of OL extraction methods

Plasmid-based overexpression of *CsOLS* (KSV47) in rBOX optimized strain *yr*BOX1 and analysis OL production (orange bars) after 72 h in selective buffered YPD media using various OL extraction methods. C_6-FA accumulation in the media was also analyzed (gray squares). OL – olivetol; *Cs* – *Cannabis sativa*; *OLS* – olivetol synthase; C_6-FA – hexanoic acid; ACN – acetonitrile; FA – formic acid; EtAc – ethyl acetate. *n* = 3 biologically independent samples. Data represent mean ± s.d. Statistical analysis was performed using the one-way ANOVA with Tukey's multiple comparisons test.

We performed 15 biological replicates, and each extraction method was performed as a triplicate. Four methods were based on the addition of 870 µL of an organic solvent mixed with 30 µL formic acid. The acid organic solvent mixtures used were acetonitrile with formic acid (ACN/FA) or ethyl acetate with formic acid (EtAc/FA). These were added to a 300 µL cell suspension sample taken directly from the culture, thereby generating a final formic acid concentration of 2.5% (v/v). The samples were thoroughly mixed and incubated at 4 °C with either the acidic solvent mix alone or with the addition of glass beads and vigorous shaking to mechanically lyse the cells. The final method tested involved extracting OL form the cells alone by pelleting the culture and lysing cells through sonification. The lysate was subsequently resuspended in the ACN/FA mixture. The OL measured using the extraction methods varied and this variance was statistically significant as determined by analyzing and comparing the

means using the one-way ANOVA test with the follow-up Tukey's multiple comparisons test (Supplementary Table 2). In contrast, hexanoic acid accumulation in the media was similar between each method tested as the means of each triplicate ranged from 36.42 mg L^{-1} to 37.2 mg L^{-1}. Moreover, the statistical analysis showed that the differences between the means were not significant (Supplementary Table 3). Thus, we can confidently assume that the biosynthesis of OL between the cultures was consistent, and that the difference observed in OL concentrations is due to the extraction method rather than OL biosynthesis or biomass accumulation. Our data show that using ACN leads to an increased extraction efficiency of OL (11.1 ± 0.39 mg L^{-1}) compared to EtAc (7.8 ± 0.42 mg L^{-1}). Moreover, mechanical lysis of the cells using glass beads improved the extraction efficiency with both solvents by approximately 14% for ACN (12.7 ± 0.80 mg L^{-1}) and 24% for EtAc (9.7 ± 0.39 mg L^{-1}). Extraction from the cells alone resulted in the lowest amount of OL being measured (2.9 ± 0.56 mg L^{-1}), indicating that the majority of the OL is released into the medium; however, a fraction does remain intracellularly. This further solidifies the requirement for mechanical lysis of the cells using glass beads in the presence of the organic solvent mix. For this reason, we proceeded to use the extraction method involving ACN/FA and glass beads for all OL and olivetolic acid extraction processes moving forward.

Having determined the most efficient extraction method, we repeated the experiment in *yr*BOX1 using an EV control (pRS42H) in order to deduce the hexanoyl-CoA turnover capacity of ^{Cs}*OLS* in our system (Figure 31Figure 1). After 72 h cultivation in selective buffered YPD, the EV control produced no OL while 9.9 ± 0.48 mg L^{-1} OL was produced following overexpression on ^{Cs}*OLS* (Figure 31A). Consequently, the EV control accumulated 23.6% more hexanoic acid (34.6 ± 0.81 mg L^{-1}) compared to the ^{Cs}*OLS* overexpressing strain (28.0 ± 1.4 mg L^{-1}; Figure 31B). By converting the mass concentrations (mg L^{-1}) of hexanoic acid (116.15 g mol^{-1}) and OL (180.25 g mol^{-1}) to the corresponding molar concentrations (µM), we observed a difference in hexanoic acid accumulation between the EV

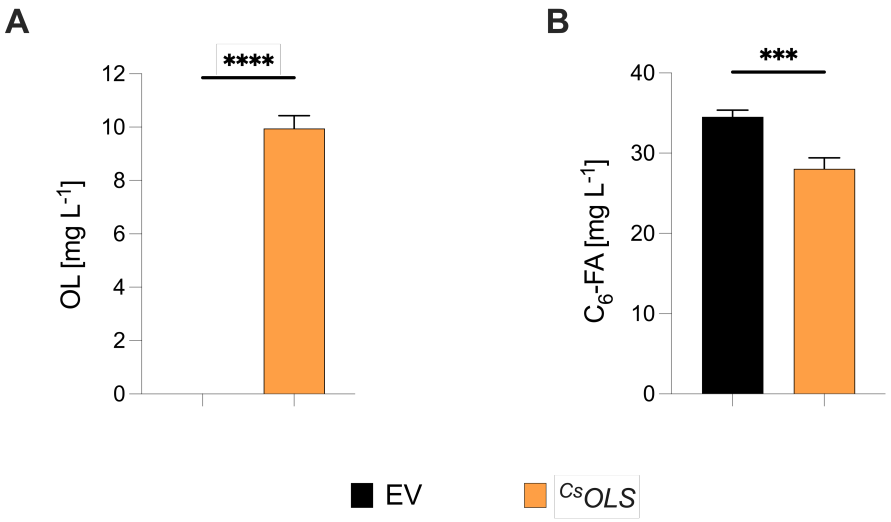

Figure 31 | Biosynthesis of OL in hexanoyl-CoA producing strain

^{Cs}OLS was overexpressed on a multicopy 2*µ* plasmid (KSV47) in the hexanoyl-CoA producing strain (*yr*BOX1) and compared to an EV control (pRS42H). **(A)** C_6-FA and **(B)** OL were measured after 72 h cultivation in selective buffered YPD media. OL – olivetol; *Cs* – Cannabis sativa; *OLS* – olivetol synthase; C_6-FA – hexanoic acid. *n* = 4 biologically independent samples. Data represent mean ± s.d. Statistical analysis was performed using the using the two-tailed unpaired *t*-test. p > 0.05 = ns (not significant); p < 0.05 = *; p < 0.01 = **; p < 0.001 = ***; p < 0.0001 = ****.

control (297.4 µM) and the *CsOLS* overexpressing strain (241.4 µM) which amounts to 56.0 µM. This is equivalent to the amount of OL produced (55.2 µM). Thus, the reduction in hexanoic acid observed can be accounted for by the turnover of hexanoyl-CoA to OL via *CsOLS* and not due to, for example, a difference in the amount of precursor synthesized. However, the total yield of OL (55.2 µM) from rBOX derived hexanoyl-CoA as a percentage, using the total molar concentration of hexanoic acid measured in the EV control (297.4 µM), was only 18.6%. The observation that the majority of the hexanoyl-CoA synthesized is subsequently hydrolyzed to hexanoic acid despite the overexpression *CsOLS* suggests that the competition for hexanoyl-CoA strongly favors TE activity within the current system. Thus, despite the proof-of-concept that *CsOLS* is capable of turning over rBOX derived hexanoyl-CoA towards the cannabinoid biosynthesis pathway, we identify a bottleneck in *CsOLS* activity.

3.3.2 The effect of PanK overexpression on OA and OL biosynthesis

Next, we aimed to increase OL biosynthesis by increasing the endogenous supply of CoA. For this, we overexpressed *CsOLS* (KSV47) in *yr*BOX1 and the PanK overexpressing strain, *yr*BOX2 (3.2.1). The strains were cultivated in selective buffered YPD media and hexanoic acid was measured after 168 h while OL was measured over time (Figure 32).

The PanK overexpressing strain (*yr*BOX2) produced approximately 2.1-fold more hexanoic acid after 168 h (85.2 ± 9.8 mg L^{-1}) than *yr*BOX1 (41.2 ± 1.7 mg L^{-1}) (Figure 32A) which was consistent with our previous data (Figure 20A). Although *yr*BOX2 synthesized higher amounts of hexanoyl-CoA, an

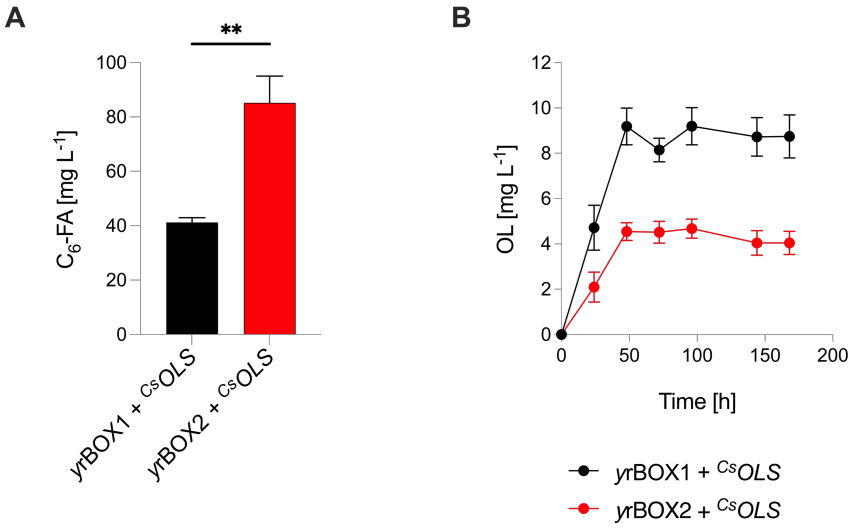

Figure 32 | Effect of PanK overexpression on OL biosynthesis

CsOLS was overexpressed using a multicopy *2µ* plasmid plasmid (KSV47) in a hexanoyl-CoA synthesizing strain (*yr*BOX1) and its PanK overexpressing daughter strain (*yr*BOX2). **(A)** C_6-FA was measured after 168 h and **(B)** OL was measured over time following cultivation of the strains in selective buffered YPD media. PanK – pantothenate kinase; OL – olivetol; *Cs* – *Cannabis sativa*; *OLS* – olivetol synthase; C_6-FA – hexanoic acid. *n* = 3 biologically independent samples. Data represent mean ± s.d. Statistical analysis was performed using the using the two-tailed unpaired *t*-test. p > 0.05 = ns (not significant); p < 0.05 = *; p < 0.01 = **; p < 0.001 = ***; p < 0.0001 = ****.

increase in OL synthesis was not expected due to the bottleneck in *CsOLS* activity identified in previous experiments (Figure 31). Paradoxically however, the data revealed a decrease in OL synthesis in the PanK overexpressing strain (*yr*BOX2), reaching a titer of 4.5 ± 0.40 mg L^{-1} after 48 h compared to 9.2 ± 0.82 mg L^{-1} *yr*BOX1 (Figure 32B). This corresponds to a 51% decrease. Moreover, OL concentrations did not change significantly after 48 h signaling that synthesis had terminated after this point. We therefore deduce that there is an additional factor limiting OL biosynthesis upon PanK overexpression. This was considered to be malonyl-CoA and will be discussed in later chapters (3.3.7).

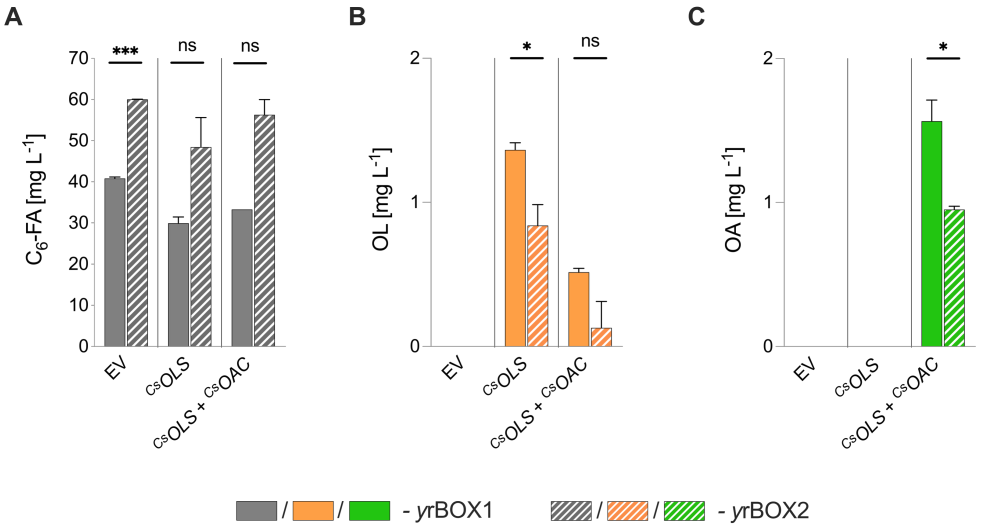

Figure 33 | Analyzing effect of PanK overexpression on OA biosynthesis

Plasmid-based overexpression of *CsOLS* and *CsOAC* (KSV74) compared to *CsOLS* alone (KSV69) and an EV control in a hexanoyl-CoA synthesizing strain (*yr*BOX1 – solid bars) and its PanK overexpressing daughter strain (*yr*BOX2 – dashed bars). **(A)** C_6-FA, **(B)** OL and **(C)** OA titers were measured after 312 h cultivation in SMD uracil$^-$ media. OA – olivetolic acid; *Cs* – *Cannabis sativa*; *OLS* – olivetol synthase; *OAC* – olivetolic acid cyclase; C_6-FA – hexanoic acid; PanK – pantothenate kinase; OL – olivetol. *n* = 2 biologically independent samples. Data represent mean ± s.d. Statistical analysis was performed using the using the two-tailed unpaired *t*-test. p > 0.05 = ns (not significant); p < 0.05 = *; p < 0.01 = **; p < 0.001 = ***; p < 0.0001 = ****.

Nevertheless, we next aimed to synthesize OA for the first time using a plasmid-based approach. For this, *CsOLS* and *CsOAC*, (KSV74) or *CsOLS* alone (KSV69) were overexpressed in either *yr*BOX2, as hexanoyl-CoA supply was higher in this strain, or in *yr*BOX1 due to our previous observations that OL biosynthesis had decreased in *yr*BOX2. Both plasmids were multicopy (*2μ*) plasmids and contained the auxotrophic marker *URA3* as well as the strongly expressed *TEF2* and *TEF1* promoters to control the expression of *CsOLS* and *CsOAC*, respectively (Figure 33).

After 312 h of cultivation in SMD uracil$^-$ media, hexanoic acid production was higher in *yr*BOX2 reaching titers between approximately 48 mg L^{-1} and 60 mg L^{-1} compared to 30 mg L^{-1} and 40 mg L^{-1} in yrBOX1 (Figure 33A). This was expected and cements that hexanoyl-CoA supply was sufficient. However, OL and OA production was very modest, reaching a maximum of 1.4 ± 0.05 mg L^{-1} and 1.6 ± 0.15 mg L^{-1}, respectively in *yr*BOX1 (Figure 33B-C). Moreover, we observed a decrease in both OL and OA production in *yr*BOX2 reaching a maximum of only 0.84 ± 0.15 mg L^{-1} and 0.95 ± 0.02 mg L^{-1}, respectively.

Finally, having now identified *yr*BOX1 as superior OA producer to *yr*BOX2, we repeated the overexpression of ^{Cs}*OLS* and ^{Cs}*OAC* (KSV74) in *yr*BOX1. However, the strains were cultivated in SCD uracil$^-$ media in an effort to increase production compared to minimal media (Figure 34). Here, we observed a higher production of OA reaching a titer of 14.8 ± 0.5 mg L^{-1}. Furthermore, 3.6 ± 0.9 mg L^{-1} OL was formed and 51.1 ± 3.9 mg L^{-1} hexanoic acid accumulated in the media.

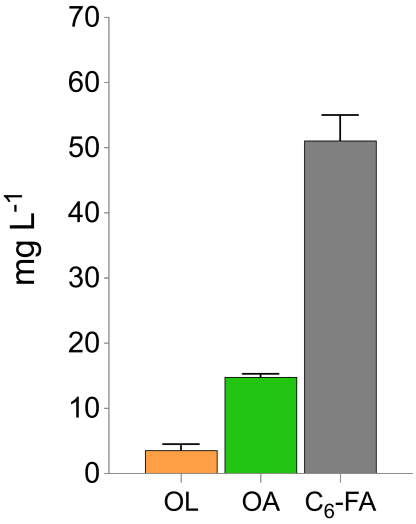

Figure 34 | Analyzing OA biosynthesis with basal PanK expression

^{Cs}*OLS* and ^{Cs}*OAC* were overexpressed in the hexanoyl-CoA producing strain without PanK overexpression (*yr*BOX1) using a multicopy *2µ* plasmid (KSV74). OL, OA and C_6-FA titers were analyzed after 120 h cultivation in SCD uracil$^-$ media. AAE – acyl-activating enzyme; OA – olivetolic acid; *Cs* – *Cannabis sativa*; *OLS* – olivetol synthase; *OAC* – olivetolic acid cyclase; C_6-FA – hexanoic acid; PanK – pantothenate kinase; OL – olivetol. *n* = 3 biologically independent samples. Data represent mean ± s.d.

3.3.3 Screening novel AAEs for hexanoyl-CoA ligase activity

S. cerevisiae is limited in its ability to activate hexanoic acid to hexanoyl-CoA cytosolically and our Δ*faa2* strains are also unable to perform this reaction within the peroxisomes. Furthermore, we previously concluded that there is a strong competition between ^{Cs}*OLS* and endogenous TEs for rBOX derived hexanoyl-CoA and that this competition is in favor of hydrolysis, as determined by the greater titers of hexanoic acid compared to OL or OA. We therefore aimed to introduce a heterologous acyl-CoA synthetase or acyl activating enzyme (AAE) capable of reactivating hexanoic acid to form hexanoyl-CoA. As early and current yeast cannabinoid biosynthesis systems rely on the exogenous supplementation of cultures with hexanoate, the *C. sativa* derived acyl activating enzyme 1 gene (^{Cs}*AAE1*) is commonly overexpressed to generate hexanoyl-CoA. We took this opportunity to search for an alternative AAE which potentially displays more efficient hexanoic acid activation activity. By conducting a literature research, we identified candidate enzymes based on their ability to activate hexanoic acid or similar organic acids, either *in vitro* or *in vivo*, and based on the presence of conserved

motifs including ATP-AMP (AMP1 and AMP2) motifs, fatty acyl-CoA synthetase (FACS) signature motifs and short/medium chain acyl-CoA synthetase domain (A8) motifs.[430–432] These were investigated and tested in comparison to *^{Cs}AAE1*. The following genes which encode AAEs were tested: acyl activating enzyme 3 from *C. sativa* (*^{Cs}AAE3*), *FAA2* from *S. cerevisiae* (*^{Sc}FAA2*), long chain fatty acid-CoA ligase and medium chain fatty acid-CoA ligase from *E. coli* (*^{Ec}fadD* and *^{Ec}fadK*, respectively), acyl activating enzyme 11 from *Arabidopsis thaliana* (At1g66120; *^{At}AAE11*), acyl activating enzyme 15 from *Taxus x media* (*^{Tm}AAE15*), and finally phenylacetate-CoA ligase from *Penicillium chrysogenum* (*^{Pc}PCL*). In addition to *^{Cs}AAE1*, *^{Cs}AAE3* is also expressed within the glandular trichomes of *C. sativa* and was shown to display acyl-CoA ligase activity for a range of substrates including hexanoate *in vitro*.[181] The two genes *fadD* and *fadK* encode acyl-CoA synthetases and constitute part of the regulon for fatty acid degradation (*fad*) in *E. coli*. FadD primarily activates LCFAs while FadK is responsible for MCFA activation.[430] A large superfamily of acyl-activating enzymes or acyl:coenzyme A synthetases exists in *A. thaliana* to allow the activation of a wide range of substrates.[433–435] Of these, ^{At}AAE11 showed the highest specificity for hexanoic and octanoic acid.[435] ^{Tm}AAE15 is involved in the activation of side chain moieties of an anti-cancer drug found in various plant species within the *Taxus* genus, taxol (also called paclitaxel), and similarly displayed hexanoic acid activation activity *in vitro*.[431] Interestingly, the kinetic values were described to be comparable to ^{Cs}AAE3 in that study. ^{Pc}PCL is involved in penicillin biosynthesis where it activates the aromatic substrate phenylacetate.[436] It has also been shown to activate a range of other substrates *in vitro*, including hexanoic acid, and the catalytic activity of ^{Pc}PCL was increased for hexanoic acid through the mutation of a threonine residue to alanine within the substrate binding pocket (T369A).[251,436] It is this construct which was used in this study and is hereafter referred to as *^{Pc}PCL* (or *^{Pc}PCL^{WT}* when compared to mutant *^{Pc}PCL* constructs engineered in this study). Finally, *^{Sc}FAA2* encodes the medium chain fatty acyl-CoA ligase involved in peroxisomal β-oxidation and was already shown to efficiently activate hexanoic acid in this study, resulting in its degradation (3.1.6). ^{Cs}AAE1, ^{Ec}FadD and ^{Ec}FadK are cytosolic enyzmes whereas all the other AAEs are likely localized to the peroxisomes or glyoxysomes in their respective organisms and are predicted to contain a C-terminal peroxisomal targeting signal (PTS1) (Table 21).[437,438]

Table 21 | Overview of candidate acyl-activating enzymes (AAEs) with hexanoyl-CoA ligase activity

Gene	Species	Localization	Predicted PTS1	Source
AAE1	*C. sativa*	Cytosol	-	(181)
AAE3	*C. sativa*	Peroxisome	-SNM	(181)
FAA2	*S. cerevisiae*	Peroxisome	-EKL	(432)
fadD	*E. coli*	Cytosol	-	(430)
fadK	*E. coli*	Cytosol	-	(430)
PCL	*P. chrysogenum*	Peroxisome	-SKI	(439)
AAE11	*A. thaliana*	Peroxisome	-SRL	(440)
AAE15	*T. x media*	Unknown	-SKL	This study

To investigate the hexanoyl-CoA ligase activity of the enzymes in *S. cerevisiae* and to determine the localization of this activity is, we used a plasmid-based approach. ^{Cs}*OLS* was overexpressed either alone or with each AAE on a multicopy (2*μ*) plasmid with the selection marker *URA3*: ^{Cs}*AAE1* (LCV6), ^{Cs}*AAE3* (LCV7), ^{Sc}*FAA2* (LCV8), ^{Ec}*fadD* (LCV9), ^{Ec}*fadK* (LCV10), ^{Pc}*PCL* (LCV11), ^{At}*AAE11* (LCV12), or ^{Tm}*AAE15* (LCV13). These constructs were overexpressed in the strain KSY12 which was generated by knocking out Δ*faa2* in GDY15.[393] KSY12 therefore contained the same metabolic modifications as *yr*BOX1 (Δ*adh1-5*, Δ*gpd2*, Δ*faa2*) but lacked the rBOX pathway. By using this strain, it allowed us to mimic our hexanoyl-CoA producer strains, however, without the endogenous biosynthesis of hexanoyl-CoA. Thus, we were able to accurately compare the activity of the AAE constructs as OL biosynthesis primarily relied on exogenous hexanoic acid. For the initial experiment, strains were cultivated in SMD uracil$^-$ media and the cultures were supplemented with 100 mg L^{-1} (0.86 mM) of hexanoic acid, as this was within the range of the titers produced by our hexanoyl-CoA synthesizing strains. Finally, three negative controls were used. In the first, we used an EV control devoid of either of the genes (SiHV005). In the second, ^{Cs}*OLS* was overexpressed alone (KSV69). In the third, no cells were added to the media in order to confirm the stability of hexanoic acid in the media after cultivation and to measure the true concentration in the media following addition of hexanoic acid. OL and extracellular hexanoic acid were measured after 196 h, once glucose had been fully consumed (Figure 35).

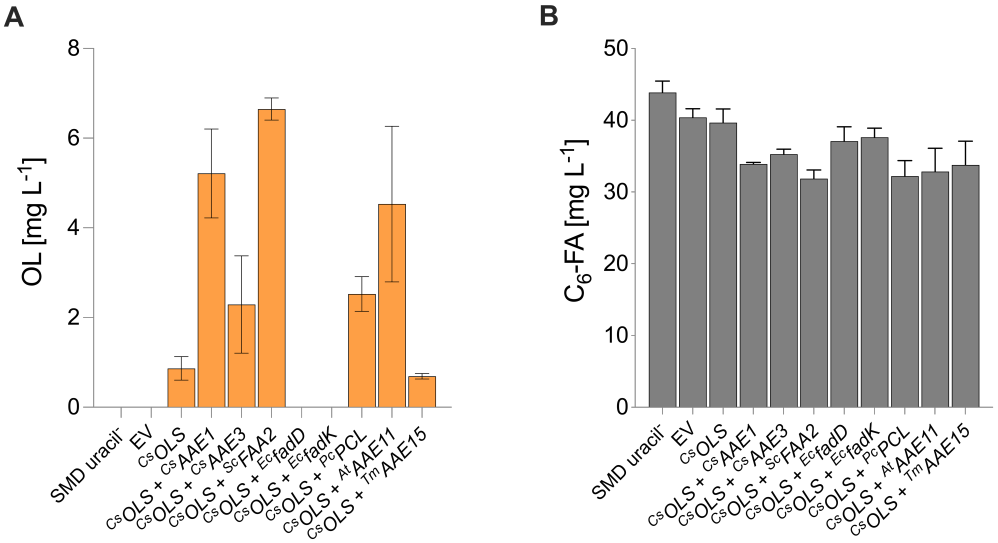

Figure 35 | Assessing AAEs for hexanoyl-CoA ligase activity in *S. cerevisiae* in minimal medium

^{Cs}*OLS* was overexpressed alone or in combination with various AAEs on a single plasmid in KSY12 (Δ*adh1-5* Δ*gpd2* Δ*faa2*). Strains were cultivated in SMD uracil$^-$ supplemented with 100 mg L^{-1} hexanoic acid for 196 h and **(A)** olivetol production and **(B)** C_6-FA in the media were analyzed after cultivation. AAE – acyl-activating enzyme; OL – olivetol; *OLS* – olivetol synthase; C_6-FA – hexanoic acid; EV – empty vector; *Cs* – *Cannabis sativa*; *Sc* – *Saccharomyces cerevisiae*; *Ec* – *E. coli*; *Pc* – *Penicillium chrysogenum*; *At* – *Arabidopsis thaliana*; *Tm* – *Taxus x media*. *n* = 2 biologically independent samples. Data represent mean ± s.d.

No OL was detected in the EV control and a mild production of OL was observed when *CsOLS* was overexpressed alone (0.87 ± 0.26 mg L^{-1}; Figure 35A). This is consistent with reports that a low endogenous supply of hexanoyl-CoA exists which allows OA production upon the expression of *CsOLS* and *CsOAC* in yeast.[243] An increase in OL production was observed following overexpression of most *AAE* constructs together with *CsOLS*. The only exceptions were the two *E. coli* constructs *fadD* and *fadK*, which synthesized no OL, and *TmAAE15* which resulted in slightly reduced OL biosynthesis (0.69 ± 0.06 mg L^{-1}) compared to *CsOLS* alone. The maximum OL titer was measured with *ScFAA2* (6.6 ± 0.25 mg L^{-1}) followed by *CsAAE1* (5.2 ± 0.99 mg L^{-1}) and *AtAAE11* (4.5 ± 1.7 mg L^{-1}). A smaller increase in OL titer compared to the *CsOLS* control was observed with *CsAAE3* (2.3 ± 1.1 mg L^{-1}) and *PcPCL* (2.5 ± 0.39 mg L^{-1}). Furthermore, although 100 mg L^{-1} (0.86 mM) hexanoic acid were supplemented to the media, only approximately 43.9 mg L^{-1} (0.38 mM) was measured after 196 h in the control without cells (Figure 35B). This is likely due to the poor solubility of pure hexanoic acid in aqueous media. The use of a salt such as sodium hexanoate would have improved solubility. Nevertheless, the amount of hexanoic acid which dissolved was not limiting in this context and in subsequent experiments. Similar amounts of hexanoic acid were measured in the EV control (40.4 ± 1.2 mg L^{-1}) and the *CsOLS* control (39.7 ± 1.9 mg L^{-1}). The slight reduction in hexanoic acid observed in the EV control compared to the SMD uracil$^-$ control may be explained by hexanoic acid embedding into the cell membrane or being retained within the cell, and the slight reduction in the *CsOLS* control might be explained by its activation and turnover to OL. In line with this, the concentration of hexanoic acid was further reduced in the constructs which produced OL, whereas slightly more hexanoic acid was measured in cultures which did not synthesize OL. However, when calculating the molar turnover of hexanoic acid to OL, we observed a difference in the amount of hexanoic acid between the AAEs and the EV control which was greater than the difference in OL titers. Thus, the decrease in hexanoic acid cannot be completely explained due to its conversion to OL, suggesting that hexanoic acid is lost in another way. The biggest molar difference between hexanoic acid reduction and OL formation was observed with *PcPCL* (56.5 µM) followed by *TmAAE15* (53.5 µM), *AtAAE11* (39.9 µM), *ScFAA2* (36.8 µM) and AAE3 (31.5 µM). The lowest differences were observed with *CsAAE1* (27.1 µM) *EcfadD* (28.6 µM) and *EcfadK* (24.0 µM). As the *ScFAA2* construct is known to localize to the peroxisome and initiate hexanoic acid degradation by activating it within the peroxisome, an explanation for the excess loss of hexanoic acid may be its degradation via β-oxidation. It can therefore act a positive control for hexanoic acid degradation in this system. As we predicted the *CsAAE3*, *AtAAE11*, *TmAAE15* and *PcPCL* constructs to localize to the peroxisome, it is possible that the molar differences in hexanoic acid consumption and OL biosynthesis may be due to peroxisomal localization of the constructs. However, as the *CsAAE1* construct is known to be cytosolic and a small molar difference was observed here too, a further explanation may be the retention of hexanoyl-CoA within the cells at the time of measurement coupled with a limitation in CsOLS activity, which we had previously established (3.3.1). To examine this further, we repeated the experiment, however, the cells were cultivated in SCD uracil$^-$ media to allow better growth (Figure 36). Furthermore, we extended the cultivation time to 216 h to provide sufficient time for the

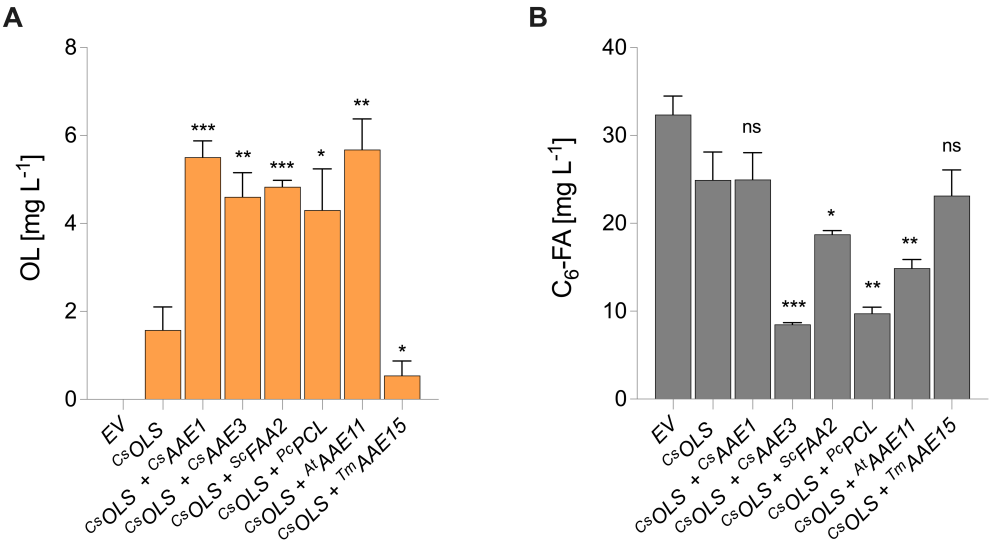

Figure 36 | Assessing AAEs for hexanoyl-CoA ligase activity in *S. cerevisiae* in complete medium

[Cs]OLS was overexpressed alone or in combination with various AAEs on a single plasmid in KSY12 (Δ*adh1-5* Δ*gpd2* Δ*faa2*). Strains were cultivated in buffered SCD uracil$^-$ supplemented with 100 mg L^{-1} hexanoic acid for 216 h and **(A)** olivetol production and **(B)** C_6-FA in the media were analyzed after cultivation. OL – olivetol; *OLS* – olivetol synthase; C_6-FA – hexanoic acid; EV – empty vector; *Cs* – *Cannabis sativa*; *Sc* – *Saccharomyces cerevisiae*; *Pc* – *Penicillium chrysogenum*; *At* – *Arabidopsis thaliana*; *Tm* – *Taxus x media*. *n* = 3 biologically independent samples. Data represent mean ± s.d. Statistical analysis was performed using the using the two-tailed unpaired *t*-test and compared to *[Cs]OLS* alone. p > 0.05 = ns (not significant); p < 0.05 = *; p < 0.01 = **; p < 0.001 = ***; p < 0.0001 = ****.

hydrolysis of cytosolic hexanoyl-CoA and the subsequent release of free hexanoic acid into the media or to allow time for the peroxisomal degradation of hexanoyl-CoA, as this occurs in later growth stages after glucose has been consumed.[441] The *E. coli* derived constructs were left out due to the apparent lack of activity as no OL was produced in the previous experiment.

As before, we observed a low amount of OL biosynthesis when *[Cs]OLS* was overexpressed alone (1.6 ± 0.52 mg L^{-1}). Consistent with our observation in the previous experiment, OL biosynthesis decreased following the overexpression of *[Tm]AAE15* (0.54 ± 0.33 mg L^{-1}) compared to *[Cs]OLS* alone while all other AAE constructs led to an increase in OL biosynthesis, ranging from 4.3 ± 0.94 mg L^{-1} (*[Pc]PCL*) to 5.7 ± 0.70 mg L^{-1} (*[At]AAE11*; Figure 36A). However, titers did not differ greatly between the constructs. In contrast, when analyzing the accumulation of hexanoic acid in the media, we observed strong differences between the individual constructs. In the EV control, 32.4 ± 2.1 mg L^{-1} hexanoic acid was measured, and this fell to 24.9 ± 3.2 mg L^{-1} following overexpression of *[Cs]OLS* alone (Figure 36B). Despite the mild increase in OL production with *[Cs]AAE1*, no significant difference in hexanoic acid accumulation was observed when compared to *[Cs]OLS* alone (25.0 ± 3.0 mg L^{-1}). This would reinforce the idea that [Cs]OLS activity is limiting as *[Cs]AAE1* is known to activate hexanoic acid in yeast more efficiently than these data imply. Moreover, *[Cs]AAE1* increased OL production by approximately 3.9 mg L^{-1} compared to *[Cs]OLS* alone. When converting the amount to the molar concentration (21.6 µM), this corresponds to a difference of

approximately 2.5 mg L^{-1} hexanoic acid which is within the standard deviation of the extracellular hexanoic acid measured. Thus, we can presume that hexanoic acid was turned over to OL, however, the amount is too small to be accurately measured in this context due to statistical variation between the replicates. Furthermore, the restoration of hexanoic acid into the media in *^{Cs}AAE1* and *^{Tm}AAE15* suggests that any intracellular hexanoyl-CoA that had not been turned over to OL was fully hydrolyzed and released into the medium at the time of measurement.

In contrast, overexpression of the AAE constructs which were hypothesized to localize to the peroxisomes (*^{Cs}AAE3*, *^{Sc}FAA2*, *^{Pc}PCL* and *^{At}AAE11*) resulted in a significant decrease in hexanoic acid which did not correspond to the amount of OL synthesized. This strongly suggests that hexanoic acid was degraded following activation inside the peroxisomes. Interestingly, despite *^{Sc}FAA2* being the native enzyme and acting as a positive control for hexanoic acid degradation, we observed the highest amount of extracellular hexanoic acid with this construct (18.7 $\pm$ 0.4 mg L^{-1}). This indicates that plasmid-based overexpression of *^{Sc}FAA2* does not fully complement the Δ*faa2* mutation, as we had previously observed complete degradation of hexanoic acid in the presence of the WT *FAA2* allele (3.1.6). A slightly lower concentration of hexanoic acid was measured with *^{At}AAE11* (14.9 $\pm$ 1.0 mg L^{-1}) while the lowest titers were measured with *^{Pc}PCL* (9.7 $\pm$ 0.7 mg L^{-1}) and *^{Cs}AAE3* (8.50 $\pm$ 0.20 mg L^{-1}), indicating that these may be more efficient in activating hexanoic acid than *^{Sc}FAA2*.

To further confirm this hypothesis, we aimed to prevent AAE mediated degradation of hexanoic acid by disrupting the predicted PTS1 of *^{Cs}AAE3*, *^{At}AAE11*, *^{Sc}FAA2* and *^{Pc}PCL*. We implemented two approaches to achieve this. The first was by truncating the constructs by three amino acids at the C-terminus (Δ*PTS1*). Truncation of Faa2p by 10 amino acids has been shown to be sufficient in preventing peroxisomal localization, thereby retaining it in the cytosol.[442] However, as the aim of that study was to investigate PTS1 dependent targeting of proteins, any potential loss of enzyme activity due to truncation was not considered. In contrast, we desired to limit the extent of the truncation in order to minimize any loss of activity. Alternatively, we aimed to add a C-terminal lysine residue (K) by incorporating the codon AGA, as we predicted this to sterically block the machinery responsible for PTS1 recognition. Adding a C-terminal lysine residue has been demonstrated to retain ^{Sc}Faa2p in the cytosol.[443] We then repeated the hexanoic acid feeding experiments using these mutant constructs. Moreover, we discontinued the use of *^{Tm}AAE15* due to negative results in the previous two experiments. Due to difficulties in cloning, we were unable to generate every construct with each modification. Nevertheless, at least one modification was achieved for each AAE, and these were subsequently tested under the same conditions as the previous experiment (Figure 37).

We observed a similar pattern for OL production as in the previous experiments. Each mutant AAE resulted in a small increase in OL biosynthesis compared to *^{Cs}OLS* alone (1.9 $\pm$ 0.72 mg L^{-1}), similar to their WT counterparts (Figure 37A). OL titers ranged from 4.6 $\pm$ 0.70 mg L^{-1} (*^{Cs}AAE3-K*) to 6.5 $\pm$ 0.19 mg L^{-1} (*^{At}AAE11-K*). This again suggested a limitation in ^{Cs}OLS activity, although this allowed us to conclude that the mutant constructs were still active. In contrast to the WT constructs however, all mutant constructs resulted in the restoration of 83-99%

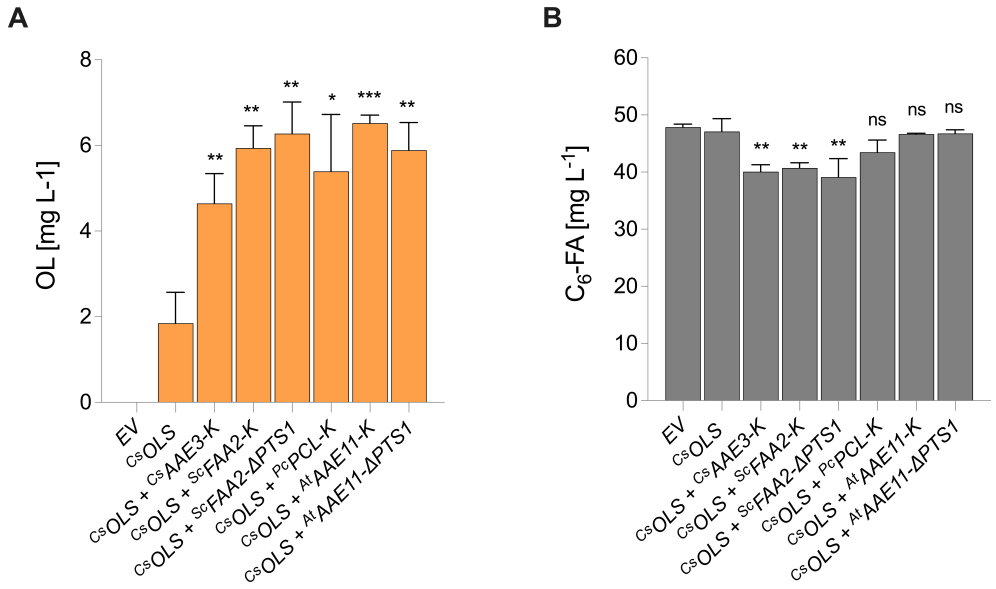

Figure 37 | Effect of disrupting the peroxisomal targeting signal 1 (PTS1) of AAEs

[Cs]OLS was overexpressed alone or in combination with various AAEs on a single plasmid in KSY12 (Δ*adh1-5* Δ*gpd2* Δ*faa2*). Strains were cultivated in buffered SCD uracil$^-$ supplemented with 100 mg L^{-1} hexanoic acid for 216 h. AAE – Acyl activating enzyme; OL – olivetol; OLS – olivetol synthase; C_6-FA – hexanoic acid; EV – empty vector; *Cs* – *Cannabis sativa*; *Sc* – *Saccharomyces cerevisiae*; *Pc* – *Penicillium chrysogenum*; *At* – *Arabidopsis thaliana*; *Tm* – *Taxus x media*. *n* = 3 biologically independent samples. Data represent mean ± s.d. Statistical analysis was performed using the using the two-tailed unpaired *t*-test and compared to [Cs]OLS alone. p > 0.05 = ns (not significant); p < 0.05 = *; p < 0.01 = **; p < 0.001 = ***; p < 0.0001 = ****.

of the hexanoic acid compared to *[Cs]OLS* alone (47.1 ± 2.3 mg L^{-1}), ranging from 39.1 ± 3.3 mg L^{-1} (*[Sc]FAA2-ΔPTS1*) to 46.8 ± 0.6 mg L^{-1} (*[At]AAE11-ΔPTS1*; Figure 37B). This strongly suggests that the enzymes no longer localize to the peroxisome and therefore do not initiate hexanoic acid degradation via β-oxidation. Thus, excess cytosolic hexanoyl-CoA, which was not converted to OL, is likely hydrolyzed by endogenous TEs, thereby reforming hexanoic acid which is released back into the medium. Taken together, we conclude that the heterologous genes *[Cs]AAE3*, *[At]AAE11*, and *[Pc]PCL* display hexanoyl-CoA ligase activity in *S. cerevisiae*, however, the proteins localize to the peroxisomes resulting in hexanoic acid degradation. Furthermore, we demonstrate here that peroxisomal localization can be prevented by mutating the C-terminus which disrupts the PTS1 and results in cytosolic hexanoic acid activation.

3.3.4 Stable genomic integration of multiple copies of *[Cs]OLS* and *[Cs]OAC*

Having previously demonstrated the ability to synthesize OA *de novo* using rBOX derived hexanoyl-CoA (3.3.2), we continually encountered bottlenecks in OA production. We concluded this to be due to low *[Cs]OLS* and *[Cs]OAC* activity when using plasmid-based approaches. Furthermore, we were unable to conclusively identify which AAE exhibits the most efficient cytosolic hexanoyl-

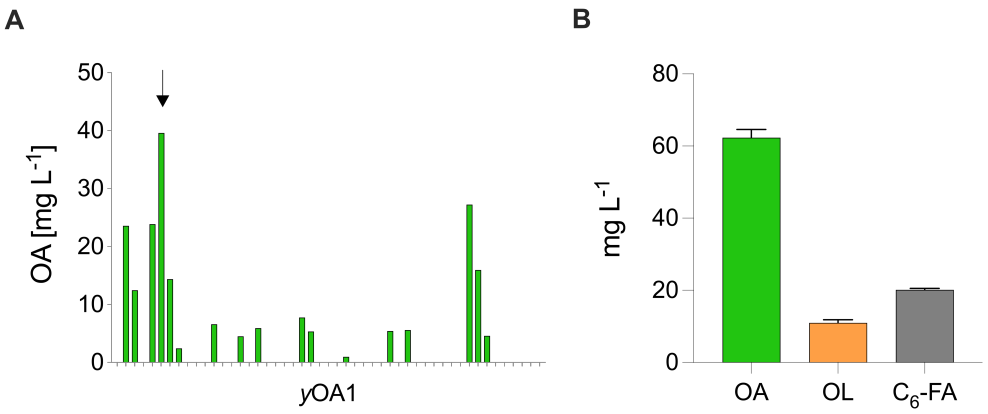

Figure 38 | Genomic integration of multiple *CsOLS* and *CsOAC* copies.

Multiple copies of a construct comprising a single CsOLS expression cassette, two CsOAC expression cassettes and a URA3 marker containing a degradation tag (dURA3) were integrated into the genome of KSY29 in a single step via HR with Ty4 elements to generate yOA1. (A) 50 individual yOA1 clones were screened for OA biosynthesis following cultivation in YPD for 48 h without the use of a pre-culture. (B) The most promising clone (black arrow) was selected, and OA, OL and C_6-FA production was analyzed after 48 h cultivation in YPD after growth in SCD uracil$^-$ as a pre-culture. n = 2 biologically independent samples. OA – olivetolic acid; OL – olivetol; C_6-FA – hexanoic acid; Cs – Cannabis sativa; OLS – olivetol synthase; OAC – olivetolic acid cyclase.

CoA ligase activity due to these limitations (3.3.3). To overcome these limitations, we aimed to stably integrate the *CsOLS* and *CsOAC* genes into the genome *y*rBOX1, a strain which previously achieved the highest OA titers in plasmid-based experiments (Figure 34). Stably integrating expression cassettes within the genome integration can sometimes lead to improved expression and therefore greater activity. For example, we had observed this in our experiments as plasmid-based overexpression of *FAA2* only partially complemented the *faa2* KO mutation, despite the use of a strong promoter and a multicopy expression plasmid (Figure 36). Furthermore, genomic integration of the pathway genes is generally advantageous as the strain is genetically more stable and can grow in non-selective media. This makes handling of the strain less complicated and improves growth. We therefore integrated the *CsOLS* and *CsOAC* expression cassettes into the Δ*ura3* locus of *y*rBOX1, thereby replacing the *kanMX4* cassette which lies downstream of the rBOX pathway genes and had previously been used to provide selection pressure for its integration. The resultant strain, KSY29, was subsequently analyzed for OA production after cultivation in buffered YPD media. However, we were unable to produce detectable amounts of OL and OA via HPLC analysis, despite verification of successful integration via PCR and sequencing analysis.

To address the insufficient production of OA, we proceeded by increasing the copy number of each gene. We also aimed to ensure an excess in *CsOAC* copy number compared to *CsOLS* to increase the likelihood of the enzyme-catalyzed conversion of the linear tetraketide intermediate to OA and in so doing minimize the spontaneous and irreversible formation of OL. This was done by incorporating two copies of *CsOAC* for each copy of *CsOLS*. Furthermore, we utilized the *Ty4* sites within *S. cerevisiae* to allow the integration of multiple copies of the construct in a single step.[43] As the construct also contained a *URA3* marker tagged with a degradation tag (*dURA3*), transformants were subject to increased selection pressure, forcing them to integrate multiple copies of the construct in order to compensate for the instability of Ura3p when grown in uracil$^-$ media. After

transformation of KSY29 with the integration construct (pCS_Can10), the transformants were screened by inoculating 50 individual colonies in 5 mL YPD and measuring OA production after 48 h (Figure 38A). From this initial screen, we selected the most promising OA producer strain and cultivated this following our standard protocol. However, for this strain, precultures were grown in SCD uracil$^-$ prior to inoculation of main cultures in buffered YPD media (Figure 38B). This strain, hereafter named *y*OA1, was able to synthesize 62.3 ± 2.2 mg L^{-1} OA from glucose after 48 h. Furthermore, 11.0 ± 0.9 mg L^{-1} OL was synthesized, suggesting a limitation in OAC activity, despite the higher copy number of *^{Cs}OAC*. Finally, 20.2 ± 0.4 mg L^{-1} extracellular hexanoic acid was also produced which suggests an ongoing competition between OLS and endogenous TEs. Nevertheless, the competition had shifted in favor of OA biosynthesis, in contrast to plasmid-based overexpression of *^{Cs}OLS* and *^{Cs}OAC* (3.3.1). Due to the presence of the *dURA3* marker and the fact that multiple copies of the same sequence are present within the genome of *y*OA1, this strain and all strains engineered from this one were cultivated in SCD uracil$^-$ during propagation. This way, we aimed to uphold selection pressure during strain propagation and engineering and thereby minimize the likelihood of recombination events. For OA biosynthesis purposes, pre-cultures were cultivated in SCD uracil$^-$ and main cultures were inoculated in buffered YPD, according to our standard procedures.

3.3.5 Investigating the effect of pH on OA biosynthesis

Until this point, strains were cultivated in YPD media buffered with 0.1 M KP_i set to pH 6.5. This was to protect our MCFA and hexanoic acid overproducing strains against MCFA induced toxicity.[444] Various mechanisms have been proposed as to how MCFA mediated toxicity occurs. *S. cerevisiae* can survive in a low pH environment as they secrete organic acids such as acetic acid during fermentative growth on sugars or other carbohydrates.[445] Thus, the cultivation media naturally becomes acidified over time. Following the biosynthesis of MCFAs in our recombinant strains, they are secreted into the media. When exposed to a pH in the media which is lower than their acid-base dissociation constant (pK_a), the molecules exist in their protonated form. In this nonionized form, the molecules are able to reenter the cell by traversing the hydrophobic phospholipid of the cell membrane. The ability of a molecule to cross the membrane is measured by its membrane permeability coefficient which, concerning MCFAs, increases with the length of the acyl chain.[446] In this proposed mechanism of crossing the membrane and entering into the cell, the pH neutral environment of the cytosol renders the MCFAs to exist as conjugate acids and they become deprotonated, thereby releasing H^+ within the cell.[447] An alternative mechanism proposed for MCFA toxicity is for the MCFAs to embed themselves into the phospholipid bilayer, thereby compromising the integrity of the membrane structure. This, in turn, increases cell permeability and allows the entrance of H^+ from the acidic extracellular environment.[448] Irrespective of the mechanism of action, the consequences of both proposals is the acidification of the intracellular milieu. Some proposed detoxification methods include the expulsion of the MCFAs through various

transporters (including Aqr1p, Pdr12p and Tpo1p), the esterification of MCFAs via Eeb1p to form ethyl esters and β-oxidation mediated degradation via Faa1p or, as also demonstrated in this work, Faa2p.[403,404] Alternatively, H^+ is pumped out of the cell against its concentration gradient in an ATP-dependent manner.[449] Indeed, octanoic acid upregulates the expression of the plasma membrane H^+-ATPases, *PMA1* and *PMA2*, and decanoic acid increases H^+-ATPase activity in *S. cerevisiae*.[450,448] This process exerts a high demand of energy and therefore compromises cell fitness. Thus, by stabilizing the pH of the cultures above the pK_a of hexanoic acid (pK_a = 4.89) using KP_i, hexanoic acid will exist in its deprotonated form in the media, making it less lipophilic and therefore less able to cross or embed itself within the phospholipid bilayer. This therefore reduces toxicity and promotes growth which ultimately increases hexanoic acid biosynthesis. A more recent study investigated the transcriptomic regulation of *S. cerevisiae* upon internal octanoic acid biosynthesis via a mutant FAB pathway (FAS^{R1834K}) when grown in buffered medium. This study revealed that *PMA2* was only upregulated during the glucose consumption phase, in which low levels of octanoic acid were synthesized.[402] At later growth stages, the expression of *PMA2* actually decreased over time as octanoic acid titers increased. Similarly, *PMA1* expression was downregulated during all growth and production phases. This reinforces the hypothesis that buffering the media limits reentry of MCFAs into the cell after their release into the media, as the plasma membrane H^+-ATPases are not upregulated.

Consequently, we desired to investigate whether this concept holds true for the biosynthesis of OA which has a predicted pK_a of 3.41. *y*OA1 was cultivated in unbuffered and buffered YPD and growth (OD_{600}) and the production of OA and OL were analyzed (Figure 39). Indeed, buffering of the media led to a 32% increase in OA biosynthesis, from 50.0 ± 4.0 mg L^{-1} to

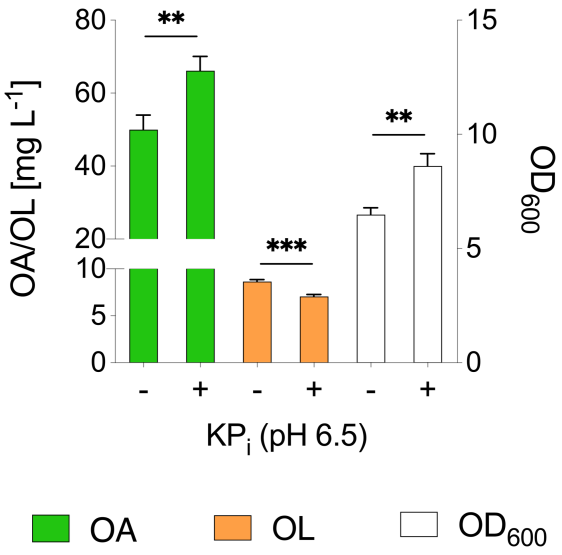

Figure 39 | Effect of buffering cultivation medium on OA biosynthesis

The OA producing strain *y*OA1 was cultivated in either unbuffered YPD media (-) or YPD media buffered with 0.1 M KP_i at pH 6.5 (+). OA and OL production and growth (OD_{600}) were measured after 48 h. OA – olivetolic acid; OL – olivetol; OD_{600} – optical density at 600 nm; KP_i – potassium phosphate buffer. *n* = 3 biologically independent samples. Data represent mean ± s.d. Statistical analysis was performed using the using the two-tailed unpaired *t*-test. p > 0.05 = ns (not significant); p < 0.05 = *; p < 0.01 = **; p < 0.001 = ***; p < 0.0001 = ****.

66.1 ± 3.9 mg L^{-1}. Growth was similarly increased by 33%, reaching an OD_{600} of 8.6 ± 0.54. When normalized to growth, OA production was the same in both unbuffered and buffered media (7.7 mg L^{-1} OD_{600}^{-1}), suggesting that production per cell remained the same and that the increase in production can be attributed to an improvement in growth. Although hexanoic acid was not measured in this experiment, we know from our previous data that approximately 20 mg L^{-1} accumulated in this strain (Figure 38). It is therefore plausible that the positive effects of buffering the media may at least partly be due to an increased tolerance against hexanoic acid. The possibility of OA mediated toxicity was not investigated in this context. Interestingly, OL formation was reduced by 19% from 8.7 ± 0.20 mg L^{-1} to 7.0 ± 0.21 mg L^{-1} which may suggest an increase in OAC activity or turnover efficiency. Indeed, pH plays a pivotal role in cannabinoid biosynthesis as the activity and product spectra of downstream enzymes such as THCAS and CBDAS have been shown to vary depending on pH. A proposed reason for this may be due to the ionization state of the catalytic histidine residue (H292) which has a pK_a of 6.04.[223] Although data for the pH optimum of OAC is not available, we observe a parallel improvement in OA titers and decrease in OL formation which would suggest that OAC activity is improved when buffered at pH 6.5. This was also observed in *Y. lipolytica*, as buffering of the media with 20 g L^{-1} calcium carbonate ($CaCO_3$) improved OA titers three-fold compared to unbuffered cultures in which the pH fell below 3.5.[248] Furthermore, as the pH optimums of THCAS, CBDAS, CBGAS and OLS range from 5.0-7.0,[451] it is plausible to assume a similar optimum for OAC. For this reason, all following OA producing strains were cultivated in YPD buffered at pH 6.5.

3.3.6 Screening mutant AAEs in multicopy *CsOLS* and *CsOAC* strain

Having now improved the activity of OLS and OAC through the genomic integration of multiple copies of their respective overexpression cassettes (*y*OA1), we reverted to testing our mutant, cytosolic AAE constructs for the reactivation of endogenously synthesized hexanoic acid. The following constructs were re-cloned under the control of the *TEF1* promoter using a multicopy (*2μ*) plasmid which contained the dominant marker *hphNT1*: *CsAAE1* (KSV103), *CsAAE3-K* (KSV105), *ScFAA2-ΔPTS1* (KSV100), *PcPCL-K* (KSV102), *AtAAE11-K* (KSV107), *AtAAE11-ΔPTS1* (KSV108). OA and OL production was analyzed after 48 h following overexpression of these constructs in *y*OA1 in selective buffered YPD media (Figure 40).

Here, we could observe clear differences between the individual constructs, in contrast to our preliminary experiments (3.3.3). Compared to the EV control (68.2 ± 5.8 mg L^{-1}), a significant increase in OA biosynthesis was observed with *ScFAA2-ΔPTS1*, *PcPCL-K*, *AtAAE11-K* and *AtAAE11-ΔPTS1*. The highest titer was reached with *PcPCL-K* (99.8 ± 4.3 mg L^{-1}; Figure 40A). Although an increase was measured with both *CsAAE1* (82.8 ± 7.1 mg L^{-1}) and *CsAAE3-K* (72.9 ± 7.4 mg L^{-1}), the increase was not significant in this experiment. Furthermore, as we were searching for viable alternative to *CsAAE1*, it is important to note that *PcPCL-K* was the only construct to achieve a statistically higher biosynthesis than *CsAAE1*, corresponding to a 20% increase. A similar pattern

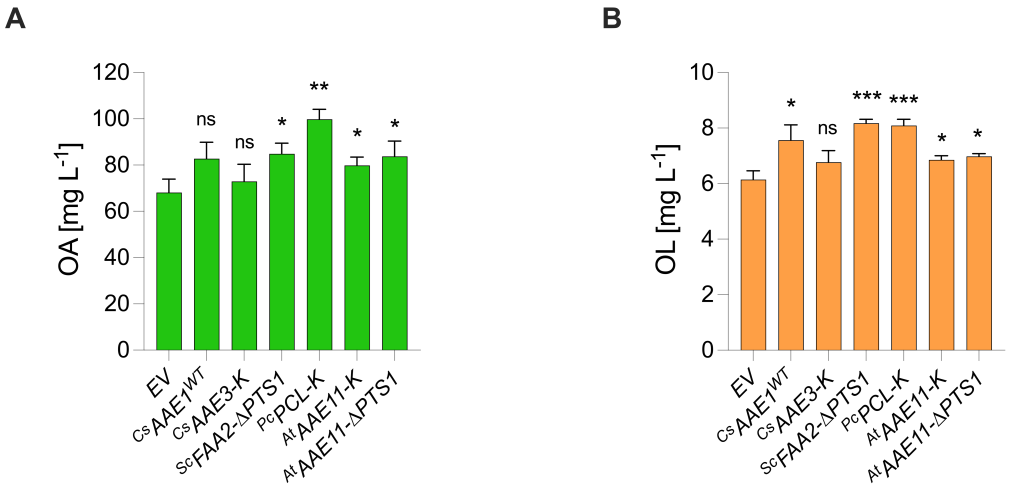

Figure 40 | Screening mutant AAEs for cytosolic hexanoyl-CoA ligase activity

Heterologous AAEs were screened for hexanoyl-CoA ligase activity in *y*OA1. WT AAEs were compared to their mutated counterparts in which the PTS1 was disrputed by either incorporating a C-terminal lysine residue (K) or by removing three amino acids at the C-terminus (ΔPTS1). **(A)** OA and **(B)** OL biosynthesis was analyzed following 48 h cultivation in selective buffered YPD media. AAE – acyl activating enzyme; EV – empty vector; WT – wildtype; PTS1 – peroxisomal targeting signal 1; OA – olivetolic acid; OL – olivetol; *Cs* – *Cannabis sativa*; *Sc* – *Saccharomyces cerevisiae*; *Pc* – *Penicillium chrysogenum*; *At* – *Arabidopsis thaliana*. *n* = 3 biologically independent samples. Data represent mean ± s.d. Statistical analysis was performed using the using the two-tailed unpaired *t*-test and compared to the EV control. p > 0.05 = ns (not significant); p < 0.05 = *; p < 0.01 = **; p < 0.001 = ***; p < 0.0001 = ****.

was observed with OL production; however, titers were substantially lower than OA titers, representing only approximately 9% (Figure 40B).

3.3.7 Increasing cytosolic malonyl-CoA supply for OA biosynthesis

We previously described that an upregulation of the CoA biosynthesis pathway through the overexpression of an *E. coli* derived PanK (*^{Ec}coaA*) resulted in an increase in hexanoyl-CoA biosynthesis (3.2.1). However, this also resulted in a decrease in OL and OA production when *^{Cs}OLS* and *^{Cs}OAC* were overexpressed (3.3.2). Similarly, we had previously deduced that the contribution of MCFA biosynthesis by the mutant FAB pathway was reduced upon PanK overexpression (3.2.3). As a common factor for both pathways is the utilization of malonyl-CoA as a substrate, we considered there to be a limitation in its supply. Cytosolic malonyl-CoA in *S. cerevisiae* is exclusively derived from acetyl-CoA through a reaction catalyzed by Acc1p. Moreover, as the upregulation of CoA biosynthesis increases rBOX mediated hexanoyl-CoA biosynthesis, using cytosolic acetyl-CoA as a substrate, we can conclude that the formation of acetyl-CoA from acetate is also upregulated. This reaction is catalyzed by acetyl-CoA synthetase (ACS) during which ATP is consumed and AMP is released. This would result in an increase in the cytosolic AMP:ATP ratio, thus activating the AMP-activated kinase, Snf1p. Amongst many other roles, Snf1p is involved in the negative regulation Acc1p via phosphorylation.[361] We therefore hypothesized that PanK overexpression indirectly results in the Snf1p mediated downregulation of Acc1p, thus limiting the levels of cytosolic malonyl-CoA. This was reflected by a decrease in the biosynthesis of the malonyl-CoA derived molecules, OL and FAB derived

MCFAs. These two independent observations strengthened our hypothesis that malonyl-CoA availability is reduced through increased Snf1p mediated regulation of Acc1p. We therefore decided to address this directly by deregulating Acc1p on the protein level. To achieve this, we introduced serine to alanine amino acid substitutions of known phosphorylation sites of Acc1p at the positions 659, 686 and 1157.[353,360,361] We mutated the *ACC1* gene in our best hexanoic acid producing strain, *yr*BOX3, in which PanK and *FMS1* were overexpressed (3.2.5). Moreover, we decided to directly incorporate the mutations into the native *ACC1* allele as all examples within the literature hitherto had overexpressed a mutant construct in addition to the WT allele.[353,360,361] This may be due to the inability to knock out *ACC1* in advance as it is an essential gene. Additionally, due to the overwhelming homology of the WT and mutant sequences, there may be difficulty in specifically knocking out the WT gene, for example using CRISPR/Cas9, after incorporation of the mutant gene into the genome. It may be possible to lower sequence homology through codon-optimization or the use of alternative codons. However, changing the sequence of large proteins which form complex structures, particularly those which are vital for growth and survival, may lead to misfolding and potential degradation or the proteins. Furthermore, as Acc1p dimerizes to form an active complex, we contemplated that the existence of both a WT and a mutant allele would lead to a heterologous population of Acc1p complexes, thus reducing the efficacy of the deregulatory modifications. Therefore, we implemented a strategy in which we specifically targeted the phosphorylation sites within *ACC1* using CRISPR/Cas9 and co-transformed the strains with synthetic oligonucleotides which contained the desired mutation to repair the DSB. Furthermore, to prevent recognition by the sgRNA and consequently Cas9 mediated endonuclease activity against the regions of the newly engineered mutations, we incorporated additional silent mutations within the protospacer recognition sequence or the protospacer-adjacent motif (PAM) of the donor oligonucleotides, choosing codons which exist in frequencies close to those of the WT codons. We initially aimed to sequentially mutate the phosphorylation sites and generate strains containing each possible combination of the three mutations. Despite successfully generating $ACC1^{S659A}$ (KSY31) and $ACC1^{S1157A}$ (KSY33) single mutants and subsequently an $ACC1^{S659A/S1157A}$ double mutant (KSY34), we were unable to introduce the S686A mutation into any strain using this approach. For this reason, we investigated whether the malonyl-CoA supply was increased within strain KSY34 ($ACC1^{S659A/S1157A}$) by analyzing rBOX mediated MCFA biosynthesis and comparing this to its parent strain, *yr*BOX3 ($ACC1^{WT}$) after 72 h cultivation in buffered YPD media (Figure 41).

Deregulation of *ACC1* resulted in a decrease in MCFA biosynthesis (Figure 41A). Hexanoic acid, the principal product, decreased by 12% in from 107.4 ± 0.85 mg L^{-1} ($ACC1^{WT}$) to 94.4 ± 1.1 mg L^{-1} ($ACC1^{S659A/S1157A}$) while the already modest biosynthesis of octanoic acid and decanoic acid decreased further by 28% from 4.54 ± 0.15 mg L^{-1} to 3.3 ± 0.03 mg L^{-1} and by 52% from 0.59 ± 0.06 mg L^{-1} to 0.29 ± 0.02 mg L^{-1}, respectively. Growth was not significantly affected, although a slight increase was observed which may be attributed to increased LCFA biosynthesis, resulting in more lipid biosynthesis (Figure 41B). Thus, we deduce that the reduction in MCFA production is due to an increased carboxylation of acetyl-CoA to malonyl-CoA which consequently reduces the supply of acetyl-CoA for the rBOX pathway. However, our analysis relies partly on

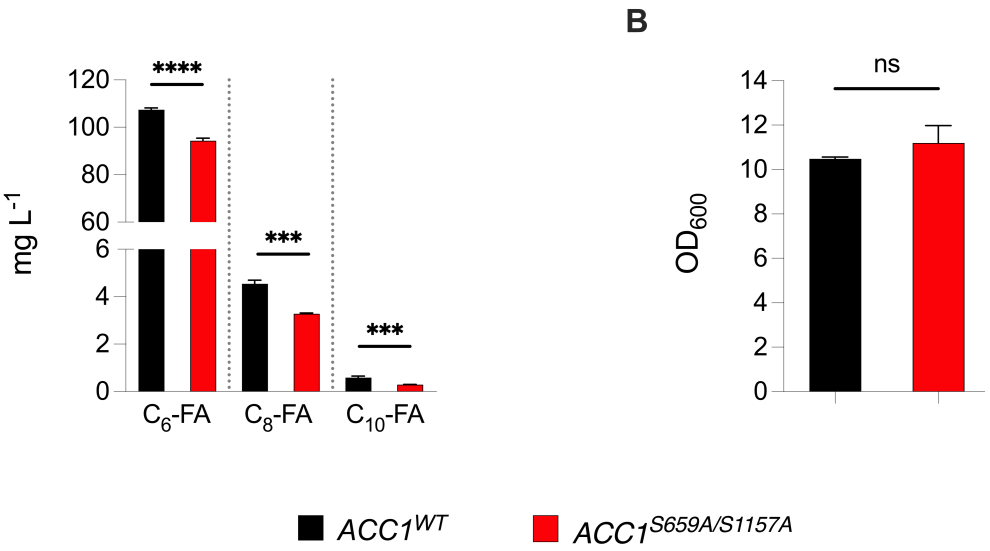

Figure 41 | Effect of deregulating Acc1p on rBOX mediated MCFA biosynthesis

Two phosphorylation sites of Acc1p were mutated from serine to alanine at the positions 659 and 1157 (*ACC1*$^{S659A/S1157A}$) in the hexanoic acid producing strain *yr*BOX3 (*ACC1*^{WT}). **(A)** MCFA biosynthesis and **(B)** growth (OD_{600}) was analyzed after 72 h cultivation in buffered YPD. *ACC1* – acetyl-CoA carboxylase 1; MCFA – medium chain fatty acid; rBOX – reverse β-oxidation; WT – wildtype; C_6-FA – hexanoic acid; C_8-FA – octanoic acid; C_{10}-FA – decanoic acid; OD_{600} – optical density at 600 nm. *n* = 3 biologically independent samples. Data represent mean ± s.d. Statistical analysis was performed using the using the two-tailed unpaired *t*-test. $p > 0.05$ = ns (not significant); $p < 0.05$ = *; $p < 0.01$ = **; $p < 0.001$ = ***; $p < 0.0001$ = ****.

speculation as we only observed an indirect effect and did not measure malonyl-CoA directly. Various methods can be applied for the measurement of short chain acyl-CoAs, including malonyl-CoA, such as via liquid chromatography-mass spectrometry (LC-MS) or the use of a biosensor system.[452–454] However, an alternative method commonly used in *S. cerevisiae* is to measure the biosynthesis of a malonyl-CoA derived product.[361,455,456] We therefore applied the latter method by analyzing the MCFA output following the overexpression of *fusFAS*^{IAGSMWFY} in *yr*BOX3 (*ACC1*^{WT}) and KSY34 (*ACC1*$^{S659A/S1157A}$), as FAS utilizes malonyl-CoA as a substrate. Strains were cultivated in selective buffered YPD for 96 h (Figure 42).

Here, hexanoic acid production fell by approximately 16% from the EV control of *ACC1*^{WT} (90.7 ± 2.6 mg L^{-1}) to the EV control of *ACC1*$^{S659A/S1157A}$ (76.5 ± 1.1 mg L^{-1}; Figure 42A). This was similar to our previous data. In contrast, octanoic acid and decanoic acid production was very low in the EV controls, as the major product of the rBOX pathway is hexanoic acid. Here we also observed a decrease in octanoic acid production in *ACC1*$^{S659A/S1157A}$, although a minor increase was observed for decanoic acid. Interestingly, upon overexpression of *fusFAS*^{IAGSMWFY}, we observed a reduction in total MCFA biosynthesis in *ACC1*$^{S659A/S1157A}$ compared to *ACC1*^{WT} (Figure 42B). Contrary to expectation, hexanoic acid production decreased by approximately 13% (from 92.18 ± 2.0 mg L^{-1} to 80.1 ± 2.3 mg L^{-1}), while a more substantial effect was observed for octanoic acid and decanoic acid. Octanoic acid was reduced by 77% from 12.84 ± 2.4 mg L^{-1} to 2.99 ± 0.10 mg L^{-1} while decanoic acid biosynthesis was almost abolished, falling from 5.6 ± 1.6 mg L^{-1} to 0.45 ± 0.05 mg L^{-1}. Nevertheless, these observations can be explained as follows: following an increase in malonyl-CoA biosynthesis through the deregulation of Acc1p, the

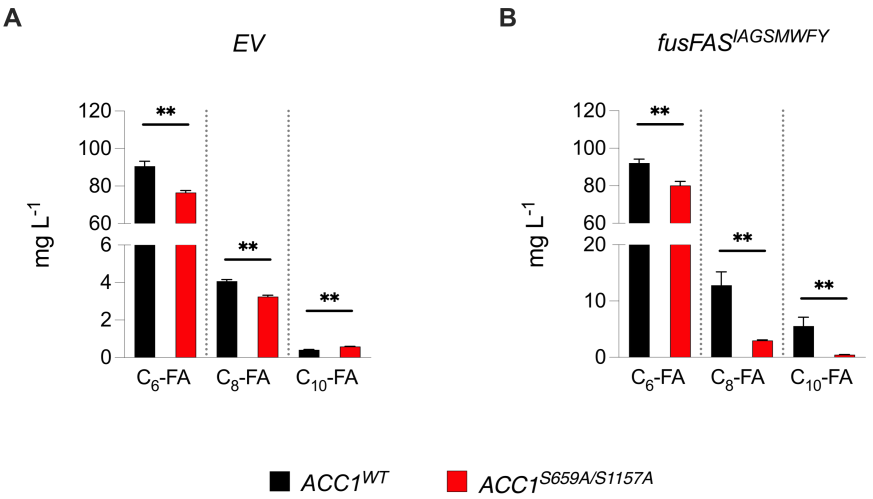

Figure 42 | Effect of deregulating Acc1p on fusFAS mediated MCFA biosynthesis

Two phosphorylation sites of Acc1p were mutated from serine to alanine at the positions 659 and 1157 in the hexanoic acid producing strain *yr*BOX3 (*ACC1*^{WT}) to generate KSY34 (*ACC1*$^{S659A/S1157A}$). MCFA biosynthesis was analyzed after 96 h cultivation in selective buffered YPD media in **(A)** the EV control and **(B)** following overexpression of *fusFAS*^{lAGSMWFY}. *ACC1* – acetyl-CoA carboxylase 1; *fusFAS* – fused fatty acid synthase; MCFA – medium chain fatty acid; WT – wildtype; EV – empty vector; C_6-FA – hexanoic acid; C_8-FA – octanoic acid; C_{10}-FA – decanoic acid. *n* = 3 biologically independent samples. Data represent mean ± s.d. Statistical analysis was performed using the using the two-tailed unpaired *t*-test. p > 0.05 = ns (not significant); p < 0.05 = *; p < 0.01 = **; p < 0.001 = ***; p < 0.0001 = ****.

ratio of cytosolic malonyl-CoA to acetyl-CoA increases. In turn, this would have an effect on FAS mediated FAB, as elongation of the growing acyl-CoA would be favored over initiation. The decrease in FAS mediated MCFA biosynthesis may therefore be due to an enhanced rate of elongation. This may be a further example of the dynamic biosynthesis spectrum of the mutant FAS constructs as the MCFA output of the same construct is strongly influenced by the genomic background (3.1.2) as well as the supply of acetyl-CoA and malonyl-CoA.

Despite this, we were still unable to directly measure a malonyl-CoA derived molecule in the KSY34 strain. Moreover, plasmid-based overexpression of ^{Cs}*OLS* and ^{Cs}*OAC* in a PanK overexpression strain had previously shown to limit OA biosynthesis making it an unsuitable system for cytosolic malonyl-CoA analysis (3.3.2). However, through the generation of the multicopy ^{Cs}*OLS* ^{Cs}*OAC* strain, *y*OA1 (3.3.4), we were able to improve the turnover of hexanoyl-CoA to OA. Thus, this strain was deemed as a suitable host to investigate the mutant *ACC1*. We therefore incorporated the mutations into the native *ACC1* gene of *y*OA1, as described above, thereby generating a single *ACC1*^{S659A} mutant (KSY46) and a double *ACC1*$^{S659A/S1157A}$ mutant (KSY45). Due to the difficulties previously encountered in incorporating the S686A mutation, we adapted our approach and introduced this mutation via mutagenic PCR. The primers used contained no additional silent mutations to prevent recognition by the sgRNA as this was no longer required. We amplified the region of interest from the *ACC1*$^{S659A/S1557A}$ mutant strain (KSY34) as two overlapping fragments which together contained the S659A, S686A and S1157A mutations. These were then fused via a second PCR step to generate a single double stranded DNA fragment which contained all three mutations. Next, by co-transforming *y*OA1 with the triple mutant fragment and two

CRISPR/Cas9 expression plasmids, one which targeted the S659 locus (KSV96) and one the S1157 locus (KSV80) simultaneously, we successfully generated the triple mutant *ACC1*$^{S659A/S686A/S1157A}$ strain, KSY52, later referred to as *y*OA1_ACC1*. OA biosynthesis of all three *ACC1* mutants was compared to the parent strain, *y*OA1, after 48 h cultivation in buffered YPD media (Figure 43).

We observed a slight decrease in OA biosynthesis in the single *ACC1*^{S659A} mutant (KSY46; 58.3 ± 5.6 mg L^{-1}) although this was not statistically significant compared to *ACC1*^{WT} (67.9 ± 3.9 mg L^{-1}; Figure 43A). Should activity really be slightly compromised, a reason for this may be the insertion of the additional silent mutations which may affect protein folding. Although abolishing the recognition of a single phosphorylation site at S1157 enhances activity of Acc1p 9-fold,[360] the S659A mutation had previously only been shown to enhance activity in conjunction with S1157A and has not yet been investigated alone.[353] S659A may therefore not be sufficient to increase malonyl-CoA biosynthesis by itself. Regardless, no statistically significant difference was

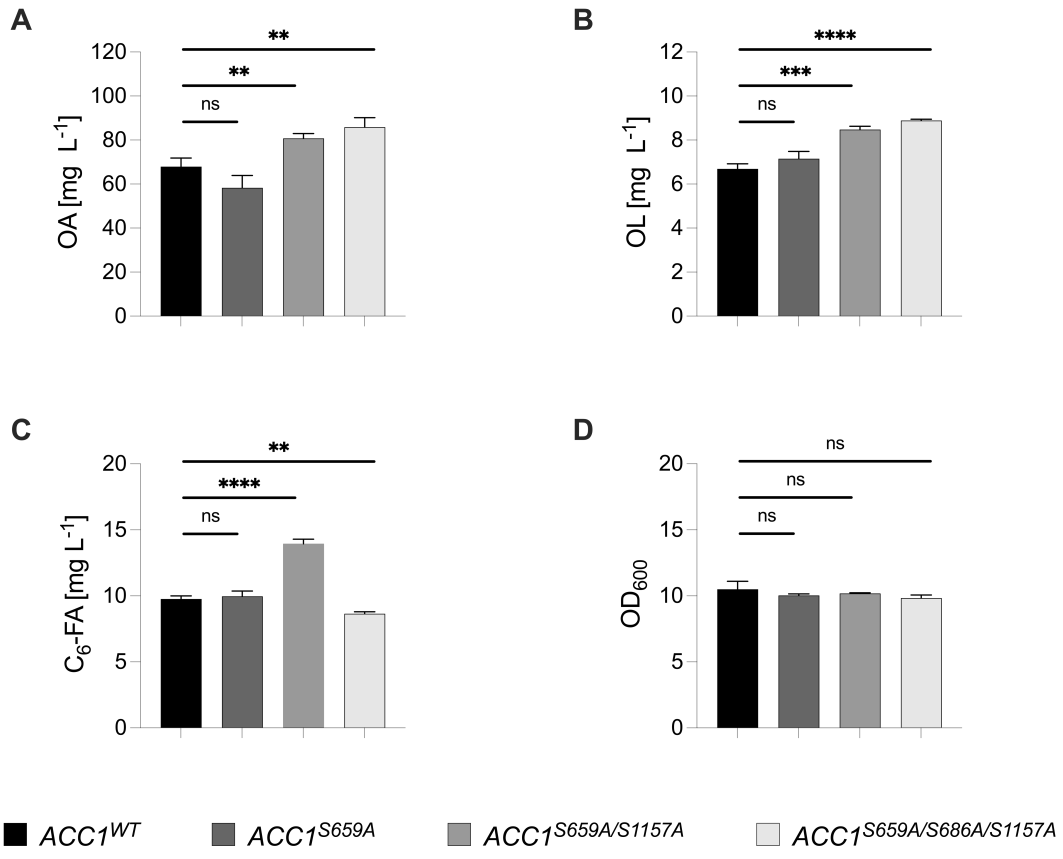

Figure 43 | Effect of deregulating Acc1p on OA biosynthesis

Mutations were incorporated into *ACC1* to introduce serine to alanine amino acid substitutions at positions S659, S686 and S1157 within the OA producing strain *y*OA1. The resultant strains, containing a single mutation (*ACC1*^{S659A}), a double mutation (*ACC1*$^{S659A/S1157A}$) or a triple mutation (*ACC1*$^{S659A/S686A/S1157A}$), were analyzed for **(A)** OA and **(B)** OL biosynthesis, **(C)** C_6-FA accumulation and **(D)** growth (OD_{600}) after 48 h cultivation in buffered YPD media. *ACC1* – acetyl-CoA carboxylase 1; OA – olivetolic acid; OL – olivetol; C_6-FA – hexanoic acid; OD_{600} – optical density at 600 nm; WT – wildtype. *n* = 3 biologically independent samples. Data represent mean ± s.d. Statistical analysis was performed using the using the two-tailed unpaired *t*-test. $p > 0.05$ = ns (not significant); $p < 0.05$ = *; $p < 0.01$ = **; $p < 0.001$ = ***; $p < 0.0001$ = ****.

observed for either OL biosynthesis, hexanoic acid accumulation or growth in the single *ACC1*^{S659A} strain, suggesting that S659A alone has no effect on Acc1p regulation (Figure 43B-D). In contrast, a 19% increase in OA biosynthesis was observed in the double *ACC1*$^{S659A/S1157A}$ mutant (KSY45; 80.7 ± 2.2 mg L^{-1}) indicating that regulation is significantly reduced. This is consistent with previous reports which demonstrate an increase in cytosolic malonyl-CoA levels and the biosynthesis of other malonyl-CoA derived products.[353] Finally, combining all three mutations in the triple mutant *ACC1*$^{S659A/S686A/S1157A}$ strain (*y*OA1_ACC1*) increased OA biosynthesis by 26% (85.9 ± 4.3 mg L^{-1}). This is also in accordance with previous studies which demonstrated an increased malonyl-CoA supply.[361] Thus, together, these mutations have a positive effect on OA biosynthesis. A similar effect was seen on OL biosynthesis as titers also increased from 6.7 ± 0.23 mg L^{-1} to 8.5 ± 0.15 mg L^{-1} and 8.9 ± 0.06 mg L^{-1} in the double and triple mutants, respectively. Interestingly, more hexanoic acid accumulated in the double mutant (14.0 ± 0.35 mg L^{-1}) than in the *ACC1*^{WT} strain (9.8 ± 0.23 mg L^{-1}) while hexanoic acid slightly decreased in the triple mutant (8.6 ± 0.16 mg L^{-1}). A decrease in hexanoic acid would be expected if OA and OL biosynthesis is increased, however, the increase in the double mutant cannot be fully explained. Nevertheless, the difference in the absolute values is minor (approximately 3 mg L^{-1}) and may therefore be overlooked in this context.

Increasing malonyl-CoA biosynthesis through the overexpression of *ACC1* for cannabinoid biosynthesis in yeast has been suggested previously[451] and has since been applied in metabolic engineering strategies to increase OA production in *Y. lipolytica* by lowering transcriptional regulation of the endogenous *ACC1* gene.[248] However, incorporating the corresponding mutations into the transcriptionally deregulated gene to prevent phosphorylation mediated regulation of Acc1p (^{Yl}*ACC1*$^{S667A/S1178A}$) actually resulted in a decrease in OA production, indicating possible differential mechanisms of Acc1p regulation in *Y. lipolytica*. More recently, the overexpression of *ACC1*$^{S659A/S686A/S1157A}$ was successfully implemented for the biosynthesis of CBG in *S. cerevisiae*.[362] Here, overexpression of *ACC1*$^{S659A/S686A/S1157A}$ led to an increase in OA and CBG biosynthesis, although titers were modest, reaching 1.85 mg L^{-1} and 3.75 mg L^{-1}, respectively. However, this was one of the initial steps made during metabolic engineering in that study. This approach would however have the limitation of generating a heterologous Acc1p population, a concern which was addressed above. Interestingly, they continued engineering by additionally targeting *ACC1*$^{S659A/S686A/S1157A}$ to the peroxisomes, together with the GPP and OA biosynthesis pathways. This way, they were able to improve CBG production by utilizing both the cytosolic and peroxisomal pools of acetyl-CoA in a dual compartmentalization approach. As Acc1p is not present in the peroxisome, this method would ensure a homologous *ACC1*$^{S659A/S686A/S1157A}$ population within this organelle. Exploiting the peroxisomes for the biosynthesis of acetyl-CoA derived products, including polyketides, is a common approach and has previously been shown for the biosynthesis of CGBA as a proof-of-concept.[457–459] As the cytoplasmic acetyl-CoA pool is limited, it is a promising approach to either utilize both acetyl-CoA pools for cannabinoid biosynthesis or partition each arm of the pathway in separate compartments. As the engineering strategy in the current work was focused on increasing the cytosolic acetyl-CoA and malonyl-CoA pool for OA biosynthesis, we

conclude that the best approach was to deregulate the native cytosolic Acc1p. This was successfully achieved.

3.3.8 Increasing CoA biosynthesis in multicopy *^{Cs}OLS* and *^{Cs}OAC* strain

Finally, we had previously discussed that the supply of free CoA was limiting hexanoyl-CoA biosynthesis via the rBOX pathway and we demonstrated that this could be overcome by overexpressing the *E. coli* derived PanK (*^{Ec}coaA*; 3.2.1) or its feedback resistant variant (*^{Ec}coaA^{R106A}*; 3.2.2). Although we had established that PanK overexpression decreased OL and OA biosynthesis, which we argued may be caused by a limitation in malonyl-CoA supply due to increased Snf1p mediated Acc1p phosphorylation, we aimed to investigate the effect of increasing CoA biosynthesis on OA biosynthesis in multicopy *^{Cs}OLS* and *^{Cs}OAC* strain, *y*OA1, as this was previously not attempted. We therefore integrated the *^{Ec}coaA^{R106A}* expression cassette into the *LEU2* locus of *y*OA1 using the construct containing the selection marker *natNT2* (KSV81) which we had previously implemented in the engineering of KSY28 (3.2.2). The resultant strain, KSY48, hereafter referred to as *y*OA2, was analyzed for OA, OL and hexanoic acid biosynthesis as well as growth (OD_{600}) and compared to its parent strain (*y*OA1) after 48 h cultivation in buffered YPD media (Figure 44).

Genomic integration of *^{Ec}coaA^{R106A}* (*y*OA2) resulted in a 61% increase in OA biosynthesis (82.5 ± 0.50 mg L^{-1}) compared to *y*OA1 (51.2 ± 4.5 mg L^{-1}) while OL and hexanoic acid were both

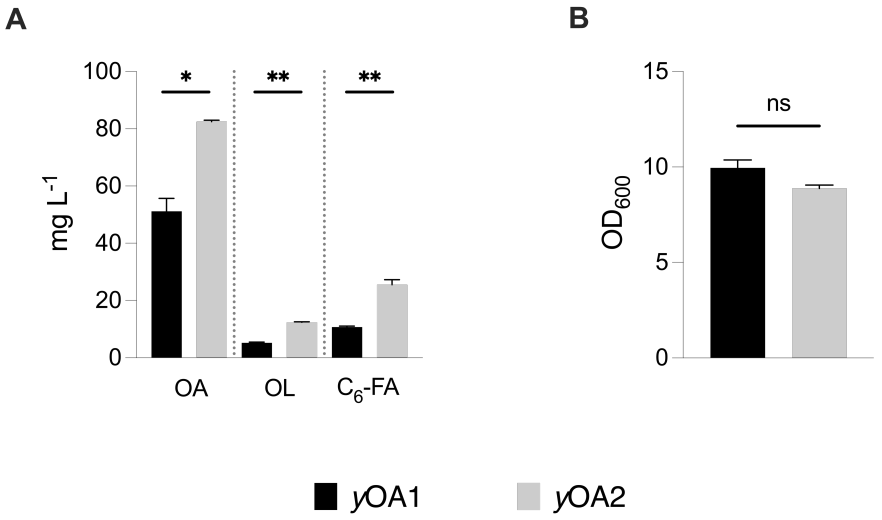

Figure 44 | Effect of increasing CoA biosynthesis on OA biosynthesis

CoA biosynthesis was upregulated in the multicopy *^{Cs}OLS* and *^{Cs}OAC* strain, *y*OA1, through the genomic integration of an *E. coli* derived, feedback resistant PanK mutant (*^{Ec}coaA^{R106A}*) to generate *y*OA2. **(A)** OA, OL and C_6-FA and **(B)** growth (OD_{600}) were measured after 48 h cultivation in buffered YPD media. OA – olivetolic acid; OL – olivetol; C_6-FA – hexanoic acid; OD_{600} – optical density at 600 nm. *n* = 2 biologically independent samples. Data represent mean ± s.d. Statistical analysis was performed using the using the two-tailed unpaired *t*-test. p > 0. 05 = ns (not significant); p < 0.05 = *; p < 0.01 = **; p < 0.001 = ***; p < 0.0001 = ****.

increased approximately 2.4-fold to 12.4 ± 0.21 mg L^{-1} and 25.5 ± 0.18 mg L^{-1}, respectively (Figure 44A). Thus, we observed a substantial increase in precursor supply which ultimately leads to an increase in OA biosynthesis. Moreover, the increased accumulation of hexanoic acid in *y*OA2 implies that there is a continued competition for hexanoyl-CoA between OLS and endogenous TEs. This can be addressed through the overexpression of cytosolic AAEs (3.3.6). Alternatively, this may be due to a limitation in malonyl-CoA supply which, in light of the previous subchapter, we had expected and can be addressed through deregulation of Acc1p (3.3.7). The increase in OL may suggest a limitation in OAC activity. Finally, growth was reduced by 11% from OD_{600} 10.0 ± 0.42 to 8.9 ± 0.18, although the difference was not statistically significant (Figure 44B). Nevertheless, this growth phenotype is consistent with our previous observations following PanK overexpression.

3.4 Combining metabolic engineering approaches to optimize OA biosynthesis

3.4.1 Combining PanK and AAE overexpression

Although OL formation cannot be reversed and therefore results in a loss of precursor, hexanoic acid can reenter the cannabinoid biosynthesis pathway by overexpressing cytosolic AAEs. This was demonstrated in *y*OA1 (3.3.6). Genomic introduction of *E. coli* PanK ($^{Ec}coaA^{R106A}$) to upregulate CoA biosynthesis (*y*OA2) increased OA production but also resulted in an increased amount of hexanoic acid released into the media (3.3.8). We therefore hypothesized that overexpression of cytosolic AAEs may have a greater effect in combination with PanK overexpression, assuming no limitation in their activity with higher substrate concentrations. This assumption is plausible as hexanoate concentrations typically fed in heterologous cannabinoid biosynthesis systems using $^{Cs}AAE1$ range from 1 mM to 3 mM which is substantially higher than the excess hexanoic acid which was generated in our current system.[243,252,362] We therefore performed plasmid-based overexpression experiments in *y*OA2 and narrowed our selection of AAEs to the most promising candidates based on our previous data: $^{Sc}FAA2$-Δ$PTS1$ (KSV100) and ^{Pc}PCL-K (KSV102). These were compared to $^{Cs}AAE1$ (KSV103). Finally, as we were unable to conclusively confirm higher hexanoyl-CoA ligase activity of the mutant constructs compared to their WT counterparts from our initial experiments, we also overexpressed $^{Sc}FAA2^{WT}$ (KSV99) and

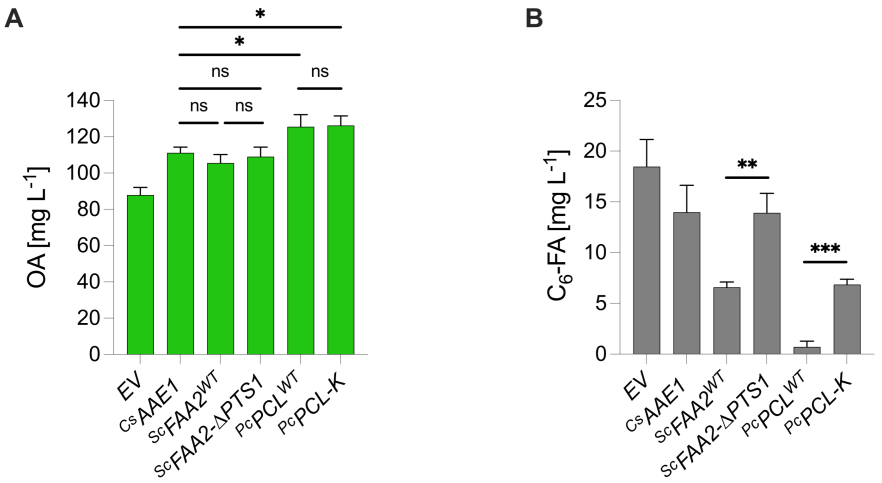

Figure 45 | Overexpression of AAEs and CoA biosynthesis pathway for OA biosynthesis

Plasmid-based overexpression of WT or mutant AAEs in an OA producing strain (*y*OA2) which contained an upregulated CoA biosynthesis pathway through the overexpression of an *E. coli* derived PanK ($^{Ec}coaA^{R106A}$). **(A)** OA biosynthesis and **(B)** C_6-FA accumulation was analyzed following 48 h cultivation in selective buffered YPD media. AAE – acyl-activating enzyme; CoA – coenzyme A; OA – olivetolic acid; PanK – Pantothenate kinase; C_6-FA – hexanoic acid; *Cs* – *C. sativa*; *Sc* – *S. cerevisiae*; *Pc* – *P. chrysogenum*; PTS1 – peroxisomal targeting signal 1. *n* = 3 biologically independent samples. Data represent mean ± s.d. Statistical analysis was performed using the using the two-tailed unpaired *t*-test. $p > 0.05$ = ns (not significant); $p < 0.05$ = *; $p < 0.01$ = **; $p < 0.001$ = ***; $p < 0.0001$ = ****.

[Pc]PCL[WT] (KSV101) which we know are, or strongly predict to be, targeted to the peroxisome (3.3.3). The strains were cultivated in selective buffered YPD media and OA and hexanoic acid titers were analyzed after 48 h (Figure 45).

Consistent with our previous experiments, overexpression of *[Cs]AAE1*, *[Sc]FAA2-ΔPTS1* and *[Pc]PCL-K* resulted in an increase in OA biosynthesis compared to the EV control (87.9 ± 4.3 mg L^{-1}; Figure 45A). The greatest improvement was obtained using *[Pc]PCL-K* (126.3 ± 5.3 mg L^{-1}) which was also significantly higher than both *[Cs]AAE1* (111.2 ± 3.2 mg L^{-1}) and *[Sc]FAA2-ΔPTS1* (109 ± 5.3 mg L^{-1}). The difference between *[Cs]AAE1* and *[Sc]FAA2-ΔPTS1* was, however, not statistically significant. To our surprise, we observed no significant difference in OA production between *[Pc]PCL[WT]* (125.6 ± 6.6 mg L^{-1}) and *[Pc]PCL-K* or between *[Sc]FAA2[WT]* (105.6 ± 4.7 mg L^{-1}) and *[Sc]FAA2-ΔPTS1*. This may raise the question as to whether the mutant constructs are actually localized to the cytosol or whether *[Pc]PCL[WT]* is localized to the peroxisomes. Nevertheless, we did observe a significant reduction in hexanoic acid accumulation with the WT AAEs which indicates degradation of the excess hexanoic acid and would suggest peroxisomal localization, as was initially hypothesized (Figure 45B). Overexpression of *[Sc]FAA2[WT]* resulted in the accumulation of 47% of the hexanoic acid (6.58 ± 0.52 mg L^{-1}) compared to *[Sc]FAA2-ΔPTS1* (13.9 ± 1.9 mg L^{-1}) while *[Pc]PCL[WT]* overexpression almost completely depleted hexanoic acid (0.70 ± 0.2 mg L^{-1}) compared to *[Pc]PCL-K* (6.84 ± 0.52 mg L^{-1}). This would again indicate that the activity of *[Pc]PCL* for hexanoic acid exceeds that of *[Sc]FAA2*.

To clarify the uncertainty concerning the enzymes' subcellular localization, we visualized their localization using fluorescence microscopy. (Figure 46). For this, we first allowed visualization of the peroxisomes by tagging the red fluorescent protein, mRuby2, with a C-terminal PTS1 consisting of the tripeptide sequence serine-lysine-leucine (SKL). mRuby2-SKL was integrated into the genome of CEN.PK2-1C to generate (KSY39). WT and mutant *[Sc]FAA2* and *[Pc]PCL* constructs were tagged with an N-terminal enhanced green fluorescent protein (eGFP) and introduced into the genome of KSY39 to generate KSY42 (eGFP-[Sc]FAA2[WT]), KSY44 (eGFP-[Sc]FAA2-ΔPTS1), KSY49 (eGFP-[Pc]PCL[WT]) and KSY50 (eGFP-[Pc]PCL-K). We opted to genomically integrate the constructs rather than perform plasmid-based overexpression in order to allow a more homogenous distribution of the fluorescent signal, thereby simplifying analysis and increasing its reliability.[36] As expected, we observed co-localization of eGFP-[Sc]Faa2p[WT] with mRuby2-SKL, as Faa2p is known to localize to the peroxisomes. In contrast, eGFP-[Sc]Faa2p-ΔPTS1 localized to the cytosol, confirming successful disruption of PTS1. However, there seems to be some overlapping signals between mRuby2-SKL and eGFP-[Sc]Faa2p-ΔPTS1 which may suggest some localization to the peroxisome. This may be due to a low levels of peroxisomal targeting as our construct only contained a C-terminal truncation of three amino acids and it has been shown that removal of 10 amino acids at the C-terminus completely prevents peroxisomal targeting.[442] Similarly, eGFP-[Pc]PCL[WT] co-localized with mRuby2-SKL while the mutant eGFP-[Pc]PCL-K primarily localized to the cytosol, despite some possible signal overlap. We can therefore conclude that disruption of PTS1 in *[Sc]FAA2* and *[Pc]PCL* was successful. As a result, a possible explanation for the increase in OA biosynthesis following overexpression of the WT AAE constructs is that soluble peroxisomal matrix

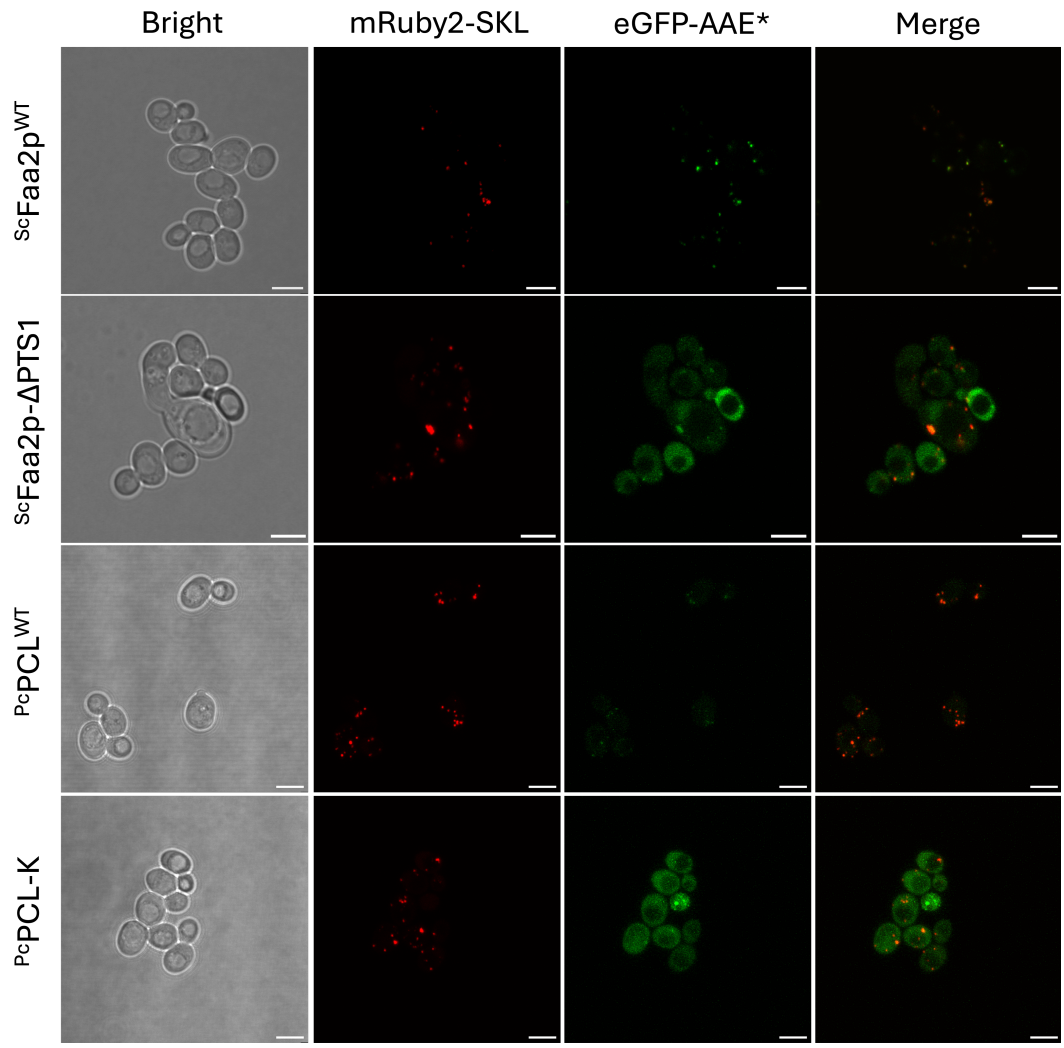

Figure 46 | Visualization of AAE subcellular localization

Fluorescence microscopy images of *S. cerevisiae* (CEN.PK2-1C). Peroxisomes were visualized by overexpressing the fluorophore mRuby2 tagged with a C-terminal PTS1 (mRuby2-SKL). The localization of WT and mutant ^{Sc}Faa2p and ^{Pc}PCL were visualized by overexpressing the constructs tagged with an N-terminal eGPF fluorophore. The mutant Faa2p was truncated by three amino acids at its C-terminus (ΔPTS1) while the mutant ^{Pc}PCL contained a C-terminus lysine residue (-K). Scale bars represent 5 µm. *Sc* – *S. cerevisiae*; *Pc* – *P. chrysogenum*; PTS1 – peroxisomal targeting signal 1.

proteins, including ^{Sc}Faa2p, are targeted to the peroxisome post-translationally.[442,460,461] Indeed, Faa2p has been shown to be localized to the cytosol as well as the peroxisome in *S. cerevisiae*.[462] Thus, we suggest that ^{Sc}*FAA2*^{WT} and ^{Pc}*PCL*^{WT} are initially expressed and fully functional in the cytosol during growth on glucose, as a result of the strong constitutive promoter used for their expression (P_{TEF1}). Therefore, they are able to activate hexanoic acid cytosolically during glucose consumption. However, following growth and proliferation of peroxisomes at later growth stages or upon the accumulation of free fatty acids, the WT variants are targeted to the peroxisomes and degrade the remaining hexanoic acid. In contrast, the mutant variants remain in the cytosol. We therefore recommend the use of a hexanoyl-CoA ligase that is permanently localized to the cytosol, for example ^{Pc}*PCL-K*. This may particularly be beneficial during fed-batch fermentations for OA

production as it would prevent peroxisomal targeting at later growth stages while glucose is continuously fed to the system.

3.4.2 Combining PanK overexpression with deregulated Acc1p

After successfully combining an increased CoA supply with increased hexanoyl-CoA ligase activity for OA biosynthesis, we continued our investigations by combining the upregulated CoA biosynthesis pathway with an upregulation in malonyl-CoA biosynthesis. We therefore overexpressed *E. coli* PanK (*^{Ec}coaA*) in our *ACC1$^{S659A/S686/S1157A}$* strain (*y*OA1_ACC1*). The previous data had pointed to a limitation in hexanoyl-CoA turnover to OA following the genomic integration of *^{Ec}coaA^{R106A}*, given the accumulation of hexanoic acid in the *ACC1^{WT}* strain, *y*OA2 (3.3.8). As discussed, this may be attributed to competition with endogenous TEs and due to a limitation in malonyl-CoA supply. We had previously established that a limitation in malonyl-CoA supply exists during OA biosynthesis and demonstrated how this can be overcome by deregulating Acc1p (3.3.7). To confirm and address the limitation of malonyl-CoA in the current context, we began by overexpressing *^{Ec}coaA* in *y*OA1_ACC1* and the *ACC1^{WT}* parent strain, *y*OA1, using a plasmid-based approach (KSV52). OA and OL biosynthesis were analyzed after 48 h cultivation in selective buffered YPD media (Figure 47).

As previously observed, OA biosynthesis was higher in the EV control for *y*OA1_ACC1* (79.0 ± 3.8 mg L^{-1}) than *y*OA1 (61.2 ± 4.1 mg L^{-1}), corresponding to an increase of 29% (Figure

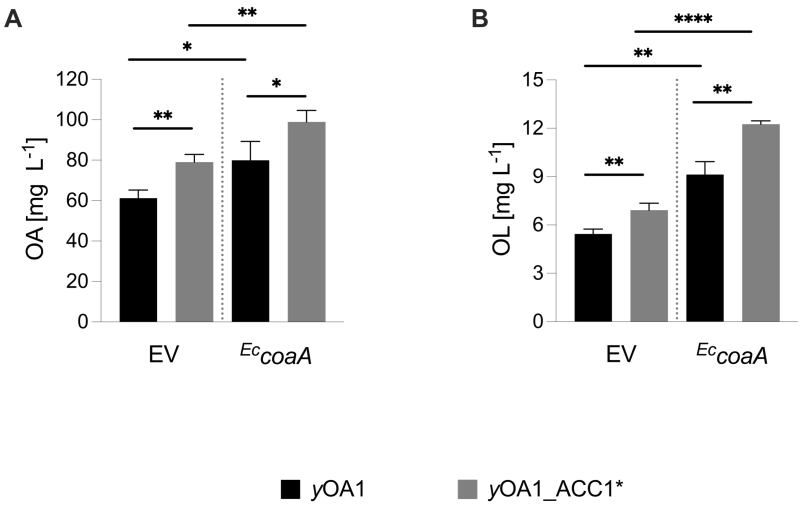

Figure 47 | Overexpressing PanK in Acc1p deregulated strain

Plasmid-based overexpression of an *E. coli* derived PanK (*^{Ec}coaA*) in an *ACC1^{WT}* (*y*OA1) and a mutant *ACC1$^{S659A/S686A/S1157A}$* (*y*OA1_ACC1*) strain. **(A)** OA and **(B)** OL titers were measured after 48 h cultivation in selective buffered YPD and compared to an EV control. PanK = pantothenate kinase; *ACC1* = acetyl-CoA carboxylase; OA – olivetolic acid; OL – olivetol; EV – empty vector; *Ec* – *E. coli*. *n* = 3 biologically independent samples. Data represent mean ± s.d. Statistical analysis was performed using the using the two-tailed unpaired t-test. $p > 0.05$ = ns (not significant); $p < 0.05$ = *; $p < 0.01$ = **; $p < 0.001$ = ***; $p < 0.0001$ = ****.

47A). Furthermore, overexpression of PanK increased OA production in both strains compared to their respective EV controls with *y*OA1_ACC1* producing the highest titer (98.9 ± 5.7 mg L^{-1}). This was 24% higher than PanK overexpression in *y*OA1 (79.9 ± 9.3 mg L^{-1}). Thus, each engineering strategy acts to improve OA biosynthesis individually, as seen in the EV control of *y*OA1_ACC1* (deregulated Acc1p) and in the overexpression of ^{Ec}*coaA* in *y*OA1 (upregulated CoA biosynthesis). This is consistent with our previous data. Furthermore, we also see that combining both strategies improves OA production further. Thus, the increased demand for malonyl-CoA due to the increased availability of hexanoyl-CoA through PanK overexpression, can be met through Acc1p deregulation. Similar trends were also observed for OL as levels increased from 5.4 ± 0.31 mg L^{-1} in the EV control of *y*OA1 to 12.25 ± 0.21 mg L^{-1} following overexpression of ^{Ec}*coaA* in *y*OA1_ACC1* (Figure 47B).

3.4.3 Engineering of a single optimized OA producer strain

Finally, we combined the key metabolic engineering steps which were described throughout this work by introducing the various genetic modifications into a single, optimized OA producer strain. We began by introducing the feedback resistant PanK gene (^{Ec}*coaA*^{R106A}) into the genome of *y*OA1_ACC1*. We opted to perform this modification via CRISPR/Cas9, in contrast to the engineering of PanK overexpressing strains previously generated in this work. By doing so, we omitted the parallel introduction of the *natNT2* expression cassette into the genome. This prevents the overexpression of an unrequired heterologous gene in our final OA production strain. Moreover, *natNT2* encodes an *N*-acetyl transferase (NAT) which uses acetyl-CoA as a substrate to confer resistance to the antibiotic nourseothricin via acetylation.[463,464] Despite the absence of nourseothricin, the enzyme may compete for the binding of acetyl-CoA, thereby interfering with OA biosynthesis. We therefore co-transformed *y*OA1_ACC1* with the CRISPR/Cas9 plasmid SARV84, which targets the strongly expressed neutral site *NSII-3* on Chr III,[42] and the linearized integration plasmid (KSV114), which contained the ^{Ec}*coaA*^{R106A} expression cassette and overhangs for the target locus. This generated the strain KSY59, hereafter referred to as *y*OA3.

In parallel, we introduced ^{Pc}*PCL-K*, the AAE which showed the most efficient cytosolic hexanoyl-CoA ligase activity in our strains, into the genome of *y*OA1_ACC1*, thereby generating KSY60, hereafter referred to as *y*OA4. Similar to the integration of ^{Ec}*coaA*^{R106A} mentioned above, we integrated ^{Pc}*PCL-K* into the strongly expressed *416d* locus on Chr IV via CRISPR/Cas9.[39] We did this by co-transforming *y*OA1_ACC1* with the CRISPR/Cas9 plasmid (KSV115) and the PCR product of the ^{Pc}*PCL-K* expression cassette amplified from KSV102 using primers with overhangs for the *416d* locus. We subsequently analyzed OA, OL and hexanoic acid production in *y*OA3 and *y*OA4 and compared them to their common parent strain, *y*OA1_ACC1* (Figure 48).

OA production was increased by 35% in *y*OA3 (109.7 ± 5.2 mg L^{-1}) over *y*OA1_ACC1* (81.4 ± 2.0 mg L^{-1}). A greater improvement was achieved by *y*OA4 (123.5 ± 6.5 mg L^{-1}), corresponding to 52% over *y*OA1_ACC1* and 13% over *y*OA3 (Figure 48A). Interestingly, a

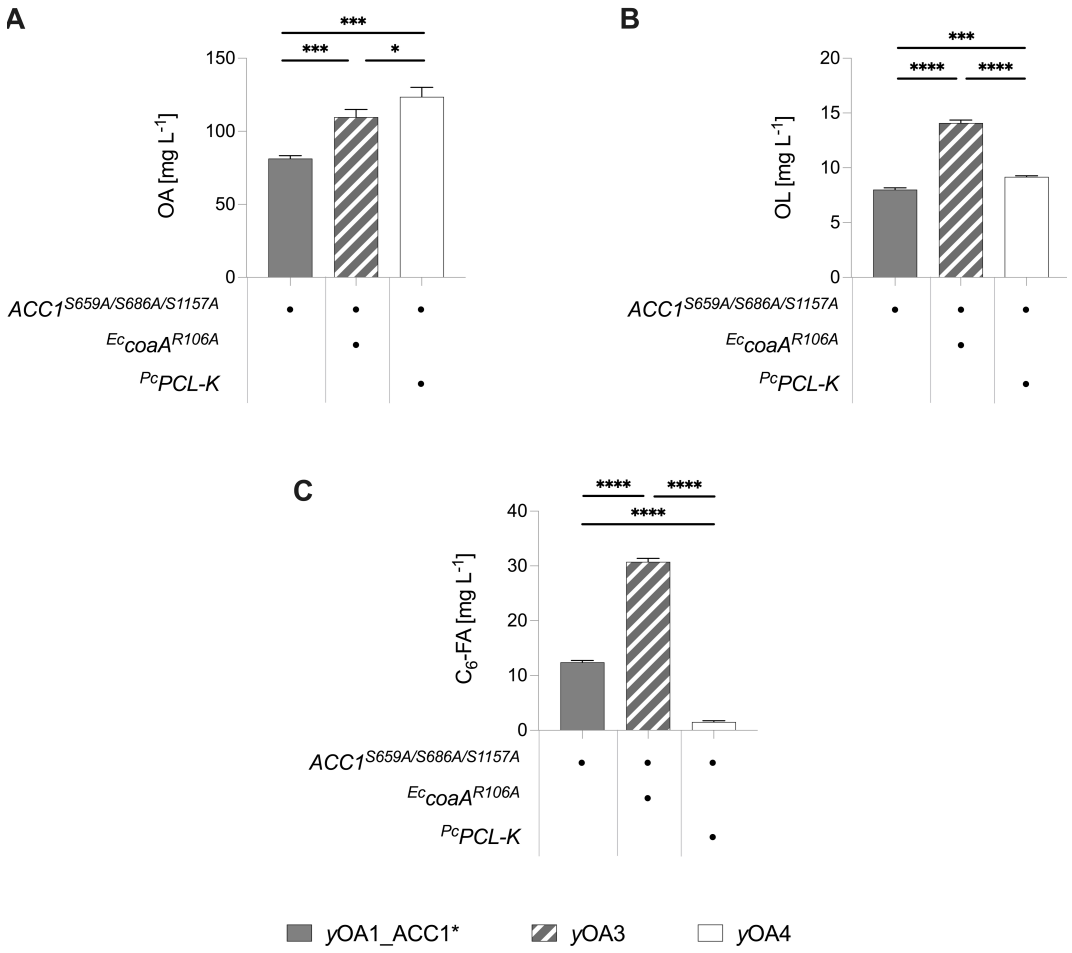

Figure 48 | Genomic integration of PanK and hexanoyl-CoA ligase in *ACC1* mutant strain

Overexpression cassettes of the *E. coli* derived feedback resistent PanK ($^{Ec}coaA^{R106A}$) and the *P. chrysogenum* derived cytosolic AAE mutant with the greatest hexanoyl-CoA ligase activity ($^{Pc}PCL\text{-}K$) were each introduced into the genome of the $ACC1^{S659A/S686A/S1157A}$ strain, yOA1_ACC1*, to generate *y*OA3 and *y*OA4, respectively. **(A)** OA **(B)** OL and **(C)** C_6-FA titers were measured after 48 h cultivation in buffered YPD media. PanK = pantothenate kinase; *ACC1* = acetyl-CoA carboxylase; OA – olivetolic acid; OL – olivetol; C_6-FA – hexanoic acid; *Ec* – *E. coli*; *Pc* – *Penicillium chrysogenum*. *n* = 3 biologically independent samples. Data represent mean ± s.d. Statistical analysis was performed using the using the two-tailed unpaired *t*-test. p > 0.05 = ns (not significant); p < 0.05 = *; p < 0.01 = **; p < 0.001 = ***; p < 0.0001 = ****.

different pattern was observed between the strains when analyzing OL and hexanoic acid production (Figure 48B-C). Overexpression of PanK ($^{Ec}coaA^{R106A}$) resulted in the greatest increase in OL (14.1 ± 0.26 mg L^{-1}) and hexanoic acid (30.8 ± 0.63 mg L^{-1}) production, corresponding to a 76% and 2.5-fold increase over *y*OA1_ACC1*, respectively. This is consistent with our previous observations and is likely due to a substantial increase in precursor supply which exceeds the capacity of OLS and OAC (3.3.8). In contrast, overexpression of the hexanoyl-CoA ligase ($^{Pc}PCL\text{-}K$) only resulted in a 15% increase in OL (9.2 ± 0.10 mg L^{-1}) and accumulated 88% less hexanoic acid (1.50 ± 0.24 mg L^{-1}) than *y*OA1_ACC1* (12.4 ± 0.32 mg L). This is expected as $^{Pc}PCL\text{-}K$ does not enhance precursor biosynthesis but does rescue the hexanoyl-CoA which was lost as hexanoic acid, thereby providing OLS and OAC with a steadier precursor supply over an extended time period. Limitations in OAC activity may explain the slight increase in OL production once hexanoyl-

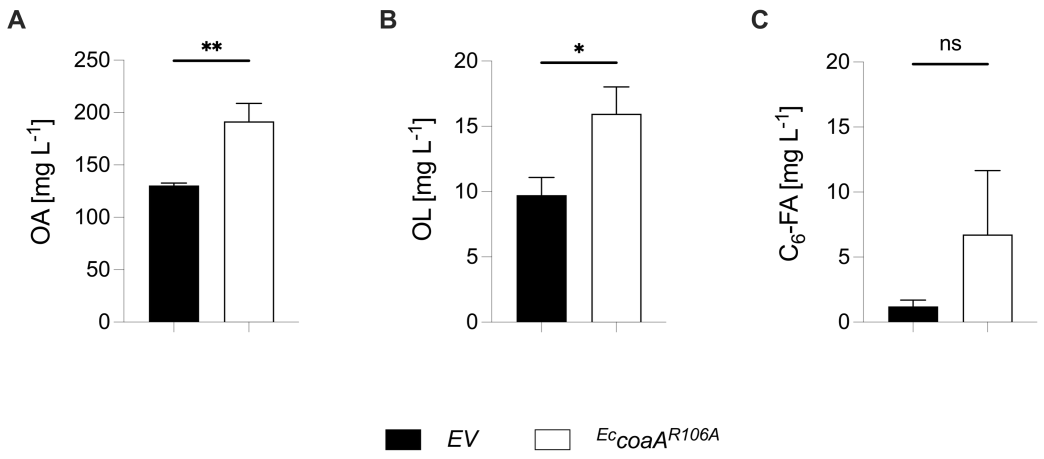

Figure 49 | Combining increased hexanoyl-CoA supply and hexanoyl-CoA ligase activity

Overexpression of the *E. coli* derived PanK ($^{Ec}coaA^{R106A}$) using the plasmid TFV3 in *y*OA4 in which hexanoyl-CoA ligase activity is increased through the genomic integration of $^{Pc}PCL\text{-}K$ and malonyl-CoA supply is increased through the mutant $ACC1^{S659A/S686A/S1157A}$ gene. **(A)** OA **(B)** OL and **(C)** C_6-FA titers were measured after 48 h cultivation in selective buffered YPD media and compared to an EV control. PanK – pantothenate kinase; OA – olivetolic acid; OL – olivetol; C_6-FA – hexanoic acid; EV – empty vector; *Ec* – *E. coli*; *Pc* – *Penicillium chrysogenum*. *n* = 3 biologically independent samples. Data represent mean ± s.d. Statistical analysis was performed using the using the two-tailed unpaired *t*-test. p > 0.05 = ns (not significant); p < 0.05 = *; p < 0.01 = **; p < 0.001 = ***; p < 0.0001 = ****.

CoA is regenerated. Otherwise, hexanoyl-CoA supply seems to become limiting as hexanoic acid was almost completely depleted in *y*OA4. Therefore, to increase the supply of hexanoyl-CoA, we cloned the feedback resistant $^{Ec}coaA^{R106A}$ gene into a multicopy expression plasmid containing the *hphNT1* selection marker (TFV3) and overexpressed this in *y*OA4 (Figure 49).

Indeed, doing so increased OA biosynthesis by approximately 47% reaching a titer of 191.5 ± 17.2 mg L^{-1} compared to the EV control (130.4 ± 2.3 mg L^{-1}; Figure 49A). Similarly, OL increased by 64% to 16.0 ± 2.1 mg L^{-1} (Figure 49B) which follows the previous trends when overexpressing PanK. However, in contrast to previous experiments in which PanK was overexpressed, hexanoic acid accumulation was modest, reaching only 6.7 ± 4.9 mg L^{-1} (Figure 49C) This was not statistically significantly higher than the EV control (1.2 ± 0.48 mg L^{-1}). One of the three replicates measured only 1.1 mg L^{-1} hexanoic acid while approximately 9.5 mg L^{-1} was measured in the other two. It is likely that the cultures first accumulate hexanoic acid extracellularly and this is subsequently taken up reactivated to hexanoyl-CoA by $^{Pc}PCL\text{-}K$ over time. It may therefore be that, given enough time, these cultures would have also reactivated the remainder of the hexanoic acid, as was observed in the one replicate. We therefore proceeded to integrate $^{Ec}coaA^{R106A}$ into the *NSII-3* locus of *y*OA4 as previously described, thus generating the strain KSY61, hereafter referred to as yOA5 (Figure 50).

We observed an increase in OA biosynthesis of 33% from 138.0 ± 11.5 mg L^{-1} in *y*OA4 to 183.2 ± 16.7 mg L^{-1} in *y*OA5 (Figure 50A). The increase in absolute titers was slightly lower than in the plasmid-based overexpression experiment (Figure 49A). This may be due to increased expression of PanK using a multicopy plasmid in complex media compared to integration of a single copy within the genome. This therefore suggests that integrating a second copy of $^{Ec}coaA$ into the

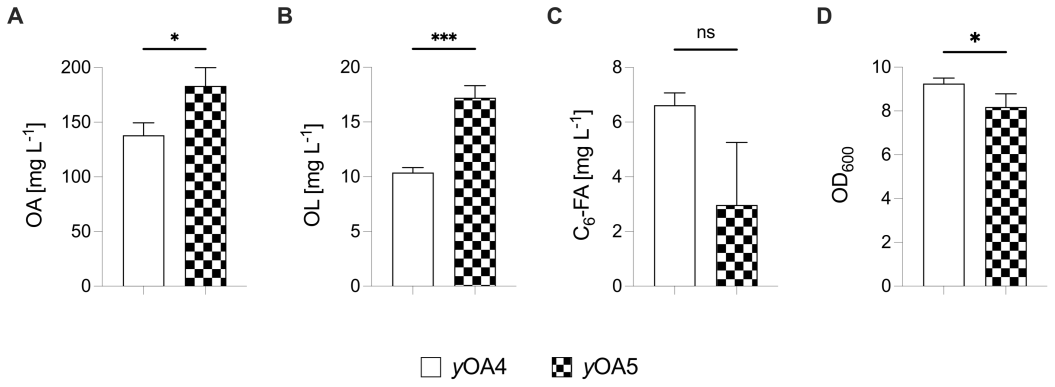

Figure 50 | Generation of a single optimized OA producer strain

Genomic integration of the *E. coli* derived PanK ($^{Ec}coaA^{R106A}$) overexpression cassette into the *NSII-3* locus of *y*OA4 in which hexanoyl-CoA ligase activity is increased through the genomic integration of $^{Pc}PCL\text{-}K$ and malonyl-CoA supply is increased through the mutant $ACC1^{S659A/S686A/S1157A}$ gene to generate *y*OA5. **(A)** OA **(B)** OL and **(C)** C_6-FA titers as we ll as (D) growth (OD_{600}) were measured after 48 h cultivation in selective buffered YPD media and compared to an EV control. PanK – pantothenate kinase; OA – olivetolic acid; OL – olivetol; C_6-FA – hexanoic acid; OD_{600} – optical density at 600 nm; EV – empty vector; *Ec* – *E. coli*; *Pc* – *Penicillium chrysogenum*. *n* = 3 biologically independent samples. Data represent mean ± s.d. Statistical analysis was performed using the using the two-tailed unpaired *t*-test. $p > 0.05$ = ns (not significant); $p < 0.05$ = *; $p < 0.01$ = **; $p < 0.001$ = ***; $p < 0.0001$ = ****.

genome could potentially increase OA biosynthesis due to higher expression. Similarly, OL production increased by 66% to 17.2 ± 1.1 mg L^{-1} (Figure 50B). In contrast, hexanoic acid titers fell from 6.6 ± 0.45 mg L^{-1} in *y*OA4 to 3.0 ± 2.3 mg L^{-1} in *y*OA5, although this difference was again not statistically significant (Figure 50C). Moreover, one of the three *y*OA5 replicates accumulated only 0.66 mg L^{-1} hexanoic acid. Thus, it is plausible that hexanoic acid was being actively converted to hexanoyl-CoA and, given more cultivation time, may have been fully converted in the remaining replicates. Finally, *y*OA5 biomass accumulation was slightly less than *y*OA4, reaching an OD of 8.2 ± 0.60 compared to 9.3 ± 0.25 (Figure 50D). Although we observed a gradual downward trend in strain growth with each generation of OA producing strains, the overall fitness of the final optimized OA producer *y*OA5 was not greatly reduced compared to the first generation of an OA producing strain, *y*OA1, which reached OD_{600} values of between 8.6 (Figure 39) and 10.5 (Figure 43).

4 CONCLUSION AND OUTLOOK

We began our aim of generating a recombinant *S. cerevisiae* strain capable of synthesizing olivetolic acid from glucose by first tackling the challenge of an insufficient hexanoyl-CoA supply. To achieve the *de novo* biosynthesis of hexanoyl-CoA, we explored the use of two distinct pathways. We initially engineered the FAB pathway by overexpressing different engineered fusFAS constructs using a plasmid-based approach. These constructs contained various mutations within the catalytic domains involved in chain length control during FAB. In addition to previously described mutation combinations, new combinations of these mutations were tested in this study. Strains expressing the engineered fusFAS constructs were subsequently analyzed for their capacity to specifically synthesize hexanoic acid as an indirect measurement of hexanoyl-CoA biosynthesis. Furthermore, the total MCFA output, which included octanoic acid and decanoic acid, was also monitored. The constructs were first expressed in a FAB deficient strain in order to test their ability to complement the *fas1* and *fas2* KO mutations. The rationale behind this was to reduce the competition for acetyl-CoA and malonyl-CoA with WT FAS, thereby increasing flux towards MCFA and specifically hexanoyl-CoA biosynthesis. Strikingly, we observed that introducing the F1279Y mutation into the *FAS2* gene, which lies within the KS domain, resulted in the inability to complement the *fas* KO mutations, as reflected by the lack of growth of these strains. We therefore tested the constructs in a WT *FAS* strain. Here, we observed a trend in which the product spectrum shifted towards the biosynthesis of hexanoic acid compared to octanoic acid and decanoic acid for each engineered construct when WT FAS was present. We then confirmed this observation experimentally by demonstrating that the production spectrum the mutant *fusFAS*^{IARKGS} construct is altered in favor of hexanoic acid production in the presence of WT *FAS* compared to in a *fas* KO strain. This suggests that the regulation of MCFA biosynthesis is dynamic and depends on metabolic pressure. We therefore conclude that introducing the F1279Y mutation results in a more stringent blockade of the growing acyl chain within the binding tunnel of the KS domain and that this consequently promotes the premature release of medium chain acyl-CoAs with little flexibility. As such, there is insufficient leaky production of LCFAs to complement the *fas* KO mutations. In this regard, we identify the overexpression of *fusFAS*^{IAGSMWFY} in a WT *FAS* strain as the most efficient system for the total biosynthesis of MCFAs (91.9 mg L^{-1}) and for the best production of hexanoic acid (36 mg L^{-1}) after 48 h. The production of hexanoic acid was further increased to 57 mg L^{-1} when the cultivation time was extended to 96 h. Next, we demonstrated that *FAA2* is responsible for degrading MCFAs in a metabolically optimized rBOX strain (GDY27) by introducing a *faa2* KO mutation (*yr*BOX1). This mutation resulted in a great improvement in hexanoic acid titers which, importantly, remained stable over time, reaching 56 mg L^{-1}. Finally, rBOX occurs during glucose consumption and FAB occurs during ethanol consumption, both engineered pathways were combined in a single strain in order to exploit both growth phases for hexanoic acid production. This resulted in a further 10% increase in hexanoic acid biosynthesis, reaching 65 mg L^{-1} compared to

the rBOX pathway alone. As each pathway produced approximately 50-60 mg L^{-1} hexanoic acid when overexpressed alone, this improvement was lower than expected. Despite this, the production of total MCFAs was elevated more strongly, increasing from 64 mg L^{-1} to 101 mg L^{-1} when combining both pathways. This was primarily due to a substantial increase in octanoic acid and decanoic acid production which almost exclusively derived from the engineered FAB pathway.

Next, we continued to optimize hexanoyl-CoA production by increasing the supply of cytosolic acetyl-CoA. This aimed to both increase rBOX mediated hexanoyl-CoA production and to alleviate a potential bottleneck in acetyl-CoA supply when combining both the rBOX and engineered FAB pathways. By overexpressing an *E. coli* derived PanK (^{Ec}*coaA*) to upregulate the CoA biosynthesis pathway within *yr*BOX1, hexanoic acid production via the rBOX pathway increased 2.2-fold (*yr*BOX2). When combining the engineered FAB pathway with the rBOX pathway in the strain *yr*BOX2, up to 120 mg L^{-1} hexanoic acid production was achieved. However, closer analysis revealed that the contribution of hexanoic acid from the FAB pathway was still very small and actually decreased upon PanK overexpression. We discussed that this may have been due to a limitation in malonyl-CoA supply.

Furthermore, we demonstrated that a sufficient supply of pantothenate is essential for the positive effects of PanK upregulation to be exerted and we consequently engineered a strain capable of meeting the higher demand of pantothenate by overexpressing *FMS1* in plasmid-based experiments. This resulted in increased hexanoic acid production in synthetic media. However, after exchanging the native *FMS1* promoter within the genome (*yr*BOX3), only a minimal improvement in hexanoic acid biosynthesis was observed in complex media. This was likely due to sufficient concentrations of pantothenate being available in the media. Upon further analysis, upregulating *FMS1* had a detrimental effect on growth in pantothenate-free synthetic media, possibly due to toxic byproduct formation. As such, further engineering steps or an alteration to the media composition would be required to balance the metabolic pathways within this strain. For these reasons, we omitted the upregulation of *FMS1* in our subsequent metabolic engineering approaches directed towards OA biosynthesis.

In light of our data, we established that the most efficient pathway for specifically synthesizing hexanoic acid is the rBOX pathway and opted to move forward using only the rBOX pathway to provide hexanoyl-CoA for OA biosynthesis. We therefore concluded our experiments in optimizing hexanoic acid biosynthesis, having engineered a strain (*yr*BOX2) capable of producing approximately 100-115 mg L^{-1} (0.86-0.99 mM) hexanoic acid from 20 g L^{-1} glucose in complex media in shake flask cultivations. Nevertheless, we suggest that combining both the rBOX and engineered FAB pathways in a single strain may be an interesting option for increasing total MCFA biosynthesis, where chain-length specificity is not necessarily required. Industrial applications for this may include biofuel production. Further fine-tuning of the engineered FAB pathway may additionally improve hexanoic acid production, for example by downregulating WT *FAS* expression to reduce precursor competition while still upholding strain viability.

During the continuation of metabolically engineering a strain capable of synthesizing OA using only endogenously produced hexanoyl-CoA, various bottlenecks were identified. These were

subsequently overcome through a series of genetic and protein engineering steps. We initially began by overexpressing *Cs*OLS alone in a hexanoyl-CoA producer strain (*yr*BOX1) and measuring OL production to analyze the efficiency of hexanoyl-CoA entry into the cannabinoid biosynthesis pathway. We also tested various OL extraction methods and identified an efficient method for extracting OL from yeast cultures. Although the majority of OL was present in the culture supernatant, we consistently observed the retention of a smaller proportion of OL within the cells which was successfully extracted from culture suspensions. This also remained true for OA. Next, we overexpressed *Cs*OAC in addition to *Cs*OLS to enable the biosynthesis of OA. Although, titers remained low reaching only approximately 15 mg L^{-1} (0.07 mM), these corresponded to the highest OA titers produced without the supplementation of hexanoate hitherto to the best of our knowledge. Moreover, we consistently observed a large accumulation of extracellular hexanoic acid. This demonstrated that hexanoyl-CoA supply was sufficient in our strains, however, the turnover by OLS remained limited which we concluded to be due to strong competition with endogenous TEs for hexanoyl-CoA. We therefore screened various AAEs with hexanoyl-CoA ligase activity in order to reactivate hexanoic acid and funnel the carbon flux back into the cannabinoid biosynthesis pathway. We also used this opportunity to search for a more efficient enzyme as an alternative to the commonly used *C. sativa* derived AAE1. However, limitations in OLS activity restricted our ability to completely determine *in vivo* hexanoyl-CoA ligase activity. Nevertheless, by analyzing the effect of AAE overexpression on hexanoic acid degradation through feeding experiments, we hypothesized that a number of AAEs localized to the peroxisomes in *S. cerevisiae*. We therefore mutated these by disrupting their predicted PTS1s to prevent their localization to the peroxisomes and were thereby able to prevent hexanoic acid degradation. Despite this, the turnover of hexanoic acid to OL remained low, again suggesting a limitation in OLS activity. This limitation was addressed by integrating multiple copies *Cs*OLS and *Cs*OAC into the genome of a hexanoyl-CoA producing strain (*yr*BOX1) using the *Ty4* elements as integration sites. This approach generated a strain capable of synthesizing up to 66 mg L^{-1} (0.29 mM) OA from 20 g L^{-1} glucose in complex media (*y*OA1). Moreover, we demonstrate that buffering the media at pH 6.5 using 0.1 M KP_i increased OA production by 32% and strain growth by 33% while OL formation was reduced by 19%.

Subsequently, we applied three main metabolic engineering strategies and tested these individually using the multicopy *Cs*OLS and *Cs*OAC strain, *y*OA1. First, by screening our mutant AAE constructs in *y*OA1 using a plasmid-based approach, the greatest increase in OA production was observed with *Pc*PCL-*K* reaching titers of up to 100 mg L^{-1} (0.45 mM). Notably, production was also significantly greater than *Cs*AAE1. Next, we identified a limitation in malonyl-CoA supply within *y*OA1 and overcame this by deregulating Acc1p. This was achieved by directly mutating three phosphorylation sites within the endogenous *ACC1* gene (*y*OA1_ACC1*) which led to a 26% increase in OA production reaching 86 mg L^{-1} (0.38 mM). Directly mutating the endogenous *ACC1* gene represents a unique and novel strategy which has not been reported to date and we argue that this is more efficient than current approaches used to manipulate Acc1p regulation in *S. cerevisiae*. Third, we increased CoA biosynthesis in *y*OA1 through the genomic introduction of the

feedback resistant *E. coli* derived PanK $^{Ec}coaA^{R106A}$ (*y*OA2). This resulted in a 61% increase in OA production reaching approximately 82 mg L^{-1} (0.37 mM).

Finally, we combined the most promising engineering strategies to generate a single OA producer strain. We started by conducting plasmid-based overexpression experiments and these approaches proved complementary in increasing OA biosynthesis. We first combined the upregulation of CoA biosynthesis with increased hexanoyl-CoA ligase activity. This was achieved by overexpressing the most promising AAEs in *y*OA2. Following this, $^{Pc}PCL\text{-}K$ was concluded to exhibit the best hexanoyl-CoA ligase capability amongst the constructs tested in this study and, importantly, it displayed superior ligase activity to $^{Cs}AAE1$ in our system. Moreover, localization of

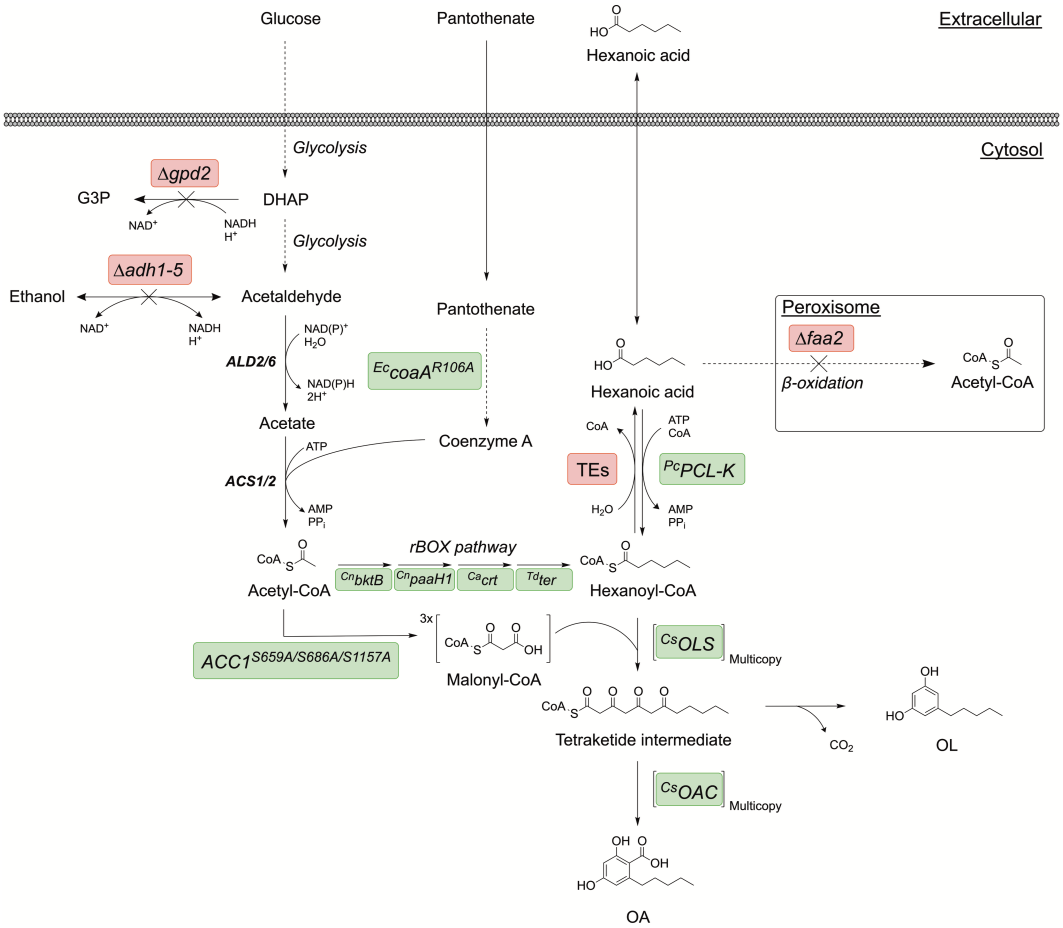

Figure 51 | Schematic overview of metabolic engineering strategies in the final *S. cerevisiae* OA producer strain

Genes invovled in competing pathways are highlighed in red and were kocked out (Δ) where possible. Heterelogous or mutated endogenous genes which were overexpressed are highlighted in green. Endogenous genes which were not genetically manipulated are written in bold. DHAP – dihydroxyacetone phosphate; *gpd* – glycerol 3-phosphate dehydrogenase; G3P – glycerol 3-phosphate; *adh* – alcohol dehydrogenase; *ALD* – aldehyde dehydrogenase; *ACS* – acetyl-CoA synthetase; rBOX – reverse β-oxidation; TEs – thioesterases; *faa2* – medium chain fatty acyl-CoA synthase; *PCL-K* – phenylacetate-CoA ligase with C-terminal lysine; *OLS* – olivetol synthase; *OAC* – olivetolic acid cyclase; OA – olivetolic acid; OL – olivetol; *bktB* – β-ketothiolase; *paaH1* - β-hydroxyacyl-CoA dehydrogenase; *crt* – crotonase; *ter* – *trans*-enoyl-CoA reductase; *Ec* – *E. coli*; *Cs*-*C. sativa*; *Pc* – *P. chrysogenum*; *Cn* – *C. necator*; *Ca* – *C. acetobutylicum*; *Td* – *T. denticola*. This figure was created using ChemDraw 22.2.0 (PerkinElmer).

*Pc*PCL^{WT} to the peroxisomes and *Pc*PCL-K to the cytosol was also confirmed via fluorescence microscopy.

Next, we investigated the combination of an increased malonyl-CoA supply with increased CoA biosynthesis and the combination of an increased malonyl-CoA supply with increased hexanoyl-CoA ligase activity. These approaches functioned to increase the supply of hexanoyl-CoA via two distinct metabolic routes: (i) an increase in cytosolic acetyl-CoA through more available CoA or (ii) the reactivation of hexanoyl-CoA which was lost as hexanoic acid. First, the *Ec*coaA^{R106A} overexpression cassette was stably integrated into the genome of *y*OA1_ACC1* (*y*OA3) to combine increased CoA biosynthesis with an increased malonyl-CoA supply. This resulted in a 35% increase in OA production, reaching titers of up to approximately 110 mg L^{-1} (0.49 mM). Similarly, combining an increased malonyl-CoA supply with an increase in hexanoyl-CoA ligase activity through the introduction of *Pc*PCL-K in *y*OA1_ACC1* (*y*OA4) significantly boosted OA production, reaching titers of close to 125 mg L^{-1} (0.56 mM). Thus, both engineering strategies successfully increased OA biosynthesis in *y*OA1_ACC1*. Following analysis of the pathway intermediates and side-products, the data proved promising for a positive combinatorial effect of all three approaches. Consequently, the genomic overexpression of *Ec*coaA^{R106A} and *Pc*PCL-K and the mutant *ACC1*$^{S659A/S686A/S1157A}$ were combined in a single strain (*y*OA5). This strain was capable of producing approximately 180 mg L^{-1} (0.80 mM) OA from 20 g L^{-1} glucose in shake-flask cultures. A schematic overview of all the engineered pathways within our metabolically optimized OA producer strain *y*OA5 is illustrated in Figure 51. These titers are substantially higher than those reported to date for cultures lacking hexanoate supplementation. We anticipate that cultivating this strain in bioreactors using fed-batch fermentations will significantly increase production titers.

5 REFERENCES

(1) Lesage, G.; Bussey, H. Cell Wall Assembly in *Saccharomyces Cerevisiae*. *Microbiol. Mol. Biol. Rev.* **2006**, *70* (2), 317–343. https://doi.org/10.1128/MMBR.00038-05.

(2) Trivellin, C.; Rugbjerg, P.; Olsson, L. Performance and Robustness Analysis Reveals Phenotypic Trade-Offs in Yeast. *Life Sci. Alliance* **2024**, *7* (1), e202302215. https://doi.org/10.26508/lsa.202302215.

(3) Trivellin, C.; Olsson, L.; Rugbjerg, P. Quantification of Microbial Robustness in Yeast. *ACS Synth. Biol.* **2022**, *11* (4), 1686–1691. https://doi.org/10.1021/acssynbio.1c00615.

(4) Diaz-Ruiz, R.; Rigoulet, M.; Devin, A. The Warburg and Crabtree Effects: On the Origin of Cancer Cell Energy Metabolism and of Yeast Glucose Repression. *Biochim. Biophys. Acta BBA - Bioenerg.* **2011**, *1807* (6), 568–576. https://doi.org/10.1016/j.bbabio.2010.08.010.

(5) Crabtree, H. G. Observations on the Carbohydrate Metabolism of Tumours. *Biochem. J.* **1929**, *23* (3), 536–545. https://doi.org/10.1042/bj0230536.

(6) Yu, T.; Zhou, Y. J.; Huang, M.; Liu, Q.; Pereira, R.; David, F.; Nielsen, J. Reprogramming Yeast Metabolism from Alcoholic Fermentation to Lipogenesis. *Cell* **2018**, *174* (6), 1549-1558.e14. https://doi.org/10.1016/j.cell.2018.07.013.

(7) Petranovic, D.; Tyo, K.; Vemuri, G. N.; Nielsen, J. Prospects of Yeast Systems Biology for Human Health: Integrating Lipid, Protein and Energy Metabolism: Yeast Systems Biology for Human Health. *FEMS Yeast Res.* **2010**, *10* (8), 1046–1059. https://doi.org/10.1111/j.1567-1364.2010.00689.x.

(8) Gastelum, S.; Michael, A. F.; Bolger, T. A. *Saccharomyces Cerevisiae* as a Research Tool for RNA -mediated Human Disease. *WIREs RNA* **2024**, *15* (1), e1814. https://doi.org/10.1002/wrna.1814.

(9) Cervelli, T.; Galli, A. Yeast as a Tool to Understand the Significance of Human Disease-Associated Gene Variants. *Genes* **2021**, *12* (9), 1303. https://doi.org/10.3390/genes12091303.

(10) Bayandina, S. V.; Mukha, D. V. Saccharomyces Cerevisiae as a Model for Studying Human Neurodegenerative Disorders: Viral Capsid Protein Expression. *Int. J. Mol. Sci.* **2023**, *24* (24), 17213. https://doi.org/10.3390/ijms242417213.

(11) Baudin, A.; Ozier-Kalogeropoulos, O.; Denouel, A.; Lacroute, F.; Cullin, C. A Simple and Efficient Method for Direct Gene Deletion in *Saccharomyces Cerevisiae*. *Nucleic Acids Res.* **1993**, *21* (14), 3329–3330. https://doi.org/10.1093/nar/21.14.3329.

(12) Li, X.; Heyer, W.-D. Homologous Recombination in DNA Repair and DNA Damage Tolerance. *Cell Res.* **2008**, *18* (1), 99–113. https://doi.org/10.1038/cr.2008.1.

(13) Lorenz, M. C.; Muir, R. S.; Lim, E.; McElver, J.; Weber, S. C.; Heitman, J. Gene Disruption with PCR Products in Saccharomyces Cerevisiae. *Gene* **1995**, *158* (1), 113–117. https://doi.org/10.1016/0378-1119(95)00144-U.

(14) Brachmann, C. B.; Davies, A.; Cost, G. J.; Caputo, E.; Li, J.; Hieter, P.; Boeke, J. D. Designer Deletion Strains Derived from Saccharomyces Cerevisiae S288C: A Useful Set of Strains and Plasmids for PCR-Mediated Gene Disruption and Other Applications. *Yeast Chichester Engl.* **1998**, *14* (2), 115–132.

https://doi.org/10.1002/(SICI)1097-0061(19980130)14:2%253C115::AID-YEA204%253E3.0.CO;2-2.

(15) Sauer, B. Functional Expression of the *Cre-Lox* Site-Specific Recombination System in the Yeast *Saccharomyces Cerevisiae*. *Mol. Cell. Biol.* **1987**, *7* (6), 2087–2096. https://doi.org/10.1128/mcb.7.6.2087-2096.1987.

(16) Cautereels, C.; Smets, J.; De Saeger, J.; Cool, L.; Zhu, Y.; Zimmermann, A.; Steensels, J.; Gorkovskiy, A.; Jacobs, T. B.; Verstrepen, K. J. Orthogonal LoxPsym Sites Allow Multiplexed Site-Specific Recombination in Prokaryotic and Eukaryotic Hosts. *Nat. Commun.* **2024**, *15* (1), 1113. https://doi.org/10.1038/s41467-024-44996-8.

(17) Jinek, M.; Chylinski, K.; Fonfara, I.; Hauer, M.; Doudna, J. A.; Charpentier, E. A Programmable Dual-RNA–Guided DNA Endonuclease in Adaptive Bacterial Immunity. *Science* **2012**, *337* (6096), 816–821. https://doi.org/10.1126/science.1225829.

(18) Cong, L.; Ran, F. A.; Cox, D.; Lin, S.; Barretto, R.; Habib, N.; Hsu, P. D.; Wu, X.; Jiang, W.; Marraffini, L. A.; Zhang, F. Multiplex Genome Engineering Using CRISPR/Cas Systems. *Science* **2013**, *339* (6121), 819–823. https://doi.org/10.1126/science.1231143.

(19) Ran, F. A.; Hsu, P. D.; Wright, J.; Agarwala, V.; Scott, D. A.; Zhang, F. Genome Engineering Using the CRISPR-Cas9 System. *Nat. Protoc.* **2013**, *8* (11), 2281–2308. https://doi.org/10.1038/nprot.2013.143.

(20) Ran, F. A.; Hsu, P. D.; Lin, C.-Y.; Gootenberg, J. S.; Konermann, S.; Trevino, A. E.; Scott, D. A.; Inoue, A.; Matoba, S.; Zhang, Y.; Zhang, F. Double Nicking by RNA-Guided CRISPR Cas9 for Enhanced Genome Editing Specificity. *Cell* **2013**, *154* (6), 1380–1389. https://doi.org/10.1016/j.cell.2013.08.021.

(21) Deltcheva, E.; Chylinski, K.; Sharma, C. M.; Gonzales, K.; Chao, Y.; Pirzada, Z. A.; Eckert, M. R.; Vogel, J.; Charpentier, E. CRISPR RNA Maturation by Trans-Encoded Small RNA and Host Factor RNase III. *Nature* **2011**, *471* (7340), 602–607. https://doi.org/10.1038/nature09886.

(22) Gasiunas, G.; Barrangou, R.; Horvath, P.; Siksnys, V. Cas9–crRNA Ribonucleoprotein Complex Mediates Specific DNA Cleavage for Adaptive Immunity in Bacteria. *Proc. Natl. Acad. Sci.* **2012**, *109* (39). https://doi.org/10.1073/pnas.1208507109.

(23) Nishimasu, H.; Ran, F. A.; Hsu, P. D.; Konermann, S.; Shehata, S. I.; Dohmae, N.; Ishitani, R.; Zhang, F.; Nureki, O. Crystal Structure of Cas9 in Complex with Guide RNA and Target DNA. *Cell* **2014**, *156* (5), 935–949. https://doi.org/10.1016/j.cell.2014.02.001.

(24) Brouns, S. J. J.; Jore, M. M.; Lundgren, M.; Westra, E. R.; Slijkhuis, R. J. H.; Snijders, A. P. L.; Dickman, M. J.; Makarova, K. S.; Koonin, E. V.; Van Der Oost, J. Small CRISPR RNAs Guide Antiviral Defense in Prokaryotes. *Science* **2008**, *321* (5891), 960–964. https://doi.org/10.1126/science.1159689.

(25) Kalderon, D.; Roberts, B. L.; Richardson, W. D.; Smith, A. E. A Short Amino Acid Sequence Able to Specify Nuclear Location. *Cell* **1984**, *39* (3), 499–509. https://doi.org/10.1016/0092-8674(84)90457-4.

(26) Mojica, F. J. M.; Díez-Villaseñor, C.; García-Martínez, J.; Almendros, C. Short Motif Sequences Determine the Targets of the Prokaryotic CRISPR Defence System. *Microbiology* **2009**, *155* (3), 733–740. https://doi.org/10.1099/mic.0.023960-0.

(27) Mali, P.; Yang, L.; Esvelt, K. M.; Aach, J.; Guell, M.; DiCarlo, J. E.; Norville, J. E.; Church, G. M. RNA-Guided Human Genome Engineering via Cas9. *Science* **2013**, *339* (6121), 823–826. https://doi.org/10.1126/science.1232033.
(28) Friedland, A. E.; Baral, R.; Singhal, P.; Loveluck, K.; Shen, S.; Sanchez, M.; Marco, E.; Gotta, G. M.; Maeder, M. L.; Kennedy, E. M.; Kornepati, A. V. R.; Sousa, A.; Collins, M. A.; Jayaram, H.; Cullen, B. R.; Bumcrot, D. Characterization of Staphylococcus Aureus Cas9: A Smaller Cas9 for All-in-One Adeno-Associated Virus Delivery and Paired Nickase Applications. *Genome Biol.* **2015**, *16* (1), 257. https://doi.org/10.1186/s13059-015-0817-8.
(29) Nishimasu, H.; Cong, L.; Yan, W. X.; Ran, F. A.; Zetsche, B.; Li, Y.; Kurabayashi, A.; Ishitani, R.; Zhang, F.; Nureki, O. Crystal Structure of Staphylococcus Aureus Cas9. *Cell* **2015**, *162* (5), 1113–1126. https://doi.org/10.1016/j.cell.2015.08.007.
(30) Ran, F. A.; Cong, L.; Yan, W. X.; Scott, D. A.; Gootenberg, J. S.; Kriz, A. J.; Zetsche, B.; Shalem, O.; Wu, X.; Makarova, K. S.; Koonin, E. V.; Sharp, P. A.; Zhang, F. In Vivo Genome Editing Using Staphylococcus Aureus Cas9. *Nature* **2015**, *520* (7546), 186–191. https://doi.org/10.1038/nature14299.
(31) Jedrzejczyk, D. J.; Poulsen, L. D.; Mohr, M.; Damas, N. D.; Schoffelen, S.; Barghetti, A.; Baumgartner, R.; Weinert, B. T.; Warnecke, T.; Gill, R. T. CRISPR-Cas12a Nucleases Function with Structurally Engineered crRNAs: SynThetic trAcrRNA. *Sci. Rep.* **2022**, *12* (1), 12193. https://doi.org/10.1038/s41598-022-15388-z.
(32) Paul, B.; Montoya, G. CRISPR-Cas12a: Functional Overview and Applications. *Biomed. J.* **2020**, *43* (1), 8–17. https://doi.org/10.1016/j.bj.2019.10.005.
(33) Gilbert, L. A.; Horlbeck, M. A.; Adamson, B.; Villalta, J. E.; Chen, Y.; Whitehead, E. H.; Guimaraes, C.; Panning, B.; Ploegh, H. L.; Bassik, M. C.; Qi, L. S.; Kampmann, M.; Weissman, J. S. Genome-Scale CRISPR-Mediated Control of Gene Repression and Activation. *Cell* **2014**, *159* (3), 647–661. https://doi.org/10.1016/j.cell.2014.09.029.
(34) Dreissig, S.; Schiml, S.; Schindele, P.; Weiss, O.; Rutten, T.; Schubert, V.; Gladilin, E.; Mette, M. F.; Puchta, H.; Houben, A. Live-cell CRISPR Imaging in Plants Reveals Dynamic Telomere Movements. *Plant J.* **2017**, *91* (4), 565–573. https://doi.org/10.1111/tpj.13601.
(35) Zhang, Z.; Rong, X.; Xie, T.; Li, Z.; Song, H.; Zhen, S.; Wang, H.; Wu, J.; Jaffrey, S. R.; Li, X. Fluorogenic CRISPR for Genomic DNA Imaging. *Nat. Commun.* **2024**, *15* (1), 934. https://doi.org/10.1038/s41467-024-45163-9.
(36) Lee, M. E.; DeLoache, W. C.; Cervantes, B.; Dueber, J. E. A Highly Characterized Yeast Toolkit for Modular, Multipart Assembly. *ACS Synth. Biol.* **2015**, *4* (9), 975–986. https://doi.org/10.1021/sb500366v.
(37) Lian, J.; Mishra, S.; Zhao, H. Recent Advances in Metabolic Engineering of Saccharomyces Cerevisiae: New Tools and Their Applications. *Metab. Eng.* **2018**, *50*, 85–108. https://doi.org/10.1016/j.ymben.2018.04.011.
(38) Redden, H.; Morse, N.; Alper, H. S. The Synthetic Biology Toolbox for Tuning Gene Expression in Yeast. *FEMS Yeast Res.* **2014**, n/a-n/a. https://doi.org/10.1111/1567-1364.12188.
(39) Apel, A. R.; d'Espaux, L.; Wehrs, M.; Sachs, D.; Li, R. A.; Tong, G. J.; Garber, M.; Nnadi, O.; Zhuang, W.; Hillson, N. J.; Keasling, J. D.; Mukhopadhyay, A. A Cas9-Based Toolkit to Program Gene Expression in *Saccharomyces Cerevisiae*. *Nucleic Acids Res.* **2017**, *45* (1), 496–508. https://doi.org/10.1093/nar/gkw1023.

(40) Generoso, W. C.; Gottardi, M.; Oreb, M.; Boles, E. Simplified CRISPR-Cas Genome Editing for Saccharomyces Cerevisiae. *J. Microbiol. Methods* **2016**, *127*, 203–205. https://doi.org/10.1016/j.mimet.2016.06.020.
(41) Jakočiūnas, T.; Bonde, I.; Herrgård, M.; Harrison, S. J.; Kristensen, M.; Pedersen, L. E.; Jensen, M. K.; Keasling, J. D. Multiplex Metabolic Pathway Engineering Using CRISPR/Cas9 in Saccharomyces Cerevisiae. *Metab. Eng.* **2015**, *28*, 213–222. https://doi.org/10.1016/j.ymben.2015.01.008.
(42) Kong, S.; Yu, W.; Gao, N.; Zhai, X.; Zhou, Y. J. Expanding the Neutral Sites for Integrated Gene Expression in *Saccharomyces Cerevisiae*. *FEMS Microbiol. Lett.* **2022**, *369* (1), fnac081. https://doi.org/10.1093/femsle/fnac081.
(43) Maury, J.; Germann, S. M.; Baallal Jacobsen, S. A.; Jensen, N. B.; Kildegaard, K. R.; Herrgård, M. J.; Schneider, K.; Koza, A.; Forster, J.; Nielsen, J.; Borodina, I. EasyCloneMulti: A Set of Vectors for Simultaneous and Multiple Genomic Integrations in Saccharomyces Cerevisiae. *PLOS ONE* **2016**, *11* (3), e0150394. https://doi.org/10.1371/journal.pone.0150394.
(44) Mans, R.; van Rossum, H. M.; Wijsman, M.; Backx, A.; Kuijpers, N. G. A.; van den Broek, M.; Daran-Lapujade, P.; Pronk, J. T.; van Maris, A. J. A.; Daran, J.-M. G. CRISPR/Cas9: A Molecular Swiss Army Knife for Simultaneous Introduction of Multiple Genetic Modifications in Saccharomyces Cerevisiae. *FEMS Yeast Res.* **2015**, *15* (2), fov004. https://doi.org/10.1093/femsyr/fov004.
(45) Feng, X.; Marchisio, M. Saccharomyces Cerevisiae Promoter Engineering before and during the Synthetic Biology Era. *Biology* **2021**, *10* (6), 504. https://doi.org/10.3390/biology10060504.
(46) Oldenburg, K.; Kham, V.; Michaelis, S.; Paddon, C. Recombination-Mediated PCR-Directed Plasmid Construction in Vivo in Yeast. *Nucleic Acids Res.* **1997**, *25* (2), 451–452. https://doi.org/10.1093/nar/25.2.451.
(47) Partow, S.; Siewers, V.; Bjørn, S.; Nielsen, J.; Maury, J. Characterization of Different Promoters for Designing a New Expression Vector in *Saccharomyces Cerevisiae*. *Yeast* **2010**, *27* (11), 955–964. https://doi.org/10.1002/yea.1806.
(48) Peng, B.; Williams, T. C.; Henry, M.; Nielsen, L. K.; Vickers, C. E. Controlling Heterologous Gene Expression in Yeast Cell Factories on Different Carbon Substrates and across the Diauxic Shift: A Comparison of Yeast Promoter Activities. *Microb. Cell Factories* **2015**, *14* (1), 91. https://doi.org/10.1186/s12934-015-0278-5.
(49) Sun, J.; Shao, Z.; Zhao, H.; Nair, N.; Wen, F.; Xu, J.; Zhao, H. Cloning and Characterization of a Panel of Constitutive Promoters for Applications in Pathway Engineering in *Saccharomyces Cerevisiae*. *Biotechnol. Bioeng.* **2012**, *109* (8), 2082–2092. https://doi.org/10.1002/bit.24481.
(50) Taxis, C.; Knop, M. System of Centromeric, Episomal, and Integrative Vectors Based on Drug Resistance Markers for *Saccharomyces Cerevisiae*. *BioTechniques* **2006**, *40* (1), 73–78. https://doi.org/10.2144/000112040.
(51) Cherry, J. M. The Saccharomyces Genome Database: A Tool for Discovery. *Cold Spring Harb. Protoc.* **2015**, *2015* (12), pdb.top083840. https://doi.org/10.1101/pdb.top083840.
(52) Cherry, J. M.; Hong, E. L.; Amundsen, C.; Balakrishnan, R.; Binkley, G.; Chan, E. T.; Christie, K. R.; Costanzo, M. C.; Dwight, S. S.; Engel, S. R.; Fisk, D. G.; Hirschman, J. E.; Hitz, B. C.; Karra, K.; Krieger, C. J.; Miyasato, S. R.; Nash, R. S.; Park, J.; Skrzypek, M. S.; Simison, M.; Weng, S.; Wong, E. D. Saccharomyces Genome Database: The Genomics Resource of Budding Yeast. *Nucleic Acids Res.* **2012**, *40* (D1), D700–D705. https://doi.org/10.1093/nar/gkr1029.

(53) Gülck, T.; Møller, B. L. Phytocannabinoids: Origins and Biosynthesis. *Trends Plant Sci.* **2020**, *25* (10), 985–1004. https://doi.org/10.1016/j.tplants.2020.05.005.
(54) Hill, M. N.; Hillard, C. J.; Bambico, F. R.; Patel, S.; Gorzalka, B. B.; Gobbi, G. The Therapeutic Potential of the Endocannabinoid System for the Development of a Novel Class of Antidepressants. *Trends Pharmacol. Sci.* **2009**, *30* (9), 484–493. https://doi.org/10.1016/j.tips.2009.06.006.
(55) Howlett, A. C. The Cannabinoid Receptors. *Prostaglandins Other Lipid Mediat.* **2002**, *68–69*, 619–631. https://doi.org/10.1016/S0090-6980(02)00060-6.
(56) Ahmed, S. A.; Ross, S. A.; Slade, D.; Radwan, M. M.; Khan, I. A.; ElSohly, M. A. Minor Oxygenated Cannabinoids from High Potency Cannabis Sativa L. *Phytochemistry* **2015**, *117*, 194–199. https://doi.org/10.1016/j.phytochem.2015.04.007.
(57) ElSohly, M. A.; Radwan, M. M.; Gul, W.; Chandra, S.; Galal, A. Phytochemistry of Cannabis Sativa L. In *Phytocannabinoids*; Kinghorn, A. D., Falk, H., Gibbons, S., Kobayashi, J., Eds.; Progress in the Chemistry of Organic Natural Products; Springer International Publishing: Cham, 2017; Vol. 103, pp 1–36. https://doi.org/10.1007/978-3-319-45541-9_1.
(58) ElSohly, M. A.; Mehmedic, Z.; Foster, S.; Gon, C.; Chandra, S.; Church, J. C. Changes in Cannabis Potency Over the Last 2 Decades (1995–2014): Analysis of Current Data in the United States. *Biol. Psychiatry* **2016**, *79* (7), 613–619. https://doi.org/10.1016/j.biopsych.2016.01.004.
(59) ElSohly, M. A.; Gul, W. Constituents of Cannabis Sativa. In *Handbook of Cannabis*; Pertwee, R., Ed.; Oxford University Press, 2014; pp 3–22. https://doi.org/10.1093/acprof:oso/9780199662685.003.0001.
(60) ElSohly, M. A.; Slade, D. Chemical Constituents of Marijuana: The Complex Mixture of Natural Cannabinoids. *Life Sci.* **2005**, *78* (5), 539–548. https://doi.org/10.1016/j.lfs.2005.09.011.
(61) Turner, C. E.; Elsohly, M. A.; Boeren, E. G. Constituents of Cannabis Sativa L. XVII. A Review of the Natural Constituents. *J. Nat. Prod.* **1980**, *43* (2), 169–234. https://doi.org/10.1021/np50008a001.
(62) Hanuš, L. O.; Meyer, S. M.; Muñoz, E.; Taglialatela-Scafati, O.; Appendino, G. Phytocannabinoids: A Unified Critical Inventory. *Nat. Prod. Rep.* **2016**, *33* (12), 1357–1392. https://doi.org/10.1039/C6NP00074F.
(63) Shoyama, Y.; Hirano, H.; Makino, H.; Umekita, N.; Nishioka, I. Cannabis. X. The Isolation and Structures of Four New Propyl Cannabinoid Acids, Tetrahydrocannabivarinic Acid, Cannabidivarinic Acid, Cannabichromevarinic Acid and Cannabigerovarinic Acid, from Thai Cannabis, "Meao Variant". *Chem. Pharm. Bull. (Tokyo)* **1977**, *25* (9), 2306–2311. https://doi.org/10.1248/cpb.25.2306.
(64) Citti, C.; Linciano, P.; Russo, F.; Luongo, L.; Iannotta, M.; Maione, S.; Laganà, A.; Capriotti, A. L.; Forni, F.; Vandelli, M. A.; Gigli, G.; Cannazza, G. A Novel Phytocannabinoid Isolated from Cannabis Sativa L. with an in Vivo Cannabimimetic Activity Higher than Δ9-Tetrahydrocannabinol: Δ9-Tetrahydrocannabiphorol. *Sci. Rep.* **2019**, *9* (1), 20335. https://doi.org/10.1038/s41598-019-56785-1.
(65) Vega-García, A.; Feria-Romero, I.; García-Juárez, A.; Munguia-Madera, A. Ch.; Montes-Aparicio, A. V.; Zequeida-Muñoz, E.; Garcia-Albavera, E.; Orozco-Suárez, S. Cannabinoids: A New Perspective on Epileptogenesis and Seizure Treatment in Early Life in Basic and Clinical Studies. *Front. Behav. Neurosci.* **2021**, *14*, 610484. https://doi.org/10.3389/fnbeh.2020.610484.

(66) Aizpurua-Olaizola, O.; Soydaner, U.; Öztürk, E.; Schibano, D.; Simsir, Y.; Navarro, P.; Etxebarria, N.; Usobiaga, A. Evolution of the Cannabinoid and Terpene Content during the Growth of *Cannabis Sativa* Plants from Different Chemotypes. *J. Nat. Prod.* **2016**, *79* (2), 324–331. https://doi.org/10.1021/acs.jnatprod.5b00949.

(67) Aizpurua-Olaizola, O.; Omar, J.; Navarro, P.; Olivares, M.; Etxebarria, N.; Usobiaga, A. Identification and Quantification of Cannabinoids in Cannabis Sativa L. Plants by High Performance Liquid Chromatography-Mass Spectrometry. *Anal. Bioanal. Chem.* **2014**, *406* (29), 7549–7560. https://doi.org/10.1007/s00216-014-8177-x.

(68) Flores-Sanchez, I. J.; Verpoorte, R. Secondary Metabolism in Cannabis. *Phytochem. Rev.* **2008**, *7* (3), 615–639. https://doi.org/10.1007/s11101-008-9094-4.

(69) *Cannabinoids as Therapeutic Agents*; Mechoulam, R., Ed.; CRC Press: Boca Raton, Flor, 1986.

(70) Zlas, J.; Stark, H.; Seligman, J.; Levy, R.; Werker, E.; Breuer, A.; Mechoulam, R. Early Medical Use of Cannabis. *Nature* **1993**, *363* (6426), 215–215. https://doi.org/10.1038/363215a0.

(71) Wood, T. B.; Spivey, W. T. N.; Easterfield, T. H. III.—Cannabinol. Part I. *J Chem Soc Trans* **1899**, *75* (0), 20–36. https://doi.org/10.1039/CT8997500020.

(72) Adams, R.; Hunt, M.; Clark, J. H. Structure of Cannabidiol, a Product Isolated from the Marihuana Extract of Minnesota Wild Hemp. I. *J. Am. Chem. Soc.* **1940**, *62* (1), 196–200. https://doi.org/10.1021/ja01858a058.

(73) Mechoulam, R.; Shvo, Y. Hashish—I. The Structure of Cannabidiol. *Tetrahedron* **1963**, *19* (12), 2073–2078. https://doi.org/10.1016/0040-4020(63)85022-X.

(74) Gaoni, Y.; Mechoulam, R. Isolation, Structure, and Partial Synthesis of an Active Constituent of Hashish. *J. Am. Chem. Soc.* **1964**, *86* (8), 1646–1647. https://doi.org/10.1021/ja01062a046.

(75) Russo, E. B. History of Cannabis and Its Preparations in Saga, Science, and Sobriquet. *Chem. Biodivers.* **2007**, *4* (8), 1614–1648. https://doi.org/10.1002/cbdv.200790144.

(76) Burstein, S. Cannabidiol (CBD) and Its Analogs: A Review of Their Effects on Inflammation. *Bioorg. Med. Chem.* **2015**, *23* (7), 1377–1385. https://doi.org/10.1016/j.bmc.2015.01.059.

(77) Pisanti, S.; Malfitano, A. M.; Ciaglia, E.; Lamberti, A.; Ranieri, R.; Cuomo, G.; Abate, M.; Faggiana, G.; Proto, M. C.; Fiore, D.; Laezza, C.; Bifulco, M. Cannabidiol: State of the Art and New Challenges for Therapeutic Applications. *Pharmacol. Ther.* **2017**, *175*, 133–150. https://doi.org/10.1016/j.pharmthera.2017.02.041.

(78) Capodice, J. L.; Kaplan, S. A. The Endocannabinoid System, Cannabis, and Cannabidiol: Implications in Urology and Men's Health. *Curr. Urol.* **2021**, *15* (2), 95–100. https://doi.org/10.1097/CU9.0000000000000023.

(79) Lu, H.-C.; Mackie, K. An Introduction to the Endogenous Cannabinoid System. *Biol. Psychiatry* **2016**, *79* (7), 516–525. https://doi.org/10.1016/j.biopsych.2015.07.028.

(80) Marzo, V. D.; Bifulco, M.; Petrocellis, L. D. The Endocannabinoid System and Its Therapeutic Exploitation. *Nat. Rev. Drug Discov.* **2004**, *3* (9), 771–784. https://doi.org/10.1038/nrd1495.

(81) Felder, C. C.; Glass, M. CANNABINOID RECEPTORS AND THEIR ENDOGENOUS AGONISTS. *Annu. Rev. Pharmacol. Toxicol.* **1998**, *38* (1), 179–200. https://doi.org/10.1146/annurev.pharmtox.38.1.179.

(82) Matsuda, L. A.; Lolait, S. J.; Brownstein, M. J.; Young, A. C.; Bonner, T. I. Structure of a Cannabinoid Receptor and Functional Expression of the Cloned cDNA. *Nature* **1990**, *346* (6284), 561–564. https://doi.org/10.1038/346561a0.
(83) Herkenham, M.; Lynn, A. B.; Little, M. D.; Johnson, M. R.; Melvin, L. S.; De Costa, B. R.; Rice, K. C. Cannabinoid Receptor Localization in Brain. *Proc. Natl. Acad. Sci.* **1990**, *87* (5), 1932–1936. https://doi.org/10.1073/pnas.87.5.1932.
(84) Devane, W. A.; Dysarz, F. A.; Johnson, M. R.; Melvin, L. S.; Howlett, A. C. Determination and Characterization of a Cannabinoid Receptor in Rat Brain. *Mol. Pharmacol.* **1988**, *34* (5), 605–613.
(85) Matias, I.; Bisogno, T.; Di Marzo, V. Endogenous Cannabinoids in the Brain and Peripheral Tissues: Regulation of Their Levels and Control of Food Intake. *Int. J. Obes.* **2006**, *30* (S1), S7–S12. https://doi.org/10.1038/sj.ijo.0803271.
(86) Cavuoto, P.; McAinch, A. J.; Hatzinikolas, G.; Janovská, A.; Game, P.; Wittert, G. A. The Expression of Receptors for Endocannabinoids in Human and Rodent Skeletal Muscle. *Biochem. Biophys. Res. Commun.* **2007**, *364* (1), 105–110. https://doi.org/10.1016/j.bbrc.2007.09.099.
(87) Galiègue, S.; Mary, S.; Marchand, J.; Dussossoy, D.; Carrière, D.; Carayon, P.; Bouaboula, M.; Shire, D.; Le Fur, G.; Casellas, P. Expression of Central and Peripheral Cannabinoid Receptors in Human Immune Tissues and Leukocyte Subpopulations. *Eur. J. Biochem.* **1995**, *232* (1), 54–61. https://doi.org/10.1111/j.1432-1033.1995.tb20780.x.
(88) Roche, R.; Hoareau, L.; Bes-Houtmann, S.; Gonthier, M.-P.; Laborde, C.; Baron, J.-F.; Haffaf, Y.; Cesari, M.; Festy, F. Presence of the Cannabinoid Receptors, CB1 and CB2, in Human Omental and Subcutaneous Adipocytes. *Histochem. Cell Biol.* **2006**, *126* (2), 177–187. https://doi.org/10.1007/s00418-005-0127-4.
(89) Munro, S.; Thomas, K. L.; Abu-Shaar, M. Molecular Characterization of a Peripheral Receptor for Cannabinoids. *Nature* **1993**, *365* (6441), 61–65. https://doi.org/10.1038/365061a0.
(90) Benito, C.; Núñez, E.; Tolón, R. M.; Carrier, E. J.; Rábano, A.; Hillard, C. J.; Romero, J. Cannabinoid CB $_2$ Receptors and Fatty Acid Amide Hydrolase Are Selectively Overexpressed in Neuritic Plaque-Associated Glia in Alzheimer's Disease Brains. *J. Neurosci.* **2003**, *23* (35), 11136–11141. https://doi.org/10.1523/JNEUROSCI.23-35-11136.2003.
(91) Ashton, J. C.; Rahman, R. M. A.; Nair, S. M.; Sutherland, B. A.; Glass, M.; Appleton, I. Cerebral Hypoxia-Ischemia and Middle Cerebral Artery Occlusion Induce Expression of the Cannabinoid CB2 Receptor in the Brain. *Neurosci. Lett.* **2007**, *412* (2), 114–117. https://doi.org/10.1016/j.neulet.2006.10.053.
(92) Ramírez, B. G.; Blázquez, C.; Del Pulgar, T. G.; Guzmán, M.; De Ceballos, M. L. Prevention of Alzheimer's Disease Pathology by Cannabinoids: Neuroprotection Mediated by Blockade of Microglial Activation. *J. Neurosci.* **2005**, *25* (8), 1904–1913. https://doi.org/10.1523/JNEUROSCI.4540-04.2005.
(93) Atwood, B. K.; Mackie, K. CB_2 : A Cannabinoid Receptor with an Identity Crisis. *Br. J. Pharmacol.* **2010**, *160* (3), 467–479. https://doi.org/10.1111/j.1476-5381.2010.00729.x.
(94) Callén, L.; Moreno, E.; Barroso-Chinea, P.; Moreno-Delgado, D.; Cortés, A.; Mallol, J.; Casadó, V.; Lanciego, J. L.; Franco, R.; Lluis, C.; Canela, E. I.; McCormick, P. J. Cannabinoid Receptors CB1 and CB2 Form Functional Heteromers in Brain. *J. Biol. Chem.* **2012**, *287* (25), 20851–20865. https://doi.org/10.1074/jbc.M111.335273.

(95) Devane, W. A.; Hanuš, L.; Breuer, A.; Pertwee, R. G.; Stevenson, L. A.; Griffin, G.; Gibson, D.; Mandelbaum, A.; Etinger, A.; Mechoulam, R. Isolation and Structure of a Brain Constituent That Binds to the Cannabinoid Receptor. *Science* **1992**, *258* (5090), 1946–1949. https://doi.org/10.1126/science.1470919.

(96) Mechoulam, R.; Ben-Shabat, S.; Hanus, L.; Ligumsky, M.; Kaminski, N. E.; Schatz, A. R.; Gopher, A.; Almog, S.; Martin, B. R.; Compton, D. R.; Pertwee, R. G.; Griffin, G.; Bayewitch, M.; Barg, J.; Vogel, Z. Identification of an Endogenous 2-Monoglyceride, Present in Canine Gut, That Binds to Cannabinoid Receptors. *Biochem. Pharmacol.* **1995**, *50* (1), 83–90. https://doi.org/10.1016/0006-2952(95)00109-D.

(97) Sugiura, T.; Kondo, S.; Sukagawa, A.; Nakane, S.; Shinoda, A.; Itoh, K.; Yamashita, A.; Waku, K. 2-Arachidonoylgylcerol: A Possible Endogenous Cannabinoid Receptor Ligand in Brain. *Biochem. Biophys. Res. Commun.* **1995**, *215* (1), 89–97. https://doi.org/10.1006/bbrc.1995.2437.

(98) Murataeva, N.; Straiker, A.; Mackie, K. Parsing the Players: 2-arachidonoylglycerol Synthesis and Degradation in the CNS. *Br. J. Pharmacol.* **2014**, *171* (6), 1379–1391. https://doi.org/10.1111/bph.12411.

(99) Liu, J.; Wang, L.; Harvey-White, J.; Osei-Hyiaman, D.; Razdan, R.; Gong, Q.; Chan, A. C.; Zhou, Z.; Huang, B. X.; Kim, H.-Y.; Kunos, G. A Biosynthetic Pathway for Anandamide. *Proc. Natl. Acad. Sci.* **2006**, *103* (36), 13345–13350. https://doi.org/10.1073/pnas.0601832103.

(100) Kelly, R. B. Storage and Release of Neurotransmitters. *Cell* **1993**, *72*, 43–53. https://doi.org/10.1016/S0092-8674(05)80027-3.

(101) Simon, G. M.; Cravatt, B. F. Characterization of Mice Lacking Candidate N-Acyl Ethanolamine Biosynthetic Enzymes Provides Evidence for Multiple Pathways That Contribute to Endocannabinoid Production in Vivo. *Mol. Biosyst.* **2010**, *6* (8), 1411. https://doi.org/10.1039/c000237b.

(102) Bisogno, T.; Howell, F.; Williams, G.; Minassi, A.; Cascio, M. G.; Ligresti, A.; Matias, I.; Schiano-Moriello, A.; Paul, P.; Williams, E.-J.; Gangadharan, U.; Hobbs, C.; Di Marzo, V.; Doherty, P. Cloning of the First Sn1-DAG Lipases Points to the Spatial and Temporal Regulation of Endocannabinoid Signaling in the Brain. *J. Cell Biol.* **2003**, *163* (3), 463–468. https://doi.org/10.1083/jcb.200305129.

(103) Nakane, S.; Oka, S.; Arai, S.; Waku, K.; Ishima, Y.; Tokumura, A.; Sugiura, T. 2-Arachidonoyl-Sn-Glycero-3-Phosphate, an Arachidonic Acid-Containing Lysophosphatidic Acid: Occurrence and Rapid Enzymatic Conversion to 2-Arachidonoyl-Sn-Glycerol, a Cannabinoid Receptor Ligand, in Rat Brain. *Arch. Biochem. Biophys.* **2002**, *402* (1), 51–58. https://doi.org/10.1016/S0003-9861(02)00038-3.

(104) Jung, K.-M.; Astarita, G.; Zhu, C.; Wallace, M.; Mackie, K.; Piomelli, D. A Key Role for Diacylglycerol Lipase-α in Metabotropic Glutamate Receptor-Dependent Endocannabinoid Mobilization. *Mol. Pharmacol.* **2007**, *72* (3), 612–621. https://doi.org/10.1124/mol.107.037796.

(105) Gyombolai, P.; Pap, D.; Turu, G.; Catt, K. J.; Bagdy, G.; Hunyady, L. Regulation of Endocannabinoid Release by G Proteins: A Paracrine Mechanism of G Protein-Coupled Receptor Action. *Mol. Cell. Endocrinol.* **2012**, *353* (1–2), 29–36. https://doi.org/10.1016/j.mce.2011.10.011.

(106) Ohno-Shosaku, T.; Shosaku, J.; Tsubokawa, H.; Kano, M. Cooperative Endocannabinoid Production by Neuronal Depolarization and Group I Metabotropic Glutamate Receptor Activation. *Eur. J. Neurosci.* **2002**, *15* (6), 953–961. https://doi.org/10.1046/j.1460-9568.2002.01929.x.

(107) Stella, N.; Schweitzer, P.; Piomelli, D. A Second Endogenous Cannabinoid That Modulates Long-Term Potentiation. *Nature* **1997**, *388* (6644), 773–778. https://doi.org/10.1038/42015.
(108) Luk, T.; Jin, W.; Zvonok, A.; Lu, D.; Lin, X.; Chavkin, C.; Makriyannis, A.; Mackie, K. Identification of a Potent and Highly Efficacious, yet Slowly Desensitizing CB1 Cannabinoid Receptor Agonist. *Br. J. Pharmacol.* **2004**, *142* (3), 495–500. https://doi.org/10.1038/sj.bjp.0705792.
(109) Nomura, D. K.; Morrison, B. E.; Blankman, J. L.; Long, J. Z.; Kinsey, S. G.; Marcondes, M. C. G.; Ward, A. M.; Hahn, Y. K.; Lichtman, A. H.; Conti, B.; Cravatt, B. F. Endocannabinoid Hydrolysis Generates Brain Prostaglandins That Promote Neuroinflammation. *Science* **2011**, *334* (6057), 809–813. https://doi.org/10.1126/science.1209200.
(110) Wilson, R. I.; Nicoll, R. A. Endogenous Cannabinoids Mediate Retrograde Signalling at Hippocampal Synapses. *Nature* **2001**, *410* (6828), 588–592. https://doi.org/10.1038/35069076.
(111) Kreitzer, A. C.; Regehr, W. G. Retrograde Inhibition of Presynaptic Calcium Influx by Endogenous Cannabinoids at Excitatory Synapses onto Purkinje Cells. *Neuron* **2001**, *29* (3), 717–727. https://doi.org/10.1016/S0896-6273(01)00246-X.
(112) Ohno-Shosaku, T.; Maejima, T.; Kano, M. Endogenous Cannabinoids Mediate Retrograde Signals from Depolarized Postsynaptic Neurons to Presynaptic Terminals. *Neuron* **2001**, *29* (3), 729–738. https://doi.org/10.1016/S0896-6273(01)00247-1.
(113) Guo, J.; Ikeda, S. R. Endocannabinoids Modulate N-Type Calcium Channels and G-Protein-Coupled Inwardly Rectifying Potassium Channels via CB1 Cannabinoid Receptors Heterologously Expressed in Mammalian Neurons. *Mol. Pharmacol.* **2004**, *65* (3), 665–674. https://doi.org/10.1124/mol.65.3.665.
(114) Lauckner, J. E.; Jensen, J. B.; Chen, H.-Y.; Lu, H.-C.; Hille, B.; Mackie, K. GPR55 Is a Cannabinoid Receptor That Increases Intracellular Calcium and Inhibits M Current. *Proc. Natl. Acad. Sci.* **2008**, *105* (7), 2699–2704. https://doi.org/10.1073/pnas.0711278105.
(115) Kohno, M.; Hasegawa, H.; Inoue, A.; Muraoka, M.; Miyazaki, T.; Oka, K.; Yasukawa, M. Identification of N-Arachidonylglycine as the Endogenous Ligand for Orphan G-Protein-Coupled Receptor GPR18. *Biochem. Biophys. Res. Commun.* **2006**, *347* (3), 827–832. https://doi.org/10.1016/j.bbrc.2006.06.175.
(116) McHugh, D.; Page, J.; Dunn, E.; Bradshaw, H. B. Δ^9 -Tetrahydrocannabinol and *N* -arachidonyl Glycine Are Full Agonists at GPR18 Receptors and Induce Migration in Human Endometrial HEC-1B Cells. *Br. J. Pharmacol.* **2012**, *165* (8), 2414–2424. https://doi.org/10.1111/j.1476-5381.2011.01497.x.
(117) De Petrocellis, L.; Ligresti, A.; Moriello, A. S.; Allarà, M.; Bisogno, T.; Petrosino, S.; Stott, C. G.; Di Marzo, V. Effects of Cannabinoids and Cannabinoid-enriched *Cannabis* Extracts on TRP Channels and Endocannabinoid Metabolic Enzymes. *Br. J. Pharmacol.* **2011**, *163* (7), 1479–1494. https://doi.org/10.1111/j.1476-5381.2010.01166.x.
(118) Marzo, V.; Petrocellis, L. Endocannabinoids as Regulators of Transient Receptor Potential (TRP)Channels: A Further Opportunity to Develop New Endocannabinoid-Based Therapeutic Drugs. *Curr. Med. Chem.* **2010**, *17* (14), 1430–1449. https://doi.org/10.2174/092986710790980078.
(119) Meza, R. C.; Ancatén-González, C.; Chiu, C. Q.; Chávez, A. E. Transient Receptor Potential Vanilloid 1 Function at Central Synapses in Health and Disease. *Front. Cell. Neurosci.* **2022**, *16*, 864828. https://doi.org/10.3389/fncel.2022.864828.

(120) Sigel, E.; Baur, R.; Rácz, I.; Marazzi, J.; Smart, T. G.; Zimmer, A.; Gertsch, J. The Major Central Endocannabinoid Directly Acts at $GABA_A$ Receptors. *Proc. Natl. Acad. Sci.* **2011**, *108* (44), 18150–18155. https://doi.org/10.1073/pnas.1113444108.
(121) Howlett, A. C.; Mukhopadhyay, S. Cellular Signal Transduction by Anandamide and 2-Arachidonoylglycerol. *Chem. Phys. Lipids* **2000**, *108* (1–2), 53–70. https://doi.org/10.1016/S0009-3084(00)00187-0.
(122) Kano, M.; Ohno-Shosaku, T.; Hashimotodani, Y.; Uchigashima, M.; Watanabe, M. Endocannabinoid-Mediated Control of Synaptic Transmission. *Physiol. Rev.* **2009**, *89* (1), 309–380. https://doi.org/10.1152/physrev.00019.2008.
(123) Lu, H.-C.; Mackie, K. Review of the Endocannabinoid System. *Biol. Psychiatry Cogn. Neurosci. Neuroimaging* **2021**, *6* (6), 607–615. https://doi.org/10.1016/j.bpsc.2020.07.016.
(124) Paronis, C. A.; Nikas, S. P.; Shukla, V. G.; Makriyannis, A. Δ(9)-Tetrahydrocannabinol Acts as a Partial Agonist/Antagonist in Mice. *Behav. Pharmacol.* **2012**, *23* (8), 802–805. https://doi.org/10.1097/FBP.0b013e32835a7c4d.
(125) Krishna Kumar, K.; Shalev-Benami, M.; Robertson, M. J.; Hu, H.; Banister, S. D.; Hollingsworth, S. A.; Latorraca, N. R.; Kato, H. E.; Hilger, D.; Maeda, S.; Weis, W. I.; Farrens, D. L.; Dror, R. O.; Malhotra, S. V.; Kobilka, B. K.; Skiniotis, G. Structure of a Signaling Cannabinoid Receptor 1-G Protein Complex. *Cell* **2019**, *176* (3), 448-458.e12. https://doi.org/10.1016/j.cell.2018.11.040.
(126) Hua, T.; Vemuri, K.; Nikas, S. P.; Laprairie, R. B.; Wu, Y.; Qu, L.; Pu, M.; Korde, A.; Jiang, S.; Ho, J.-H.; Han, G. W.; Ding, K.; Li, X.; Liu, H.; Hanson, M. A.; Zhao, S.; Bohn, L. M.; Makriyannis, A.; Stevens, R. C.; Liu, Z.-J. Crystal Structures of Agonist-Bound Human Cannabinoid Receptor CB1. *Nature* **2017**, *547* (7664), 468–471. https://doi.org/10.1038/nature23272.
(127) Petitet, F.; Jeantaud, B.; Reibaud, M.; Imperato, A.; Dubroeucq, M.-C. Complex Pharmacology of Natural Cannabivoids: Evidence for Partial Agonist Activity of Δ9-Tetrahydrocannabinol and Antagonist Activity of Cannabidiol on Rat Brain Cannabinoid Receptors. *Life Sci.* **1998**, *63* (1), PL1–PL6. https://doi.org/10.1016/S0024-3205(98)00238-0.
(128) Jones, P. G.; Falvello, L.; Kennard, O.; Sheldrick, G. M.; Mechoulam, R. Cannabidiol. *Acta Crystallogr. B* **1977**, *33* (10), 3211–3214. https://doi.org/10.1107/S0567740877010577.
(129) Thomas, A.; Baillie, G. L.; Phillips, A. M.; Razdan, R. K.; Ross, R. A.; Pertwee, R. G. Cannabidiol Displays Unexpectedly High Potency as an Antagonist of CB_1 and CB_2 Receptor Agonists *in Vitro*. *Br. J. Pharmacol.* **2007**, *150* (5), 613–623. https://doi.org/10.1038/sj.bjp.0707133.
(130) Pertwee, R. G. The Diverse CB_1 and CB_2 Receptor Pharmacology of Three Plant Cannabinoids: Δ^9 -tetrahydrocannabinol, Cannabidiol and Δ^9 -tetrahydrocannabivarin. *Br. J. Pharmacol.* **2008**, *153* (2), 199–215. https://doi.org/10.1038/sj.bjp.0707442.
(131) Laprairie, R. B.; Bagher, A. M.; Kelly, M. E. M.; Denovan-Wright, E. M. Cannabidiol Is a Negative Allosteric Modulator of the Cannabinoid CB_1 Receptor. *Br. J. Pharmacol.* **2015**, *172* (20), 4790–4805. https://doi.org/10.1111/bph.13250.
(132) Martínez-Pinilla, E.; Varani, K.; Reyes-Resina, I.; Angelats, E.; Vincenzi, F.; Ferreiro-Vera, C.; Oyarzabal, J.; Canela, E. I.; Lanciego, J. L.; Nadal, X.; Navarro, G.; Borea, P. A.; Franco, R. Binding and Signaling Studies Disclose a Potential Allosteric Site for Cannabidiol in Cannabinoid CB2 Receptors. *Front. Pharmacol.* **2017**, *8*, 744. https://doi.org/10.3389/fphar.2017.00744.

(133) Leweke, F. M.; Piomelli, D.; Pahlisch, F.; Muhl, D.; Gerth, C. W.; Hoyer, C.; Klosterkötter, J.; Hellmich, M.; Koethe, D. Cannabidiol Enhances Anandamide Signaling and Alleviates Psychotic Symptoms of Schizophrenia. *Transl. Psychiatry* **2012**, *2* (3), e94–e94. https://doi.org/10.1038/tp.2012.15.

(134) Grosser, T.; Theken, K. N.; FitzGerald, G. A. Cyclooxygenase Inhibition: Pain, Inflammation, and the Cardiovascular System. *Clin. Pharmacol. Ther.* **2017**, *102* (4), 611–622. https://doi.org/10.1002/cpt.794.

(135) Aiello, F.; Carullo, G.; Badolato, M.; Brizzi, A. TRPV1–FAAH–COX: The *Couples Game* in Pain Treatment. *ChemMedChem* **2016**, *11* (16), 1686–1694. https://doi.org/10.1002/cmdc.201600111.

(136) Giuffrida, A.; Leweke, F. M.; Gerth, C. W.; Schreiber, D.; Koethe, D.; Faulhaber, J.; Klosterkötter, J.; Piomelli, D. Cerebrospinal Anandamide Levels Are Elevated in Acute Schizophrenia and Are Inversely Correlated with Psychotic Symptoms. *Neuropsychopharmacology* **2004**, *29* (11), 2108–2114. https://doi.org/10.1038/sj.npp.1300558.

(137) Koethe, D.; Giuffrida, A.; Schreiber, D.; Hellmich, M.; Schultze-Lutter, F.; Ruhrmann, S.; Klosterkötter, J.; Piomelli, D.; Leweke, F. M. Anandamide Elevation in Cerebrospinal Fluid in Initial Prodromal States of Psychosis. *Br. J. Psychiatry* **2009**, *194* (4), 371–372. https://doi.org/10.1192/bjp.bp.108.053843.

(138) Grover, A. K. Use of Allosteric Targets in the Discovery of Safer Drugs. *Med. Princ. Pract. Int. J. Kuwait Univ. Health Sci. Cent.* **2013**, *22* (5), 418–426. https://doi.org/10.1159/000350417.

(139) Nichol, K.; Stott, C.; Jones, N.; Gray, R. A.; Bazelot, M.; Whalley, B. J. The Proposed Multimodal Mechanism of Action of Cannabidiol (CBD) in Epilepsy: Modulation of Intracellular Calcium and Adenosine-Mediated Signaling (P5.5-007). *Neurology* **2019**, *92* (15_supplement), P5.5-007. https://doi.org/10.1212/WNL.92.15_supplement.P5.5-007.

(140) Martínez-Aguirre, C.; Carmona-Cruz, F.; Velasco, A. L.; Velasco, F.; Aguado-Carrillo, G.; Cuéllar-Herrera, M.; Rocha, L. Cannabidiol Acts at 5-HT1A Receptors in the Human Brain: Relevance for Treating Temporal Lobe Epilepsy. *Front. Behav. Neurosci.* **2020**, *14*, 611278. https://doi.org/10.3389/fnbeh.2020.611278.

(141) Khan, A. A.; Shekh-Ahmad, T.; Khalil, A.; Walker, M. C.; Ali, A. B. Cannabidiol Exerts Antiepileptic Effects by Restoring Hippocampal Interneuron Functions in a Temporal Lobe Epilepsy Model. *Br. J. Pharmacol.* **2018**, *175* (11), 2097–2115. https://doi.org/10.1111/bph.14202.

(142) Scuderi, C.; Filippis, D. D.; Iuvone, T.; Blasio, A.; Steardo, A.; Esposito, G. Cannabidiol in Medicine: A Review of Its Therapeutic Potential in CNS Disorders. *Phytother. Res.* **2009**, *23* (5), 597–602. https://doi.org/10.1002/ptr.2625.

(143) Izzo, A. A.; Borrelli, F.; Capasso, R.; Di Marzo, V.; Mechoulam, R. Non-Psychotropic Plant Cannabinoids: New Therapeutic Opportunities from an Ancient Herb. *Trends Pharmacol. Sci.* **2009**, *30* (10), 515–527. https://doi.org/10.1016/j.tips.2009.07.006.

(144) Walsh, K. B.; McKinney, A. E.; Holmes, A. E. Minor Cannabinoids: Biosynthesis, Molecular Pharmacology and Potential Therapeutic Uses. *Front. Pharmacol.* **2021**, *12*, 777804. https://doi.org/10.3389/fphar.2021.777804.

(145) Sepulveda, D. E.; Vrana, K. E.; Kellogg, J. J.; Bisanz, J. E.; Desai, D.; Graziane, N. M.; Raup-Konsavage, W. M. The Potential of Cannabichromene (CBC) as a Therapeutic Agent. *J. Pharmacol. Exp. Ther.* **2024**, *391* (2), 206–213. https://doi.org/10.1124/jpet.124.002166.

(146) Zagzoog, A.; Mohamed, K. A.; Kim, H. J. J.; Kim, E. D.; Frank, C. S.; Black, T.; Jadhav, P. D.; Holbrook, L. A.; Laprairie, R. B. In Vitro and in Vivo Pharmacological Activity of Minor Cannabinoids Isolated from Cannabis Sativa. *Sci. Rep.* **2020**, *10* (1), 20405. https://doi.org/10.1038/s41598-020-77175-y.

(147) Izzo, A. A.; Capasso, R.; Aviello, G.; Borrelli, F.; Romano, B.; Piscitelli, F.; Gallo, L.; Capasso, F.; Orlando, P.; Di Marzo, V. Inhibitory Effect of Cannabichromene, a Major Non-psychotropic Cannabinoid Extracted from *Cannabis Sativa* , on Inflammation-induced Hypermotility in Mice. *Br. J. Pharmacol.* **2012**, *166* (4), 1444–1460. https://doi.org/10.1111/j.1476-5381.2012.01879.x.

(148) Calcaterra, A.; Cianfoni, G.; Tortora, C.; Manetto, S.; Grassi, G.; Botta, B.; Gasparrini, F.; Mazzoccanti, G.; Appendino, G. Natural Cannabichromene (CBC) Shows Distinct Scalemicity Grades and Enantiomeric Dominance in *Cannabis Sativa* Strains. *J. Nat. Prod.* **2023**, *86* (4), 909–914. https://doi.org/10.1021/acs.jnatprod.2c01139.

(149) Crombie, L.; Ponsford, R. Synthesis of Cannabinoids by Pyridine-Catalysed Citral–Olivetol Condensation: Synthesis and Structure of Cannabicyclol, Cannabichromen, (Hashish Extractives), Citrylidene-Cannabis, and Related Compounds. *J Chem Soc C* **1971**, *0* (0), 796–804. https://doi.org/10.1039/J39710000796.

(150) Pollastro, F.; Caprioglio, D.; Del Prete, D.; Rogati, F.; Minassi, A.; Taglialatela-Scafati, O.; Munoz, E.; Appendino, G. Cannabichromene. *Nat. Prod. Commun.* **2018**, *13* (9), 1934578X1801300922. https://doi.org/10.1177/1934578X1801300922.

(151) Quílez Del Moral, J. F.; Ruiz Martínez, C.; Pérez Del Pulgar, H.; Martín González, J. E.; Fernández, I.; López-Pérez, J. L.; Fernández-Arteaga, A.; Barrero, A. F. Synthesis of Cannabinoids: “In Water” and “On Water” Approaches: Influence of SDS Micelles. *J. Org. Chem.* **2021**, *86* (4), 3344–3355. https://doi.org/10.1021/acs.joc.0c02698.

(152) Thomas, F.; Kayser, O. Improving CBCA Synthase Activity through Rational Protein Design. *J. Biotechnol.* **2023**, *363*, 40–49. https://doi.org/10.1016/j.jbiotec.2023.01.004.

(153) Miller, S.; Daily, L.; Leishman, E.; Bradshaw, H.; Straiker, A. Δ9-Tetrahydrocannabinol and Cannabidiol Differentially Regulate Intraocular Pressure. *Invest. Ophthalmol. Vis. Sci.* **2018**, *59* (15), 5904–5911. https://doi.org/10.1167/iovs.18-24838.

(154) Abrams, D. I.; Hilton, J. F.; Leiser, R. J.; Shade, S. B.; Elbeik, T. A.; Aweeka, F. T.; Benowitz, N. L.; Bredt, B. M.; Kosel, B.; Aberg, J. A.; Deeks, S. G.; Mitchell, T. F.; Mulligan, K.; Bacchetti, P.; McCune, J. M.; Schambelan, M. Short-Term Effects of Cannabinoids in Patients with HIV-1 Infection: A Randomized, Placebo-Controlled Clinical Trial. *Ann. Intern. Med.* **2003**, *139* (4), 258. https://doi.org/10.7326/0003-4819-139-4-200308190-00008.

(155) Badowski, M.; Yanful, P. K. Dronabinol Oral Solution in the Management of Anorexia and Weight Loss in AIDS and Cancer. *Ther. Clin. Risk Manag.* **2018**, *Volume 14*, 643–651. https://doi.org/10.2147/TCRM.S126849.

(156) Beal, J. E.; Olson, R.; Laubenstein, L.; Morales, J. O.; Bellman, P.; Yangco, B.; Lefkowitz, L.; Plasse, T. F.; Shepard, K. V. Dronabinol as a Treatment for Anorexia Associated with Weight Loss in Patients with AIDS. *J. Pain Symptom Manage.* **1995**, *10* (2), 89–97. https://doi.org/10.1016/0885-3924(94)00117-4.

(157) Herman, T. S.; Einhorn, L. H.; Jones, S. E.; Nagy, C.; Chester, A. B.; Dean, J. C.; Furnas, B.; Williams, S. D.; Leigh, S. A.; Dorr, R. T.; Moon, T. E. Superiority of

Nabilone over Prochlorperazine as an Antiemetic in Patients Receiving Cancer Chemotherapy. *N. Engl. J. Med.* **1979**, *300* (23), 1295–1297. https://doi.org/10.1056/NEJM197906073002302.

(158) Hutcheon, A. W.; Palmer, J. B. D.; Soukop, M.; Cunningham, D.; McArdle, C.; Welsh, J.; Stuart, F.; Sangster, G.; Kaye, S.; Charlton, D.; Cash, H. A Randomised Multicentre Single Blind Comparison of a Cannabinoid Anti-Emetic (Levonantradol) with Chlorpromazine in Patients Receiving Their First Cytotoxic Chemotherapy. *Eur. J. Cancer Clin. Oncol.* **1983**, *19* (8), 1087–1090. https://doi.org/10.1016/0277-5379(83)90032-9.

(159) Wilsey, B.; Marcotte, T.; Deutsch, R.; Gouaux, B.; Sakai, S.; Donaghe, H. Low-Dose Vaporized Cannabis Significantly Improves Neuropathic Pain. *J. Pain* **2013**, *14* (2), 136–148. https://doi.org/10.1016/j.jpain.2012.10.009.

(160) Lynch, M. E.; Campbell, F. Cannabinoids for Treatment of Chronic Non-cancer Pain; a Systematic Review of Randomized Trials. *Br. J. Clin. Pharmacol.* **2011**, *72* (5), 735–744. https://doi.org/10.1111/j.1365-2125.2011.03970.x.

(161) Corey-Bloom, J.; Wolfson, T.; Gamst, A.; Jin, S.; Marcotte, T. D.; Bentley, H.; Gouaux, B. Smoked Cannabis for Spasticity in Multiple Sclerosis: A Randomized, Placebo-Controlled Trial. *Can. Med. Assoc. J.* **2012**, *184* (10), 1143–1150. https://doi.org/10.1503/cmaj.110837.

(162) Wade, D. T.; Makela, P.; Robson, P.; House, H.; Bateman, C. Do Cannabis-Based Medicinal Extracts Have General or Specific Effects on Symptoms in Multiple Sclerosis? A Double-Blind, Randomized, Placebo-Controlled Study on 160 Patients. *Mult. Scler. J.* **2004**, *10* (4), 434–441. https://doi.org/10.1191/1352458504ms1082oa.

(163) Akinyemi, E.; Randhawa, G.; Longoria, V.; Zeine, R. Medical Marijuana Effects in Movement Disorders, Focus on Huntington Disease; A Literature Review. *J. Pharm. Pharm. Sci.* **2020**, *23*, 389–395. https://doi.org/10.18433/jpps30967.

(164) De Petrocellis, L.; Ligresti, A.; Schiano Moriello, A.; Iappelli, M.; Verde, R.; Stott, C. G.; Cristino, L.; Orlando, P.; Di Marzo, V. Non-THC Cannabinoids Inhibit Prostate Carcinoma Growth *in Vitro* and *in Vivo* : Pro-apoptotic Effects and Underlying Mechanisms. *Br. J. Pharmacol.* **2013**, *168* (1), 79–102. https://doi.org/10.1111/j.1476-5381.2012.02027.x.

(165) Abu-Sawwa, R.; Scutt, B.; Park, Y. Emerging Use of Epidiolex (Cannabidiol) in Epilepsy. *J. Pediatr. Pharmacol. Ther.* **2020**, *25* (6), 485–499. https://doi.org/10.5863/1551-6776-25.6.485.

(166) Cunha, J. M.; Carlini, E. A.; Pereira, A. E.; Ramos, O. L.; Pimentel, C.; Gagliardi, R.; Sanvito, W. L.; Lander, N.; Mechoulam, R. Chronic Administration of Cannabidiol to Healthy Volunteers and Epileptic Patients. *Pharmacology* **1980**, *21* (3), 175–185. https://doi.org/10.1159/000137430.

(167) Kim, S. H.; Yang, J. W.; Kim, K. H.; Kim, J. U.; Yook, T. H. A Review on Studies of Marijuana for Alzheimer's Disease - Focusing on CBD, THC. *J. Pharmacopuncture* **2019**, *22* (4), 225–230. https://doi.org/10.3831/KPI.2019.22.030.

(168) Urbi, B.; Corbett, J.; Hughes, I.; Owusu, M. A.; Thorning, S.; Broadley, S. A.; Sabet, A.; Heshmat, S. Effects of Cannabis in Parkinson's Disease: A Systematic Review and Meta-Analysis. *J. Park. Dis.* **2022**, *12* (2), 495–508. https://doi.org/10.3233/JPD-212923.

(169) Van Klingeren, B.; Ten Ham, M. Antibacterial Activity of Δ9-Tetrahydrocannabinol and Cannabidiol. *Antonie Van Leeuwenhoek* **1976**, *42* (1–2), 9–12. https://doi.org/10.1007/BF00399444.

(170) Appendino, G.; Gibbons, S.; Giana, A.; Pagani, A.; Grassi, G.; Stavri, M.; Smith, E.; Rahman, M. M. Antibacterial Cannabinoids from *Cannabis Sativa* : A Structure−Activity Study. *J. Nat. Prod.* **2008**, *71* (8), 1427–1430. https://doi.org/10.1021/np8002673.
(171) Farha, M. A.; El-Halfawy, O. M.; Gale, R. T.; MacNair, C. R.; Carfrae, L. A.; Zhang, X.; Jentsch, N. G.; Magolan, J.; Brown, E. D. Uncovering the Hidden Antibiotic Potential of Cannabis. *ACS Infect. Dis.* **2020**, *6* (3), 338–346. https://doi.org/10.1021/acsinfecdis.9b00419.
(172) Manso, T.; Lores, M.; De Miguel, T. Antimicrobial Activity of Polyphenols and Natural Polyphenolic Extracts on Clinical Isolates. *Antibiotics* **2021**, *11* (1), 46. https://doi.org/10.3390/antibiotics11010046.
(173) Cham, P. S.; Deepika; Bhat, R.; Raina, D.; Manhas, D.; Kotwal, P.; Mindala, D. P.; Pandey, N.; Ghosh, A.; Saran, S.; Nandi, U.; Khan, I. A.; Singh, P. P. Exploring the Antibacterial Potential of Semisynthetic Phytocannabinoid: Tetrahydrocannabidiol (THCBD) as a Potential Antibacterial Agent against Sensitive and Resistant Strains of *Staphylococcus Aureus*. *ACS Infect. Dis.* **2024**, *10* (1), 64–78. https://doi.org/10.1021/acsinfecdis.3c00154.
(174) Niyangoda, D.; Aung, M. L.; Qader, M.; Tesfaye, W.; Bushell, M.; Chiong, F.; Tsai, D.; Ahmad, D.; Samarawickrema, I.; Sinnollareddy, M.; Thomas, J. Cannabinoids as Antibacterial Agents: A Systematic and Critical Review of In Vitro Efficacy Against Streptococcus and Staphylococcus. *Antibiotics* **2024**, *13* (11), 1023. https://doi.org/10.3390/antibiotics13111023.
(175) Happyana, N.; Agnolet, S.; Muntendam, R.; Van Dam, A.; Schneider, B.; Kayser, O. Analysis of Cannabinoids in Laser-Microdissected Trichomes of Medicinal Cannabis Sativa Using LCMS and Cryogenic NMR. *Phytochemistry* **2013**, *87*, 51–59. https://doi.org/10.1016/j.phytochem.2012.11.001.
(176) Kim, E.; Mahlberg, P. Immunochemical Localization of Tetrahydrocannabinol (THC) in Cryofixed Glandular Trichomes of Cannabis (Cannabaceae). *Am. J. Bot.* **1997**, *84* (3), 336.
(177) Ohlsson, A.; Abou-Chaar, C. I.; Agurell, S.; Nilsson, I. M.; Olofsson, K.; Sandberg, F. Cannabinoid Constituents of Male and Female Cannabis Sativa. *UN Bull. Narc.* **1971**, No. 23, 29–32.
(178) Livingston, S. J.; Quilichini, T. D.; Booth, J. K.; Wong, D. C. J.; Rensing, K. H.; Laflamme-Yonkman, J.; Castellarin, S. D.; Bohlmann, J.; Page, J. E.; Samuels, A. L. Cannabis Glandular Trichomes Alter Morphology and Metabolite Content during Flower Maturation. *Plant J.* **2020**, *101* (1), 37–56. https://doi.org/10.1111/tpj.14516.
(179) Zager, J. J.; Lange, I.; Srividya, N.; Smith, A.; Lange, B. M. Gene Networks Underlying Cannabinoid and Terpenoid Accumulation in Cannabis. *Plant Physiol.* **2019**, *180* (4), 1877–1897. https://doi.org/10.1104/pp.18.01506.
(180) Gagne, S. J.; Stout, J. M.; Liu, E.; Boubakir, Z.; Clark, S. M.; Page, J. E. Identification of Olivetolic Acid Cyclase from *Cannabis Sativa* Reveals a Unique Catalytic Route to Plant Polyketides. *Proc. Natl. Acad. Sci.* **2012**, *109* (31), 12811–12816. https://doi.org/10.1073/pnas.1200330109.
(181) Stout, J. M.; Boubakir, Z.; Ambrose, S. J.; Purves, R. W.; Page, J. E. The hexanoyl-CoA Precursor for Cannabinoid Biosynthesis Is Formed by an Acyl-activating Enzyme in *Cannabis Sativa* Trichomes. *Plant J.* **2012**, *71* (3), 353–365. https://doi.org/10.1111/j.1365-313X.2012.04949.x.
(182) Marks, M. D.; Tian, L.; Wenger, J. P.; Omburo, S. N.; Soto-Fuentes, W.; He, J.; Gang, D. R.; Weiblen, G. D.; Dixon, R. A. Identification of Candidate Genes

Affecting Δ9-Tetrahydrocannabinol Biosynthesis in Cannabis Sativa. *J. Exp. Bot.* **2009**, *60* (13), 3715–3726. https://doi.org/10.1093/jxb/erp210.
(183) Taura, F.; Tanaka, S.; Taguchi, C.; Fukamizu, T.; Tanaka, H.; Shoyama, Y.; Morimoto, S. Characterization of Olivetol Synthase, a Polyketide Synthase Putatively Involved in Cannabinoid Biosynthetic Pathway. *FEBS Lett.* **2009**, *583* (12), 2061–2066. https://doi.org/10.1016/j.febslet.2009.05.024.
(184) Kearsey, L. J.; Prandi, N.; Karuppiah, V.; Yan, C.; Leys, D.; Toogood, H.; Takano, E.; Scrutton, N. S. Structure of the *Cannabis Sativa* Olivetol-producing Enzyme Reveals Cyclization Plasticity in Type III Polyketide Synthases. *FEBS J.* **2020**, *287* (8), 1511–1524. https://doi.org/10.1111/febs.15089.
(185) Tan, Z.; Clomburg, J. M.; Gonzalez, R. Synthetic Pathway for the Production of Olivetolic Acid in *Escherichia Coli*. *ACS Synth. Biol.* **2018**, *7* (8), 1886–1896. https://doi.org/10.1021/acssynbio.8b00075.
(186) Shen, Y.; Yoon, P.; Yu, T.-W.; Floss, H. G.; Hopwood, D.; Moore, B. S. Ectopic Expression of the Minimal *whiE* Polyketide Synthase Generates a Library of Aromatic Polyketides of Diverse Sizes and Shapes. *Proc. Natl. Acad. Sci.* **1999**, *96* (7), 3622–3627. https://doi.org/10.1073/pnas.96.7.3622.
(187) Yang, X.; Matsui, T.; Mori, T.; Taura, F.; Noguchi, H.; Abe, I.; Morita, H. Expression, Purification and Crystallization of a Plant Polyketide Cyclase from *Cannabis Sativa*. *Acta Crystallogr. Sect. F Struct. Biol. Commun.* **2015**, *71* (12), 1470–1474. https://doi.org/10.1107/S2053230X15020385.
(188) Yang, X.; Matsui, T.; Kodama, T.; Mori, T.; Zhou, X.; Taura, F.; Noguchi, H.; Abe, I.; Morita, H. Structural Basis for Olivetolic Acid Formation by a Polyketide Cyclase from *Cannabis Sativa*. *FEBS J.* **2016**, *283* (6), 1088–1106. https://doi.org/10.1111/febs.13654.
(189) Do, T.-H.; Duong, T.-H.; Nguyen, H. T.; Nguyen, T.-H.; Sichaem, J.; Nguyen, C. H.; Nguyen, H.-H.; Long, N. P. Biological Activities of Lichen-Derived Monoaromatic Compounds. *Molecules* **2022**, *27* (9), 2871. https://doi.org/10.3390/molecules27092871.
(190) Yu, D.; Xu, F.; Zeng, J.; Zhan, J. Type III Polyketide Synthases in Natural Product Biosynthesis. *IUBMB Life* **2012**, *64* (4), 285–295. https://doi.org/10.1002/iub.1005.
(191) Ismed, F.; Farhan, A.; Bakhtiar, A.; Zaini, E.; Nugraha, Y. P.; Dwichandra Putra, O.; Uekusa, H. Crystal Structure of Olivetolic Acid: A Natural Product from *Cetrelia Sanguinea* (Schaer.). *Acta Crystallogr. Sect. E Crystallogr. Commun.* **2016**, *72* (11), 1587–1589. https://doi.org/10.1107/S2056989016016273.
(192) Frémont, L. Biological Effects of Resveratrol. *Life Sci.* **2000**, *66* (8), 663–673. https://doi.org/10.1016/S0024-3205(99)00410-5.
(193) Jez, J. M.; Bowman, M. E.; Noel, J. P. Structure-Guided Programming of Polyketide Chain-Length Determination in Chalcone Synthase. *Biochemistry* **2001**, *40* (49), 14829–14838. https://doi.org/10.1021/bi015621z.
(194) Winkel-Shirley, B. Flavonoid Biosynthesis. A Colorful Model for Genetics, Biochemistry, Cell Biology, and Biotechnology. *Plant Physiol.* **2001**, *126* (2), 485–493. https://doi.org/10.1104/pp.126.2.485.
(195) Austin, M. B.; Bowman, M. E.; Ferrer, J.-L.; Schröder, J.; Noel, J. P. An Aldol Switch Discovered in Stilbene Synthases Mediates Cyclization Specificity of Type III Polyketide Synthases. *Chem. Biol.* **2004**, *11* (9), 1179–1194. https://doi.org/10.1016/j.chembiol.2004.05.024.
(196) Heath, R. J.; Rock, C. O. The Claisen Condensation in Biology. *Nat. Prod. Rep.* **2002**, *19* (5), 581–596. https://doi.org/10.1039/b110221b.

(197) Tropf, S.; Kärcher, B.; Schröder, G.; Schröder, J. Reaction Mechanisms of Homodimeric Plant Polyketide Synthases (Stilbene and Chalcone Synthase). *J. Biol. Chem.* **1995**, *270* (14), 7922–7928. https://doi.org/10.1074/jbc.270.14.7922.
(198) Vranová, E.; Coman, D.; Gruissem, W. Network Analysis of the MVA and MEP Pathways for Isoprenoid Synthesis. *Annu. Rev. Plant Biol.* **2013**, *64* (1), 665–700. https://doi.org/10.1146/annurev-arplant-050312-120116.
(199) Hunter, W. N. The Non-Mevalonate Pathway of Isoprenoid Precursor Biosynthesis. *J. Biol. Chem.* **2007**, *282* (30), 21573–21577. https://doi.org/10.1074/jbc.R700005200.
(200) Carvalho, Â.; Hansen, E. H.; Kayser, O.; Carlsen, S.; Stehle, F. Designing Microorganisms for Heterologous Biosynthesis of Cannabinoids. *FEMS Yeast Res.* **2017**, *17* (4), fox037. https://doi.org/10.1093/femsyr/fox037.
(201) Fellermeier, M.; Zenk, M. H. Prenylation of Olivetolate by a Hemp Transferase Yields Cannabigerolic Acid, the Precursor of Tetrahydrocannabinol. *FEBS Lett.* **1998**, *427* (2), 283–285. https://doi.org/10.1016/S0014-5793(98)00450-5.
(202) Gülck, T.; Booth, J. K.; Carvalho, Â.; Khakimov, B.; Crocoll, C.; Motawia, M. S.; Møller, B. L.; Bohlmann, J.; Gallage, N. J. Synthetic Biology of Cannabinoids and Cannabinoid Glucosides in *Nicotiana Benthamiana* and *Saccharomyces Cerevisiae*. *J. Nat. Prod.* **2020**, *83* (10), 2877–2893. https://doi.org/10.1021/acs.jnatprod.0c00241.
(203) Tanaya, R.; Kodama, T.; Lee, Y.-E.; Yasuno, Y.; Shinada, T.; Takahashi, H.; Ito, T.; Morita, H.; Awale, S.; Taura, F. Catalytic Potential of *Cannabis* Prenyltransferase to Expand Cannabinoid Scaffold Diversity. *Org. Lett.* **2023**, *25* (48), 8601–8605. https://doi.org/10.1021/acs.orglett.3c03410.
(204) Yamauchi, T.; Shoyama, Y.; Aramaki, H.; Azuma, T.; Nishioka, I. Tetrahydrocannabinolic Acid, a Genuine Substance of Tetrahydrocannabinol. *Chem. Pharm. Bull. (Tokyo)* **1967**, *15* (7), 1075–1076. https://doi.org/10.1248/cpb.15.1075.
(205) Veress, T.; Szanto, J. I.; Leisztner, L. Determination of Cannabinoid Acids by High-Performance Liquid Chromatography of Their Neutral Derivatives Formed by Thermal Decarboxylation. *J. Chromatogr. A* **1990**, *520*, 339–347. https://doi.org/10.1016/0021-9673(90)85118-F.
(206) Kimura, M.; Okamoto, K. Distribution of Tetrahydrocannabinolic Acid in Fresh Wild Cannabis. *Experientia* **1970**, *26* (8), 819–820. https://doi.org/10.1007/BF02114192.
(207) Kim, A. L.; Yun, Y. J.; Choi, H. W.; Hong, C.-H.; Shim, H. J.; Lee, J. H.; Kim, Y.-C. Profiling Cannabinoid Contents and Expression Levels of Corresponding Biosynthetic Genes in Commercial Cannabis (Cannabis Sativa L.) Cultivars. *Plants* **2022**, *11* (22), 3088. https://doi.org/10.3390/plants11223088.
(208) Laverty, K. U.; Stout, J. M.; Sullivan, M. J.; Shah, H.; Gill, N.; Holbrook, L.; Deikus, G.; Sebra, R.; Hughes, T. R.; Page, J. E.; Van Bakel, H. A Physical and Genetic Map of *Cannabis Sativa* Identifies Extensive Rearrangements at the *THC/CBD Acid Synthase* Loci. *Genome Res.* **2019**, *29* (1), 146–156. https://doi.org/10.1101/gr.242594.118.
(209) Taura, F.; Sirikantaramas, S.; Shoyama, Y.; Yoshikai, K.; Shoyama, Y.; Morimoto, S. Cannabidiolic-acid Synthase, the Chemotype-determining Enzyme in the Fiber-type *Cannabis Sativa*. *FEBS Lett.* **2007**, *581* (16), 2929–2934. https://doi.org/10.1016/j.febslet.2007.05.043.
(210) Stuyt, E. The Problem with the Current High Potency THC Marijuana from the Perspective of an Addiction Psychiatrist. *Mo. Med.* **2018**, *115* (6), 482–486.

(211) Pennypacker, S. D.; Cunnane, K.; Cash, M. C.; Romero-Sandoval, E. A. Potency and Therapeutic THC and CBD Ratios: U.S. Cannabis Markets Overshoot. *Front. Pharmacol.* **2022**, *13*, 921493. https://doi.org/10.3389/fphar.2022.921493.
(212) Tahir, M. N.; Shahbazi, F.; Rondeau-Gagné, S.; Trant, J. F. The Biosynthesis of the Cannabinoids. *J. Cannabis Res.* **2021**, *3* (1), 7. https://doi.org/10.1186/s42238-021-00062-4.
(213) Taura, F.; Morimoto, S.; Shoyama, Y.; Mechoulam, R. First Direct Evidence for the Mechanism of .DELTA.1-Tetrahydrocannabinolic Acid Biosynthesis. *J. Am. Chem. Soc.* **1995**, *117* (38), 9766–9767. https://doi.org/10.1021/ja00143a024.
(214) Taura, F.; Morimoto, S.; Shoyama, Y. Purification and Characterization of Cannabidiolic-Acid Synthase from Cannabis Sativa L. *J. Biol. Chem.* **1996**, *271* (29), 17411–17416. https://doi.org/10.1074/jbc.271.29.17411.
(215) Morimoto, S.; Komatsu, K.; Taura, F.; Shoyama, Y. Enzymological Evidence for Cannabichromenic Acid Biosynthesis. *J. Nat. Prod.* **1997**, *60* (8), 854–857. https://doi.org/10.1021/np970210y.
(216) Morimoto, S.; Komatsu, K.; Taura, F.; Shoyama, Y. Purification and Characterization of Cannabichromenic Acid Synthase from Cannabis Sativa. *Phytochemistry* **1998**, *49* (6), 1525–1529. https://doi.org/10.1016/S0031-9422(98)00278-7.
(217) Page, J. E.; Stout, J. M. Cannabichromenic Acid Synthase from Cannabis Sativa. WO2015196275A1, December 30, 2015.
(218) Rodziewicz, P.; Loroch, S.; Marczak, Ł.; Sickmann, A.; Kayser, O. Cannabinoid Synthases and Osmoprotective Metabolites Accumulate in the Exudates of Cannabis Sativa L. Glandular Trichomes. *Plant Sci.* **2019**, *284*, 108–116. https://doi.org/10.1016/j.plantsci.2019.04.008.
(219) Tanney, C. A. S.; Backer, R.; Geitmann, A.; Smith, D. L. Cannabis Glandular Trichomes: A Cellular Metabolite Factory. *Front. Plant Sci.* **2021**, *12*, 721986. https://doi.org/10.3389/fpls.2021.721986.
(220) Sirikantaramas, S.; Taura, F.; Tanaka, Y.; Ishikawa, Y.; Morimoto, S.; Shoyama, Y. Tetrahydrocannabinolic Acid Synthase, the Enzyme Controlling Marijuana Psychoactivity, Is Secreted into the Storage Cavity of the Glandular Trichomes. *Plant Cell Physiol.* **2005**, *46* (9), 1578–1582. https://doi.org/10.1093/pcp/pci166.
(221) Sirikantaramas, S.; Morimoto, S.; Shoyama, Y.; Ishikawa, Y.; Wada, Y.; Shoyama, Y.; Taura, F. The Gene Controlling Marijuana Psychoactivity. *J. Biol. Chem.* **2004**, *279* (38), 39767–39774. https://doi.org/10.1074/jbc.M403693200.
(222) Geissler, M.; Volk, J.; Stehle, F.; Kayser, O.; Warzecha, H. Subcellular Localization Defines Modification and Production of Δ9-Tetrahydrocannabinolic Acid Synthase in Transiently Transformed Nicotiana Benthamiana. *Biotechnol. Lett.* **2018**, *40* (6), 981–987. https://doi.org/10.1007/s10529-018-2545-0.
(223) Zirpel, B.; Kayser, O.; Stehle, F. Elucidation of Structure-Function Relationship of THCA and CBDA Synthase from Cannabis Sativa L. *J. Biotechnol.* **2018**, *284*, 17–26. https://doi.org/10.1016/j.jbiotec.2018.07.031.
(224) Cao, J.; Shen, C.; Wang, H.; Shen, H.; Chen, Y.; Nie, A.; Yan, G.; Lu, H.; Liu, Y.; Yang, P. Identification of N-Glycosylation Sites on Secreted Proteins of Human Hepatocellular Carcinoma Cells with a Complementary Proteomics Approach. *J. Proteome Res.* **2009**, *8* (2), 662–672. https://doi.org/10.1021/pr800826u.
(225) Taura, F.; Dono, E.; Sirikantaramas, S.; Yoshimura, K.; Shoyama, Y.; Morimoto, S. Production of Δ1-Tetrahydrocannabinolic Acid by the Biosynthetic Enzyme Secreted from Transgenic Pichia Pastoris. *Biochem. Biophys. Res. Commun.* **2007**, *361* (3), 675–680. https://doi.org/10.1016/j.bbrc.2007.07.079.

(226) Van Velzen, R.; Schranz, M. E. Origin and Evolution of the Cannabinoid Oxidocyclase Gene Family. *Genome Biol. Evol.* **2021**, *13* (8), evab130. https://doi.org/10.1093/gbe/evab130.
(227) Croteau, Rodney. Biosynthesis and Catabolism of Monoterpenoids. *Chem. Rev.* **1987**, *87* (5), 929–954. https://doi.org/10.1021/cr00081a004.
(228) Christianson, D. W. Structural and Chemical Biology of Terpenoid Cyclases. *Chem. Rev.* **2017**, *117* (17), 11570–11648. https://doi.org/10.1021/acs.chemrev.7b00287.
(229) Shoyama, Y.; Tamada, T.; Kurihara, K.; Takeuchi, A.; Taura, F.; Arai, S.; Blaber, M.; Shoyama, Y.; Morimoto, S.; Kuroki, R. Structure and Function of Δ1-Tetrahydrocannabinolic Acid (THCA) Synthase, the Enzyme Controlling the Psychoactivity of Cannabis Sativa. *J. Mol. Biol.* **2012**, *423* (1), 96–105. https://doi.org/10.1016/j.jmb.2012.06.030.
(230) Taura, F.; Sirikantaramas, S.; Shoyama, Y.; Shoyama, Y.; Morimoto, S. Phytocannabinoids in *Cannabis Sativa* : Recent Studies on Biosynthetic Enzymes. *Chem. Biodivers.* **2007**, *4* (8), 1649–1663. https://doi.org/10.1002/cbdv.200790145.
(231) Yang, X.; Liang, W.; Lin, X.; Zhao, M.; Zhang, Q.; Tao, Y.; Huang, J.; Ke, C. Efficient *Escherichia Coli* Platform for Cannabinoid Precursor Olivetolic Acid Biosynthesis from Inexpensive Inputs. *J. Agric. Food Chem.* **2025**, *73* (6), 3611–3621. https://doi.org/10.1021/acs.jafc.4c11867.
(232) Zirpel, B.; Stehle, F.; Kayser, O. Production of Δ9-Tetrahydrocannabinolic Acid from Cannabigerolic Acid by Whole Cells of Pichia (Komagataella) Pastoris Expressing Δ9-Tetrahydrocannabinolic Acid Synthase from Cannabis Sativa l. *Biotechnol. Lett.* **2015**, *37* (9), 1869–1875. https://doi.org/10.1007/s10529-015-1853-x.
(233) Chen, R.; Gao, B.; Liu, X.; Ruan, F.; Zhang, Y.; Lou, J.; Feng, K.; Wunsch, C.; Li, S.-M.; Dai, J.; Sun, F. Molecular Insights into the Enzyme Promiscuity of an Aromatic Prenyltransferase. *Nat. Chem. Biol.* **2017**, *13* (2), 226–234. https://doi.org/10.1038/nchembio.2263.
(234) Kearsey, L. J.; Yan, C.; Prandi, N.; Toogood, H. S.; Takano, E.; Scrutton, N. S. Biosynthesis of Cannabigerol and Cannabigerolic Acid: The Gateways to Further Cannabinoid Production. *Synth. Biol. Oxf. Engl.* **2023**, *8* (1), ysad010. https://doi.org/10.1093/synbio/ysad010.
(235) Karbalaei, M.; Rezaee, S. A.; Farsiani, H. *Pichia Pastoris* : A Highly Successful Expression System for Optimal Synthesis of Heterologous Proteins. *J. Cell. Physiol.* **2020**, *235* (9), 5867–5881. https://doi.org/10.1002/jcp.29583.
(236) Xu, S.; Wu, S.; Li, Y. Investigating Plant Biosynthetic Pathways Using Heterologous Gene Expression: Yeast as a Heterologous Host. *Methods Mol. Biol. Clifton NJ* **2022**, *2489*, 369–393. https://doi.org/10.1007/978-1-0716-2273-5_19.
(237) Popova, L. G.; Khramov, D. E.; Nedelyaeva, O. I.; Volkov, V. S. Yeast Heterologous Expression Systems for the Study of Plant Membrane Proteins. *Int. J. Mol. Sci.* **2023**, *24* (13), 10768. https://doi.org/10.3390/ijms241310768.
(238) Zirpel, B.; Degenhardt, F.; Martin, C.; Kayser, O.; Stehle, F. Engineering Yeasts as Platform Organisms for Cannabinoid Biosynthesis. *J. Biotechnol.* **2017**, *259*, 204–212. https://doi.org/10.1016/j.jbiotec.2017.07.008.
(239) Kuzuyama, T.; Noel, J. P.; Richard, S. B. Structural Basis for the Promiscuous Biosynthetic Prenylation of Aromatic Natural Products. *Nature* **2005**, *435* (7044), 983–987. https://doi.org/10.1038/nature03668.
(240) Page, J. E.; Boubakir, Z. Aromatic Prenyltransferase from Cannabis. US8884100B2, November 11, 2014.

(241) Kayser, O.; Stehle, F. Biotechnological Production of Cannabinoids. WO2020016287A1, January 23, 2020.
(242) Valliere, M. A.; Korman, T. P.; Woodall, N. B.; Khitrov, G. A.; Taylor, R. E.; Baker, D.; Bowie, J. U. A Cell-Free Platform for the Prenylation of Natural Products and Application to Cannabinoid Production. *Nat. Commun.* **2019**, *10* (1), 565. https://doi.org/10.1038/s41467-019-08448-y.
(243) Luo, X.; Reiter, M. A.; d'Espaux, L.; Wong, J.; Denby, C. M.; Lechner, A.; Zhang, Y.; Grzybowski, A. T.; Harth, S.; Lin, W.; Lee, H.; Yu, C.; Shin, J.; Deng, K.; Benites, V. T.; Wang, G.; Baidoo, E. E. K.; Chen, Y.; Dev, I.; Petzold, C. J.; Keasling, J. D. Complete Biosynthesis of Cannabinoids and Their Unnatural Analogues in Yeast. *Nature* **2019**, *567* (7746), 123–126. https://doi.org/10.1038/s41586-019-0978-9.
(244) Hedl, M.; Sutherlin, A.; Wilding, E. I.; Mazzulla, M.; McDevitt, D.; Lane, P.; Burgner, J. W.; Lehnbeuter, K. R.; Stauffacher, C. V.; Gwynn, M. N.; Rodwell, V. W. *Enterococcus Faecalis* Acetoacetyl-Coenzyme A Thiolase/3-Hydroxy-3-Methylglutaryl-Coenzyme A Reductase, a Dual-Function Protein of Isopentenyl Diphosphate Biosynthesis. *J. Bacteriol.* **2002**, *184* (8), 2116–2122. https://doi.org/10.1128/JB.184.8.2116-2122.2002.
(245) Sutherlin, A.; Hedl, M.; Sanchez-Neri, B.; Burgner, J. W.; Stauffacher, C. V.; Rodwell, V. W. *Enterococcus Faecalis* 3-Hydroxy-3-Methylglutaryl Coenzyme A Synthase, an Enzyme of Isopentenyl Diphosphate Biosynthesis. *J. Bacteriol.* **2002**, *184* (15), 4065–4070. https://doi.org/10.1128/JB.184.15.4065-4070.2002.
(246) Ignea, C.; Pontini, M.; Maffei, M. E.; Makris, A. M.; Kampranis, S. C. Engineering Monoterpene Production in Yeast Using a Synthetic Dominant Negative Geranyl Diphosphate Synthase. *ACS Synth. Biol.* **2014**, *3* (5), 298–306. https://doi.org/10.1021/sb400115e.
(247) Spitzer, S.; Wloka, J.; Pietruszka, J.; Kayser, O. Generation of Cannabigerolic Acid Derivatives and Their Precursors by Using the Promiscuity of the Aromatic Prenyltransferase NphB. *ChemBioChem* **2023**, *24* (22), e202300441. https://doi.org/10.1002/cbic.202300441.
(248) Ma, J.; Gu, Y.; Xu, P. Biosynthesis of Cannabinoid Precursor Olivetolic Acid in Genetically Engineered Yarrowia Lipolytica. *Commun. Biol.* **2022**, *5* (1), 1239. https://doi.org/10.1038/s42003-022-04202-1.
(249) Starai, V. J.; Gardner, J. G.; Escalante-Semerena, J. C. Residue Leu-641 of Acetyl-CoA Synthetase Is Critical for the Acetylation of Residue Lys-609 by the Protein Acetyltransferase Enzyme of Salmonella Enterica. *J. Biol. Chem.* **2005**, *280* (28), 26200–26205. https://doi.org/10.1074/jbc.M504863200.
(250) Liu, H.; Marsafari, M.; Wang, F.; Deng, L.; Xu, P. Engineering Acetyl-CoA Metabolic Shortcut for Eco-Friendly Production of Polyketides Triacetic Acid Lactone in Yarrowia Lipolytica. *Metab. Eng.* **2019**, *56*, 60–68. https://doi.org/10.1016/j.ymben.2019.08.017.
(251) Schmidt, C.; Aras, M.; Kayser, O. Engineering Cannabinoid Production in *Saccharomyces Cerevisiae*. *Biotechnol. J.* **2024**, *19* (2), 2300507. https://doi.org/10.1002/biot.202300507.
(252) Zhang, Y.; Guo, J.; Gao, P.; Yan, W.; Shen, J.; Luo, X.; Keasling, J. D. Development of an Efficient Yeast Platform for Cannabigerolic Acid Biosynthesis. *Metab. Eng.* **2023**, *80*, 232–240. https://doi.org/10.1016/j.ymben.2023.10.004.
(253) Schuck, S.; Prinz, W. A.; Thorn, K. S.; Voss, C.; Walter, P. Membrane Expansion Alleviates Endoplasmic Reticulum Stress Independently of the Unfolded Protein

Response. *J. Cell Biol.* **2009**, *187* (4), 525–536. https://doi.org/10.1083/jcb.200907074.
(254) Ambroziak, J.; Henry, S. A. INO2 and INO4 Gene Products, Positive Regulators of Phospholipid Biosynthesis in Saccharomyces Cerevisiae, Form a Complex That Binds to the INO1 Promoter. *J. Biol. Chem.* **1994**, *269* (21), 15344–15349.
(255) Okorafor, I. C.; Chen, M.; Tang, Y. High-Titer Production of Olivetolic Acid and Analogs in Engineered Fungal Host Using a Nonplant Biosynthetic Pathway. *ACS Synth. Biol.* **2021**, *10* (9), 2159–2166. https://doi.org/10.1021/acssynbio.1c00309.
(256) Resh, M. D. Fatty Acylation of Proteins: The Long and the Short of It. *Prog. Lipid Res.* **2016**, *63*, 120–131. https://doi.org/10.1016/j.plipres.2016.05.002.
(257) Van Meer, G.; Voelker, D. R.; Feigenson, G. W. Membrane Lipids: Where They Are and How They Behave. *Nat. Rev. Mol. Cell Biol.* **2008**, *9* (2), 112–124. https://doi.org/10.1038/nrm2330.
(258) Graber, R.; Sumida, C.; Nunez, E. A. Fatty Acids and Cell Signal Transduction. *J. Lipid Mediat. Cell Signal.* **1994**, *9* (2), 91–116.
(259) Biermann, U.; Bornscheuer, U.; Meier, M. A. R.; Metzger, J. O.; Schäfer, H. J. Oils and Fats as Renewable Raw Materials in Chemistry. *Angew. Chem. Int. Ed.* **2011**, *50* (17), 3854–3871. https://doi.org/10.1002/anie.201002767.
(260) Marella, E. R.; Holkenbrink, C.; Siewers, V.; Borodina, I. Engineering Microbial Fatty Acid Metabolism for Biofuels and Biochemicals. *Curr. Opin. Biotechnol.* **2018**, *50*, 39–46. https://doi.org/10.1016/j.copbio.2017.10.002.
(261) Yu, A.-Q.; Pratomo Juwono, N. K.; Leong, S. S. J.; Chang, M. W. Production of Fatty Acid-Derived Valuable Chemicals in Synthetic Microbes. *Front. Bioeng. Biotechnol.* **2014**, *2*. https://doi.org/10.3389/fbioe.2014.00078.
(262) Zhou, Y. J.; Buijs, N. A.; Zhu, Z.; Qin, J.; Siewers, V.; Nielsen, J. Production of Fatty Acid-Derived Oleochemicals and Biofuels by Synthetic Yeast Cell Factories. *Nat. Commun.* **2016**, *7* (1), 11709. https://doi.org/10.1038/ncomms11709.
(263) Yusoff, M. F. M.; Xu, X.; Guo, Z. Comparison of Fatty Acid Methyl and Ethyl Esters as Biodiesel Base Stock: A Review on Processing and Production Requirements. *J. Am. Oil Chem. Soc.* **2014**, *91* (4), 525–531. https://doi.org/10.1007/s11746-014-2443-0.
(264) Krishnan, A.; McNeil, B. A.; Stuart, D. T. Biosynthesis of Fatty Alcohols in Engineered Microbial Cell Factories: Advances and Limitations. *Front. Bioeng. Biotechnol.* **2020**, *8*, 610936. https://doi.org/10.3389/fbioe.2020.610936.
(265) Wenning, L.; Yu, T.; David, F.; Nielsen, J.; Siewers, V. Establishing Very Long-chain Fatty Alcohol and Wax Ester Biosynthesis in *Saccharomyces Cerevisiae*. *Biotechnol. Bioeng.* **2017**, *114* (5), 1025–1035. https://doi.org/10.1002/bit.26220.
(266) Folan, M.A., O'Brien, C., Dunne, C. Free Fatty Acid Blends and Use Thereof. US20100317734, December 16, 2010.
(267) P. Desbois, A. Potential Applications of Antimicrobial Fatty Acids in Medicine, Agriculture and Other Industries. *Recent Patents Anti-Infect. Drug Disc.* **2012**, *7* (2), 111–122. https://doi.org/10.2174/157489112801619728.
(268) Royce, L. A.; Liu, P.; Stebbins, M. J.; Hanson, B. C.; Jarboe, L. R. The Damaging Effects of Short Chain Fatty Acids on Escherichia Coli Membranes. *Appl. Microbiol. Biotechnol.* **2013**, *97* (18), 8317–8327. https://doi.org/10.1007/s00253-013-5113-5.
(269) Hu, K.; Jin, G.-J.; Mei, W.-C.; Li, T.; Tao, Y.-S. Increase of Medium-Chain Fatty Acid Ethyl Ester Content in Mixed H. Uvarum/S. Cerevisiae Fermentation Leads to Wine Fruity Aroma Enhancement. *Food Chem.* **2018**, *239*, 495–501. https://doi.org/10.1016/j.foodchem.2017.06.151.

(270) Henritzi, S.; Fischer, M.; Grininger, M.; Oreb, M.; Boles, E. An Engineered Fatty Acid Synthase Combined with a Carboxylic Acid Reductase Enables de Novo Production of 1-Octanol in Saccharomyces Cerevisiae. *Biotechnol. Biofuels* **2018**, *11* (1), 150. https://doi.org/10.1186/s13068-018-1149-1.
(271) Kremer, F.; Blank, L. M.; Jones, P. R.; Akhtar, M. K. A Comparison of the Microbial Production and Combustion Characteristics of Three Alcohol Biofuels: Ethanol, 1-Butanol, and 1-Octanol. *Front. Bioeng. Biotechnol.* **2015**, *3*. https://doi.org/10.3389/fbioe.2015.00112.
(272) Çelebi, Y.; Cengiz, M.; Aydın, H. A Review on the Utilization of Octanol and Its Blends in Diesel Engines. *J. Energy Inst.* **2025**, *118*, 101925. https://doi.org/10.1016/j.joei.2024.101925.
(273) Boateng, L.; Ansong, R.; Owusu, W. B.; Steiner-Asiedu, M. Coconut Oil and Palm Oil's Role in Nutrition, Health and National Development: A Review. *Ghana Med. J.* **2016**, *50* (3), 189–196.
(274) Jadhav, H. B.; Annapure, U. Designer Lipids -Synthesis and Application – A Review. *Trends Food Sci. Technol.* **2021**, *116*, 884–902. https://doi.org/10.1016/j.tifs.2021.08.020.
(275) Djordjevic, J.; Ledina, T.; Baltic, M. Z.; Trbovic, D.; Babic, M.; Bulajic, S. Fatty Acid Profile of Milk. *IOP Conf. Ser. Earth Environ. Sci.* **2019**, *333*, 012057. https://doi.org/10.1088/1755-1315/333/1/012057.
(276) Choi, K.; Jeon, B. S.; Kim, B.-C.; Oh, M.-K.; Um, Y.; Sang, B.-I. In Situ Biphasic Extractive Fermentation for Hexanoic Acid Production from Sucrose by Megasphaera Elsdenii NCIMB 702410. *Appl. Biochem. Biotechnol.* **2013**, *171* (5), 1094–1107. https://doi.org/10.1007/s12010-013-0310-3.
(277) Nelson, R.; Peterson, D.; Karp, E.; Beckham, G.; Salvachúa, D. Mixed Carboxylic Acid Production by Megasphaera Elsdenii from Glucose and Lignocellulosic Hydrolysate. *Fermentation* **2017**, *3* (1), 10. https://doi.org/10.3390/fermentation3010010.
(278) Seedorf, H.; Fricke, W. F.; Veith, B.; Brüggemann, H.; Liesegang, H.; Strittmatter, A.; Miethke, M.; Buckel, W.; Hinderberger, J.; Li, F.; Hagemeier, C.; Thauer, R. K.; Gottschalk, G. The Genome of *Clostridium Kluyveri* , a Strict Anaerobe with Unique Metabolic Features. *Proc. Natl. Acad. Sci.* **2008**, *105* (6), 2128–2133. https://doi.org/10.1073/pnas.0711093105.
(279) Roghair, M.; Liu, Y.; Strik, D. P. B. T. B.; Weusthuis, R. A.; Bruins, M. E.; Buisman, C. J. N. Development of an Effective Chain Elongation Process From Acidified Food Waste and Ethanol Into N-Caproate. *Front. Bioeng. Biotechnol.* **2018**, *6*, 50. https://doi.org/10.3389/fbioe.2018.00050.
(280) Jeon, B. S.; Choi, O.; Um, Y.; Sang, B.-I. Production of Medium-Chain Carboxylic Acids by Megasphaera Sp. MH with Supplemental Electron Acceptors. *Biotechnol. Biofuels* **2016**, *9* (1), 129. https://doi.org/10.1186/s13068-016-0549-3.
(281) Dekishima, Y.; Lan, E. I.; Shen, C. R.; Cho, K. M.; Liao, J. C. Extending Carbon Chain Length of 1-Butanol Pathway for 1-Hexanol Synthesis from Glucose by Engineered *Escherichia Coli*. *J. Am. Chem. Soc.* **2011**, *133* (30), 11399–11401. https://doi.org/10.1021/ja203814d.
(282) Kim, S.; Clomburg, J. M.; Gonzalez, R. Synthesis of Medium-Chain Length (C6–C10) Fuels and Chemicals via β-Oxidation Reversal in *Escherichia Coli*. *J. Ind. Microbiol. Biotechnol.* **2015**, *42* (3), 465–475. https://doi.org/10.1007/s10295-015-1589-6.

(283) Lian, J.; Zhao, H. Reversal of the β-Oxidation Cycle in *Saccharomyces Cerevisiae* for Production of Fuels and Chemicals. *ACS Synth. Biol.* **2015**, *4* (3), 332–341. https://doi.org/10.1021/sb500243c.
(284) Gajewski, J.; Pavlovic, R.; Fischer, M.; Boles, E.; Grininger, M. Engineering Fungal de Novo Fatty Acid Synthesis for Short Chain Fatty Acid Production. *Nat. Commun.* **2017**, *8* (1), 14650. https://doi.org/10.1038/ncomms14650.
(285) Tan, Z.; Yoon, J. M.; Chowdhury, A.; Burdick, K.; Jarboe, L. R.; Maranas, C. D.; Shanks, J. V. Engineering of E. Coli Inherent Fatty Acid Biosynthesis Capacity to Increase Octanoic Acid Production. *Biotechnol. Biofuels* **2018**, *11* (1), 87. https://doi.org/10.1186/s13068-018-1078-z.
(286) Torella, J. P.; Ford, T. J.; Kim, S. N.; Chen, A. M.; Way, J. C.; Silver, P. A. Tailored Fatty Acid Synthesis via Dynamic Control of Fatty Acid Elongation. *Proc. Natl. Acad. Sci.* **2013**, *110* (28), 11290–11295. https://doi.org/10.1073/pnas.1307129110.
(287) Zhu, Z.; Hu, Y.; Teixeira, P. G.; Pereira, R.; Chen, Y.; Siewers, V.; Nielsen, J. Multidimensional Engineering of Saccharomyces Cerevisiae for Efficient Synthesis of Medium-Chain Fatty Acids. *Nat. Catal.* **2020**, *3* (1), 64–74. https://doi.org/10.1038/s41929-019-0409-1.
(288) Chen, L.; Zhang, J.; Chen, W. N. Engineering the Saccharomyces Cerevisiae β-Oxidation Pathway to Increase Medium Chain Fatty Acid Production as Potential Biofuel. *PLoS ONE* **2014**, *9* (1), e84853. https://doi.org/10.1371/journal.pone.0084853.
(289) Elad, N.; Baron, S.; Peleg, Y.; Albeck, S.; Grunwald, J.; Raviv, G.; Shakked, Z.; Zimhony, O.; Diskin, R. Structure of Type-I Mycobacterium Tuberculosis Fatty Acid Synthase at 3.3 Å Resolution. *Nat. Commun.* **2018**, *9* (1), 3886. https://doi.org/10.1038/s41467-018-06440-6.
(290) Gago, G.; Diacovich, L.; Arabolaza, A.; Tsai, S.-C.; Gramajo, H. Fatty Acid Biosynthesis in Actinomycetes. *FEMS Microbiol. Rev.* **2011**, *35* (3), 475–497. https://doi.org/10.1111/j.1574-6976.2010.00259.x.
(291) Hiltunen, J. K.; Schonauer, M. S.; Autio, K. J.; Mittelmeier, T. M.; Kastaniotis, A. J.; Dieckmann, C. L. Mitochondrial Fatty Acid Synthesis Type II: More than Just Fatty Acids. *J. Biol. Chem.* **2009**, *284* (14), 9011–9015. https://doi.org/10.1074/jbc.R800068200.
(292) Radmacher, E.; Alderwick, L. J.; Besra, G. S.; Brown, A. K.; Gibson, K. J. C.; Sahm, H.; Eggeling, L. Two Functional FAS-I Type Fatty Acid Synthases in Corynebacterium Glutamicum. *Microbiology* **2005**, *151* (7), 2421–2427. https://doi.org/10.1099/mic.0.28012-0.
(293) White, S. W.; Zheng, J.; Zhang, Y.-M.; Rock, C. O. THE STRUCTURAL BIOLOGY OF TYPE II FATTY ACID BIOSYNTHESIS. *Annu. Rev. Biochem.* **2005**, *74* (1), 791–831. https://doi.org/10.1146/annurev.biochem.74.082803.133524.
(294) Leibundgut, M.; Maier, T.; Jenni, S.; Ban, N. The Multienzyme Architecture of Eukaryotic Fatty Acid Synthases. *Curr. Opin. Struct. Biol.* **2008**, *18* (6), 714–725. https://doi.org/10.1016/j.sbi.2008.09.008.
(295) Maier, T.; Leibundgut, M.; Ban, N. The Crystal Structure of a Mammalian Fatty Acid Synthase. *Science* **2008**, *321* (5894), 1315–1322. https://doi.org/10.1126/science.1161269.
(296) Lomakin, I. B.; Xiong, Y.; Steitz, T. A. The Crystal Structure of Yeast Fatty Acid Synthase, a Cellular Machine with Eight Active Sites Working Together. *Cell* **2007**, *129* (2), 319–332. https://doi.org/10.1016/j.cell.2007.03.013.

(297) Jenni, S.; Leibundgut, M.; Maier, T.; Ban, N. Architecture of a Fungal Fatty Acid Synthase at 5 Å Resolution. *Science* **2006**, *311* (5765), 1263–1267. https://doi.org/10.1126/science.1123251.
(298) Bukhari, H. S. T.; Jakob, R. P.; Maier, T. Evolutionary Origins of the Multienzyme Architecture of Giant Fungal Fatty Acid Synthase. *Structure* **2014**, *22* (12), 1775–1785. https://doi.org/10.1016/j.str.2014.09.016.
(299) Fischer, M.; Joppe, M.; Mulinacci, B.; Vollrath, R.; Konstantinidis, K.; Kötter, P.; Ciccarelli, L.; Vonck, J.; Oesterhelt, D.; Grininger, M. Analysis of the Co-Translational Assembly of the Fungal Fatty Acid Synthase (FAS). *Sci. Rep.* **2020**, *10* (1), 895. https://doi.org/10.1038/s41598-020-57418-8.
(300) Buyachuihan, L.; Stegemann, F.; Grininger, M. How Acyl Carrier Proteins (ACPs) Direct Fatty Acid and Polyketide Biosynthesis. *Angew. Chem. Int. Ed.* **2024**, *63* (4), e202312476. https://doi.org/10.1002/anie.202312476.
(301) Cronan, J. E.; Thomas, J. Bacterial Fatty Acid Synthesis and Its Relationships with Polyketide Synthetic Pathways. *Methods Enzymol.* **2009**, *459*, 395–433. https://doi.org/10.1016/S0076-6879(09)04617-5.
(302) Leibundgut, M.; Jenni, S.; Frick, C.; Ban, N. Structural Basis for Substrate Delivery by Acyl Carrier Protein in the Yeast Fatty Acid Synthase. *Science* **2007**, *316* (5822), 288–290. https://doi.org/10.1126/science.1138249.
(303) Samani, E. K.; Chen, A. C.; Lou, J. W.; Dai, D. L.; Keszei, A. F. A.; Tan, G.; Boone, C.; Grininger, M.; Mazhab-Jafari, M. T. Direct Structural Analysis of a Single Acyl Carrier Protein Domain in Fatty Acid Synthase from the Fungus Saccharomyces Cerevisiae. *Commun. Biol.* **2024**, *7* (1), 92. https://doi.org/10.1038/s42003-024-05777-7.
(304) Crosby, J.; Crump, M. P. The Structural Role of the Carrier Protein – Active Controller or Passive Carrier. *Nat. Prod. Rep.* **2012**, *29* (10), 1111. https://doi.org/10.1039/c2np20062g.
(305) Bunkoczi, G.; Pasta, S.; Joshi, A.; Wu, X.; Kavanagh, K. L.; Smith, S.; Oppermann, U. Mechanism and Substrate Recognition of Human Holo ACP Synthase. *Chem. Biol.* **2007**, *14* (11), 1243–1253. https://doi.org/10.1016/j.chembiol.2007.10.013.
(306) Fichtlscherer, F.; Wellein, C.; Mittag, M.; Schweizer, E. A Novel Function of Yeast Fatty Acid Synthase: Subunit α Is Capable of Self-pantetheinylation. *Eur. J. Biochem.* **2000**, *267* (9), 2666–2671. https://doi.org/10.1046/j.1432-1327.2000.01282.x.
(307) Johansson, P.; Mulinacci, B.; Koestler, C.; Vollrath, R.; Oesterhelt, D.; Grininger, M. Multimeric Options for the Auto-Activation of the Saccharomyces Cerevisiae FAS Type I Megasynthase. *Structure* **2009**, *17* (8), 1063–1074. https://doi.org/10.1016/j.str.2009.06.014.
(308) Flugel, R. S.; Hwangbo, Y.; Lambalot, R. H.; Cronan, J. E.; Walsh, C. T. Holo-(Acyl Carrier Protein) Synthase and Phosphopantetheinyl Transfer in Escherichia Coli. *J. Biol. Chem.* **2000**, *275* (2), 959–968. https://doi.org/10.1074/jbc.275.2.959.
(309) Rittner, A.; Paithankar, K. S.; Huu, K. V.; Grininger, M. Characterization of the Polyspecific Transferase of Murine Type I Fatty Acid Synthase (FAS) and Implications for Polyketide Synthase (PKS) Engineering. *ACS Chem. Biol.* **2018**, *13* (3), 723–732. https://doi.org/10.1021/acschembio.7b00718.
(310) Engeser, H.; HuBNER, K.; Straub, J.; Lynen, F. Identity of Malonyl and Palmitoyl Transferase of Fatty Acid Synthetase from Yeast. 2. A Comparison of Active-Site Peptides. *Eur. J. Biochem.* **1979**, *101* (2), 413–422. https://doi.org/10.1111/j.1432-1033.1979.tb19734.x.

(311) Smith, S.; Tsai, S.-C. The Type I Fatty Acid and Polyketide Synthases: A Tale of Two Megasynthases. *Nat. Prod. Rep.* **2007**, *24* (5), 1041. https://doi.org/10.1039/b603600g.
(312) Tehlivets, O.; Scheuringer, K.; Kohlwein, S. D. Fatty Acid Synthesis and Elongation in Yeast. *Biochim. Biophys. Acta BBA - Mol. Cell Biol. Lipids* **2007**, *1771* (3), 255–270. https://doi.org/10.1016/j.bbalip.2006.07.004.
(313) Steen, E. J.; Kang, Y.; Bokinsky, G.; Hu, Z.; Schirmer, A.; McClure, A.; Del Cardayre, S. B.; Keasling, J. D. Microbial Production of Fatty-Acid-Derived Fuels and Chemicals from Plant Biomass. *Nature* **2010**, *463* (7280), 559–562. https://doi.org/10.1038/nature08721.
(314) Deng, X.; Chen, L.; Hei, M.; Liu, T.; Feng, Y.; Yang, G.-Y. Structure-Guided Reshaping of the Acyl Binding Pocket of 'TesA Thioesterase Enhances Octanoic Acid Production in E. Coli. *Metab. Eng.* **2020**, *61*, 24–32. https://doi.org/10.1016/j.ymben.2020.04.010.
(315) Gipson, P.; Mills, D. J.; Wouts, R.; Grininger, M.; Vonck, J.; Kühlbrandt, W. Direct Structural Insight into the Substrate-Shuttling Mechanism of Yeast Fatty Acid Synthase by Electron Cryomicroscopy. *Proc. Natl. Acad. Sci.* **2010**, *107* (20), 9164–9169. https://doi.org/10.1073/pnas.0913547107.
(316) Singh, K.; Bunzel, G.; Graf, B.; Yip, K. M.; Neumann-Schaal, M.; Stark, H.; Chari, A. Reconstruction of a Fatty Acid Synthesis Cycle from Acyl Carrier Protein and Cofactor Structural Snapshots. *Cell* **2023**, *186* (23), 5054-5067.e16. https://doi.org/10.1016/j.cell.2023.10.009.
(317) Johansson, P.; Wiltschi, B.; Kumari, P.; Kessler, B.; Vonrhein, C.; Vonck, J.; Oesterhelt, D.; Grininger, M. Inhibition of the Fungal Fatty Acid Synthase Type I Multienzyme Complex. *Proc. Natl. Acad. Sci.* **2008**, *105* (35), 12803–12808. https://doi.org/10.1073/pnas.0805827105.
(318) Chirala, S. S.; Kuziora, M. A.; Spector, D. M.; Wakil, S. J. Complementation of Mutations and Nucleotide Sequence of FAS1 Gene Encoding Beta Subunit of Yeast Fatty Acid Synthase. *J. Biol. Chem.* **1987**, *262* (9), 4231–4240. https://doi.org/10.1016/S0021-9258(18)61337-7.
(319) Mohamed, A. H.; Chirala, S. S.; Mody, N. H.; Huang, W. Y.; Wakil, S. J. Primary Structure of the Multifunctional Alpha Subunit Protein of Yeast Fatty Acid Synthase Derived from FAS2 Gene Sequence. *J. Biol. Chem.* **1988**, *263* (25), 12315–12325.
(320) Shiber, A.; Döring, K.; Friedrich, U.; Klann, K.; Merker, D.; Zedan, M.; Tippmann, F.; Kramer, G.; Bukau, B. Cotranslational Assembly of Protein Complexes in Eukaryotes Revealed by Ribosome Profiling. *Nature* **2018**, *561* (7722), 268–272. https://doi.org/10.1038/s41586-018-0462-y.
(321) Schüller, H.-J.; Richter, K.; Hoffmann, B.; Ebbert, R.; Schweizer, E. DNA Binding Site of the Yeast Heteromeric Ino2p/Ino4p Basic Helix-loop-helix Transcription Factor: Structural Requirements as Defined by Saturation Mutagenesis. *FEBS Lett.* **1995**, *370* (1–2), 149–152. https://doi.org/10.1016/0014-5793(95)00818-T.
(322) Schüller, H. J.; Hahn, A.; Tröster, F.; Schütz, A.; Schweizer, E. Coordinate Genetic Control of Yeast Fatty Acid Synthase Genes FAS1 and FAS2 by an Upstream Activation Site Common to Genes Involved in Membrane Lipid Biosynthesis. *EMBO J.* **1992**, *11* (1), 107–114. https://doi.org/10.1002/j.1460-2075.1992.tb05033.x.
(323) Wenz, P. A Downstream Regulatory Element Located within the Coding Sequence Mediates Autoregulated Expression of the Yeast Fatty Acid Synthase Gene FAS2

by the FAS1 Gene Product. *Nucleic Acids Res.* **2001**, *29* (22), 4625–4632. https://doi.org/10.1093/nar/29.22.4625.
(324) Anselmi, C.; Grininger, M.; Gipson, P.; Faraldo-Gómez, J. D. Mechanism of Substrate Shuttling by the Acyl-Carrier Protein within the Fatty Acid Mega-Synthase. *J. Am. Chem. Soc.* **2010**, *132* (35), 12357–12364. https://doi.org/10.1021/ja103354w.
(325) Lou, J. W.; Mazhab-Jafari, M. T. Steric Occlusion Regulates Proximal Interactions of Acyl Carrier Protein Domain in Fungal Fatty Acid Synthase. *Commun. Biol.* **2020**, *3* (1), 274. https://doi.org/10.1038/s42003-020-0997-y.
(326) Stuible, H.; Meurer, G.; Schweizer, E. Heterologous Expression and Biochemical Characterization of Two Functionally Different Type I Fatty Acid Synthases from *Brevibacterium Ammoniagenes*. *Eur. J. Biochem.* **1997**, *247* (1), 268–273. https://doi.org/10.1111/j.1432-1033.1997.00268.x.
(327) Jayakumar, A.; Tai, M. H.; Huang, W. Y.; al-Feel, W.; Hsu, M.; Abu-Elheiga, L.; Chirala, S. S.; Wakil, S. J. Human Fatty Acid Synthase: Properties and Molecular Cloning. *Proc. Natl. Acad. Sci.* **1995**, *92* (19), 8695–8699. https://doi.org/10.1073/pnas.92.19.8695.
(328) Omura, S. The Antibiotic Cerulenin, a Novel Tool for Biochemistry as an Inhibitor of Fatty Acid Synthesis. *Bacteriol. Rev.* **1976**, *40* (3), 681–697. https://doi.org/10.1128/br.40.3.681-697.1976.
(329) Aritomi, K.; Hirosawa, I.; Hoshida, H.; Shiigi, M.; Nishizawa, Y.; Kashiwagi, S.; Akada, R. Self-Cloning Yeast Strains Containing Novel *FAS2* Mutations Produce a Higher Amount of Ethyl Caproate in Japanese Sake. *Biosci. Biotechnol. Biochem.* **2004**, *68* (1), 206–214. https://doi.org/10.1271/bbb.68.206.
(330) Pirson, W.; Schuhmann, L.; Lynen, F. The Specificity of Yeast Fatty-Acid Synthetase with Respect to the "Priming" Substrate: Decanoyl-CoA and Derivatives as "Primers" of Fatty-Acid Synthesis *in Vitro*. *Eur. J. Biochem.* **1973**, *36* (1), 16–24. https://doi.org/10.1111/j.1432-1033.1973.tb02879.x.
(331) Gajewski, J.; Buelens, F.; Serdjukow, S.; Janßen, M.; Cortina, N.; Grubmüller, H.; Grininger, M. Engineering Fatty Acid Synthases for Directed Polyketide Production. *Nat. Chem. Biol.* **2017**, *13* (4), 363–365. https://doi.org/10.1038/nchembio.2314.
(332) Sumper, M.; Riepertinger, C.; Lynen, F.; Oesterhelt, D. Die Synthese Verschiedener Carbonsäuren Durch Den Multienzymkomplex Der Fettsäuresynthese Aus Hefe Und Die Erklärung Ihrer Bildung. *Eur. J. Biochem.* **1969**, *10* (2), 377–387. https://doi.org/10.1111/j.1432-1033.1969.tb00701.x.
(333) Wei, J.; Tong, L. Crystal Structure of the 500-kDa Yeast Acetyl-CoA Carboxylase Holoenzyme Dimer. *Nature* **2015**, *526* (7575), 723–727. https://doi.org/10.1038/nature15375.
(334) Cronan, J. E.; Waldrop, G. L. Multi-Subunit Acetyl-CoA Carboxylases. *Prog. Lipid Res.* **2002**, *41* (5), 407–435. https://doi.org/10.1016/S0163-7827(02)00007-3.
(335) Attwood, P. V.; Wallace, J. C. Chemical and Catalytic Mechanisms of Carboxyl Transfer Reactions in Biotin-Dependent Enzymes. *Acc. Chem. Res.* **2002**, *35* (2), 113–120. https://doi.org/10.1021/ar000049+.
(336) Tong, L. Structure and Function of Biotin-Dependent Carboxylases. *Cell. Mol. Life Sci. CMLS* **2013**, *70* (5), 863–891. https://doi.org/10.1007/s00018-012-1096-0.
(337) Ivessa, A. S.; Schneiter, R.; Kohlwein, S. D. Yeast Acetyl-CoA Carboxylase Is Associated with the Cytoplasmic Surface of the Endoplasmic Reticulum. *Eur. J. Cell Biol.* **1997**, *74* (4), 399–406.

(338) Schneiter, R.; Hitomi, M.; Ivessa, A. S.; Fasch, E.-V.; Kohlwein, S. D.; Tartakoff, A. M. A Yeast Acetyl Coenzyme A Carboxylase Mutant Links Very-Long-Chain Fatty Acid Synthesis to the Structure and Function of the Nuclear Membrane-Pore Complex. *Mol. Cell. Biol.* **1996**, *16* (12), 7161–7172. https://doi.org/10.1128/MCB.16.12.7161.
(339) Al-Feel, W.; Chirala, S. S.; Wakil, S. J. Cloning of the Yeast FAS3 Gene and Primary Structure of Yeast Acetyl-CoA Carboxylase. *Proc. Natl. Acad. Sci.* **1992**, *89* (10), 4534–4538. https://doi.org/10.1073/pnas.89.10.4534.
(340) Guerra, C. E.; Klein, H. L. Mapping of the *ACC1/FAS3* Gene to the Right Arm of Chromosome XIV of *Saccharomyces Cerevisiae*. *Yeast* **1995**, *11* (7), 697–700. https://doi.org/10.1002/yea.320110711.
(341) Hunkeler, M.; Stuttfeld, E.; Hagmann, A.; Imseng, S.; Maier, T. The Dynamic Organization of Fungal Acetyl-CoA Carboxylase. *Nat. Commun.* **2016**, *7* (1), 11196. https://doi.org/10.1038/ncomms11196.
(342) Hoja, U.; Marthol, S.; Hofmann, J.; Stegner, S.; Schulz, R.; Meier, S.; Greiner, E.; Schweizer, E. HFA1 Encoding an Organelle-Specific Acetyl-CoA Carboxylase Controls Mitochondrial Fatty Acid Synthesis in Saccharomyces Cerevisiae. *J. Biol. Chem.* **2004**, *279* (21), 21779–21786. https://doi.org/10.1074/jbc.M401071200.
(343) Shen, Y.; Volrath, S. L.; Weatherly, S. C.; Elich, T. D.; Tong, L. A Mechanism for the Potent Inhibition of Eukaryotic Acetyl-Coenzyme A Carboxylase by Soraphen A, a Macrocyclic Polyketide Natural Product. *Mol. Cell* **2004**, *16* (6), 881–891. https://doi.org/10.1016/j.molcel.2004.11.034.
(344) Gerth, K.; Bedorf, N.; Irschik, H.; Höfle, G.; Reichenbach, H. The Soraphens: A Family of Novel Antifungal Compounds from Sorangium Cellulosum (Myxobacteria). I. Soraphen A1.ALPHA.: Fermentation, Isolation, Biological Properties. *J. Antibiot. (Tokyo)* **1994**, *47* (1), 23–31. https://doi.org/10.7164/antibiotics.47.23.
(345) Hedbacker, K. SNF1/AMPK Pathways in Yeast. *Front. Biosci.* **2008**, *13* (13), 2408. https://doi.org/10.2741/2854.
(346) Woods, A.; Munday, M. R.; Scott, J.; Yang, X.; Carlson, M.; Carling, D. Yeast SNF1 Is Functionally Related to Mammalian AMP-Activated Protein Kinase and Regulates Acetyl-CoA Carboxylase in Vivo. *J. Biol. Chem.* **1994**, *269* (30), 19509–19515.
(347) Witters, L. A.; Watts, T. D. Yeast Acetyl-CoA Carboxylase: In Vitro Phosphorylation by Mammalian and Yeast Protein Kinases. *Biochem. Biophys. Res. Commun.* **1990**, *169* (2), 369–376. https://doi.org/10.1016/0006-291X(90)90341-J.
(348) Kayikci, Ö.; Nielsen, J. Glucose Repression in *Saccharomyces Cerevisiae*. *FEMS Yeast Res.* **2015**, *15* (6), fov068. https://doi.org/10.1093/femsyr/fov068.
(349) McCartney, R. R.; Schmidt, M. C. Regulation of Snf1 Kinase. *J. Biol. Chem.* **2001**, *276* (39), 36460–36466. https://doi.org/10.1074/jbc.M104418200.
(350) Dale, S.; Wilson, W. A.; Edelman, A. M.; Hardie, D. G. Similar Substrate Recognition Motifs for Mammalian AMP-activated Protein Kinase, Higher Plant HMG-CoA Reductase kinase-A, Yeast SNF1, and Mammalian Calmodulin-dependent Protein Kinase I. *FEBS Lett.* **1995**, *361* (2–3), 191–195. https://doi.org/10.1016/0014-5793(95)00172-6.
(351) Ficarro, S. B.; McCleland, M. L.; Stukenberg, P. T.; Burke, D. J.; Ross, M. M.; Shabanowitz, J.; Hunt, D. F.; White, F. M. Phosphoproteome Analysis by Mass Spectrometry and Its Application to Saccharomyces Cerevisiae. *Nat. Biotechnol.* **2002**, *20* (3), 301–305. https://doi.org/10.1038/nbt0302-301.

(352) Hofbauer, H. F.; Schopf, F. H.; Schleifer, H.; Knittelfelder, O. L.; Pieber, B.; Rechberger, G. N.; Wolinski, H.; Gaspar, M. L.; Kappe, C. O.; Stadlmann, J.; Mechtler, K.; Zenz, A.; Lohner, K.; Tehlivets, O.; Henry, S. A.; Kohlwein, S. D. Regulation of Gene Expression through a Transcriptional Repressor That Senses Acyl-Chain Length in Membrane Phospholipids. *Dev. Cell* **2014**, *29* (6), 729–739. https://doi.org/10.1016/j.devcel.2014.04.025.
(353) Shi, S.; Chen, Y.; Siewers, V.; Nielsen, J. Improving Production of Malonyl Coenzyme A-Derived Metabolites by Abolishing Snf1-Dependent Regulation of Acc1. *mBio* **2014**, *5* (3), e01130-14. https://doi.org/10.1128/mBio.01130-14.
(354) Wattanachaisaereekul, S.; Lantz, A. E.; Nielsen, M. L.; Nielsen, J. Production of the Polyketide 6-MSA in Yeast Engineered for Increased Malonyl-CoA Supply. *Metab. Eng.* **2008**, *10* (5), 246–254. https://doi.org/10.1016/j.ymben.2008.04.005.
(355) Li, X.; Guo, D.; Cheng, Y.; Zhu, F.; Deng, Z.; Liu, T. Overproduction of Fatty Acids in Engineered *Saccharomyces Cerevisiae*. *Biotechnol. Bioeng.* **2014**, *111* (9), 1841–1852. https://doi.org/10.1002/bit.25239.
(356) Davis, M. S.; Solbiati, J.; Cronan, J. E. Overproduction of Acetyl-CoA Carboxylase Activity Increases the Rate of Fatty Acid Biosynthesis in Escherichia Coli. *J. Biol. Chem.* **2000**, *275* (37), 28593–28598. https://doi.org/10.1074/jbc.M004756200.
(357) Tai, M.; Stephanopoulos, G. Engineering the Push and Pull of Lipid Biosynthesis in Oleaginous Yeast Yarrowia Lipolytica for Biofuel Production. *Metab. Eng.* **2013**, *15*, 1–9. https://doi.org/10.1016/j.ymben.2012.08.007.
(358) Kamiryo, T.; Parthasarathy, S.; Numa, S. Evidence That Acyl Coenzyme A Synthetase Activity Is Required for Repression of Yeast Acetyl Coenzyme A Carboxylase by Exogenous Fatty Acids. *Proc. Natl. Acad. Sci.* **1976**, *73* (2), 386–390. https://doi.org/10.1073/pnas.73.2.386.
(359) Pham, T.; Walden, E.; Huard, S.; Pezacki, J.; Fullerton, M. D.; Baetz, K. Fine-Tuning Acetyl-CoA Carboxylase 1 Activity through Localization: Functional Genomics Reveals a Role for the Lysine Acetyltransferase NuA4 and Sphingolipid Metabolism in Regulating Acc1 Activity and Localization. *Genetics* **2022**, *221* (4), iyac086. https://doi.org/10.1093/genetics/iyac086.
(360) Choi, J. W.; Da Silva, N. A. Improving Polyketide and Fatty Acid Synthesis by Engineering of the Yeast Acetyl-CoA Carboxylase. *J. Biotechnol.* **2014**, *187*, 56–59. https://doi.org/10.1016/j.jbiotec.2014.07.430.
(361) Chen, X.; Yang, X.; Shen, Y.; Hou, J.; Bao, X. Screening Phosphorylation Site Mutations in Yeast Acetyl-CoA Carboxylase Using Malonyl-CoA Sensor to Improve Malonyl-CoA-Derived Product. *Front. Microbiol.* **2018**, *9*, 47. https://doi.org/10.3389/fmicb.2018.00047.
(362) Ding, Y.; Ning, Y.; Xin, D.; Fu, Y. Dual Cytoplasmic-peroxisomal Compartmentalization Engineering and Multiple Metabolic Engineering Strategies for High Yield Non-psychoactive Cannabinoid in *Saccharomyces Cerevisiae*. *Biotechnol. J.* **2024**, *19* (2), 2300590. https://doi.org/10.1002/biot.202300590.
(363) Dellomonaco, C.; Clomburg, J. M.; Miller, E. N.; Gonzalez, R. Engineered Reversal of the β-Oxidation Cycle for the Synthesis of Fuels and Chemicals. *Nature* **2011**, *476* (7360), 355–359. https://doi.org/10.1038/nature10333.
(364) Haapalainen, A. M.; Meriläinen, G.; Wierenga, R. K. The Thiolase Superfamily: Condensing Enzymes with Diverse Reaction Specificities. *Trends Biochem. Sci.* **2006**, *31* (1), 64–71. https://doi.org/10.1016/j.tibs.2005.11.011.
(365) Liu, L.; Zhou, S.; Deng, Y. The 3-Ketoacyl-CoA Thiolase: An Engineered Enzyme for Carbon Chain Elongation of Chemical Compounds. *Appl. Microbiol.*

Biotechnol. **2020**, *104* (19), 8117–8129. https://doi.org/10.1007/s00253-020-10848-w.

(366) Cintolesi, A.; Clomburg, J. M.; Gonzalez, R. In Silico Assessment of the Metabolic Capabilities of an Engineered Functional Reversal of the β-Oxidation Cycle for the Synthesis of Longer-Chain (C≥4) Products. *Metab. Eng.* **2014**, *23*, 100–115. https://doi.org/10.1016/j.ymben.2014.02.011.

(367) Clomburg, J. M.; Contreras, S. C.; Chou, A.; Siegel, J. B.; Gonzalez, R. Combination of Type II Fatty Acid Biosynthesis Enzymes and Thiolases Supports a Functional β-Oxidation Reversal. *Metab. Eng.* **2018**, *45*, 11–19. https://doi.org/10.1016/j.ymben.2017.11.003.

(368) Clomburg, J. M.; Vick, J. E.; Blankschien, M. D.; Rodríguez-Moyá, M.; Gonzalez, R. A Synthetic Biology Approach to Engineer a Functional Reversal of the β-Oxidation Cycle. *ACS Synth. Biol.* **2012**, *1* (11), 541–554. https://doi.org/10.1021/sb3000782.

(369) Bond-Watts, B. B.; Bellerose, R. J.; Chang, M. C. Y. Enzyme Mechanism as a Kinetic Control Element for Designing Synthetic Biofuel Pathways. *Nat. Chem. Biol.* **2011**, *7* (4), 222–227. https://doi.org/10.1038/nchembio.537.

(370) Slater, S.; Houmiel, K. L.; Tran, M.; Mitsky, T. A.; Taylor, N. B.; Padgette, S. R.; Gruys, K. J. Multiple β-Ketothiolases Mediate Poly(β-Hydroxyalkanoate) Copolymer Synthesis in *Ralstonia Eutropha*. *J. Bacteriol.* **1998**, *180* (8), 1979–1987. https://doi.org/10.1128/JB.180.8.1979-1987.1998.

(371) Vandamme, P. Taxonomy of the Genus Cupriavidus: A Tale of Lost and Found. *Int. J. Syst. Evol. Microbiol.* **2004**, *54* (6), 2285–2289. https://doi.org/10.1099/ijs.0.63247-0.

(372) Machado, H. B.; Dekishima, Y.; Luo, H.; Lan, E. I.; Liao, J. C. A Selection Platform for Carbon Chain Elongation Using the CoA-Dependent Pathway to Produce Linear Higher Alcohols. *Metab. Eng.* **2012**, *14* (5), 504–511. https://doi.org/10.1016/j.ymben.2012.07.002.

(373) Martin, C. H.; Dhamankar, H.; Tseng, H.-C.; Sheppard, M. J.; Reisch, C. R.; Prather, K. L. J. A Platform Pathway for Production of 3-Hydroxyacids Provides a Biosynthetic Route to 3-Hydroxy-γ-Butyrolactone. *Nat. Commun.* **2013**, *4* (1), 1414. https://doi.org/10.1038/ncomms2418.

(374) Kim, S.; Cheong, S.; Gonzalez, R. Engineering Escherichia Coli for the Synthesis of Short- and Medium-Chain α,β-Unsaturated Carboxylic Acids. *Metab. Eng.* **2016**, *36*, 90–98. https://doi.org/10.1016/j.ymben.2016.03.005.

(375) Schadeweg, V.; Boles, E. N-Butanol Production in Saccharomyces Cerevisiae Is Limited by the Availability of Coenzyme A and Cytosolic Acetyl-CoA. *Biotechnol. Biofuels* **2016**, *9* (1), 44. https://doi.org/10.1186/s13068-016-0456-7.

(376) Steen, E. J.; Chan, R.; Prasad, N.; Myers, S.; Petzold, C. J.; Redding, A.; Ouellet, M.; Keasling, J. D. Metabolic Engineering of Saccharomyces Cerevisiae for the Production of N-Butanol. *Microb. Cell Factories* **2008**, *7* (1), 36. https://doi.org/10.1186/1475-2859-7-36.

(377) Lee, S. Y.; Park, J. H.; Jang, S. H.; Nielsen, L. K.; Kim, J.; Jung, K. S. Fermentative Butanol Production by Clostridia. *Biotechnol. Bioeng.* **2008**, *101* (2), 209–228. https://doi.org/10.1002/bit.22003.

(378) Hiser, L.; Basson, M. E.; Rine, J. ERG10 from Saccharomyces Cerevisiae Encodes Acetoacetyl-CoA Thiolase. *J. Biol. Chem.* **1994**, *269* (50), 31383–31389.

(379) Bond-Watts, B. B.; Weeks, A. M.; Chang, M. C. Y. Biochemical and Structural Characterization of the *Trans* -Enoyl-CoA Reductase from *Treponema Denticola*. *Biochemistry* **2012**, *51* (34), 6827–6837. https://doi.org/10.1021/bi300879n.

(380) Krink-Koutsoubelis, N.; Loechner, A. C.; Lechner, A.; Link, H.; Denby, C. M.; Vögeli, B.; Erb, T. J.; Yuzawa, S.; Jakociunas, T.; Katz, L.; Jensen, M. K.; Sourjik, V.; Keasling, J. D. Engineered Production of Short-Chain Acyl-Coenzyme A Esters in *Saccharomyces Cerevisiae*. *ACS Synth. Biol.* **2018**, *7* (4), 1105–1115. https://doi.org/10.1021/acssynbio.7b00466.

(381) Chen, Y.; Daviet, L.; Schalk, M.; Siewers, V.; Nielsen, J. Establishing a Platform Cell Factory through Engineering of Yeast Acetyl-CoA Metabolism. *Metab. Eng.* **2013**, *15*, 48–54. https://doi.org/10.1016/j.ymben.2012.11.002.

(382) Chen, Y.; Bao, J.; Kim, I.-K.; Siewers, V.; Nielsen, J. Coupled Incremental Precursor and Co-Factor Supply Improves 3-Hydroxypropionic Acid Production in Saccharomyces Cerevisiae. *Metab. Eng.* **2014**, *22*, 104–109. https://doi.org/10.1016/j.ymben.2014.01.005.

(383) Kozak, B. U.; Van Rossum, H. M.; Benjamin, K. R.; Wu, L.; Daran, J.-M. G.; Pronk, J. T.; Van Maris, A. J. A. Replacement of the Saccharomyces Cerevisiae Acetyl-CoA Synthetases by Alternative Pathways for Cytosolic Acetyl-CoA Synthesis. *Metab. Eng.* **2014**, *21*, 46–59. https://doi.org/10.1016/j.ymben.2013.11.005.

(384) Lian, J.; Si, T.; Nair, N. U.; Zhao, H. Design and Construction of Acetyl-CoA Overproducing Saccharomyces Cerevisiae Strains. *Metab. Eng.* **2014**, *24*, 139–149. https://doi.org/10.1016/j.ymben.2014.05.010.

(385) Liu, W.; Zhang, B.; Jiang, R. Improving Acetyl-CoA Biosynthesis in Saccharomyces Cerevisiae via the Overexpression of Pantothenate Kinase and PDH Bypass. *Biotechnol. Biofuels* **2017**, *10* (1), 41. https://doi.org/10.1186/s13068-017-0726-z.

(386) Nielsen, J. Synthetic Biology for Engineering Acetyl Coenzyme A Metabolism in Yeast. *mBio* **2014**, *5* (6), e02153-14. https://doi.org/10.1128/mBio.02153-14.

(387) Zhang, Y.; Su, M.; Qin, N.; Nielsen, J.; Liu, Z. Expressing a Cytosolic Pyruvate Dehydrogenase Complex to Increase Free Fatty Acid Production in Saccharomyces Cerevisiae. *Microb. Cell Factories* **2020**, *19* (1), 226. https://doi.org/10.1186/s12934-020-01493-z.

(388) Van Rossum, H. M.; Kozak, B. U.; Pronk, J. T.; Van Maris, A. J. A. Engineering Cytosolic Acetyl-Coenzyme A Supply in Saccharomyces Cerevisiae: Pathway Stoichiometry, Free-Energy Conservation and Redox-Cofactor Balancing. *Metab. Eng.* **2016**, *36*, 99–115. https://doi.org/10.1016/j.ymben.2016.03.006.

(389) Pronk, J. T.; Yde Steensma, H.; Van Dijken, J. P. Pyruvate Metabolism in Saccharomyces Cerevisiae. *Yeast Chichester Engl.* **1996**, *12* (16), 1607–1633. https://doi.org/10.1002/(sici)1097-0061(199612)12:16%253C1607::aid-yea70%253E3.0.co;2-4.

(390) Galdieri, L.; Mehrotra, S.; Yu, S.; Vancura, A. Transcriptional Regulation in Yeast during Diauxic Shift and Stationary Phase. *OMICS J. Integr. Biol.* **2010**, *14* (6), 629–638. https://doi.org/10.1089/omi.2010.0069.

(391) Schadeweg, V.; Boles, E. Increasing N-Butanol Production with Saccharomyces Cerevisiae by Optimizing Acetyl-CoA Synthesis, NADH Levels and Trans-2-Enoyl-CoA Reductase Expression. *Biotechnol. Biofuels* **2016**, *9* (1), 257. https://doi.org/10.1186/s13068-016-0673-0.

(392) Membrillo-Hernández, J.; Echave, P.; Cabiscol, E.; Tamarit, J.; Ros, J.; Lin, E. C. C. Evolution of the adhE Gene Product ofEscherichia Coli from a Functional Reductase to a Dehydrogenase. *J. Biol. Chem.* **2000**, *275* (43), 33869–33875. https://doi.org/10.1074/jbc.M005464200.

(393) Garces Daza, F.; Haitz, F.; Born, A.; Boles, E. An Optimized Reverse β-Oxidation Pathway to Produce Selected Medium-Chain Fatty Acids in Saccharomyces Cerevisiae. *Biotechnol. Biofuels Bioprod.* **2023**, *16* (1), 71. https://doi.org/10.1186/s13068-023-02317-z.
(394) Entian, K.-D.; Kötter, P. 25 Yeast Genetic Strain and Plasmid Collections. In *Methods in Microbiology*; Elsevier, 2007; Vol. 36, pp 629–666. https://doi.org/10.1016/S0580-9517(06)36025-4.
(395) Wernig, F.; Born, S.; Boles, E.; Grininger, M.; Oreb, M. Fusing α and β Subunits of the Fungal Fatty Acid Synthase Leads to Improved Production of Fatty Acids. *Sci. Rep.* **2020**, *10* (1), 9780. https://doi.org/10.1038/s41598-020-66629-y.
(396) Gietz, R. D.; Schiestl, R. H. High-Efficiency Yeast Transformation Using the LiAc/SS Carrier DNA/PEG Method. *Nat. Protoc.* **2007**, *2* (1), 31–34. https://doi.org/10.1038/nprot.2007.13.
(397) Lõoke, M.; Kristjuhan, K.; Kristjuhan, A. Extraction of Genomic DNA from Yeasts for PCR-Based Applications. *BioTechniques* **2011**, *50* (5), 325–328. https://doi.org/10.2144/000113672.
(398) Wiedemann, B.; Boles, E. Codon-Optimized Bacterial Genes Improve L -Arabinose Fermentation in Recombinant *Saccharomyces Cerevisiae*. *Appl. Environ. Microbiol.* **2008**, *74* (7), 2043–2050. https://doi.org/10.1128/AEM.02395-07.
(399) Leber, C.; Da Silva, N. A. Engineering of *Saccharomyces Cerevisiae* for the Synthesis of Short Chain Fatty Acids. *Biotechnol. Bioeng.* **2014**, *111* (2), 347–358. https://doi.org/10.1002/bit.25021.
(400) Ichihara, K.; Fukubayashi, Y. Preparation of Fatty Acid Methyl Esters for Gas-Liquid Chromatography. *J. Lipid Res.* **2010**, *51* (3), 635–640. https://doi.org/10.1194/jlr.D001065.
(401) Schindelin, J.; Arganda-Carreras, I.; Frise, E.; Kaynig, V.; Longair, M.; Pietzsch, T.; Preibisch, S.; Rueden, C.; Saalfeld, S.; Schmid, B.; Tinevez, J.-Y.; White, D. J.; Hartenstein, V.; Eliceiri, K.; Tomancak, P.; Cardona, A. Fiji: An Open-Source Platform for Biological-Image Analysis. *Nat. Methods* **2012**, *9* (7), 676–682. https://doi.org/10.1038/nmeth.2019.
(402) Baumann, L.; Doughty, T.; Siewers, V.; Nielsen, J.; Boles, E.; Oreb, M. Transcriptomic Response of *Saccharomyces Cerevisiae* to Octanoic Acid Production. *FEMS Yeast Res.* **2021**, *21* (2), foab011. https://doi.org/10.1093/femsyr/foab011.
(403) Tenreiro, S.; Nunes, P. A.; Viegas, C. A.; Neves, M. S.; Teixeira, M. C.; Cabral, M. G.; Sá-Correia, I. AQR1 Gene (ORF YNL065w) Encodes a Plasma Membrane Transporter of the Major Facilitator Superfamily That Confers Resistance to Short-Chain Monocarboxylic Acids and Quinidine in Saccharomyces Cerevisiae. *Biochem. Biophys. Res. Commun.* **2002**, *292* (3), 741–748. https://doi.org/10.1006/bbrc.2002.6703.
(404) Legras, J. L.; Erny, C.; Le Jeune, C.; Lollier, M.; Adolphe, Y.; Demuyter, C.; Delobel, P.; Blondin, B.; Karst, F. Activation of Two Different Resistance Mechanisms in *Saccharomyces Cerevisiae* upon Exposure to Octanoic and Decanoic Acids. *Appl. Environ. Microbiol.* **2010**, *76* (22), 7526–7535. https://doi.org/10.1128/AEM.01280-10.
(405) Knoll, L. J.; Johnson, D. R.; Gordon, J. I. Biochemical Studies of Three Saccharomyces Cerevisiae Acyl-CoA Synthetases, Faa1p, Faa2p, and Faa3p. *J. Biol. Chem.* **1994**, *269* (23), 16348–16356. https://doi.org/10.1016/S0021-9258(17)34014-0.

(406) Liu, W.; Zhang, B.; Jiang, R. Improving Acetyl-CoA Biosynthesis in Saccharomyces Cerevisiae via the Overexpression of Pantothenate Kinase and PDH Bypass. *Biotechnol. Biofuels* **2017**, *10* (1), 41. https://doi.org/10.1186/s13068-017-0726-z.
(407) Pampulha, M. E.; Loureiro-Dias, M. C. Combined Effect of Acetic Acid, pH and Ethanol on Intracellular pH of Fermenting Yeast. *Appl. Microbiol. Biotechnol.* **1989**, *31–31* (5–6), 547–550. https://doi.org/10.1007/BF00270792.
(408) Mira, N. P.; Palma, M.; Guerreiro, J. F.; Sá-Correia, I. Genome-Wide Identification of Saccharomyces Cerevisiae Genes Required for Tolerance to Acetic Acid. *Microb. Cell Factories* **2010**, *9* (1), 79. https://doi.org/10.1186/1475-2859-9-79.
(409) Guaragnella, N.; Bettiga, M. Acetic Acid Stress in Budding Yeast: From Molecular Mechanisms to Applications. *Yeast* **2021**, *38* (7), 391–400. https://doi.org/10.1002/yea.3651.
(410) Cunha, J. T.; Romaní, A.; Costa, C. E.; Sá-Correia, I.; Domingues, L. Molecular and Physiological Basis of Saccharomyces Cerevisiae Tolerance to Adverse Lignocellulose-Based Process Conditions. *Appl. Microbiol. Biotechnol.* **2019**, *103* (1), 159–175. https://doi.org/10.1007/s00253-018-9478-3.
(411) Ding, J.; Holzwarth, G.; Penner, M. H.; Patton-Vogt, J.; Bakalinsky, A. T. Overexpression of Acetyl-CoA Synthetase in Saccharomyces Cerevisiae Increases Acetic Acid Tolerance. *FEMS Microbiol. Lett.* **2015**, *362* (3), 1–7. https://doi.org/10.1093/femsle/fnu042.
(412) Qin, L.; Dong, S.; Yu, J.; Ning, X.; Xu, K.; Zhang, S.-J.; Xu, L.; Li, B.-Z.; Li, J.; Yuan, Y.-J.; Li, C. Stress-Driven Dynamic Regulation of Multiple Tolerance Genes Improves Robustness and Productive Capacity of Saccharomyces Cerevisiae in Industrial Lignocellulose Fermentation. *Metab. Eng.* **2020**, *61*, 160–170. https://doi.org/10.1016/j.ymben.2020.06.003.
(413) Rock, C. O.; Park, H.-W.; Jackowski, S. Role of Feedback Regulation of Pantothenate Kinase (CoaA) in Control of Coenzyme A Levels in *Escherichia Coli*. *J. Bacteriol.* **2003**, *185* (11), 3410–3415. https://doi.org/10.1128/JB.185.11.3410-3415.2003.
(414) Olzhausen, J.; Grigat, M.; Seifert, L.; Ulbricht, T.; Schüller, H.-J. Increased Biosynthesis of Acetyl-CoA in the Yeast Saccharomyces Cerevisiae by Overexpression of a Deregulated Pantothenate Kinase Gene and Engineering of the Coenzyme A Biosynthetic Pathway. *Appl. Microbiol. Biotechnol.* **2021**, *105* (19), 7321–7337. https://doi.org/10.1007/s00253-021-11523-4.
(415) Calder, R. B.; Williams, R. S. B.; Ramaswamy, G.; Rock, C. O.; Campbell, E.; Unkles, S. E.; Kinghorn, J. R.; Jackowski, S. Cloning and Characterization of a Eukaryotic Pantothenate Kinase Gene (panK) from Aspergillus Nidulans. *J. Biol. Chem.* **1999**, *274* (4), 2014–2020. https://doi.org/10.1074/jbc.274.4.2014.
(416) White, W. H.; Gunyuzlu, P. L.; Toyn, J. H. Saccharomyces Cerevisiae Is Capable of de Novo Pantothenic Acid Biosynthesis Involving a Novel Pathway of β-Alanine Production from Spermine. *J. Biol. Chem.* **2001**, *276* (14), 10794–10800. https://doi.org/10.1074/jbc.M009804200.
(417) White, W. H.; Skatrud, P. L.; Xue, Z.; Toyn, J. H. Specialization of Function Among Aldehyde Dehydrogenases: The *ALD2* and *ALD3* Genes Are Required for β-Alanine Biosynthesis in *Saccharomyces Cerevisiae*. *Genetics* **2003**, *163* (1), 69–77. https://doi.org/10.1093/genetics/163.1.69.
(418) Marinho, H. S.; Real, C.; Cyrne, L.; Soares, H.; Antunes, F. Hydrogen Peroxide Sensing, Signaling and Regulation of Transcription Factors. *Redox Biol.* **2014**, *2*, 535–562. https://doi.org/10.1016/j.redox.2014.02.006.

(419) Shenton, D.; Smirnova, J. B.; Selley, J. N.; Carroll, K.; Hubbard, S. J.; Pavitt, G. D.; Ashe, M. P.; Grant, C. M. Global Translational Responses to Oxidative Stress Impact upon Multiple Levels of Protein Synthesis. *J. Biol. Chem.* **2006**, *281* (39), 29011–29021. https://doi.org/10.1074/jbc.M601545200.
(420) Prousek, J. Fenton Chemistry in Biology and Medicine. *Pure Appl. Chem.* **2007**, *79* (12), 2325–2338. https://doi.org/10.1351/pac200779122325.
(421) Strotmann, L.; Harter, C.; Gerasimova, T.; Ritter, K.; Jessen, H. J.; Wohlwend, D.; Friedrich, T. H2O2 Selectively Damages the Binuclear Iron-Sulfur Cluster N1b of Respiratory Complex I. *Sci. Rep.* **2023**, *13* (1), 7652. https://doi.org/10.1038/s41598-023-34821-5.
(422) Davies, M. J. Protein Oxidation and Peroxidation. *Biochem. J.* **2016**, *473* (7), 805–825. https://doi.org/10.1042/BJ20151227.
(423) Koppenol, W. H. The Haber-Weiss Cycle – 70 Years Later. *Redox Rep.* **2001**, *6* (4), 229–234. https://doi.org/10.1179/135100001101536373.
(424) Switala, J.; Loewen, P. C. Diversity of Properties among Catalases. *Arch. Biochem. Biophys.* **2002**, *401* (2), 145–154. https://doi.org/10.1016/S0003-9861(02)00049-8.
(425) Godon, C.; Lagniel, G.; Lee, J.; Buhler, J.-M.; Kieffer, S.; Perrot, M.; Boucherie, H.; Toledano, M. B.; Labarre, J. The H2O2 Stimulon in Saccharomyces Cerevisiae. *J. Biol. Chem.* **1998**, *273* (35), 22480–22489. https://doi.org/10.1074/jbc.273.35.22480.
(426) Jamieson, D. J.; Rivers, S. L.; Stephen, D. W. S. Analysis of Saccharomyces Cerevisiae Proteins Induced by Peroxide and Superoxide Stress. *Microbiology* **1994**, *140* (12), 3277–3283. https://doi.org/10.1099/13500872-140-12-3277.
(427) Martins, D.; English, A. M. Catalase Activity Is Stimulated by H2O2 in Rich Culture Medium and Is Required for H2O2 Resistance and Adaptation in Yeast. *Redox Biol.* **2014**, *2*, 308–313. https://doi.org/10.1016/j.redox.2013.12.019.
(428) Šebela, M.; Rašková, M. Polyamine-Derived Aminoaldehydes and Acrolein: Cytotoxicity, Reactivity and Analysis of the Induced Protein Modifications. *Molecules* **2023**, *28* (21), 7429. https://doi.org/10.3390/molecules28217429.
(429) Kim, J.-E.; Jang, I.-S.; Sung, B. H.; Kim, S. C.; Lee, J. Y. Rerouting of NADPH Synthetic Pathways for Increased Protopanaxadiol Production in Saccharomyces Cerevisiae. *Sci. Rep.* **2018**, *8* (1), 15820. https://doi.org/10.1038/s41598-018-34210-3.
(430) Morgan-Kiss, R. M.; Cronan, J. E. The Escherichia Coli fadK (ydiD) Gene Encodes an Anerobically Regulated Short Chain Acyl-CoA Synthetase. *J. Biol. Chem.* **2004**, *279* (36), 37324–37333. https://doi.org/10.1074/jbc.M405233200.
(431) Srividya, N.; Lange, I.; Hartmann, M.; Li, Q.; Mirzaei, M.; Lange, B. M. Biochemical Characterization of Acyl Activating Enzymes for Side Chain Moieties of Taxol and Its Analogs. *J. Biol. Chem.* **2020**, *295* (15), 4963–4973. https://doi.org/10.1074/jbc.RA120.012663.
(432) Black, P. N.; DiRusso, C. C. Yeast Acyl-CoA Synthetases at the Crossroads of Fatty Acid Metabolism and Regulation. *Biochim. Biophys. Acta BBA - Mol. Cell Biol. Lipids* **2007**, *1771* (3), 286–298. https://doi.org/10.1016/j.bbalip.2006.05.003.
(433) De Azevedo Souza, C.; Barbazuk, B.; Ralph, S. G.; Bohlmann, J.; Hamberger, B.; Douglas, C. J. Genome-wide Analysis of a Land Plant-specific *Acyl:coenzymeA Synthetase* (*ACS*) Gene Family in *Arabidopsis* , Poplar, Rice and *Physcomitrella*. *New Phytol.* **2008**, *179* (4), 987–1003. https://doi.org/10.1111/j.1469-8137.2008.02534.x.

(434) Shockey, J.; Browse, J. Genome-level and Biochemical Diversity of the Acyl-activating Enzyme Superfamily in Plants. *Plant J.* **2011**, *66* (1), 143–160. https://doi.org/10.1111/j.1365-313X.2011.04512.x.
(435) Shockey, J. M.; Fulda, M. S.; Browse, J. Arabidopsis Contains a Large Superfamily of Acyl-Activating Enzymes. Phylogenetic and Biochemical Analysis Reveals a New Class of Acyl-Coenzyme A Synthetases. *Plant Physiol.* **2003**, *132* (2), 1065–1076. https://doi.org/10.1104/pp.103.020552.
(436) Koetsier, M. J.; Jekel, P. A.; van den Berg, M. A.; Bovenberg, R. A. L.; Janssen, D. B. Characterization of a Phenylacetate–CoA Ligase from *Penicillium Chrysogenum*. *Biochem. J.* **2009**, *417* (2), 467–476. https://doi.org/10.1042/BJ20081257.
(437) Gould, S. J.; Keller, G. A.; Hosken, N.; Wilkinson, J.; Subramani, S. A Conserved Tripeptide Sorts Proteins to Peroxisomes. *J. Cell Biol.* **1989**, *108* (5), 1657–1664. https://doi.org/10.1083/jcb.108.5.1657.
(438) Reumann, S. Specification of the Peroxisome Targeting Signals Type 1 and Type 2 of Plant Peroxisomes by Bioinformatics Analyses. *Plant Physiol.* **2004**, *135* (2), 783–800. https://doi.org/10.1104/pp.103.035584.
(439) Gidijala, L.; Van Der Klei, I. J.; Veenhuis, M.; Kiel, J. A. K. W. Reprogramming *Hansenula Polymorpha* for Penicillin Production: Expression of the *Penicillium Chrysogenum Pcl* Gene. *FEMS Yeast Res.* **2007**, *7* (7), 1160–1167. https://doi.org/10.1111/j.1567-1364.2007.00228.x.
(440) Kamada, T.; Nito, K.; Hayashi, H.; Mano, S.; Hayashi, M.; Nishimura, M. Functional Differentiation of Peroxisomes Revealed by Expression Profiles of Peroxisomal Genes in Arabidopsis Thaliana. *Plant Cell Physiol.* **2003**, *44* (12), 1275–1289. https://doi.org/10.1093/pcp/pcg173.
(441) Hiltunen, J. K.; Mursula, A. M.; Rottensteiner, H.; Wierenga, R. K.; Kastaniotis, A. J.; Gurvitz, A. The Biochemistry of Peroxisomal β-Oxidation in the Yeast *Saccharomyces Cerevisiae*. *FEMS Microbiol. Rev.* **2003**, *27* (1), 35–64. https://doi.org/10.1016/S0168-6445(03)00017-2.
(442) Rosenthal, M.; Metzl-Raz, E.; Bürgi, J.; Yifrach, E.; Drwesh, L.; Fadel, A.; Peleg, Y.; Rapaport, D.; Wilmanns, M.; Barkai, N.; Schuldiner, M.; Zalckvar, E. Uncovering Targeting Priority to Yeast Peroxisomes Using an In-Cell Competition Assay. *Proc. Natl. Acad. Sci.* **2020**, *117* (35), 21432–21440. https://doi.org/10.1073/pnas.1920078117.
(443) Hettema, E. H.; van Roermund, C. W.; Distel, B.; van den Berg, M.; Vilela, C.; Rodrigues-Pousada, C.; Wanders, R. J.; Tabak, H. F. The ABC Transporter Proteins Pat1 and Pat2 Are Required for Import of Long-Chain Fatty Acids into Peroxisomes of Saccharomyces Cerevisiae. *EMBO J.* **1996**, *15* (15), 3813–3822.
(444) Viegas, C. A.; Rosa, M. F.; Sá-Correia, I.; Novais, J. M. Inhibition of Yeast Growth by Octanoic and Decanoic Acids Produced during Ethanolic Fermentation. *Appl. Environ. Microbiol.* **1989**, *55* (1), 21–28. https://doi.org/10.1128/aem.55.1.21-28.1989.
(445) Pinto, I.; Cardoso, H.; Leão, C.; Van Uden, N. High Enthalpy and Low Enthalpy Death in *Saccharomyces Cerevisiae* Induced by Acetic Acid. *Biotechnol. Bioeng.* **1989**, *33* (10), 1350–1352. https://doi.org/10.1002/bit.260331019.
(446) Kamp, F.; Guo, W.; Souto, R.; Pilch, P. F.; Corkey, B. E.; Hamilton, J. A. Rapid Flip-Flop of Oleic Acid across the Plasma Membrane of Adipocytes. *J. Biol. Chem.* **2003**, *278* (10), 7988–7995. https://doi.org/10.1074/jbc.M206648200.
(447) Viegas, C. Effects of Low Temperatures (9–33 °C) and pH (3.3–5.7) in the Loss of Saccharomyces Cerevisiae Viability by Combining Lethal Concentrations of

Ethanol with Octanoic and Decanoic Acids. *Int. J. Food Microbiol.* **1997**, *34* (3), 267–277. https://doi.org/10.1016/S0168-1605(96)01200-7.

(448) Alexandre, H.; Mathieu, B.; Charpentier, C. Alteration in Membrane Fluidity and Lipid Composition, and Modulation of H+-ATPase Activity in Saccharomyces Cerevisiae Caused by Decanoic Acid. *Microbiology* **1996**, *142* (3), 469–475. https://doi.org/10.1099/13500872-142-3-469.

(449) Guan, N.; Liu, L. Microbial Response to Acid Stress: Mechanisms and Applications. *Appl. Microbiol. Biotechnol.* **2020**, *104* (1), 51–65. https://doi.org/10.1007/s00253-019-10226-1.

(450) Viegas, C. A.; Supply, P.; Capieaux, E.; Van Dyck, L.; Goffeau, A.; Sá-Correia, I. Regulation of the Expression of the H+-ATPase Genes PMA1 and PMA2 during Growth and Effects of Octanoic Acid in Saccharomyces Cerevisiae. *Biochim. Biophys. Acta BBA - Gene Struct. Expr.* **1994**, *1217* (1), 65–73. https://doi.org/10.1016/0167-4781(94)90126-0.

(451) Thomas, F.; Schmidt, C.; Kayser, O. Bioengineering Studies and Pathway Modeling of the Heterologous Biosynthesis of Tetrahydrocannabinolic Acid in Yeast. *Appl. Microbiol. Biotechnol.* **2020**, *104* (22), 9551–9563. https://doi.org/10.1007/s00253-020-10798-3.

(452) He, S.; Zhang, Z.; Zhang, C.; Lu, W. Construction and Optimization of Malonyl-CoA Sensors in Saccharomyces Cerevisiae by Combining Promoter Engineering Strategies. *Processes* **2022**, *10* (12), 2660. https://doi.org/10.3390/pr10122660.

(453) Jones, A. E.; Arias, N. J.; Acevedo, A.; Reddy, S. T.; Divakaruni, A. S.; Meriwether, D. A Single LC-MS/MS Analysis to Quantify CoA Biosynthetic Intermediates and Short-Chain Acyl CoAs. *Metabolites* **2021**, *11* (8), 468. https://doi.org/10.3390/metabo11080468.

(454) Tsuchiya, Y.; Pham, U.; Gout, I. Methods for Measuring CoA and CoA Derivatives in Biological Samples. *Biochem. Soc. Trans.* **2014**, *42* (4), 1107–1111. https://doi.org/10.1042/BST20140123.

(455) Kildegaard, K. R.; Jensen, N. B.; Schneider, K.; Czarnotta, E.; Özdemir, E.; Klein, T.; Maury, J.; Ebert, B. E.; Christensen, H. B.; Chen, Y.; Kim, I.-K.; Herrgård, M. J.; Blank, L. M.; Forster, J.; Nielsen, J.; Borodina, I. Engineering and Systems-Level Analysis of Saccharomyces Cerevisiae for Production of 3-Hydroxypropionic Acid via Malonyl-CoA Reductase-Dependent Pathway. *Microb. Cell Factories* **2016**, *15* (1), 53. https://doi.org/10.1186/s12934-016-0451-5.

(456) Hitschler, J.; Boles, E. Improving 3-Methylphenol (*m* -Cresol) Production in Yeast via *in Vivo* Glycosylation or Methylation. *FEMS Yeast Res.* **2020**, *20* (8), foaa063. https://doi.org/10.1093/femsyr/foaa063.

(457) Dusséaux, S.; Wajn, W. T.; Liu, Y.; Ignea, C.; Kampranis, S. C. Transforming Yeast Peroxisomes into Microfactories for the Efficient Production of High-Value Isoprenoids. *Proc. Natl. Acad. Sci.* **2020**, *117* (50), 31789–31799. https://doi.org/10.1073/pnas.2013968117.

(458) Kulagina, N.; Besseau, S.; Papon, N.; Courdavault, V. Peroxisomes: A New Hub for Metabolic Engineering in Yeast. *Front. Bioeng. Biotechnol.* **2021**, *9*, 659431. https://doi.org/10.3389/fbioe.2021.659431.

(459) Lin, P.; Fu, Z.; Liu, X.; Liu, C.; Bai, Z.; Yang, Y.; Li, Y. Direct Utilization of Peroxisomal Acetyl-CoA for the Synthesis of Polyketide Compounds in *Saccharomyces Cerevisiae*. *ACS Synth. Biol.* **2023**, *12* (6), 1599–1607. https://doi.org/10.1021/acssynbio.2c00678.

(460) Lazarow, P. B.; Fujiki, Y. Biogenesis of Peroxisomes. *Annu. Rev. Cell Biol.* **1985**, *1* (1), 489–530. https://doi.org/10.1146/annurev.cb.01.110185.002421.

(461) Sibirny, A. A. Yeast Peroxisomes: Structure, Functions and Biotechnological Opportunities. *FEMS Yeast Res.* **2016**, *16* (4), fow038. https://doi.org/10.1093/femsyr/fow038.
(462) Natter, K.; Leitner, P.; Faschinger, A.; Wolinski, H.; McCraith, S.; Fields, S.; Kohlwein, S. D. The Spatial Organization of Lipid Synthesis in the Yeast Saccharomyces Cerevisiae Derived from Large Scale Green Fluorescent Protein Tagging and High Resolution Microscopy. *Mol. Cell. Proteomics* **2005**, *4* (5), 662–672. https://doi.org/10.1074/mcp.M400123-MCP200.
(463) Seltmann, G.; Beer, W. Nourseothricin (Streptothricin) Inactivated by a Plasmid pIE636 Encoded Acetyl Transferase: Nature of the Inactivated Nourseothricin. *Acta Microbiol. Hung.* **1987**, *34* (1), 19–24.
(464) Zähringer, U.; Voigt, W.; Seltmann, G. Noureseothricin (Streptothricin) Inactivated by a Plasmid pIE636 Encoded Acetyl Transferase of *Escherichia Coli* : Location of the Acetyl Group. *FEMS Microbiol. Lett.* **1993**, *110* (3), 331–334. https://doi.org/10.1111/j.1574-6968.1993.tb06344.x.

6 SUPPLEMENTARY INFORMATION

Supplementary Table 1 | Coding sequences of heterologous or mutated genes used in this study

Codon optimized pantothenate kinase from *E. coli* (*^{Ec}coaA*)
ATGTCTATTAAGGAACAAACCTTGATGACCCCATACTTGCAATTCGACAGAAACCAATGGG CTGCTTTGAGAGATTCCGTTCCAATGACCTTGTCTGAAGATGAAATCGCTAGATTGAAGGG TATTAACGAAGATTTGTCTTTGGAAGAAGTTGCTGAAATCTACTTGCCATTGTCTAGATTGT TGAACTTCTACATTTCTTCTAACTTGAGAAGACAAGCTGTTTTGGAACAATTCTTGGGTACC AACGGTCAAAGAATTCCATACATTATCTCTATTGCTGGTTCTGTCGCTGTTGGTAAGTCTAC CACCGCTAGAGTTTTGCAAGCTTTGTTGTCTAGATGGCCAGAACACAGAAGAGTTGAATTG ATCACTACCGATGGTTTCTTGCACCCAAACCAAGTTTTGAAGGAAAGAGGTTTGATGAAGA AGAAGGGTTTCCCAGAATCTTACGATATGCACAGATTGGTTAAGTTCGTTTCCGATTTGAA GTCCGGTGTTCCAAACGTTACCGCTCCAGTTTACTCTCACTTGATTTACGATGTTATCCCA GATGGTGATAAGACCGTTGTTCAACCAGATATTTTGATTTTGGAAGGTTTGAACGTCTTGC AATCTGGTATGGATTACCCACACGATCCACACCACGTTTTCGTTTCTGATTTCGTCGATTTC TCTATTTACGTTGATGCTCCAGAAGACTTGTTGCAAACCTGGTACATCAACAGATTCTTGAA GTTCAGAGAAGGTGCTTTCACCGACCCAGATTCCTACTTCCACAACTACGCTAAGTTGACT AAGGAAGAAGCTATTAAGACTGCTATGACCTTGTGGAAGGAAATCAACTGGTTGAACTTGA AGCAAAACATTTTGCCAACTAGAGAAAGAGCTTCTTTGATCTTGACCAAGTCTGCTAACCA CGCTGTTGAAGAAGTCAGATTGAGAAAGTAA

Codon optimized pantothenate kinase (R106A) from *E. coli* (*^{Ec}coaA^{R106A}*)
ATGTCTATTAAGGAACAAACCTTGATGACCCCATACTTGCAATTCGACAGAAACCAATGGG CTGCTTTGAGAGATTCCGTTCCAATGACCTTGTCTGAAGATGAAATCGCTAGATTGAAGGG TATTAACGAAGATTTGTCTTTGGAAGAAGTTGCTGAAATCTACTTGCCATTGTCTAGATTGT TGAACTTCTACATTTCTTCTAACTTGAGAAGACAAGCTGTTTTGGAACAATTCTTGGGTACC AACGGTCAAAGAATTCCATACATTATCTCTATTGCTGGTTCTGTCGCTGTTGGTAAGTCTAC CACCGCTGCTGTTTTGCAAGCTTTGTTGTCTAGATGGCCAGAACACAGAAGAGTTGAATTG ATCACTACCGATGGTTTCTTGCACCCAAACCAAGTTTTGAAGGAAAGAGGTTTGATGAAGA AGAAGGGTTTCCCAGAATCTTACGATATGCACAGATTGGTTAAGTTCGTTTCCGATTTGAA GTCCGGTGTTCCAAACGTTACCGCTCCAGTTTACTCTCACTTGATTTACGATGTTATCCCA GATGGTGATAAGACCGTTGTTCAACCAGATATTTTGATTTTGGAAGGTTTGAACGTCTTGC AATCTGGTATGGATTACCCACACGATCCACACCACGTTTTCGTTTCTGATTTCGTCGATTTC TCTATTTACGTTGATGCTCCAGAAGACTTGTTGCAAACCTGGTACATCAACAGATTCTTGAA GTTCAGAGAAGGTGCTTTCACCGACCCAGATTCCTACTTCCACAACTACGCTAAGTTGACT AAGGAAGAAGCTATTAAGACTGCTATGACCTTGTGGAAGGAAATCAACTGGTTGAACTTGA AGCAAAACATTTTGCCAACTAGAGAAAGAGCTTCTTTGATCTTGACCAAGTCTGCTAACCA CGCTGTTGAAGAAGTCAGATTGAGAAAGTAA

Codon optimized olivetol synthase from *C. sativa* (*^{Cs}OLS*) in KSV74
ATGAACCACTTGAGAGCTGAAGGTCCAGCTTCTGTTTTGGCTATCGGTACTGCTAACCCAG AAAACATCTTGTTGCAAGACGAATTCCCAGACTACTACTTCAGAGTTACTAAGTCTGAACA CATGACTCAATTGAAGGAAAAGTTCAGAAAGATCTGTGACAAGTCTATGATCAGAAAGAGA AACTGTTTCTTGAACGAAGAACACTTGAAGCAAAACCCAAGATTGGTTGAACACGAAATGC AAACTTTGGACGCTAGACAAGACATGTTGGTTGTTGAAGTTCCAAAGTTGGGTAAGGACG CTTGTGCTAAGGCTATCAAGGAATGGGGTCAACCAAAGTCTAAGATCACTCACTTGATCTT CACTTCTGCTTCTACTACTGACATGCCAGGTGCTGACTACCACTGTGCTAAGTTGTTGGGT TTGTCTCCATCTGTTAAGAGAGTTATGATGTACCAATTGGGTTGTTACGGTGGTGGTACTG TTTTGAGAATCGCTAAGGACATCGCTGAAAACAACAAGGGTGCTAGAGTTTTGGCTGTTTG TTGTGACATCATGGCTTGTTTGTTCAGAGGTCCATCTGAATCTGACTTGGAATTGTTGGTT GGTCAAGCTATCTTCGGTGACGGTGCTGCTGCTGTTATCGTTGGTGCTGAACCAGACGAA TCTGTTGGTGAAAGACCAATCTTCGAATTGGTTTCTACTGGTCAAACTATCTTGCCAAACTC TGAAGGTACTATCGGTGGTCACATCAGAGAAGCTGGTTTGATCTTCGACTTGCACAAGGA CGTTCCAATGTTGATCTCTAACAACATCGAAAAGTGTTTGATCGAAGCTTTCACTCCAATCG GTATCTCTGACTGGAACTCTATCTTCTGGATCACTCACCCAGGTGGTAAGGCTATCTTGGA

CAAGGTTGAAGAAAAGTTGCACTTGAAGTCTGACAAGTTCGTTGACTCTAGACACGTTTTG
TCTGAACACGGTAACATGTCTTCTTCTACTGTTTTGTTCGTTATGGACGAATTGAGAAAGAG
ATCTTTGGAAGAAGGTAAGTCTACTACTGGTGACGGTTTCGAATGGGGTGTTTTGTTCGGT
TTCGGTCCAGGTTTGACTGTTGAAAGAGTTGTTGTTAGATCTGTTCCAATCAAGTACTAA

Codon optimized olivetolic acid cyclase from *C. sativa* (*^{Cs}OAC*) in KSV74

ATGGCTGTTAAGCACTTGATCGTTTTGAAGTTCAAGGACGAAATCACTGAAGCTCAAAAGG
AAGAATTCTTCAAGACTTACGTTAACTTGGTTAACATCATCCCAGCTATGAAGGACGTTTAC
TGGGGTAAGGACGTTACTCAAAAGAACAAGGAAGAAGGTTACACTCACATCGTTGAAGTTA
CTTTCGAATCTGTTGAAACTATCCAAGACTACATCATCCACCCAGCTCACGTTGGTTTCGG
TGACGTTTACAGATCTTTCTGGGAAAAGTTGTTGATCTTCGACTACACTCCAAGAAAGTAA

Codon optimized olivetol synthase from *C. sativa* (*^{Cs}OLS*) in pCS_Can10

ATGAACCACTTGAGAGCTGAAGGTCCAGCTTCTGTTTTGGCTATTGGTACTGCTAATCCAG
AGAACATCTTGTTGCAAGATGAATTTCCAGACTACTACTTCAGAGTCACTAAGTCTGAACA
CATGACCCAGTTGAAAGAGAAGTTCAGAAAGATTTGCGACAAGTCCATGATCAGAAAGAG
AAACTGTTTCTTGAACGAGGAACACTTGAAGCAAAACCCAAGATTGGTTGAACACGAAATG
CAAACATTGGATGCCAGACAAGATATGTTGGTTGTTGAAGTTCCAAAGTTGGGTAAAGATG
CTTGTGCTAAGGCTATCAAAGAATGGGGTCAACCTAAATCCAAGATCACCCATTTGATTTT
CACCTCTGCTTCTACTACTGATATGCCAGGTGCTGATTACCATTGTGCCAAATTATTGGGT
TTGTCCCCATCTGTAAAAAGGGTCATGATGTATCAATTGGGTTGTTATGGTGGTGGTACTG
TTTTGAGAATTGCTAAGGATATTGCCGAGAACAACAAAGGTGCTAGAGTTTTGGCTGTTTG
CTGTGATATTATGGCTTGTTTGTTCAGAGGTCCATCCGAATCTGATTTGGAATTATTGGTTG
GTCAAGCCATCTTTGGTGATGGTGCTGCTGCTGTTATAGTTGGTGCTGAACCAGATGAATC
TGTTGGTGAAAGACCAATCTTCGAATTGGTTTCTACTGGTCAAACTATCTTGCCAAACTCC
GAAGGTACTATTGGTGGTCATATCAGAGAAGCCGGTTTGATTTTTGACTTGCATAAGGATG
TTCCCATGCTGATCTCTAACAACATTGAAAAGTGTTTGATCGAGGCTTTCACCCCAATTGG
TATTTCTGATTGGAACTCCATTTTCTGGATTACTCATCCAGGTGGTAAAGCTATCTTGGATA
AGGTAGAAGAAAAGCTGCATCTGAAGTCCGATAAGTTCGTTGATTCAAGACACGTCTTGTC
TGAACATGGTAACATGTCATCTTCTACCGTTTTGTTCGTTATGGACGAATTGAGAAAGAGG
TCTTTGGAAGAAGGTAAATCTACTACCGGTGATGGTTTTGAATGGGGTGTTTTGTTTGGTT
TTGGTCCAGGTTTGACTGTCGAAAGAGTTGTTGTTAGGTCTGTTCCTATCAAGTACTGA

First codon optimized olivetolic acid cyclase from *C. sativa* (*^{Cs}OAC*) in pCS_Can10

ATGGCCGTTAAGCACTTAATTGTCTTGAAGTTCAAGGATGAAATCACTGAAGCTCAAAAAG
AGGAATTCTTCAAGACCTTCGTTAACTTGGTTAACATTATTCCAGCTATGAAGGACGTCTAC
TGGGGTAAGGACGTTACCCAAAAAAACAAGGAAGAGGGTTACACTCACATCGTCGAAGTT
ACCTTCGAATCTGTCGAAACTATTCAAGACTACATCATTCACCCAGCTCACGTTGGTTTCG
GTGATGTCTACAGATCTTTCTGGGAAAAGTTGTTGATCTTCGATTACACCCCTAGAAAGTA
A

Second codon optimized olivetolic acid cyclase 2 from *C. sativa* (*^{Cs}OAC*) in pCS_Can10

ATGGCCGTTAAACACTTAATAGTGTTGAAGTTTAAGGATGAGATTACTGAAGCACAAAAGG
AAGAGTTCTTCAAAACCTTTGTTAATCTAGTCAATATCATTCCAGCTATGAAAGATGTGTAT
TGGGGTAAAGATGTAACACAGAAGAACAAAGAAGAAGGCTATACGCATATAGTTGAAGTCA
CATTTGAGTCTGTTGAAACCATTCAAGACTACATCATACATCCTGCTCATGTTGGTTTTGGA
GATGTATACAGGTCATTTTGGGAAAAGTTGCTTATTTTCGACTATACTCCCAGAAAATAA

Codon optimized acyl-activating enzyme 1 from *C. sativa*

ATGGGCAAGAACTACAAGTCCTTGGATTCTGTTGTTGCCTCTGATTTTATTGCCTTGGGTA
TTACTTCTGAAGTTGCCGAAACTTTACATGGTAGATTGGCTGAAATTGTCTGTAATTATGGT
GCTGCTACTCCACAAACCTGGATTAACATTGCTAACCATATCTTGTCTCCAGACTTGCCATT
TTCCTTGCATCAAATGTTGTTCTACGGTTGCTACAAGGATTTTGGTCCAGCTCCACCAGCT
TGGATTCCAGATCCAGAAAAAGTTAAGTCTACCAACTTGGGTGCTTTGTTGGAAAAGAGAG
GCAAAGAATTTTTGGGCGTTAAGTACAAGGATCCCATCTCTTCATTTTCCCACTTCCAAGAA
TTCTCCGTTAGAAACCCAGAAGTTTATTGGAGAACTGTCTTGATGGACGAGATGAAGATTT
CATTCTCTAAGGATCCAGAGTGCATCTTGAGAAGAGATGATATTAACAATCCAGGTGGTTC
TGAATGGTTGCCTGGTGGTTATTTGAATTCTGCTAAGAACTGCTTGAACGTCAACTCCAAC
AAAAAGTTGAACGACACTATGATCGTTTGGAGAGATGAGGGTAATGATGATTTGCCATTGA

ACAAGTTGACCTTGGACCAATTGAGAAAGAGAGTTTGGTTAGTTGGTTACGCCTTGGAAGA
AATGGGTTTAGAAAAAGGTTGCGCTATTGCTATCGATATGCCAATGCATGTTGATGCCGTT
GTTATCTATTTGGCTATAGTTTTGGCTGGTTACGTCGTTGTTTCAATTGCCGATTCATTTTC
TGCTCCAGAAATCTCTACTAGGTTGAGATTGTCTAAGGCTAAGGCTATTTTCACCCAAGAT
CATATCATCAGAGGTAAGAAGAGAATTCCCTTGTACTCCAGAGTTGTTGAAGCTAAATCTC
CAATGGCTATCGTTATTCCATGTTCCGGTTCTAATATTGGTGCCGAATTGAGAGATGGTGA
TATCTCTTGGGATTATTTCTTGGAAAGGGCCAAAGAATTCAAGAACTGTGAGTTTACTGCTA
GAGAACAACCAGTTGACGCTTACACTAATATCTTGTTCTCTTCTGGTACTACCGGTGAACC
TAAAGCTATTCCATGGACTCAAGCTACTCCATTGAAAGCTGCTGCTGATGGTTGGTCACAT
TTGGATATTAGAAAGGGTGATGTTATCGTCTGGCCAACTAACTTAGGTTGGATGATGGGTC
CTTGGTTGGTTTATGCTTCTTTGTTGAATGGTGCATCCATTGCCTTGTATAATGGTTCTCCA
TTGGTTTCTGGTTTCGCCAAGTTTGTTCAAGATGCTAAGGTTACTATGTTGGGTGTTGTTCC
ATCTATCGTTAGATCTTGGAAATCCACCAATTGTGTCTCTGGTTATGATTGGTCTACTATCA
GATGCTTCTCATCTTCTGGTGAAGCTTCTAACGTTGATGAATACTTGTGGTTGATGGGTAG
AGCTAATTACAAGCCAGTTATTGAAATGTGCGGTGGTACTGAAATTGGTGGTGCTTTTTCT
GCTGGTTCATTCTTGCAAGCTCAATCCTTGTCATCCTTTTCTTCTCAATGTATGGGTTGCAC
CTTGTACATCTTGGATAAGAATGGTTATCCCATGCCAAAAAACAAACCAGGTATTGGTGAA
TTGGCTTTGGGTCCAGTTATGTTTGGTGCTTCTAAAACCTTGTTGAACGGTAACCATCACG
ATGTTTACTTTAAGGGTATGCCAACTTTGAACGGTGAAGTTTTGAGAAGGCACGGTGATAT
TTTCGAATTGACTTCTAACGGTTACTACCATGCTCACGGTAGAGCTGATGATACAATGAAT
ATCGGTGGTATCAAGATCTCCTCCATCGAAATTGAAAGAGTCTGCAACGAAGTTGACGACA
GAGTTTTTGAAACTACCGCTATTGGTGTTCCACCATTAGGTGGTGGTCCAGAACAATTGGT
TATTTTCTTCGTTCTGAAGGACTCCAACGATACCACCATTGATTTGAATCAACTGAGGCTGT
CTTTTAACTTGGGCTTGCAAAAGAAGTTGAACCCCTTGTTTAAAGTTACCAGAGTCGTTCC
ATTGTCCTCATTGCCAAGAACTGCAACTAACAAGATCATGAGAAGAGTCTTGAGACAACAG
TTCTCTCACTTCGAATGA

Codon optimized acyl-activating enzyme 3 from *C. sativa*

ATGGAAAAGTCTGGTTATGGTAGAGATGGTATCTACAGATCTTTAAGACCACCATTGCATC
TGCCAAACAACAACAATTTGTCCATGGTGTCTTTCTTGTTCCGTAACTCTTCTTCATACCCA
CAAAAGCCAGCTTTGATCGACTCTGAAACTAACCAGATTTTGTCCTTCTCACACTTCAAGTC
CACCGTTATTAAGGTTTCTCATGGCTTTTTGAACCTGGGCATCAAAAAGAACGATGTCGTT
TTGATCTACGCCCCAAACTCTATTCATTTCCCAGTTTGTTTCTTGGGCATTATTGCTTCAGG
TGCTATTGCTACTACTTCTAACCCATTATACACCGTGTCTGAATTGTCCAAGCAAGTTAAGG
ATTCCAATCCAAAGTTGATCATTACCGTTCCACAGTTGTTGGAAAAGGTTAAGGGTTTTAAC
TTGCCCACCATTTTGATTGGTCCAGACTCTGAACAAGAATCCTCTTCAGATAAGGTTATGA
CCTTCAACGACTTGGTTAACTTAGGTGGTTCTTCTGGTTCAGAATTCCCAATCGTTGATGA
CTTCAAGCAATCTGATACTGCTGCTTTGTTGTACTCTTCTGGTACTACTGGTATGTCTAAGG
GTGTTGTTTTGACCCACAAGAACTTTATTGCCTCTTCTTTGATGGTCACCATGGAACAAGAT
TTGGTTGGTGAAATGGACAACGTTTTCTTGTGTTTCTTGCCAATGTTCCACGTTTTCGGTTT
GGCTATTATTACCTACGCTCAATTGCAAAGAGGTAACACCGTTATATCTATGGCCAGATTC
GATTTGGAGAAGATGTTGAAGGATGTCGAAAAGTACAAGGTTACCCATTTGTGGGTTGTTC
CACCAGTTATTTTGGCTTTGTCTAAGAACTCCATGGTCAAGAAGTTCAACCTGTCCTCCATT
AAGTATATTGGTTCTGGTGCTGCTCCATTGGGTAAAGATTTGATGGAAGAATGCTCTAAGG
TTGTCCCATATGGTATAGTTGCTCAAGGTTACGGTATGACTGAAACTTGTGGTATCGTTAG
CATGGAAGATATTAGAGGTGGTAAGAGAAATTCTGGTTCTGCAGGTATGTTAGCTTCTGGT
GTTGAAGCTCAAATCGTTTCTGTTGATACTTTGAAACCCTTGCCACCAAATCAATTGGGTG
AAATTTGGGTCAAAGGTCCAAATATGATGCAGGGTTACTTCAACAATCCACAAGCTACTAA
GTTGACCATCGATAAGAAAGGTTGGGTTCATACTGGTGACTTGGGTTACTTTGATGAAGAT
GGTCACTTGTACGTTGTCGACAGAATCAAAGAACTGATCAAGTACAAAGGTTTCCAAGTTG
CTCCAGCTGAATTGGAAGGTTTGTTAGTTTCTCATCCAGAAATCTTGGATGCCGTTGTTATT
CCATTTCCAGATGCTGAAGCTGGTGAAGTTCCAGTTGCTTATGTTGTTAGATCTCCCAACT
CTTCCTTGACTGAAAACGATGTGAAAAAGTTCATTGCTGGTCAAGTTGCCTCTTTCAAGAG
ATTGAGAAAGGTTACCTTCATCAACTCCGTTCCAAAATCTGCTTCTGGTAAGATCTTGAGAA
GAGAGTTGATTCAAAAGGTCAGGTCCAACATGTGA

Codon optimized phenylacetate-CoA ligase (T369A) from *P. chrysogenum* (*^{Pc}PCL*)

ATGGTTTTCTTGCCACCAAAAGAATCCGGTCAATTAGATCCAATTCCAGACAACATTCCAAT
CTCCGAATTCATGTTGAACGAAAGATACGGTAGAGTTAGACATGCCTCTTCTAGAGATCCA
TACACTTGTGGTATTACTGGCAAGTCCTACTCCTCTAAAGAAGTTGCTAATAGGGTTGATT

CCTTGGCCAGATCTTTGTCTAAAGAATTTGGTTGGGCTCCAAACGAAGGTTCTGAATGGGA
TAAGACTTTGGCTGTTTTTGCCTTGAACACCATTGATTCTTTGCCTTTGTTTTGGGCCGTTC
ATAGATTAGGTGGTGTTTTGACTCCAGCTAATGCTTCTTATTCTGCTGCTGAATTGACTCAC
CAACTGTTGGATTCTAAAGCTAAGGCTTTGGTTACTTGCGTTCCTTTGTTGTCCATTTCTTT
GGAAGCTGCTGCTAAAGCTGGTTTGCCAAAGAATAGAATCTACTTGTTGGATGTCCCAGAA
CAATTACTTGGTGGTGTTAAGCCACCAGCAGGTTACAAATCTGTTTCAGAATTGACACAAG
CCGGTAAATCTTTGCCACCAGTTGATGAATTGAGATGGTCTGCTGGTGAAGGTGCTAGAA
GAACTGCTTTTGTTTGTTACTCTTCTGGTACTTCCGGTTTGCCTAAAGGTGTTATGATTTCC
CATAGAAACGTTATCGCTAACACCTTGCAAATCAAGGCTTTCGAACAAAACTATAGAGATG
GTGGTGGTACTAAGCCAGCTTCTACTGAAGTTGCTTTGGGTTTGTTGCCACAATCTCATAT
CTATGCCTTGGTTGTTATTGGTCATGCCGGTGCTTATAGAGGTGATCAAACTATCGTTTTG
CCCAAGTTCGAATTGAAGTCTTACTTGAACGCTATCCAGCAGTACAAGATTTCCGCTTTGT
TTTTGGTTCCACCAATCATCATTCACATGTTGGGTACTCAAGATGTCTGCTCTAAATACGAT
TTGTCCTCTGTTACTTCTTTGTTCACTGGTGCTGCTCCATTAGGTATGGAAACAGCTGCTG
ATTTTTTGAAGTTGTACCCCAACATCTTGATCAGACAAGGTTATGGTTTGACTGAAACCTGT
GCTGTTGTTTCTTCTACTCATCCACATGATATATGGTTGGGTTCTTCTGGTGCTTTGTTACC
AGGTGTTGAAGCTAGAATAGTTACCCCAGAAAACAAAGAAATCACCACCTATGATTCTCCA
GGTGAATTGGTTGTAAGATCCCCATCTGTTGTTTTAGGCTACTTGAACAACGAAAAGGCTA
CTGCTGAAACTTTTGTTGATGGTTGGATGAGAACTGGTGATGAAGCTGTTATTAGAAGATC
TCCAAAGGGTATCGAACACGTTTTTATCGTCGACAGGATCAAAGAATTGATCAAGGTCAAG
GGTTTACAAGTTGCTCCAGCTGAATTAGAAGCTCATATTTTGGCTCATCCAGATGTTTCTGA
TTGCGCTGTTATTGCTATTCCAGATGATAGAGCCGGTGAAGTTCCAAAAGCTATAGTTGTT
AAGTCTGCTTCTGCTGGTTCTGATGAATCAGTTTCTCAAGCTTTGGTCAAGTACGTTGAAG
ATCATAAGGCTAGACACAAGTGGTTGAAAGGTGGTATTAGATTCGTTGATGCCATTCCAAA
ATCTCCATCCGGTAAGATTTTGAGAAGATTGATCAGGGACCAAGAAAAAGAAGCCAGAAG
AAAAGCAGGTTCCAAGATCTAA

Codon optimized acyl-activating enzyme 11 from *A. thaliana* (*^{At}AAE11*)

ATGGACAACTTGGTTTTGTGTGAAGCTAACAACGTTCCATTGACTCCAATCACTTTCTTGAA
GAGAGCTTCTGAATGTTACCCAAACAGAACTTCTATCATCTACGGTCAAACTAGATTCACTT
GGCCACAAACTTACGACAGATGTTGTAGATTGGCTGCTTCTTTGTTGTCTTTGAACATCAC
TAGAAATGACGTTGTTTCTATCTTGGCTCCAAACGTTCCAGCTATGTACGAAATGCACTTCT
CTGTTCCAATGACTGGTGCTGTTTTGAACCCAATCAACACTAGATTGGACGCTAAGACTAT
CGCTATCATCTTGAGACACGCTGAACCAAAGATCTTGTTCGTTGACTACGAATTCGCTCCA
TTGATCCAAGAAGTTTTGAGATTGATCCCAACTTACCAATCTCAACCACACCCAAGAATCAT
CTTGATCAACGAAATCGACTCTACTACTAAGCCATTCTCTAAGGAATTGGACTACGAAGGT
TTGATCAGAAAGGGTGAACCAACTCCATCTTCTTCTGCTTCTATGTTCAGAGTTCACAACG
AACACGACCCAATCTCTTTGAACTACACTTCTGGTACTACTGCTGACCCAAAGGGTGTTGT
TATCTCTCACCAAGGTGCTTACTTGTCTGCTTTGTCTTCTATCATCGGTTGGGAAATGGGT
ATCTTCCCAGTTTACTTGTGGACTTTGCCAATGTTCCACTGTAACGGTTGGACTCACACTT
GGTCTGTTGCTGCTAGAGGTGGTACTAACGTTTGTATCAGACACGTTACTGCTCCAGAAAT
CTACAAGAACATCGAATTGCACGGTGTTACTCACATGTCTTGTGTTCCAACTGTTTTCAGAT
TCTTGTTGGAAGGTTCTAGAACTGACCAATCTCCAAAGTCTTCTCCAGTTCAAGTTTTGACT
GGTGGTTCTTCTCCACCAGCTGTTTTGATCAAGAAGGTTGAACAATTGGGTTTCCACGTTA
TGCACGGTTACGGTTTGACTGAAGCTACTGGTCCAGTTTTGTTCTGTGAATGGCAAGACGA
ATGGAACAAGTTGCCAGAACACCAACAAATCGAATTGCAACAAAGACAAGGTGTTAGAAAC
TTGACTTTGGCTGACGTTGACGTTAAGAACACTAAGACTTTGGAATCTGTTCCAAGAGATG
GTAAGACTATGGGTGAAATCGTTATCAAGGGTTCTTCTTTGATGAAGGGTTACTTGAAGAA
CCCAAAGGCTACTTCTGAAGCTTTCAAGCACGGTTGGTTGAACACTGGTGACATCGGTGT
TATCCACCCAGACGGTTACGTTGAAATCAAGGACAGATCTAAGGACATCATCATCTCTGGT
GGTGAAAACATCTCTTCTATCGAAGTTGAAAAGGTTTTGTACATGTACCAAGAAGTTTTGGA
AGCTGCTGTTGTTGCTATGCCACACCCATTGTGGGGTGAAACTCCATGTGCTTTCGTTGTT
TTGAAGAAGGGTGAAGAAGGTTTGGTTACTTCTGAAGGTGACTTGATCAAGTACTGTAGAG
AAAACATGCCACACTTCATGTGTCCAAAGAAGGTTGTTTTCTTCCAAGAATTGCCAAAGAA
CTCTAACGGTAAGATCTTGAAGTCTAAGTTGAGAGACATCGCTAAGGCTTTGGTTGTTAGA
GAAGACGACGCTGGTTCTAAGAAGGTTCACCAAAGATCTATCGAACACGTTTCTTCTAGAT
TGTAA

Codon optimized acyl-activating enzyme 15 from *T. x media* (*^{Tm}AAE15*)

ATGGCTTCTGACTTGGACCCATCTTCTGGTTTCTGTAGAGCTGCTGGTATCTACTACTCTA
AGAGAGATCCAATCGAATTGCCACCACCAGACCAACACTTGGACTTGACTACTTACGTTTT
CTCTCACCACCACAACACTGAAATCGCTTTCATCAACGCTCCATCTGGTGCTCAATTGTCT
TACTCTGCTTTGAGACACAACGTTAAGGCTTTGGCTGCTTCTTTGCAAAGATTGGGTATCA
GAAAGAGAGATGTTGTTTTGGTTATCTCTCCAAACTCTATCCACTTGCCATGTATCTACTTG
GCTATCGTTTACATCGGTGCTATCTTGACTACTACTAACCCATTGAACGCTGAAGCTGAAA
TCAGAAAGCAAATCGCTGACTCTAACCCAGTTTTGGTTTTCGCTGCTCCAGAATTCTTGCC
AAAGGCTAGAGCTGCTAGATTGCCAGTTGTTTTGATCCAAACTACTAACCAAACTGCTATC
CCATCTGGTTGTGTTGCTACTTTGCACGAATTGTTCCAATCTGACGTTGACGACTTCCCAT
CTGTTGACGTTAAGCAAGACGACACTGCTACTTTGTTGTACTCTTCTGGTACTACTGGTAA
GTCTAAGGGTGTTGTTGGTACTCACAGAAACCACATCGCTATGGTTGCTGGTTACGTTAAC
AAGACTAGAAAGTTCATCAACTTGTGTACTATGCCAATGTTCCACGTTTACGGTTTCTTCTA
CACTTTGTCTGCTGTTGCTTCTGGTTCTACTATGGTTGTTATGCCAAAGTTCGACTTCTCTG
AAATGTTGGCTACTGTTAAGAGATACAGAGTTACTTCTTTGCCAGCTGCTCCACCATTGTT
CGTTGCTTTGACTAAGTCTCCAATCGTTGCTCAATACGACTTGTCTTCTTTGCAATCTGTTG
GTTCTGGTGGTGCTCCATTGTCTAAGGAAATCATCGACAAGTTCATCGCTATGTTCCCAAA
CATCGAAGTTGCTCAAGGTTACGGTTTGACTGAATCTAACGGTGCTGTTACTTTCACTTCT
ACTTCTGAAGAAAACAAGAAGTACGGTACTGCTGGTTTGTTGGCTGCTAACGTTGAAGCTA
AGATCGTTGACACTGTTTCTGGTAAGGCTTTGCCACCAAACCAAAGAGGTGAATTGTGGTT
GAGAGGTCCAACTGTTATGAAGGGTTACTTCGGTAACATGGAAGCTACTGCTGCTACTTTG
GACTCTGAAGGTTGGTTGAAGACTGGTGACTTGTGTTACATCGACGAAGAAGGTTTCTTGT
TCGTTGTTGACAGAATCAAGGAATTGATCAAGTACAAGGCTTACCAAGTTGCTCCAGCTGA
ATTGGAAGAATTGTTGTTGTCTAACCCAGAAATCGCTGACGCTGCTGTTATCCCATACCCA
GACAAGGAAGCTGGTCAAATCCCAATGGCTTTCATCGTTAGAAAGTCTGACTCTAAGTTGA
AGGAAGAAGACGTTATGTCTTTCGTTTCTAAGCAAGTTGCTCCATACAAGAAGATCAGAAG
AGTTTCTTTCGTTGCTTCTATCCCAAAGTCTCCAACTGGTAAGATCTTGAGAAAGGACTTGA
TCCAACAAACTTTGTCTACTTCTAAGTTGTAA

Codon optimized acyl-activating enzyme 3 from *C. sativa* with C-terminal lysine (*^{Cs}AAE3-K*)

ATGGAAAAGTCTGGTTATGGTAGAGATGGTATCTACAGATCTTTAAGACCACCATTGCATCTGCCAAACAACAAC
AATTTGTCCATGGTGTCTTTCTTGTTCCGTAACTCTTCTTCATACCCACAAAAGCCAGCTTTGATCGACTCTGAAACT
AACCAGATTTTGTCCTTCTCACACTTCAAGTCCACCGTTATTAAGGTTTCTCATGGCTTTTTGAACCTGGGCATCAA
AAAGAACGATGTCGTTTTGATCTACGCCCCAAACTCTATTCATTTCCCAGTTTGTTTCTTGGGCATTATTGCTTCAG
GTGCTATTGCTACTACTTCTAACCCATTATACACCGTGTCTGAATTGTCCAAGCAAGTTAAGGATTCCAATCCAAAG
TTGATCATTACCGTTCCACAGTTGTTGGAAAAGGTTAAGGGTTTTAACTTGCCCACCATTTTGATTGGTCCAGACTC
TGAACAAGAATCCTCTTCAGATAAGGTTATGACCTTCAACGACTTGGTTAACTTAGGTGGTTCTTCTGGTTCAGAA
TTCCCAATCGTTGATGACTTCAAGCAATCTGATACTGCTGCTTTGTTGTACTCTTCTGGTACTACTGGTATGTCTAA
GGGTGTTGTTTTGACCCACAAGAACTTTATTGCCTCTTCTTTGATGGTCACCATGGAACAAGATTTGGTTGGTGAA
ATGGACAACGTTTTCTTGTGTTTCTTGCCAATGTTCCACGTTTTCGGTTTGGCTATTATTACCTACGCTCAATTGCAA
AGAGGTAACACCGTTATATCTATGGCCAGATTCGATTTGGAGAAGATGTTGAAGGATGTCGAAAAGTACAAGGT
TACCCATTTGTGGGTTGTTCCACCAGTTATTTTGGCTTTGTCTAAGAACTCCATGGTCAAGAAGTTCAACCTGTCCT
CCATTAAGTATATTGGTTCTGGTGCTGCTCCATTGGGTAAAGATTTGATGGAAGAATGCTCTAAGGTTGTCCCATA
TGGTATAGTTGCTCAAGGTTACGGTATGACTGAAACTTGTGGTATCGTTAGCATGGAAGATATTAGAGGTGGTAA
GAGAAATTCTGGTTCTGCAGGTATGTTAGCTTCTGGTGTTGAAGCTCAAATCGTTTCTGTTGATACTTTGAAACCC
TTGCCACCAAATCAATTGGGTGAAATTTGGGTCAAAGGTCCAAATATGATGCAGGGTTACTTCAACAATCCACAA
GCTACTAAGTTGACCATCGATAAGAAAGGTTGGGTTCATACTGGTGACTTGGGTTACTTTGATGAAGATGGTCAC
TTGTACGTTGTCGACAGAATCAAAGAACTGATCAAGTACAAAGGTTTCCAAGTTGCTCCAGCTGAATTGGAAGGT
TTGTTAGTTTCTCATCCAGAAATCTTGGATGCCGTTGTTATTCCATTTCCAGATGCTGAAGCTGGTGAAGTTCCAGT
TGCTTATGTTGTTAGATCTCCCAACTCTTCCTTGACTGAAAACGATGTGAAAAAGTTCATTGCTGGTCAAGTTGCCT
CTTTCAAGAGATTGAGAAAGGTTACCTTCATCAACTCCGTTCCAAAATCTGCTTCTGGTAAGATCTTGAGAAGAGA
GTTGATTCAAAAGGTCAGGTCCAACATGAAGTGA

Medium chain fatty acyl-CoA synthase from *S. cerevisiae* with 3 AA terminal truncation (*^{Sc}FAA2-ΔPTS1*)

ATGGCCGCTCCAGATTATGCACTTACCGATTTAATTGAATCGGATCCTCGTTTCGAAAGTTTGAAGACAAGATTAG
CCGGTTACACCAAAGGCTCTGATGAATATATTGAAGAGCTATACTCTCAATTACCACTGACCAGCTATCCCAGGTA
CAAAACATTTTTAAAGAAACAGGCGGTTGCCATTTCGAATCCGGATAATGAAGCTGGTTTTAGCTCGATTTATAGG

AGTTCTCTTTCTTCTGAAAATCTAGTGAGCTGTGTGGATAAAAACTTAAGAACTGCATACGATCACTTCATGTTTTC
TGCAAGGAGATGGCCTCAACGTGACTGTTTAGGTTCAAGGCCAATTGATAAAGCCACAGGCACCTGGGAGGAAA
CATTCCGTTTCGAGTCGTACTCCACGGTATCTAAAAGATGTCATAATATCGGAAGTGGTATATTGTCTTTGGTAAA
CACGAAAAGGAAACGTCCTTTGGAAGCCAATGATTTTGTTGTTGCTATCTTATCACACAACAACCCTGAATGGATC
CTAACAGATTTGGCCTGTCAGGCCTATTCTCTAACTAACACGGCTTTGTACGAAACATTAGGTCCAAACACCTCCG
AGTACATATTGAATTTAACCGAGGCCCCCATTCTGATTTTTGCAAAATCAAATATGTATCATGTATTGAAGATGGT
GCCTGATATGAAATTTGTTAATACTTTGGTTTGTATGGATGAATTAACTCATGACGAGCTCCGTATGCTAAATGAA
TCGTTGCTACCCGTTAAGTGCAACTCTCTCAATGAAAAAATCACATTTTTTTCATTGGAGCAGGTAGAACAAGTTG
GTTGCTTTAACAAAATTCCTGCAATTCCACCTACCCCAGATTCCTTGTATACTATTTCGTTTACTTCTGGTACTACAG
GTTTACCTAAAGGTGTGGAAATGTCTCACAGAAACATTGCGTCTGGGATAGCATTTGCTTTTTCTACCTTCAGAAT
ACCGCCAGATAAAAGAAACCAACAGTTATATGATATGTGTTTTTTGCCATTGGCTCATATTTTTGAAAGAATGGTT
ATTGCGTATGATCTAGCCATCGGGTTTGGAATAGGCTTCTTACATAAACCAGACCCAACTGTATTGGTAGAGGATT
TGAAGATTTTGAAACCTTACGCGGTTGCCCTGGTTCCTAGAATATTAACACGGTTTGAAGCCGGTATAAAAAACG
CTTTGGATAAATCGACTGTCCAGAGGAACGTAGCAAATACTATATTGGATTCTAAATCGGCCAGATTTACCGCAA
GAGGTGGTCCAGATAAATCGATTATGAATTTTCTAGTTTATCATCGCGTATTGATTGATAAAATCAGAGACTCTTT
AGGTTTGTCCAATAACTCGTTTATAATTACCGGATCAGCTCCCATATCTAAAGATACCTTACTATTTTTAAGAAGTG
CCTTGGATATTGGTATAAGACAGGGCTACGGCTTAACTGAAACTTTTGCTGGTGTCTGTTTAAGCGAACCGTTTGA
AAAAGATGTCGGATCTTGTGGTGCCATAGGTATTTCTGCAGAATGTAGATTGAAGTCTGTTCCAGAAATGGGTTA
CCATGCCGACAAGGATTTAAAAGGTGAACTGCAAATTCGTGGCCCACAGGTTTTTGAAAGATATTTTAAAAATCC
GAATGAAACTTCAAAAGCCGTTGACCAAGATGGTTGGTTTTCCACGGGAGATGTTGCATTTATCGATGGAAAAGG
TCGCATCAGCGTCATTGATCGAGTCAAGAACTTTTTCAAGCTAGCACATGGTGAATATATTGCTCCAGAGAAAATC
GAAAATATTTATTTATCATCATGCCCCTATATCACGCAAATATTTGTCTTTGGAGATCCTTTAAAGACATTTTTAGTT
GGCATCGTTGGTGTTGATGTTGATGCAGCGCAACCGATTTTAGCTGCAAAGCACCCAGAGGTGAAAACGTGGAC
TAAGGAAGTGCTAGTAGAAAACTTAAATCGTAATAAAAAGCTAAGGAAGGAATTTTTAAACAAAATTAATAAATG
CACCGATGGGCTACAAGGATTCGAAAAATTGCATAACATCAAAGTCGGACTTGAGCCTTTAACTCTCGAGGATGA
TGTTGTGACGCCAACTTTTAAAATAAAGCGTGCCAAAGCATCAAAATTCTTCAAAGATACATTAGACCAACTATAC
GCCGAAGGTTCACTAGTCAAGACATAG

Medium chain fatty acyl-CoA synthase from *S. cerevisiae* with C-terminal lysine (*^{Sc}FAA2-K*)

ATGGCCGCTCCAGATTATGCACTTACCGATTTAATTGAATCGGATCCTCGTTTCGAAAGTTTGAAGACAAGATTAG
CCGGTTACACCAAAGGCTCTGATGAATATATTGAAGAGCTATACTCTCAATTACCACTGACCAGCTATCCCAGGTA
CAAAACATTTTTAAAGAAACAGGCGGTTGCCATTTCGAATCCGGATAATGAAGCTGGTTTTAGCTCGATTTATAGG
AGTTCTCTTTCTTCTGAAAATCTAGTGAGCTGTGTGGATAAAAACTTAAGAACTGCATACGATCACTTCATGTTTTC
TGCAAGGAGATGGCCTCAACGTGACTGTTTAGGTTCAAGGCCAATTGATAAAGCCACAGGCACCTGGGAGGAAA
CATTCCGTTTCGAGTCGTACTCCACGGTATCTAAAAGATGTCATAATATCGGAAGTGGTATATTGTCTTTGGTAAA
CACGAAAAGGAAACGTCCTTTGGAAGCCAATGATTTTGTTGTTGCTATCTTATCACACAACAACCCTGAATGGATC
CTAACAGATTTGGCCTGTCAGGCCTATTCTCTAACTAACACGGCTTTGTACGAAACATTAGGTCCAAACACCTCCG
AGTACATATTGAATTTAACCGAGGCCCCCATTCTGATTTTTGCAAAATCAAATATGTATCATGTATTGAAGATGGT
GCCTGATATGAAATTTGTTAATACTTTGGTTTGTATGGATGAATTAACTCATGACGAGCTCCGTATGCTAAATGAA
TCGTTGCTACCCGTTAAGTGCAACTCTCTCAATGAAAAAATCACATTTTTTTCATTGGAGCAGGTAGAACAAGTTG
GTTGCTTTAACAAAATTCCTGCAATTCCACCTACCCCAGATTCCTTGTATACTATTTCGTTTACTTCTGGTACTACAG
GTTTACCTAAAGGTGTGGAAATGTCTCACAGAAACATTGCGTCTGGGATAGCATTTGCTTTTTCTACCTTCAGAAT
ACCGCCAGATAAAAGAAACCAACAGTTATATGATATGTGTTTTTTGCCATTGGCTCATATTTTTGAAAGAATGGTT
ATTGCGTATGATCTAGCCATCGGGTTTGGAATAGGCTTCTTACATAAACCAGACCCAACTGTATTGGTAGAGGATT
TGAAGATTTTGAAACCTTACGCGGTTGCCCTGGTTCCTAGAATATTAACACGGTTTGAAGCCGGTATAAAAAACG
CTTTGGATAAATCGACTGTCCAGAGGAACGTAGCAAATACTATATTGGATTCTAAATCGGCCAGATTTACCGCAA
GAGGTGGTCCAGATAAATCGATTATGAATTTTCTAGTTTATCATCGCGTATTGATTGATAAAATCAGAGACTCTTT
AGGTTTGTCCAATAACTCGTTTATAATTACCGGATCAGCTCCCATATCTAAAGATACCTTACTATTTTTAAGAAGTG
CCTTGGATATTGGTATAAGACAGGGCTACGGCTTAACTGAAACTTTTGCTGGTGTCTGTTTAAGCGAACCGTTTGA
AAAAGATGTCGGATCTTGTGGTGCCATAGGTATTTCTGCAGAATGTAGATTGAAGTCTGTTCCAGAAATGGGTTA
CCATGCCGACAAGGATTTAAAAGGTGAACTGCAAATTCGTGGCCCACAGGTTTTTGAAAGATATTTTAAAAATCC
GAATGAAACTTCAAAAGCCGTTGACCAAGATGGTTGGTTTTCCACGGGAGATGTTGCATTTATCGATGGAAAAGG
TCGCATCAGCGTCATTGATCGAGTCAAGAACTTTTTCAAGCTAGCACATGGTGAATATATTGCTCCAGAGAAAATC
GAAAATATTTATTTATCATCATGCCCCTATATCACGCAAATATTTGTCTTTGGAGATCCTTTAAAGACATTTTTAGTT
GGCATCGTTGGTGTTGATGTTGATGCAGCGCAACCGATTTTAGCTGCAAAGCACCCAGAGGTGAAAACGTGGAC
TAAGGAAGTGCTAGTAGAAAACTTAAATCGTAATAAAAAGCTAAGGAAGGAATTTTTAAACAAAATTAATAAATG

CACCGATGGGCTACAAGGATTCGAAAAATTGCATAACATCAAAGTCGGACTTGAGCCTTTAACTCTCGAGGATGA
TGTTGTGACGCCAACTTTTAAAATAAAGCGTGCCAAAGCATCAAAATTCTTCAAAGATACATTAGACCAACTATAC
GCCGAAGGTTCACTAGTCAAGACAGAAAAGCTTAAGTAG

Codon optimized phenylacetate-CoA ligase (T369A) from *P. chrysogenum* with C-terminal lysine (*^{Pc}PCL-K*)

ATGGTTTTCTTGCCACCAAAAGAATCCGGTCAATTAGATCCAATTCCAGACAACATTCCAATCTCCGAATTCATGTT
GAACGAAAGATACGGTAGAGTTAGACATGCCTCTTCTAGAGATCCATACACTTGTGGTATTACTGGCAAGTCCTA
CTCCTCTAAAGAAGTTGCTAATAGGGTTGATTCCTTGGCCAGATCTTTGTCTAAAGAATTTGGTTGGGCTCCAAAC
GAAGGTTCTGAATGGGATAAGACTTTGGCTGTTTTTGCCTTGAACACCATTGATTCTTTGCCTTTGTTTTGGGCCGT
TCATAGATTAGGTGGTGTTTTGACTCCAGCTAATGCTTCTTATTCTGCTGCTGAATTGACTCACCAACTGTTGGATT
CTAAAGCTAAGGCTTTGGTTACTTGCGTTCCTTTGTTGTCCATTTCTTTGGAAGCTGCTGCTAAAGCTGGTTTGCCA
AAGAATAGAATCTACTTGTTGGATGTCCCAGAACAATTACTTGGTGGTGTTAAGCCACCAGCAGGTTACAAATCT
GTTTCAGAATTGACACAAGCCGGTAAATCTTTGCCACCAGTTGATGAATTGAGATGGTCTGCTGGTGAAGGTGCT
AGAAGAACTGCTTTTGTTTGTTACTCTTCTGGTACTTCCGGTTTGCCTAAAGGTGTTATGATTTCCCATAGAAACGT
TATCGCTAACACCTTGCAAATCAAGGCTTTCGAACAAAACTATAGAGATGGTGGTGGTACTAAGCCAGCTTCTACT
GAAGTTGCTTTGGGTTTGTTGCCACAATCTCATATCTATGCCTTGGTTGTTATTGGTCATGCCGGTGCTTATAGAG
GTGATCAAACTATCGTTTTGCCCAAGTTCGAATTGAAGTCTTACTTGAACGCTATCCAGCAGTACAAGATTTCCGC
TTTGTTTTTGGTTCCACCAATCATCATTCACATGTTGGGTACTCAAGATGTCTGCTCTAAATACGATTTGTCCTCTGT
TACTTCTTTGTTCACTGGTGCTGCTCCATTAGGTATGGAAACAGCTGCTGATTTTTTGAAGTTGTACCCCAACATCT
TGATCAGACAAGGTTATGGTTTGACTGAAACCTGTGCTGTTGTTTCTTCTACTCATCCACATGATATATGGTTGGG
TTCTTCTGGTGCTTTGTTACCAGGTGTTGAAGCTAGAATAGTTACCCCAGAAAACAAAGAAATCACCACCTATGAT
TCTCCAGGTGAATTGGTTGTAAGATCCCCATCTGTTGTTTTAGGCTACTTGAACAACGAAAAGGCTACTGCTGAAA
CTTTTGTTGATGGTTGGATGAGAACTGGTGATGAAGCTGTTATTAGAAGATCTCCAAAGGGTATCGAACACGTTT
TTATCGTCGACAGGATCAAAGAATTGATCAAGGTCAAGGGTTTACAAGTTGCTCCAGCTGAATTAGAAGCTCATA
TTTTGGCTCATCCAGATGTTTCTGATTGCGCTGTTATTGCTATTCCAGATGATAGAGCCGGTGAAGTTCCAAAAGC
TATAGTTGTTAAGTCTGCTTCTGCTGGTTCTGATGAATCAGTTTCTCAAGCTTTGGTCAAGTACGTTGAAGATCATA
AGGCTAGACACAAGTGGTTGAAAGGTGGTATTAGATTCGTTGATGCCATTCCAAAATCTCCATCCGGTAAGATTTT
GAGAAGATTGATCAGGGACCAAGAAAAAGAAGCCAGAAGAAAAGCAGGTTCCAAGATCAAGTAA

Codon optimized acyl-activating enzyme 11 from *A. thaliana* with 3 AA terminal truncation (*^{At}AAE11-ΔPTS1*)

ATGGACAACTTGGTTTTGTGTGAAGCTAACAACGTTCCATTGACTCCAATCACTTTCTTGAAGAGAGCTTCTGAAT
GTTACCCAAACAGAACTTCTATCATCTACGGTCAAACTAGATTCACTTGGCCACAAACTTACGACAGATGTTGTAG
ATTGGCTGCTTCTTTGTTGTCTTTGAACATCACTAGAAATGACGTTGTTTCTATCTTGGCTCCAAACGTTCCAGCTA
TGTACGAAATGCACTTCTCTGTTCCAATGACTGGTGCTGTTTTGAACCCAATCAACACTAGATTGGACGCTAAGAC
TATCGCTATCATCTTGAGACACGCTGAACCAAAGATCTTGTTCGTTGACTACGAATTCGCTCCATTGATCCAAGAA
GTTTTGAGATTGATCCCAACTTACCAATCTCAACCACACCCAAGAATCATCTTGATCAACGAAATCGACTCTACTAC
TAAGCCATTCTCTAAGGAATTGGACTACGAAGGTTTGATCAGAAAGGGTGAACCAACTCCATCTTCTTCTGCTTCT
ATGTTCAGAGTTCACAACGAACACGACCCAATCTCTTTGAACTACACTTCTGGTACTACTGCTGACCCAAAGGGTG
TTGTTATCTCTCACCAAGGTGCTTACTTGTCTGCTTTGTCTTCTATCATCGGTTGGGAAATGGGTATCTTCCCAGTTT
ACTTGTGGACTTTGCCAATGTTCCACTGTAACGGTTGGACTCACACTTGGTCTGTTGCTGCTAGAGGTGGTACTAA
CGTTTGTATCAGACACGTTACTGCTCCAGAAATCTACAAGAACATCGAATTGCACGGTGTTACTCACATGTCTTGT
GTTCCAACTGTTTTCAGATTCTTGTTGGAAGGTTCTAGAACTGACCAATCTCCAAAGTCTTCTCCAGTTCAAGTTTT
GACTGGTGGTTCTTCTCCACCAGCTGTTTTGATCAAGAAGGTTGAACAATTGGGTTTCCACGTTATGCACGGTTAC
GGTTTGACTGAAGCTACTGGTCCAGTTTTGTTCTGTGAATGGCAAGACGAATGGAACAAGTTGCCAGAACACCAA
CAAATCGAATTGCAACAAAGACAAGGTGTTAGAAACTTGACTTTGGCTGACGTTGACGTTAAGAACACTAAGACT
TTGGAATCTGTTCCAAGAGATGGTAAGACTATGGGTGAAATCGTTATCAAGGGTTCTTCTTTGATGAAGGGTTAC
TTGAAGAACCCAAAGGCTACTTCTGAAGCTTTCAAGCACGGTTGGTTGAACACTGGTGACATCGGTGTTATCCAC
CCAGACGGTTACGTTGAAATCAAGGACAGATCTAAGGACATCATCATCTCTGGTGGTGAAAACATCTCTTCTATCG
AAGTTGAAAAGGTTTTGTACATGTACCAAGAAGTTTTGGAAGCTGCTGTTGTTGCTATGCCACACCCATTGTGGG
GTGAAACTCCATGTGCTTTCGTTGTTTTGAAGAAGGGTGAAGAAGGTTTGGTTACTTCTGAAGGTGACTTGATCA
AGTACTGTAGAGAAAACATGCCACACTTCATGTGTCCAAAGAAGGTTGTTTTCTTCCAAGAATTGCCAAAGAACTC
TAACGGTAAGATCTTGAAGTCTAAGTTGAGAGACATCGCTAAGGCTTTGGTTGTTAGAGAAGACGACGCTGGTTC
TAAGAAGGTTCACCAAAGATCTATCGAACACGTTTCTTAA

Codon optimized acyl-activating enzyme 11 from *A. thaliana* C-terminal lysine (*^{At}AAE11-K*)

ATGGACAACTTGGTTTTGTGTGAAGCTAACAACGTTCCATTGACTCCAATCACTTTCTTGAAGAGAGCTTCTGAAT
GTTACCCAAACAGAACTTCTATCATCTACGGTCAAACTAGATTCACTTGGCCACAAACTTACGACAGATGTTGTAG
ATTGGCTGCTTCTTTGTTGTCTTTGAACATCACTAGAAATGACGTTGTTTCTATCTTGGCTCCAAACGTTCCAGCTA
TGTACGAAATGCACTTCTCTGTTCCAATGACTGGTGCTGTTTTGAACCCAATCAACACTAGATTGGACGCTAAGAC
TATCGCTATCATCTTGAGACACGCTGAACCAAAGATCTTGTTCGTTGACTACGAATTCGCTCCATTGATCCAAGAA
GTTTTGAGATTGATCCCAACTTACCAATCTCAACCACACCCAAGAATCATCTTGATCAACGAAATCGACTCTACTAC
TAAGCCATTCTCTAAGGAATTGGACTACGAAGGTTTGATCAGAAAGGGTGAACCAACTCCATCTTCTTCTGCTTCT
ATGTTCAGAGTTCACAACGAACACGACCCAATCTCTTTGAACTACACTTCTGGTACTACTGCTGACCCAAAGGGTG
TTGTTATCTCTCACCAAGGTGCTTACTTGTCTGCTTTGTCTTCTATCATCGGTTGGGAAATGGGTATCTTCCCAGTTT
ACTTGTGGACTTTGCCAATGTTCCACTGTAACGGTTGGACTCACACTTGGTCTGTTGCTGCTAGAGGTGGTACTAA
CGTTTGTATCAGACACGTTACTGCTCCAGAAATCTACAAGAACATCGAATTGCACGGTGTTACTCACATGTCTTGT
GTTCCAACTGTTTTCAGATTCTTGTTGGAAGGTTCTAGAACTGACCAATCTCCAAAGTCTTCTCCAGTTCAAGTTTT
GACTGGTGGTTCTTCTCCACCAGCTGTTTTGATCAAGAAGGTTGAACAATTGGGTTTCCACGTTATGCACGGTTAC
GGTTTGACTGAAGCTACTGGTCCAGTTTTGTTCTGTGAATGGCAAGACGAATGGAACAAGTTGCCAGAACACCAA
CAAATCGAATTGCAACAAAGACAAGGTGTTAGAAACTTGACTTTGGCTGACGTTGACGTTAAGAACACTAAGACT
TTGGAATCTGTTCCAAGAGATGGTAAGACTATGGGTGAAATCGTTATCAAGGGTTCTTCTTTGATGAAGGGTTAC
TTGAAGAACCCAAAGGCTACTTCTGAAGCTTTCAAGCACGGTTGGTTGAACACTGGTGACATCGGTGTTATCCAC
CCAGACGGTTACGTTGAAATCAAGGACAGATCTAAGGACATCATCATCTCTGGTGGTGAAAACATCTCTTCTATCG
AAGTTGAAAAGGTTTTGTACATGTACCAAGAAGTTTTGGAAGCTGCTGTTGTTGCTATGCCACACCCATTGTGGG
GTGAAACTCCATGTGCTTTCGTTGTTTTGAAGAAGGGTGAAGAAGGTTTGGTTACTTCTGAAGGTGACTTGATCA
AGTACTGTAGAGAAAACATGCCACACTTCATGTGTCCAAAGAAGGTTGTTTTCTTCCAAGAATTGCCAAAGAACTC
TAACGGTAAGATCTTGAAGTCTAAGTTGAGAGACATCGCTAAGGCTTTGGTTGTTAGAGAAGACGACGCTGGTTC
TAAGAAGGTTCACCAAAGATCTATCGAACACGTTTCTTCTAGATTGAAGTAA

Supplementary Table 2 | Tukey's multiple comparisons test analysis of OL measurements following different extraction methods

Tukey's multiple comparisons test	Mean Diff.	95.00% CI of diff.	Below threshold?	Summary	Adjusted P Value
ACN/FA vs. ACN/FA + Beads	-1.595	-3.026 to -0.1637	Yes	*	0.0279
ACN/FA vs. EtAc/FA	3.342	1.911 to 4.773	Yes	***	0.0001
ACN/FA vs. EtAc/FA + Beads	1.458	0.02741 to 2.889	Yes	*	0.0453
ACN/FA vs. Sonification of Pellet	8.161	6.730 to 9.592	Yes	****	<0.0001
ACN/FA + Beads vs. EtAc/FA	4.937	3.506 to 6.368	Yes	****	<0.0001
ACN/FA + Beads vs. EtAc/FA + Beads	3.053	1.622 to 4.484	Yes	***	0.0003
ACN/FA + Beads vs. Sonification of Pellet	9.755	8.324 to 11.19	Yes	****	<0.0001
EtAc/FA vs. EtAc/FA + Beads	-1.884	-3.315 to -0.4527	Yes	*	0.0101
EtAc/FA vs. Sonification of Pellet	4.819	3.388 to 6.250	Yes	****	<0.0001
EtAc/FA + Beads vs. Sonification of Pellet	6.702	5.271 to 8.133	Yes	****	<0.0001

Supplementary Table 3 | Tukey's multiple comparisons test analysis of hexanoic acid following different extraction methods

Tukey's multiple comparisons test	Mean Diff.	95.00% CI of diff.	Below threshold?	Summary	Adjusted P Value
ACN/FA vs. ACN/FA + Beads	0.75	-2.358 to 3.858	No	ns	0.9266
ACN/FA vs. EtAc/FA	0.6067	-2.502 to 3.715	No	ns	0.9643
ACN/FA vs. EtAc/FA + Beads	0.75	-2.358 to 3.858	No	ns	0.9266
ACN/FA vs. Sonification of Pellet	0.6067	-2.502 to 3.715	No	ns	0.9643
ACN/FA + Beads vs. EtAc/FA	-0.1433	-3.252 to 2.965	No	ns	0.9999
ACN/FA + Beads vs. EtAc/FA + Beads	0	-3.108 to 3.108	No	ns	>0.9999
ACN/FA + Beads vs. Sonification of Pellet	-0.1433	-3.252 to 2.965	No	ns	0.9999
EtAc/FA vs. EtAc/FA + Beads	0.1433	-2.965 to 3.252	No	ns	0.9999
EtAc/FA vs. Sonification of Pellet	0	-3.108 to 3.108	No	ns	>0.9999
EtAc/FA + Beads vs. Sonification of Pellet	-0.1433	-3.252 to 2.965	No	ns	0.9999

Supplementary Table 4 | List of abbreviations

2-AG	2-Arachidonoylglycerol	GRAS	Generally regarded as safe
3-AP	3-Aminopropanal	h	Hours
AAE	Acyl-activating enzyme	H^+	Hydrogen ion
A-ALD	Acetylating aldehyde dehydrogenase	H_2O_2	Hydrogen peroxide
AEA	Anandamide	HDR	Homology-directed repair
ACC	Acetyl-CoA carboxylase	HPLC	High-performance liquid chromatography
ACP	Acyl carrier protein	HR	Homologous recombination
ACN	Acetonitrile	kDa	Kilo Dalton
ADH	Alcohol dehydrogenase	KO	Knockout
ALD	Aldehyde dehydrogenase	KP_i	Potassium phosphate buffer
AMP	Adenosine monophosphate	KR	β-Ketoacyl reductase
AT	Acetyl transferase	KS	β-Ketoacyl synthase
ATP	Adenosine triphosphate	KAT	3-Ketoacyl-CoA thiolase
BC	Biotin carboxylase	kV	Kilo volts
BCCP	Biotin carboxyl carrier protein	L	Liter
bp	Base pair	µL	Microliter
C-C	Carbon-Carbon bond	µM	Micromolar
C_6-FA	Hexanoic acid	MAT	Malonyl/acetyl transferase
C_8-FA	Octanoic acid	mL	Milliliter
C_{10}-FA	Decanoic acid	mM	Millimolar
Cas9	CRISPR associated protein 9	MCFA	Medium chain fatty acid
CB_1/CB_2	Cannabinoid receptor 1/2	MDa	Mega Dalton
CBC	Cannabichromene	MEP	Methylerythritol phosphate
CBCA	Cannabichromenic acid	MPT	Malonyl/palmitoyl transferase
CBCAS	Cannabigerolic acid synthase	MVA	Mevalonate
CBD	Cannabidiol	NLS	Nuclear localization sequence
CBDA	Cannabidiolic acid	Nt	Nucleotide
CBDAS	Cannabidiolic acid synthase	OAC	Olivetolic acid cyclase
CDBP	Cannabidiolphorol	OD_{600}	Optical density at 600 nm
CBG	Cannabigerol	OLS	Olivetol synthase
CBGA	Cannabigerolic acid	PAM	Protospacer adjacent motif
CGBAS	Cannabigerolic acid synthase	PanK	Pantothenate kinase
CBN	Cannabinol	PCR	Polymerase chain reaction
CHS	Chalcone synthase	PDH	Pyruvate dehydrogenase
Chr	Chromosome	PKS	Polyketide synthase

CoA	Coenzyme A	PPT	Phosphopantetheinyl transferase
CRISPR	Clustered regularly interspaced short palindromic repeats	PTM	Post-translational modifications
crRNA	CRISPR RNA	PTS1	Peroxisomal targeting signal 1
CT	Carboxyl transferase	P_{xxx}	Promoter
ddH2O	Double-distilled water	rBOX	Reverse β-oxidation
DH	Dehydratase	RNP	Ribonucleoprotein
DSB	Double-strand breaks	RT-qPCR	Real time quantitative PCR
ECS	Endocannabinoid system	s.d.	Standard deviation
eGFP	Enhance green fluorescent protein	SCD	Synthetic complete media with 2% (w/v) glucose
ER	Enoyl reductase	SMD	Synthetic minimal media with 2% (w/v) glucose
EtAc	Ethyl acetate	sgRNA	Single-guide ribonucleic acid
EtOH	Ethanol	STS	Stilbene synthase
EV	Empty vector	TE	Thioesterase
FA	Fatty acid	Ter	*trans*-enoyl-CoA reductase
FAB	Fatty acid biosynthesis	THC	Δ^9-Tetrahydrocannabinol
FAME	Fatty acid methyl ester	THCA	Δ^9-Tetrahydrocannabinolic acid
FAS	Fatty acid synthase	THCAS	Δ^9-Tetrahydrocannabinolic acid synthase
fusFAS	Fused fatty acid synthase	THCP	Δ^9-Tetrahydrocannabiphorol
GC	Gas chromatography	THCV	Δ^9-Tetrahydrocannabivarin
GFP	Green fluorescent protein	tracrRNA	Trans-activating CRISPR RNA
GOI	Gene of interest	WT	Wildtype
GPP	Geranyl pyrophosphate	YPD	Yeast extract peptone media with 2% (w/v) glucose

7 ACKNOWLEDGMENTS

At this point I would like to mention a number of people who have supported me and facilitated the completion of my PhD. First and foremost, I would like to extend my warmest thanks to Prof. Dr. Eckhard Boles who has supervised my progression in the field of yeast biotechnology starting from my master's degree in 2017 until this point today. Despite there not being space for me to undertake a practical course in your lab, you provided the space, allowing me to squeeze between work benches. After completing the course, I was able to continue the promising project for my master's thesis which I completed at the beginning of 2020. After then searching for an opportunity to start a PhD position during a time which was largely uncertain due to global circumstances, I received an Email from you describing an interesting project based on the production of cannabinoids in yeast. Very quickly, I accepted the position, being fully aware of the importance of having a supervisor, such as yourself, who is supportive and approachable. Your support continued for the next four years and beyond until today, despite personal circumstances of your own. For this, I am truly grateful.

Additionally, I would like to thank Prof. Dr. Dr. h. c. Oliver Kayser who conceptualized the project and provided the position for me. Despite limited face-to-face interactions during the first few years of the project due to the difficult circumstances, you completely trusted my work and provided the supportive framework for me to complete the project successfully. Moreover, you supported and facilitated my desire to travel to multiple conferences, including a great trip to Florence in Italy.

I would also like to thank Prof. Dr. Martin Grininger for allowing me time to work on my thesis and my publications while beginning a postdoctoral position in his group.

I also want to acknowledge the many special people in my life who have supported me in achieving my goals. This begins with my wonderful wife, Sarah, who has always supported me throughout my academic career, especially in the final phases of writing my thesis. Thank you for your love and support and working so hard both at home, being an amazing mother to our children, as well as in your job. Furthermore, I want to thank my two beautiful children, Ava and Caleb. I am extremely proud of you and grateful that you, albeit unknowingly, always provided me with the balance I needed to unwind and recalibrate, helping me remain mindful of what is truly important in life. Furthermore, I want to acknowledge those in my life who have continued supporting me from when I was a child until now. Thank you to my loving parents Sandra and Konrad, my aunties Pauline and Donna and my grandparents Carmen and Solomon for your continuous prayers and encouragement. Thank you also to my in-laws, Sandra and Achim, who supported me and my family in day-to-day life and took me in to their home when I started my master's degree in Frankfurt.

Finally, I would like to thank all those who I worked with during my PhD and who made the working environment extremely supportive and collaborative. Julia, despite your time away in Bremen, you were always a great colleague and friend, from the start of our master's until the completion of our PhD's and further. Others in Frankfurt who provided support or constructs which I was able to use for my project include Mislav, Fernando, Leonardo, Sebastian, Simon, Priti, Sina, Leonie, Christine and Charlotte. Moreover, Christina was always a great help from Dortmund and provided me with constructs which aided in my work. Clara, thank you greatly for your help and support, especially with the microscopy. Thank you also to my students who supported me in my project with their results, Lukas, Caro and Tania. A special mention goes to Sandra and Johannes who were the final PhD students with me during the last months in Eckhard's group. We really grew close in this time, had a lot of fun, supported one another and had a great last conference trip (or "Abschlussfahrt") to Regensburg. Thank you for making this time the best that it could be.

"Rejoice always, pray without ceasing, in everything give thanks; for this is the will of God in Christ Jesus for you."

I Thessalonians 5:16-18